Novel Applications of 3:1 Site-Differentiated [4Fe-4S] Clusters

Nieuwe Toepassingen van 3:1 Gedifferentieërde [4Fe-4S] Clusters

(met een samenvatting in het Nederlands)

Proefschrift

ter verkrijging van de graad van doctor aan de Universiteit Utrecht
op gezag van de rector magnificus, prof. dr. J. C. Stoof
ingevolge het besluit van het college voor promoties
in het openbaar te verdedigen
op maandag 10 maart 2008 des middags te 14.30 uur

door

Erwin Petrus Leonardus van der Geer

geboren op 29 mei 1981 te Katwijk aan den Rijn

Promotoren: Prof. dr. R. J. M. Klein Gebbink

Prof. dr. B. Hessen

Prof. dr. G. van Koten

Novel Applications of 3:1 Site-Differentiated [4Fe-4S] Clusters

Aan mijn ouders

van der Geer, Erwin Petrus Leonardus

Title: Novel Applications of 3:1 Site-Differentiated [4Fe-4S] Clusters
Utrecht, Utrecht University, Faculty of Science
Thesis Utrecht University – with ref. – with summary in Dutch –
ISBN: 978-90-393-4737-9

The work described in this thesis was carried out at the Faculty of Science, Chemical Biology & Organic Chemistry group, Utrecht University, the Netherlands.

This investigation was financially supported by the National Research School Combination–Catalysis (NRSC–C).

The printing of this thesis was financially supported by the J. E. Jurriaanse Stichting.

The cover of this thesis shows the structures of five different enzymatic active sites featuring 3:1 site-differentiated [4Fe-4S] clusters, as determined by X-ray crystallography (PDB ID codes: 7ACN, 1AOP, 1HFE, 1OAO, and 1OLT).

Table of Contents

Preface

Aim and Scope of this Thesis

One of the most common cofactors found in Nature is the [4Fe-4S] cluster, a cubic structure consisting of interlocking iron and sulfur tetrahedra. Endowed with a rich redox chemistry, the [4Fe-4S] cluster is mainly involved in electron transport but can also play direct roles in catalysis, structure stabilization, and iron sensing.[1,2] When present in enzymatic active sites, [4Fe-4S] clusters are *3:1 site-differentiated*, meaning that three of the four iron atoms are coordinated by non-bridging cysteine thiolates while the remaining iron atom is coordinated by a bridging cysteine or a non-cysteine ligand.[3] An example is the active site of aconitase (Chart 1).[4]

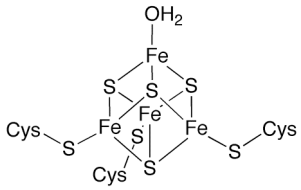

Chart 1. Schematic representation of the active site of aconitase.

In 1987, Holm *et al.* utilized the chelating, tripodal $L(SH)_3$ ligand to synthesize a synthetic 3:1 site-differentiated [4Fe-4S] cluster (Chart 2).[5] Since then, site-differentiated clusters have been successfully incorporated into several active-site models, providing a wealth of information concerning the chemistry and properties of cluster-containing active sites as well as those of [4Fe-4S] clusters in general. Nonetheless, the biomimetic potential of the 3:1 site-differentiated [4Fe-4S] cluster is far from exhausted, with many possible applications having not yet been explored. The research described in this thesis aims to investigate such novel applications and to further increase the understanding of 3:1 site-differentiated [4Fe-4S] clusters in natural and synthetic contexts.

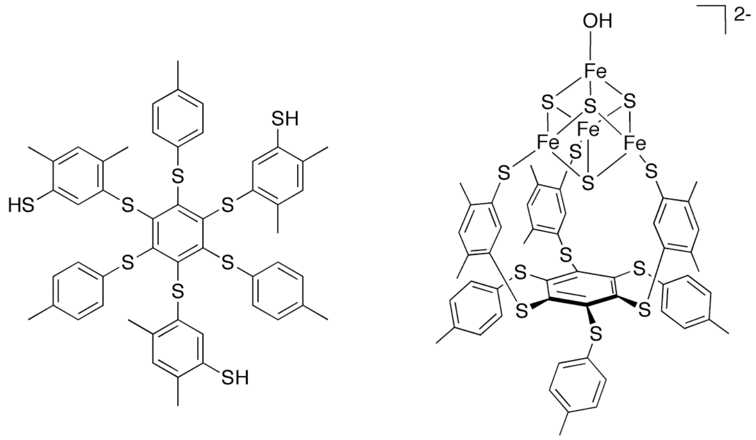

$L(SH)_3$ **$(n\text{-}Bu_4N)_2[Fe_4S_4(LS_3)(OH)]^{2-}$**

Chart 2. $L(SH)_3$ and the 3:1 site-differentiated cluster $[Fe_4S_4(LS_3)(OH)]^{2-}$.

The wealth of information concerning natural and synthetic 3:1 site-differentiated [4Fe-4S] clusters that is currently available in the literature means that all new discoveries can be placed into perspective by comparison to previous results. Hence, **Chapter 1** of this thesis aims to provide a comprehensive survey of natural and synthetic 3:1 site-differentiated [4Fe-4S] clusters and to analyze and compare the five classes of trithiols capable of effecting 3:1 site differentiation in synthetic clusters.

The most promising site-differentiating [4Fe-4S] cluster ligand currently available to the biomimetic chemist is the $TriSH_3$ ligand (Chart 3). Pohl *et al.* presented a five-step synthesis route to this trithiol in 1997 and proved crystallographically that it binds [4Fe-4S] clusters in a 1:1 reaction stoichiometry.[6] However, the reported synthesis made use of the hazardous reagents chloromethyl methyl ether, $Hg(OAc)_2$, and H_2S. The research described in **Chapter 2** seeks to make the $TriSH_3$ ligand more conveniently accessible and explores the use of the new cluster $(n\text{-}Bu_4N)_2[Fe_4S_4(TriS)(SEt)]$ in the synthesis of complex dimers with metal-containing bridges.

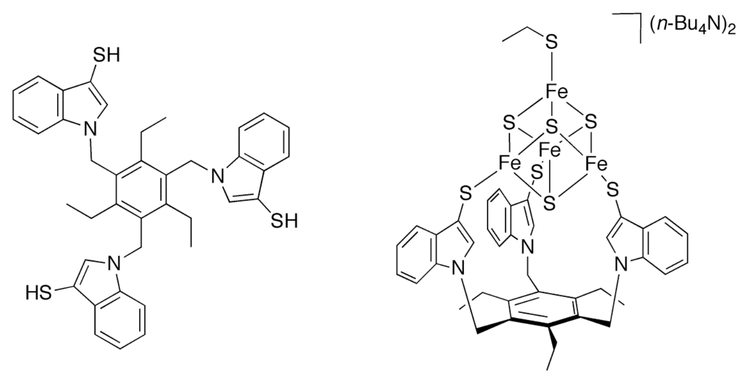

$TriSH_3$ **$(n\text{-}Bu_4N)_2[Fe_4S_4(TriS)(SEt)]$**

Chart 3. $TriSH_3$ and the 3:1 site-differentiated cluster $(n\text{-}Bu_4N)_2[Fe_4S_4(TriS)(SEt)]$.

The $TriSH_3$ ligand contains three indole-3-thiolate arms. Despite the vast number of homosubstituted, tetrathiolate [4Fe-4S] clusters described in literature, [4Fe-4S] clusters coordinated by monodentate indole-3-thiolate ligands have never been reported. Hence, **Chapter 3** describes the synthesis of a series of *N*-substituted indole-3-thiolate [4Fe-4S] clusters. The resulting cluster properties are analyzed in the context of the characteristics of the ligand, the effects of the *N*-substituent, and the relation to $TriS^{3-}$-chelated systems.

Chapter 4 further explores the chemistry of $(n\text{-}Bu_4N)_2[Fe_4S_4(TriS)(SEt)]$ by reaction with the monothiols ethyl cysteinate, *p*-fluorothiophenol, and 4-pyridinethiol. Ethyl cysteinate is an aliphatic thiol with an acidity comparable to EtSH; hence, this thiol provides a means of exploring ligand exchange when little thermodynamic driving force is present. *p*-Fluorothiophenol is a ^{19}F NMR probe ligand, allowing the use of this sensitive spectroscopic technique to analyze the substitution process. 4-Pyridinethiol contains a thiol group for cluster binding as well as an *N*-donor pyridyl group that can bind to other metal ions. To explore the viability of using 4-pyridinethiol as a cluster-to-metal bridge, 4-pyridinethiol is reacted sequentially with $(n\text{-}Bu_4N)_2[Fe_4S_4(TriS)(SEt)]$ and a ruthenium porphyrin.

Pickett *et al.* have recently reported a model for the active site of iron-only hydrogenase incorporating an LS_3^{3-}-chelated [4Fe-4S] cluster.[7] **Chapter 5** presents the $TriS^{3-}$-chelated analogue of the earlier model and explores the effects of the change in tripodal ligand on the properties of the mimic as a whole. Furthermore, the structural and electronic properties of the new model are compared with those of the native active site.

Chapters 2–5, and indeed almost all studies of [4Fe-4S] clusters conducted thus far deal with clusters in solution. In order to open the door to the study of [4Fe-4S] clusters at well-defined interfaces, the research in **Chapter 6** explores the feasibility of immobilizing $(n\text{-}Bu_4N)_2[Fe_4S_4(TriS)(SEt)]$ by reaction with a thiol-functionalized self-assembled monolayer. The SAM surface is then analyzed using X-ray photoelectron spectroscopy and secondary ion mass spectrometry.

By means of the research described in Chapters 2–6, this thesis seeks to explore the fundamental chemistry and investigate new applications of $TriS^{3-}$-chelated [4Fe-4S] clusters. The increased understanding and opening of new lines of research will hopefully facilitate further expansion in the field of 3:1 site-differentiated [4Fe-4S] cluster chemistry and lead to new insights into the properties of these intriguing and exciting compounds.

References.

[1] Beinert, H.; Holm, R. H.; Münck, E. *Science* **1997**, *277*, 653–659.
[2] Johnson, M. K. *Curr. Opin. Chem. Biol.* **1998**, *2*, 173–181.
[3] Holm, R. H. *Pure Appl. Chem.* **1998**, *70*, 931–938.
[4] Beinert, H.; Kennedy, M. C.; Stout, C. D. *Chem. Rev.* **1996**, *96*, 2335–2373.
[5] Stack, T. D. P.; Holm, R. H. *J. Am. Chem. Soc.* **1987**, *109*, 2546–2547.

[6] Walsdorff, C.; Saak, W.; Pohl, S. *J. Chem. Soc., Dalton Trans.* **1997**, 1857–1861.
[7] Tard, C.; Liu, X.; Ibrahim, S. K.; Bruschi, M.; De Gioia, L.; Davies, S. C.; Yang, X.; Wang, L.-S.; Sawers, G.; Pickett, C. J. *Nature* **2005**, *433*, 610–613.

Chapter 1

3:1 Site Differentiation in Natural and Synthetic [4Fe-4S] Clusters

Abstract. *This review covers the structural biology and biomimetic chemistry of 3:1 site-differentiated [4Fe-4S] clusters. Special emphasis is placed on the most biologically relevant results obtained from synthetic models, as well as on the differences between the five classes of site-differentiating [4Fe-4S] cluster ligands currently available to the biomimetic chemist.*

van der Geer, E. P. L.; van Putten, R.-J.; van Koten, G.; Klein Gebbink, R. J. M.; Hessen, B., manuscript in preparation.

1.1. Introduction.

Despite representing one of the oldest topics in biomimetic chemistry, the field of synthetic, cubane-type [4Fe-4S] clusters continues to change, develop, and contribute to exciting new lines of both inorganic and biomolecular research. The scientific interest stems largely from the frequent discoveries and new insights into the biological significance of [4Fe-4S] clusters, for which roles in catalysis, protein stabilization, electron transfer, and iron sensing are now well-established.[1]

In one important subclass of natural [4Fe-4S] clusters, one iron atom is catalytically active or bridged *via* a cysteinyl sulfur atom to a catalytically active metal or metal-based subsite. Such a cluster is *3:1 site-differentiated*; although each of the four iron atoms is unique by virtue of the asymmetrical protein environment, one iron atom differs more markedly from the others in that it is not coordinated by a terminal cysteine thiolate, but by a bridging cysteine or non-cysteine ligand.[2]

In an effort to model these natural systems, Stack and Holm reported the first synthetic [4Fe-4S] cluster with a stable 3:1 site-differentiated coordination sphere in 1987. In this cluster, a tripodal ligand chelated three of the four iron atoms, leaving only one iron site available for site-specific substitution.[3] Since this first report, a wealth of knowledge on these systems has been obtained, partly by virtue of the accurate reproduction of the natural site differentiation and partly due to the synthetic utility of having one rather than four coordination sites susceptible to ligand exchange.

In this review, we first provide an overview of [4Fe-4S] clusters in natural systems for which 3:1 site differentiation has been demonstrated crystallographically. Second, we describe and compare the preparation, properties, and site-specific substitution chemistry of synthetic, 3:1 site-differentiated [4Fe-4S] cluster systems, with a special emphasis on biomimetic relevance.

1.2. Natural 3:1 site-differentiated [4Fe-4S] clusters.

1.2.1. Aconitase.

The first biological [4Fe-4S] cluster recognized to display 3:1 site differentiation is located in the active site of aconitase, with the differentiated iron atom acting as catalytic site for the conversion of citrate to isocitrate. Aconitase cycles between deactivated and activated states by removal and re-insertion of the differentiated iron atom, respectively, thereby being acutely sensitive to intracellular iron concentrations.[4] First reported by Robbins and Stout in 1989, the crystal structure of pig heart aconitase shows the active mitochondrial enzyme with an oxygen ligand refined as water or hydroxide at the unique iron site.[5] Subsequent aconitase crystal structures with bound isocitrate (Figure 1) and reaction intermediate analogue

nitroisocitrate showed six-coordinate iron atoms with a bidentate substrate and an aqua ligand. In fact, the ability of the unique iron atom to expand its coordination number from four to six, together with the relative steric freedom experienced by the unique iron atom, are possible explanations for the use of a [4Fe-4S] cluster rather than a single metal ion for catalysis.[6] Recently, the structure of human cytosolic aconitase has revealed an active site almost identical to that of the mitochondrial analogue, although complete resolution of the binding modes of citrate, isocitrate, and the intermediate aconitate was not possible.[7]

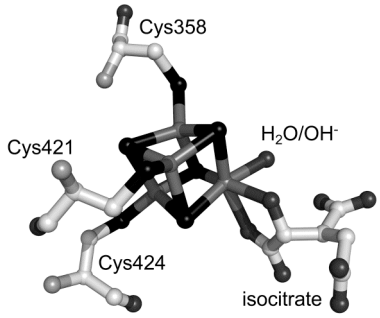

Figure 1. The isocitrate-bound active site of aconitase (PDB ID: 7ACN).[6]

1.2.2. Radical *S*-adenosylmethionine enzymes.

3:1 site-differentiated [4Fe-4S] clusters are also catalytically active in radical *S*-adenosylmethionine (SAM) enzymes. In this enzyme family, a single-electron transfer from a reduced [4Fe-4S] cofactor cleaves SAM into methionine and the 5'-deoxyadenosyl radical. This strong oxidant can then abstract a hydrogen atom from an appropriate substrate, activating it towards further transformations.[8]

The involvement of 3:1 site-differentiated [4Fe-4S] clusters in radical SAM enzymes had been predicted from their highly conserved CxxxCxxC motifs ("x" being a non-cysteine residue)[9] but was confirmed by the crystal structure of the radical SAM enzyme coproporphyrinogen III oxidase (Figure 2).[10] The structure shows that the enzyme binds both available SAM diastereomers (epimeric at the sulfonium sulfur atom), although the (*S*) configuration is favored by approximately 3:2. In both cases, the [4Fe-4S] cluster's unique iron atom is five-coordinate, with bonds to the amino nitrogen and a carboxylate oxygen atom of SAM's methionine moiety. The (*S*)-sulfonium sulfur–iron distance is 3.5 Å, demonstrating the feasibility of direct single-electron transfer from the cluster to the sulfonium group. Upon reduction, the chiral sulfonium group possibly inverts, after which the electron is most likely relayed to a second bound SAM cofactor.

Later crystallographic studies have revealed similar active sites for other radical SAM enzymes, although the mechanism of substrate reduction following SAM cleavage may differ. In biotin synthase, the generated 5'-deoxyadenosyl radical can directly abstract a hydrogen atom from its dethiobiotin substrate rather than first relaying the electron to a second SAM

cofactor.[11] The crystal structure of lysine-2,3-aminomutase shows the SAM analogue *Se*-adenosylselenomethione poised to abstract a hydrogen atom from the aldimine of pyridoxal-5'-phosphate and lysine. Together with spectroscopic evidence,[12] this suggests that SAM's sulfonium sulfur atom coordinates to the unique iron atom after single-electron transfer, leading to a six-coordinate iron site.[13]

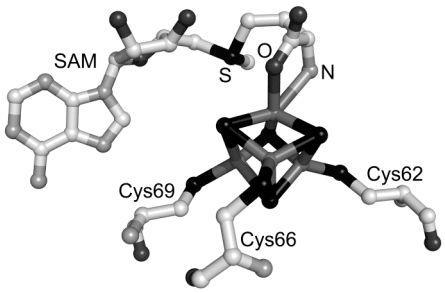

Figure 2. The active site of coproporhyrinogen III oxidase with bound SAM (only the (*S*)-sulfonium diastereomer is shown; PDB ID: 1OLT).[10]

The MoaA enzyme active in molybdenum cofactor biosynthesis is arguably the single most powerful example of the biological importance of 3:1 site-differentiated [4Fe-4S] clusters. Its N-terminal [4Fe-4S] cluster strongly resembles the SAM-binding clusters of other radical SAM enzymes, but a second, C-terminal [4Fe-4S] cluster is responsible for binding the enzyme's 5'-guanosine triphosphate substrate as an *N*,*N*-bidentate ligand. The C-terminal [4Fe-4S] cluster probably plays an important (redox) catalytic role beyond simple substrate anchoring.[14]

1.2.3. The sulfite reductase family.

While some enzymes contain [4Fe-4S] clusters with a catalytically active iron atom, others contain [4Fe-4S] clusters bridged *via* cysteinyl thiolates to various metal ions or assemblies. The first crystallographic proof came from the *Escherichia coli* NADPH-dependent sulfite reductase, which catalyzes the conversion of sulfite to sulfide. This enzyme contains a 3:1 site-differentiated [4Fe-4S] cluster bridged to a siroheme unit where substrate reduction takes place (Figure 3). Most likely, the cysteinyl thiolate bridging the electronically coupled [4Fe-4S] and siroheme cofactors participates directly in electron transfer.[15,16] Later crystal structures of a ferredoxin-dependent sulfite reductase[17] and spinach nitrate reductase[18] revealed similar structures, with the [4Fe-4S] clusters probably mediating directly between ferredoxin bound at the protein surface and the siroheme cofactors in the active sites.

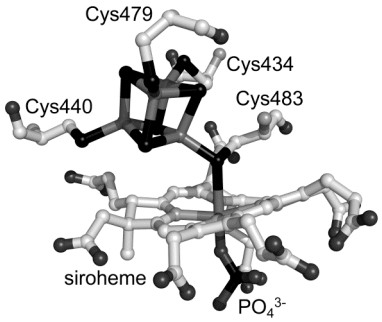

Figure 3. The active site of sulfite reductase with bound phosphate (PDB ID: 1AOP).[15]

1.2.4. Carbon monoxide dehydrogenase/acetyl coenzyme A synthase.

The bifunctional enzyme carbon monoxide dehydrogenase/acetyl coenzyme A synthase (CODH/ACS) catalyzes the reduction of atmospheric CO_2 to CO and the use of this CO in the synthesis of acetyl coenzyme A. The two reactions are related to the industrially relevant water-gas shift reaction and the Monsanto acetic acid process; consequently, the enzyme has attracted much recent attention in biomimetic chemistry. In the enzyme, the ACS function is carried out by the so-called A cluster, which is another example of a [4Fe-4S] cluster bridged to a catalytically active metal site.[19,20] A cysteinyl thiolate bridges the [4Fe-4S] cluster to a proximal metal atom, which is in turn bridged to a distal nickel atom *via* two more cysteinyl sulfur atoms. Backbone nitrogen atoms complete the square-planar coordination sphere of the distal nickel atom, while the proximal atom is also bound by an unidentified, non-protein ligand. The nature of the labile proximal metal atom varies in different crystal structures and has been resolved as square-planar Ni(II) (Figure 4),[21,22] tetrahedral Zn(II),[21] and tetrahedral Cu(I).[23] However, Ni(II) most likely occupies the proximal metal site in the catalytically active enzyme.[19,20]

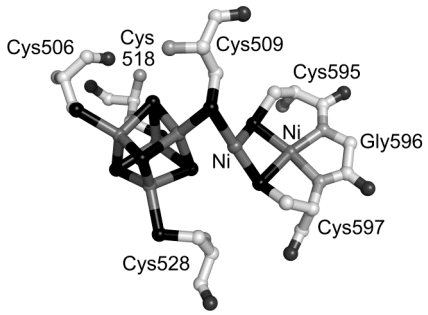

Figure 4. The A cluster of CODH/ACS (PDB ID: 1OAO).[21] The unresolved, non-protein ligand on the proximal nickel atom was not refined.

1.2.5. Iron-only hydrogenase.

Iron-only hydrogenase catalyzes the reversible redox chemistry of dihydrogen, a reaction highly relevant in fuel-cell technology and the possible development of an energy economy based on dihydrogen as energy carrier. Furthermore, iron-only hydrogenase is another example of an enzyme containing both a [4Fe-4S] cluster and a bimetallic subsite.[24,25] Peters *et al.* solved the structure of the *Clostridium pasteurianum* iron-only hydrogenase in 1998.[26] Nearly simultaneously, Fontecilla-Camps *et al.* reported the structure of the iron-only hydrogenase from *Desulfovibrio desulfuricans*.[27] The two active site structures are highly similar, displaying a [4Fe-4S] cluster bridged *via* a cysteinyl thiolate to the proximal iron atom of a [2Fe-2S] subsite. This proximal iron atom is bridged to the subsite's distal iron atom by a carbonyl ligand[26,28] and a cofactor modeled as 1,3-propanedithiolate (PDT, Figure 5),[27] although definite assignment of the bridgehead group in PDT as CH_2 or NH has not yet been possible.[24] The remaining coordination sites in the di-iron subsite are occupied by carbonyl and cyanide ligands, except for an aqua-coordinated[26] or empty[27] site on the distal iron atom, the presumed location of proton reduction and dihydrogen binding.

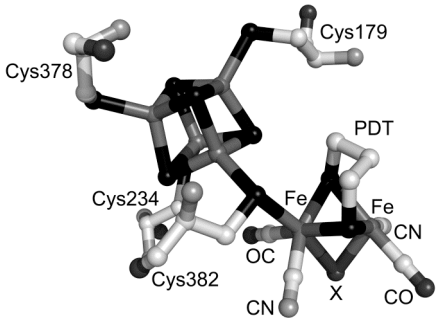

Figure 5. The active site of iron-only hydrogenase from *Desulfovibrio desulfuricans* (PDB ID: 1HFE).[27] Ligand X was initially modeled as a water molecule; later studies indicate it is a bridging carbonyl.[26,28]

In both structures, the 3:1 site-differentiated cluster resides at the end of a chain of [4Fe-4S] clusters linking the active site to the protein surface. In *Clostridium pasteurianum*, this electron-transport chain contains another 3:1 site-differentiated cluster coordinated by three cysteine thiolates and the Nε atom of a histidine residue. The reason for this cluster's histidine binding is unclear. In contrast to the marked redox effects of histidine coordination in [2Fe-2S] clusters[29] and in the site-differentiated [4Fe-4S] cluster in *Desulfovibrio gigas* nickel-iron hydrogenase[30] (*vide infra*), the potential of the histidine-bound cluster in iron-only hydrogenase has been found to be the same as that of the other, all-cysteine-bound clusters.[31]

1.2.6. Site-differentiated clusters coordinated by non-cysteine residues.

The histidine-bound [4Fe-4S] cluster in the *Clostridium pasteurianum* iron-only hydrogenase belongs to a large and growing number of known [4Fe-4S] clusters with histidine coordination. Nitrate reductase (Figure 6),[32,33] ethylbenzene dehydrogenase,[34] and

the nickel-iron and nickel-iron-selenium hydrogenases[35] all contain [4Fe-4S] clusters coordinated by histidine, although in these enzymes, Nδ is the coordinating atom. Histidine Nε coordination to a [4Fe-4S] cluster occurs in respiratory complex I[36] and in the active site of 4-hydroxybutyryl-coenzyme A dehydratase.[37] In the latter enzyme, the relatively long Fe–N bond length of 2.4 Å implies that a hydroxyl group may also coordinate to the unique iron atom in a radical-based catalytic cycle.

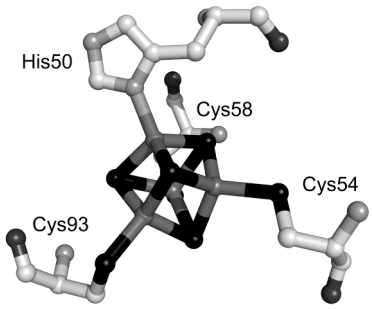

Figure 6. The active site of nitrate reductase (PDB ID: 1Q16).[32]

The nature of non-cysteine residues coordinated to natural, 3:1 site-differentiated [4Fe-4S] clusters is not limited to histidine. The enzyme dihydropyrimidine dehydrogenase contains a [4Fe-4S] cluster in which one of the iron atoms is coordinated by a glutamine residue.[38]

1.3. Synthetic 3:1 site-differentiated [4Fe-4S] clusters.

1.3.1. Peptide-bound and non-chelated clusters.

In 1974, Holm *et al.* synthesized the first synthetic 3:1 site-differentiated [4Fe-4S] cluster by coordination of a chelating nonapeptide with three cysteine residues; the fourth coordination position was occupied by *t*-BuS^-.[39] Although the flexibility of the nonapeptide ligand resulted in a mixture of diastereomeric (and possibly also oligomeric) clusters, the authors had elegantly reproduced the threefold cysteine coordination of natural 3:1 site-differentiated [4Fe-4S] clusters before these had even been discovered in an enzyme. Evans later synthesized clusters chelated by a related nonapeptide and conducted site-specific substitutions with tyrosinate and aspartate.[40] His use of a serine-rich nonapeptide further resulted in the synthesis of the first and only [4Fe-4S] clusters with *O*,*O*,*O*,*S*-ligation. Longer 3:1 site-differentiating peptide ligands of 63 residues have been used to produce [4Fe-4S]-Ni assemblies bridged by cysteinyl thiolates.[41]

3:1 site differentiation can also be achieved without the use of a chelating ligand. In principle, the conversion of any homoleptic cluster $[Fe_4S_4L_4]^{2-}$ to a second cluster $[Fe_4S_4L'_4]^{2-}$ proceeds through the 3:1 site-differentiated intermediates $[Fe_4S_4L_3L']^{2-}$ and $[Fe_4S_4LL'_3]^{2-}$. By

taking advantage of differential solubilities, several non-chelated 3:1 site-differentiated [4Fe-4S] clusters have been isolated.[42]

1.3.2. $L(SH)_3$.

The true breakthrough in 3:1 site-differentiated cluster chemistry came in 1987. In this year, Stack and Holm reported the synthesis of a tripodal trithiol capable of chelating three of the four iron atoms in a [4Fe-4S] cluster, thereby leaving one iron atom free for site-specific modification.[3] The design of this $L(SH)_3$ ligand (Scheme 1) incorporated two important structural aspects from previous work. First, it was known that neighboring groups in hexa(phenylthio)benzene are on opposite sides of the benzene plane, resulting in a so-called *ababab* conformation.[43,44] Introducing thiol functionalities on the 1,3,5-phenyl groups results in a ligand conformationally preorganized for [4Fe-4S] cluster binding, the "cavitand concept" in ligand design.[45] Second, forcing the thiol groups inward with carefully chosen substituents avoids bridging between clusters.

1.3.2.1. Synthesis.

In the originally reported, convergent synthesis, the yield of $L(SH)_3$ was 17% based on 1,3,5-trifluorobenzene and 10% based on *m*-xylene.[3,46] Later improvements increased the yields to 35% and 26%, respectively (Scheme 1),[47] although Holm *et al.* have indicated that the synthesis remains somewhat cumbersome.[48] Furthermore, care should be taken due to the use of the hazardous reagents chloromethyl ethyl ether, $Hg(OAc)_2$, and H_2S.

In order to probe the effects of ligand variations, an analogue of $L(SH)_3$ with 3-mercapto-5-*t*-butylphenyl groups instead of 4,6-dimethyl-3-mercaptophenyl groups was also synthesized, albeit in significantly lower yield. This so-called *t*-$BuL(SH)_3$ ligand has not found further application. However, it may prove useful for some purposes because *t*-$BuLS_3^{3-}$-chelated clusters are more soluble than their LS_3^{3-} counterparts.[47]

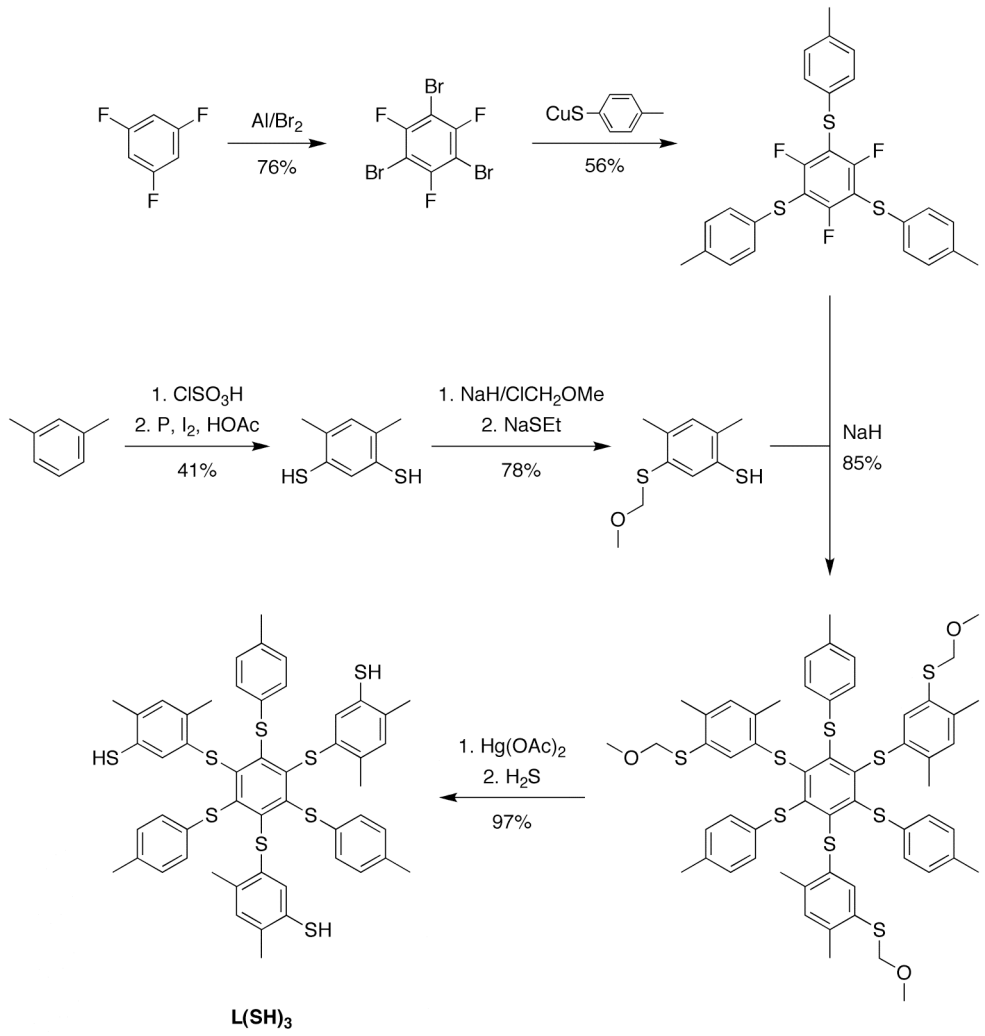

Scheme 1. Synthesis of $L(SH)_3$.

LS_3^{3-}-chelated [4Fe-4S] clusters can be prepared using the thiol-thiolate exchange reaction,[49,50] in which the tripodal ligand first protonates and then displaces three of the four alkylthiolate ligands in a symmetrically substituted $[Fe_4S_4(SR)_4]^{2-}$ cluster (R = Et or *t*-Bu, Scheme 2). The reaction is driven to completion by removal of the volatile RSH co-product. In the product cluster $[Fe_4S_4(LS_3)(SR)]^{2-}$, the remaining RS^- ligand can then be substituted by means of a fourth, subsite-specific thiol-thiolate exchange or, as in one case,[51] by a transthioesterification.

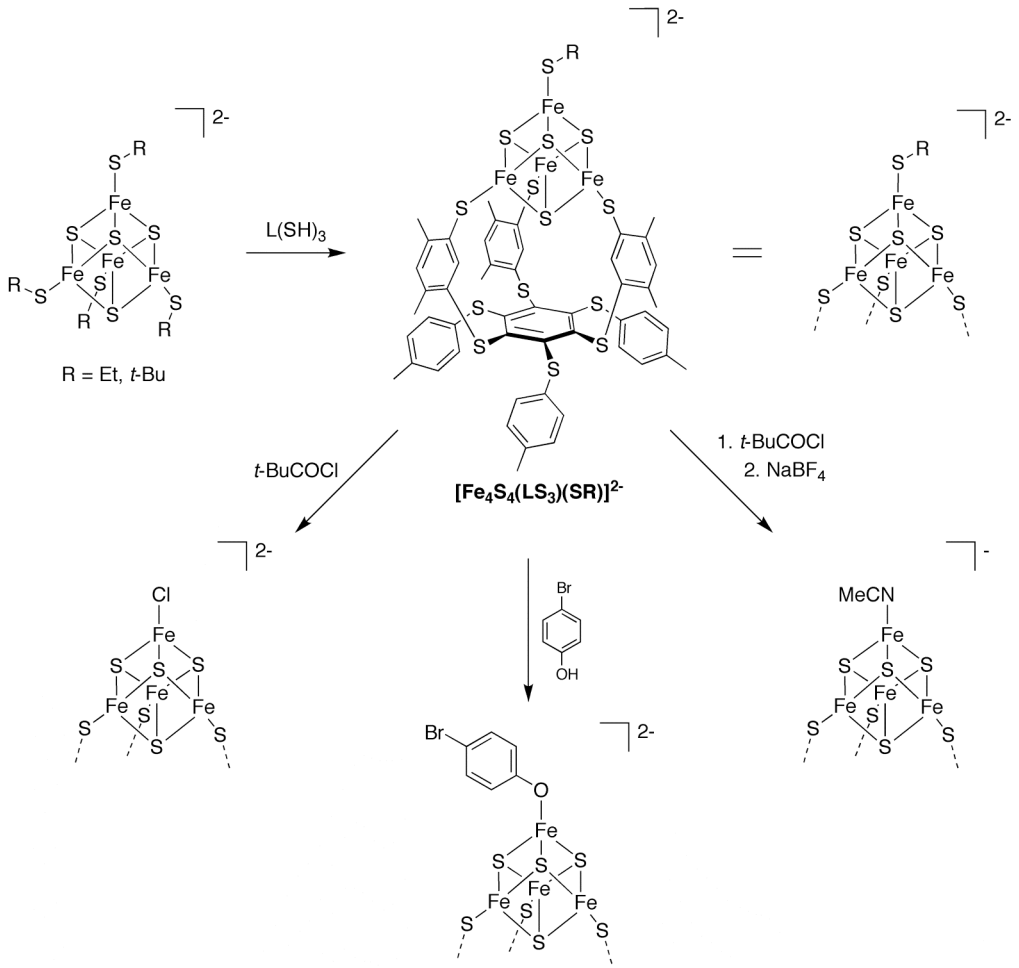

Scheme 2. Synthesis of LS_3^{3-}-chelated [4Fe-4S] clusters available for further site-specific modification.

The majority of LS_3^{3-}-chelated [4Fe-4S] clusters, however, have been synthesized *via* $[Fe_4S_4(LS_3)Cl]^{2-}$, the product of the reaction of $[Fe_4S_4(LS_3)(SR)]^{2-}$ with pivaloyl chloride (Scheme 2).[3,52] For most nucleophiles, the reaction with $[Fe_4S_4(LS_3)Cl]^{2-}$ is irreversible, making this reaction particularly convenient if the cluster under study need not be separated from its chloride salt byproduct.[53] Ligands L' that are incapable of displacing chloride can be introduced indirectly by first replacing the chloride ligand with *p*-bromophenolate to form $[Fe_4S_4(LS_3)(OC_6H_4\text{-}p\text{-}Br)]^{2-}$, followed by transsilylation with Me_3SiL'.[53] The substitution of chloride with acetonitrile to form $[Fe_4S_4(LS_3)(NCMe)_4]^{-}$ has also been applied as a method of activation (Scheme 2).[54]

1.3.2.2. Properties.

After crystallization as its PPh_4^+ salt, $[Fe_4S_4(LS_3)Cl]^{2-}$ yielded the first crystal structure of an LS_3^{3-}-chelated cluster. Surprisingly, the LS_3^{3-} ligand was found to assume an *aaabaa* conformation in the solid state, with all but one ligand arm on the same side of the central benzene ring. In solution, however, the more symmetrical *ababab* conformation is preferred.

Fe–S distances in the cluster core did not display an overall trigonal distortion; hence, 3:1 site-differentiation does not have a strong structural effect.[46]

A vast number of LS_3^{3-}-chelated cluster systems have been prepared and studied by Holm *et al.*, resulting in much fundamental insight in the structural, physical, and (bio)chemical properties of [4Fe-4S] clusters. LS_3^{3-}-chelated clusters with a series of monodentate, anionic thiolate ligands were the first to be reported.[3,46] Other sulfur ligands that have been bound at the unique site include overall neutral thiolates, which result in monoanionic clusters with cathodically shifted redox potentials,[55] and the silanethiolates Et_3SiS^- and Me_3SiS^-.[56,57] The hydrosulfide cluster $[Fe_4S_4(LS_3)(SH)]^{2-}$ readily binds other metal ions or clusters *via* a sulfide bridge, thereby mimicking the natural cysteine bridge without suffering from the lability observed with synthetic thiolate-bridged species.[56,58] The redox potential of the conjugate base, the sulfide-bound cluster $[Fe_4S_4(LS_3)S]^{3-}$,[53,59] is 200 mV more negative than that of the hydrosulfide analogue in acetonitrile.[56,59]

The nature of the atom coordinating to the unique iron atom is not restricted to chloride or sulfur. LS_3^{3-}-chelated clusters with monodentate phosphorus,[59] selenium,[53] tellurium,[53] carbon,[53,59] oxygen[48,53,52,60] and nitrogen[53,59] ligands have also been synthesized. The clusters with neutral imidazolyl ligands are close analogues of natural histidine-coordinated [Fe-4S] clusters (see Section 1.2.6).[59] Replacing the monodentate ligand in $[Fe_4S_4(LS_3)(SEt)]^{2-}$ by an imidazolyl ligand leads to an anodic shift of 320 mV, which is of the same sign, but much larger than the 60 mV difference measured between the site-differentiated and fully cysteine-coordinated clusters in the *Desulfovibrio gigas* nickel-iron hydrogenase.[30] The discrepancy illustrates the substantial redox effects of local protein environments and hydrogen bonding.

Hydroxide-substituted $[Fe_4S_4(LS_3)(OH)]^{2-}$ is a model for the catalytically active [4Fe-4S] cluster in aconitase (see Section 1.2.1).[53] The redox behavior of this cluster is similar to that of its sulfur analogue $[Fe_4S_4(LS_3)(SH)]^{2-}$, and both hydroxide and hydrosulfide clusters are in equilibrium with oxo- and sulfido-bridged species, respectively.[53,56] Citrate-bound cluster $[Fe_4S_4(LS_3)(citrate)]^{2-}$ mimics aconitase's substrate-bound form, but in contrast to the native enzyme, the citrate ligand in the synthetic cluster probably binds in a tridentate fashion.[53]

In general, LS_3^{3-}-chelated [4Fe-4S] clusters show well-defined and reversible one-electron reductions in a variety of solvents. Two reduced clusters have also been isolated, namely, $[Fe_4S_4(LS_3)(SEt)]^{3-}$ and $[Fe_4S_4(LS_3)(SPh)]^{3-}$. Reactions with sulfonium cations subsequently demonstrated that the reduced clusters are capable of reductive cleavage of sulfonium C–S bonds, in analogy to the cleavage of *S*-adenosylmethionine by radical SAM enzymes (see Section 1.2.2). Furthermore, ^{1}H NMR studies of the reduced clusters showed clear effects of site differentiation, with ligand chemical shifts differing substantially from those of homoleptic counterparts.[61]

1.3.2.3. Five- and six-coordinate subsites.

The aconitase mimic $[Fe_4S_4(LS_3)(citrate)]^{2-}$ mentioned above is one of a number of examples in which the coordination number of the unique iron atom exceeds four. Citrate acts as an *O,O,O*-donor ligand; other ligand donor atom sets reported in LS_3^{3-}-chelated clusters are *N,N*,[52] *N,S*,[52,62] *O,O*,[53] *O,S*,[52] *S,S*[52] (recently proven crystallographically),[63] *N,N,N*,[48,52,53,59] and *O,N,O*.[48,60] The stability of these higher-coordinate clusters derives from the presence of thiolate ligands at the other three iron sites; hence, the ability to study these coordination modes in [4Fe-4S] clusters is a direct consequence of the controlled 3:1 site differentiation.[52] Increased coordination numbers lead to significantly more negative redox potentials of the cluster core. This is especially the case when the extra coordinating atom is also negatively charged, probably due to a local electron density effect in the cluster rather than an overall charge effect.[52]

The realization of five- and six-coordinate iron subsites is not limited to site-specific reactions with bi- and tridentate ligands. In DMSO or MeCN solution, methanesulfonate-bound cluster $[Fe_4S_4(LS_3)(OSO_2Me)]^{2-}$ is solvolyzed to form clusters with an unknown number of solvent molecules coordinated to the unique iron atom.[53] For a series of isonitrile clusters $[Fe_4S_4(LS_3)(CNR)_3]^-$, Holm *et al.* demonstrated six-coordinate iron sites by ^1H NMR.[53,54,57,64] Site differentiation in these clusters separates the [4Fe-4S] cluster core into two isolated spin systems: an isonitrile-bound Fe(II) site and a neutral [3Fe-4S] fragment.[54,64] This extreme site differentiation effectively made the isonitrile clusters the first mimics for the [3Fe-4S] clusters found in, for example, inactive aconitase[65] and certain ferredoxins.[66,67] Nonetheless, the redox effects of isonitrile coordination were modest, with the increase in overall charge upon isonitrile binding apparently balanced by the increased σ donation.[54]

1.3.2.4. Bridged systems.

Among the first LS_3^{3-}-chelated clusters to be reported were [4Fe-4S] cluster dimers linked by dithiolates of varying nature and lengths.[58] Electrochemical analyses of the dimers elegantly revealed their distance-dependent redox coupling.[68,69] As expected, the sulfide-bridged cluster dimer $[\{(Fe_4S_4)(LS_3)\}_2(\mu\text{-}S)]^{4-}$ was the most strongly coupled. The dimer linked by benzene-1,4-dithiolate, with LS_3^{3-}-chelated clusters at a distance comparable to that found in the *Peptococcus aerogenes* ferredoxin, reproduced the redox independence observed in the natural protein.[56,58,70]

Several other ligands have been applied as linkers between LS_3^{3-}-chelated clusters, including Se^{2-}, O^{2-}, and the doubly chelating VS_4^{3-} ion.[53] The structure of labile, ethanethiolate-bridged $[\{(Fe_4S_4)(LS_3)\}_2(\mu\text{-}EtS)]^{4-}$ provided the first crystallographic proof of an unsupported thiolate bridge in a synthetic [4Fe-4S] cluster.[71] The persulfide-bridged cluster $[\{(Fe_4S_4)(LS_3)\}_2(\mu\text{-}S_2)]^{4-}$ can be used to synthesize assemblies of [4Fe-4S] clusters bridged to other metal ions by oxidative addition to the persulfide bond. Hence, this cluster was utilized

to synthesize $[Fe_4S_4(LS_3)(\mu\text{-}S)Fe(OEP)]^{2-}$ (OEP = octaethylporphyrinato dianion, Scheme 3), a model for the active site of sulfite reductase (see Section 1.2.3).[56,70]

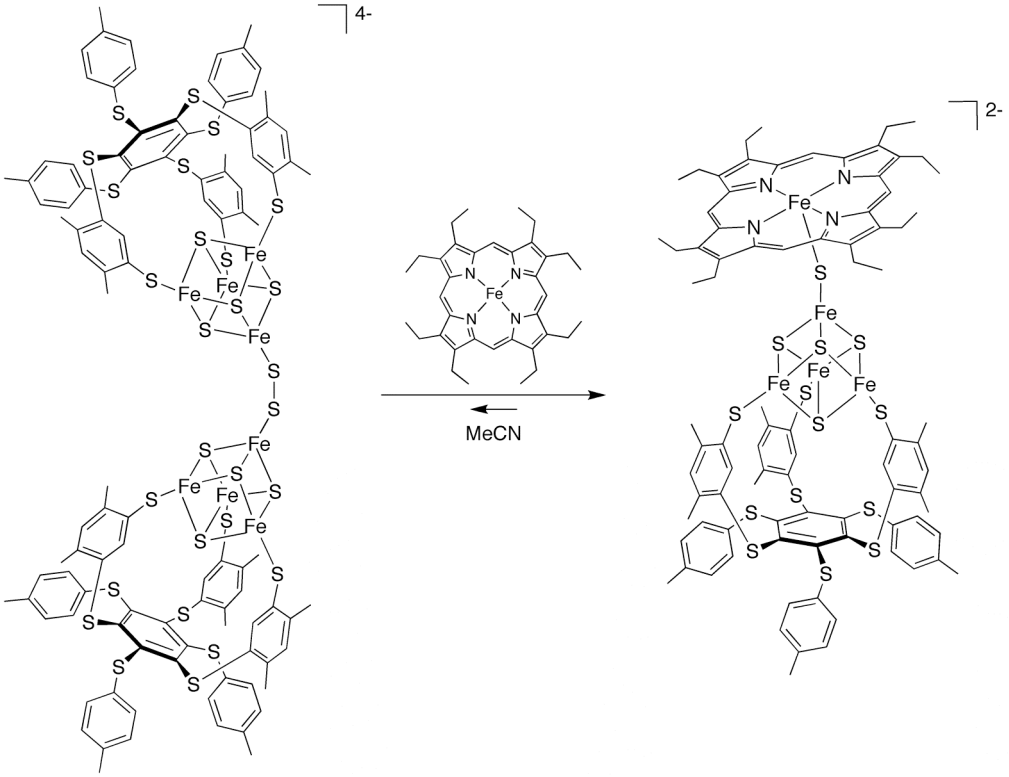

Scheme 3. Synthesis of a sulfite reductase active-site model by oxidative addition to a persulfide bond.

In accordance with the coupled siroheme and [4Fe-4S] cluster cofactors in native sulfite reductase[72] but in contrast to earlier, 3- and 4-pyridinethiolate-bridged models,[62] $[Fe_4S_4(LS_3)(\mu\text{-}S)Fe(OEP)]^{2-}$ shows extensive spin delocalization from the Fe(III) porphyrin to the [4Fe-4S] cluster.[56,70] In a later model, the octaethylporphyrinato ligand in $[Fe_4S_4(LS_3)(\mu\text{-}S)Fe(OEP)]^{2-}$ was replaced by isobacteriochlorin, a closer analogue of the native siroheme cofactor.[73] However, the Fe(III) ions in both the OEP and isobacteriochlorin-containing models are high-spin, in contrast to the siroheme Fe(III) ion in the native enzyme. The construction of a redox-coupled, low-spin [4Fe-4S]-Fe(III) assembly thus remains a biomimetic challenge.

LS_3^{3-}-chelated clusters have also been successfully applied in the synthesis of an iron-only hydrogenase active-site mimic. Pickett *et al.* prepared the model by means of a transthioesterification between $[Fe_4S_4(LS_3)(SEt)]^{2-}$ and an acetyl-protected diiron moiety (Scheme 4).[51] The resulting assembly is one of only two synthetic thiolate-bridged [4Fe-4S]-metal assemblies that have been isolated (the other being a cluster dimer, *vide supra*).[71] Interestingly, however, cyclic voltammetry provided evidence that the bridge to the model's proximal iron atom is broken reversibly upon reduction. The model further reproduced several

important features of the native active site by displaying similar Mössbauer parameters, substantial electronic communication between the [4Fe-4S] cluster and diiron subsite, and activity in electrocatalytic proton reduction.[51]

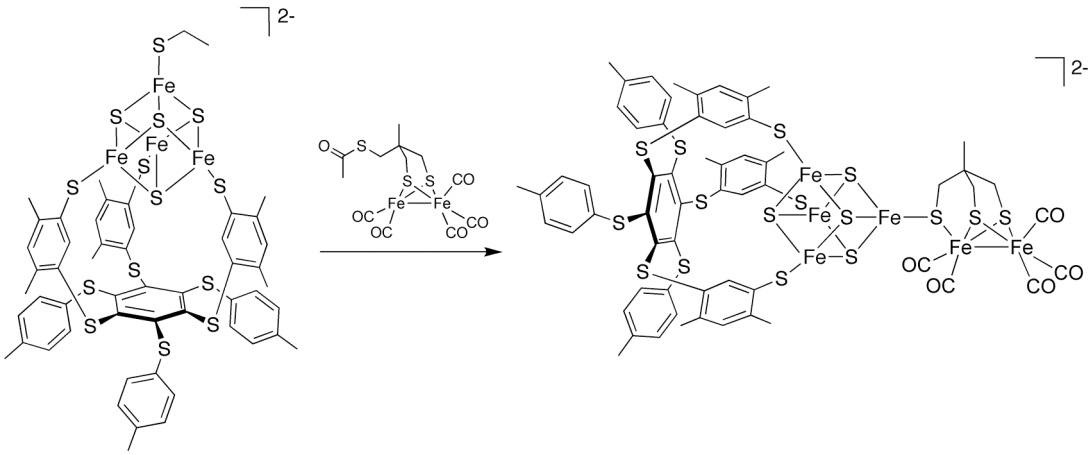

Scheme 4. Synthesis of an LS_3^{3-}-based model for the iron-only hydrogenase active site.

Finally, Holm *et al*. have recently reported considerable progress towards the synthesis of a full model for the A cluster of CODH/ACS. In an effort to create an analogue containing both a [4Fe-4S] cluster and proximal and distal nickel atoms, $[Fe_4S_4(LS_3)(OTf)]^{2-}$ was reacted with dinuclear Ni, NiPd, and NiPt complexes. The reactions indeed resulted in the first 3:1 site-differentiated [4Fe-4S]-Ni assemblies, but with concomitant cleavage of the dinuclear complexes resulting in loss of the second metal ion. A crystal structure showed one complex to be doubly bridged by two thiolate sulfur atoms, although the interaction of one of the thiolates with the site-differentiated iron atom was somewhat weaker than the other. This asymmetry was even more pronounced in a phenylenebis(acetylthio)acetamidate-bridged assembly. Monothiolate [4Fe-4S]-Ni bridges only appeared to be viable in non-coordinating solvents; the compound $[Fe_4S_4(LS_3)(\mu\text{-SEt})Ni(C_7H_7NS_2)]$ was observed by ^{1}H NMR spectroscopy in dichloromethane, but the bridging interaction was irreversibly lost in the presence of acetonitrile.[71]

1.3.3. c-L(SH)$_3$.

One of the main challenges in the early days of LS_3^{3-}-chelated cluster chemistry was the controlled removal of the unique iron atom, resulting in a model for the [3Fe-4S] clusters found in *Azetobacter vinelandii* Fd I and inactive aconitase. The feat was accomplished in 1995, eight years after the original reports on L(SH)$_3$, using the strongly chelating ligands citrate and *N*-methylimidodiacetate to abstract the differentiated iron atom.[60,73] In 1991, however, Holm *et al.* had reported a possible alternative to L(SH)$_3$ in the hope of synthesizing a 3:1 site-differentiated [4Fe-4S] cluster with a labile iron atom. The design of this polyether trithiol, called c-L(SH)$_3$ in reference to its cyclic nature, involved three 1-thio-2,6-phenylene moieties linked by two spacers containing three methylene units, and one spacer containing

only two (Scheme 5). The authors had purposefully chosen the asymmetric configuration based on modelling work, which predicted the best match of the ligand and cluster geometries while avoiding too much flexibility.[74]

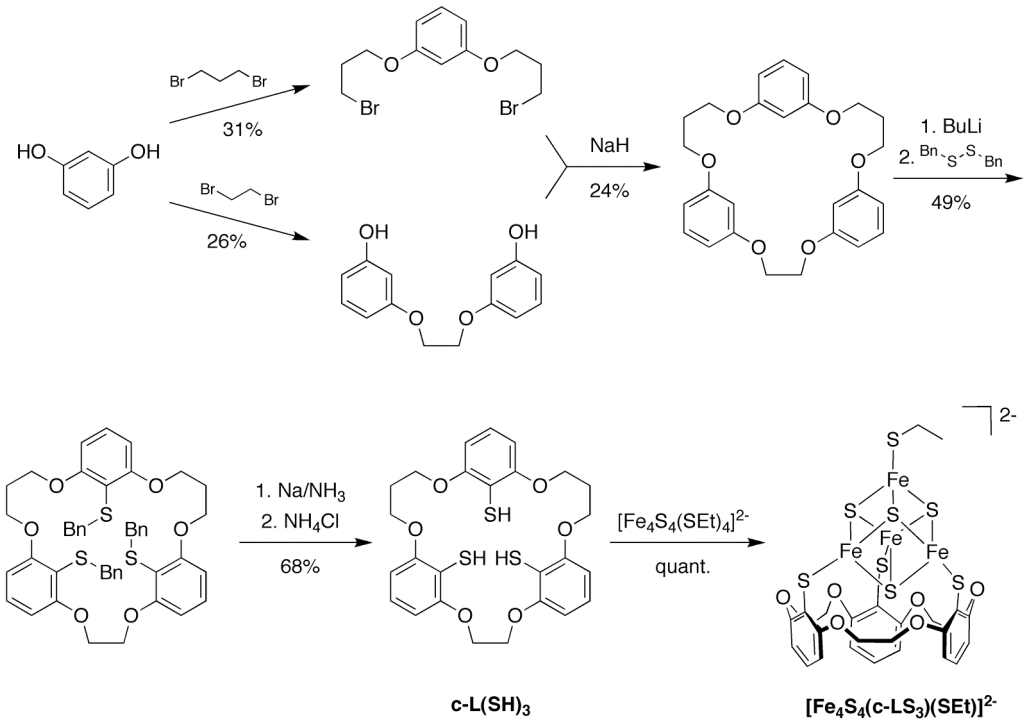

Scheme 5. Synthesis of $[Fe_4S_4(c\text{-}LS_3)(SEt)]^{2-}$.

1.3.3.1. Synthesis.

The crucial step in the synthesis of $c\text{-}L(SH)_3$ is a macrocyclization from dibromo- and dihydroxy-functionalized precursors (Scheme 5). High dilutions minimize the formation of oligomeric byproducts, although the optimized yield of the step remained low. The reactants themselves are also prepared by reactions prone to generating oligomeric byproducts, resulting in an overall yield of 0.3% for $c\text{-}L(SH)_3$ based on resorcinol. Nonetheless, the synthesis of $c\text{-}L(SH)_3$ is attractive because of its lack of highly toxic or carcinogenic reagents.[74]

$c\text{-}L(SH)_3$ reacts with $[Fe_4S_4(SEt)_4]^{2-}$ to form 3:1 site-differentiated cluster $[Fe_4S_4(c\text{-}LS_3)(SEt)]^{2-}$ in quantitative yield (Scheme 5). The cluster can be used directly in further site-specific modifications but was routinely first converted to $[Fe_4S_4(c\text{-}LS_3)Cl]^{2-}$ using pivaloyl chloride. This conversion generated an unidentified but substantial impurity, which persisted in subsequent cluster reactions.[74]

1.3.3.2. Properties.

c-LS_3^{3-}-chelated clusters display redox potentials 0.10–0.15 V more negative than their LS_3^{3-} counterparts but their reactivities are similar. Reactions of $[Fe_4S_4(c\text{-}LS_3)Cl]^{2-}$ with *p*-tolylthiolate and cyanide lead to simple ligand exchanges, while tentative evidence suggests that treatment with Li_2S results in a sulfide-bridged dimer, analogous to the LS_3^{3-} counterpart. Reactions with triazacyclononane or *t*-BuNC result in six-coordinate iron atoms. Here, the ^1H NMR shifts of the ligands at the differentiated iron site reflect the lack of C_3 symmetry in the cluster. In addition to its non-hazardous preparation, the reduced symmetry of c-$L(SH)_3$ can be an important advantage, since it allows for the differential observation of those groups not interchangeable by the cluster's mirror plane.[74] Unfortunately, the problematic purification of c-LS_3^{3-}-chelated [4Fe-4S] clusters has prevented their further application.

1.3.4. Triazacyclane trithiols.

The first alternatives to $L(SH)_3$ to be synthesized outside Holm's laboratory were L^1H_3 and L^2H_3, trithiols based on triazacyclononane and triazacyclododecane, respectively (Scheme 6).[75] Evans *et al.* based the design of L^1H_3 and L^2H_3 on previously synthesized, fully encapsulating tetradentate [4Fe-4S] cluster ligands,[76] with molecular modelling predicting preorganized ligand cavities such as that also found in $L(SH)_3$.

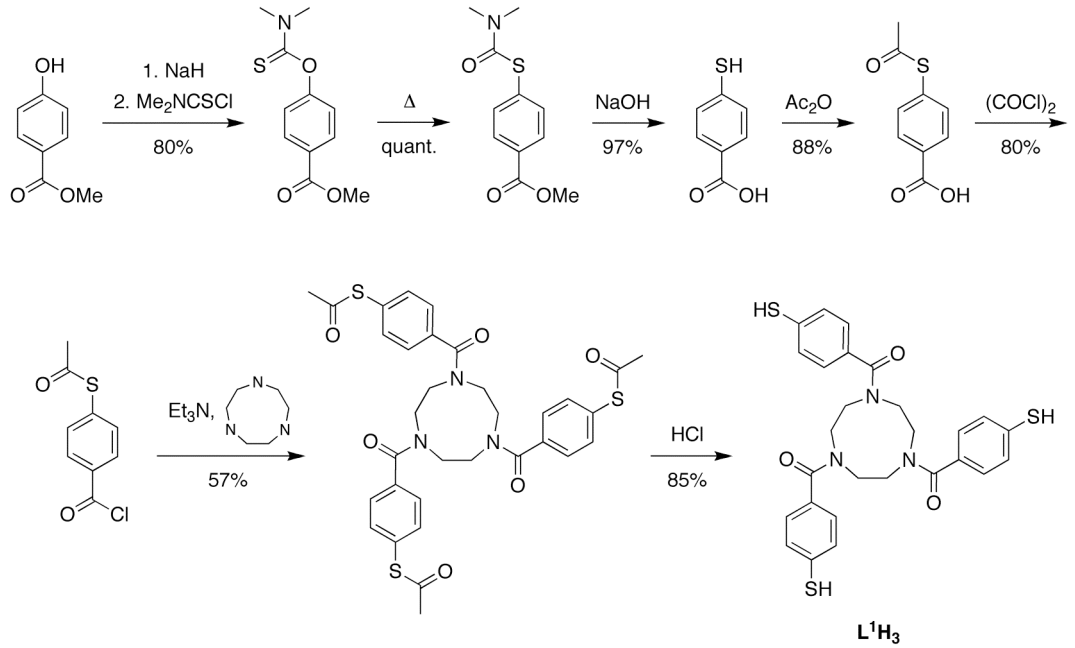

Scheme 6. Synthesis of triazacyclononane trithiol L^1H_3. The synthesis of L^2H_3 proceeds analogously, using triazacyclododecane in the penultimate step.

1.3.4.1. Synthesis.

Evans *et al.* synthesized the arms of the ligands by elegantly simple organic transformations, after which the arms were connected to the triazacyclononane or -dodecane scaffolds by amide bond formation. Thiol groups were introduced without hazardous protection and deprotection chemistry. The overall yields of the two ligands were around 40% (Scheme 6).[75,76]

Reactions of L^1H_3 and L^2H_3 with $[Fe_4S_4(SR)_4]^{2-}$ (R = Et or *t*-Bu) result in the corresponding chelated clusters. Evans *et al.* activated the site-differentiated iron atom by reaction with 2-aminobutane hydrochloride, rather than the acid chlorides used in LS_3^{3-} and c-LS_3^{3-} analogues.

1.3.4.2. Properties.

The cluster $[Fe_4S_4(L^1)(SEt)]^{2-}$ undergoes site-specific substitutions with thiophenol and *p*-methylthiophenol, as well as with the corresponding oxo analogues. In contrast to $L(SH)_3$, ^{1}H NMR resonances of $(L^1)^{3-}$ are insensitive to the nature of the monodentate ligand; hence, reactions were monitored using monodentate ligand resonances.[75] Although the NMR results supported the general contact shifting mechanism for isotropically shifted ligand signals,[77] the *m*-H signals of the (thio)phenolate clusters moved to lower chemical shifts with increasing temperature, an unexpected and as yet unexplained result. A tyrosine derivative coordinated to clusters chelated by $(L^1)^{3-}$ or $(L^2)^{3-}$ later showed similar anomalous temperature dependences for the *o*- and *m*-H signals.[78] Besides tyrosine, derivatives of the amino acids cysteine, histidine, and serine also proved capable of ligand substitution at the unique iron site in $[Fe_4S_4(L^n)(SEt)]^{2-}$ (n = 1, 2). However, the fact that PPh_4^+ and NEt_4^+ salts of the products displayed markedly different ^{1}H NMR spectra questions the identities of the obtained products. Questions also remain concerning the hypothesized formation of cysteine-bridged clusters from $[Fe_4S_4(L^n)(SEt)]^{2-}$, which would involve an unusual stability of thiolate-bridged structures not only in the presence of potentially coordinating DMSO, but also free EtS^-.

The synthetic simplicity of the triazacyclane-based trithiols is a significant advantage encouraging their use in 3:1 site-differentiated [4Fe-4S] cluster chemistry. A drawback lies in their relatively undeveloped substitution chemistry, for which important questions remain, as well as their unexplored redox properties. Elemental analyses of clusters chelated by $(L^1)^{3-}$ or $(L^2)^{3-}$ have yielded varying results. Further evidence for the absence of oligomers in the cluster products is desirable, especially since, as with c-$L(SH)_3$, the ligand design does not force the thiol groups to point into the preorganized central ligand cavity.

1.3.5. Cyclotriveratrylene-based trithiols.

In 1994, Nolte *et al.* reported another class of macrocyclic trithiols predisposed to chelate [4Fe-4S] clusters.[79] The cyclotriveratrylene (ctv) ring offered a convenient scaffold for the synthesis of a series of eight trithiols differing in the nature of the thiol donor arms (Scheme 7). By variation of the electron-donating and hydrogen-bonding properties of the arms, the authors envisioned a comprehensive study of the factors influencing the electrochemical and spectroscopic properties of chelated [4Fe-4S] clusters.[79,80]

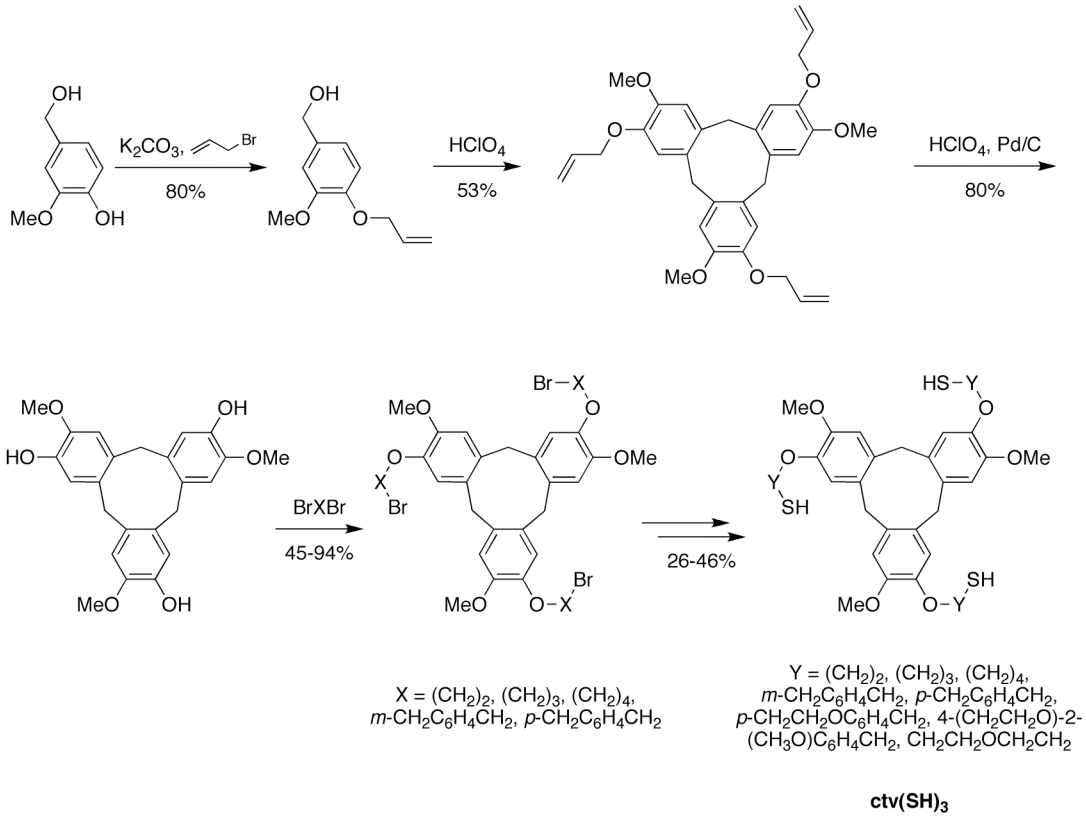

Scheme 7. Synthesis of ctv trithiols.

1.3.5.1. Synthesis.

The six-step syntheses of the ctv trithiols started from vanillyl alcohol, with the first four steps having been reported previously (Scheme 7).[81] Suitable arms were introduced on the macrocycles by reactions of the ctv hydroxyl groups with dibromo reagents, after which nucleophilic addition and reduction of dithiocarbamates yielded the desired trithiols. Alternatively, nucleophilic addition of dialcohols to the bromo-functionalized ctv rings preceded thiol introduction to give ether-functionalized arms.[79,80] Yields for the trithiols were generally low (8–17%), probably due to the formation of oligomeric byproducts (as also seen for c-L(SH)$_3$, see Section 1.3.3.1) and the ability of thiolates to cleave aryl ethers.[80,82]

Interestingly, the ctv trithiols are the only chelating ligands that allow direct synthesis of 3:1 site-differentiated [4Fe-4S] clusters from both $[Fe_4S_4Cl_4]^{2-}$ and $[Fe_4S_4(SR)_4]^{2-}$ (here, R = *t*-Bu). However, the products $[Fe(ctvS_3)(S\text{-}t\text{-}Bu)]^{2-}$ and $[Fe(ctvS_3)Cl]^{2-}$ have markedly different structures (Chart 1). The chloride ligand points towards the ctv ring and is thus protected from all but the smallest (OH^-) nucleophiles. The *t*-BuS^- ligand, in contrast, points away from the chelating ligand and displays the anticipated reactivity.[79,80]

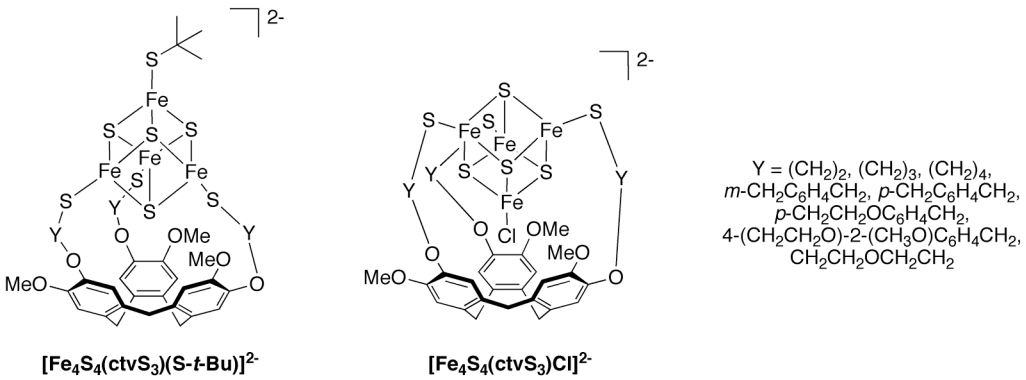

Chart 1. $[Fe_4S_4(ctvS_3)(S\text{-}t\text{-}Bu)]^{2-}$ and $[Fe_4S_4(ctvS_3)Cl]^{2-}$.

1.3.5.2. Properties.

The different electron-donating properties of the arms in the $ctvS_3^{3-}$-chelated [4Fe-4S] clusters have effects of up to 100 mV on the cluster redox potential. The addition of Ba^{2+} ions also affects the electrochemistry by shifting (modulation) and increasing the intensities (promotion) of redox waves.[79,80]

Another property influenced by the nature of the ctv arms is the site-specificity of ligand exchange. Whereas the reaction of $[Fe_4S_4(ctvS_3)(S\text{-}t\text{-}Bu)]^{2-}$ with thiophenol occurs exclusively at the unique iron atom if the ctv ligand contains *m*-xylyl spacers, no such site specificity was observed for the analogous cluster with ethyl spacers. Possibly, steric contraints destabilize the interaction between the [4Fe-4S] cluster and the ctv trithiol ligand in the case of the ethyl spacer, thereby labilizing the chelated coordination positions.[79,80]

With *m*-xylyl spacers in the ctv arms, $[Fe_4S_4(ctvS_3)(S\text{-}t\text{-}Bu)]^{2-}$ reacts with benzoyl chloride to form $[Fe_4S_4(ctvS_3)Cl]^{2-}$. Interestingly, this reaction proceeds with retention of the cluster geometry, affording a cluster in which the chloride ligand is available for substitution (Scheme 8).[79,80] In general, this more reactive isomer of $[Fe_4S_4(ctvS_3)Cl]^{2-}$ reacts similarly to its LS_3^{3-} and c-LS_3^{3-} counterparts, and the chloride ligand can be substituted by thiolates, phenolates, OH^-, N_3^-, $C_5H_5^-$, CN^-, and NCO^-. The use of *O*,*O*-, *O*,*S*-, and *S*,*S*-bidentate ligands results in five-coordinate iron sites, while reaction with Li_2S yields a sulfide-bridged [4Fe-4S] cluster dimer. The redox properties of the ctv-based clusters are also in agreement with those of the other systems. An interesting addition, however, is the use of a series of *p*-substituted phenolates as ligands. The Hammett plots for the phenolate-bound clusters

displayed a greater sensitivity of the 2–/3– redox potential towards the substituent σ_p values than their thiophenolate-based counterparts.[83]

Perhaps the most distinguishing property of the ctv(SH)$_3$ ligands is their chirality. No effects of the chiral environment on the unique iron site have been reported, but the possibility to introduce chirality *via* the chelating cluster ligand makes the family of ctvS$_3^{3-}$-chelated clusters an intriguing addition to the biomimetic toolbox. However, factors hampering further development of the chemistry of ctvS$_3^{3-}$-chelated [4Fe-4S] clusters are their low solubility in solvents other than DMF and DMSO, as well as their tendency to form oligomeric species at higher concentrations.[80] This tendency undoubtedly springs from the lack of a steric interaction that forces the thiol groups inwards and may be alleviated by the choice of an appropriate thiol arm spacer.

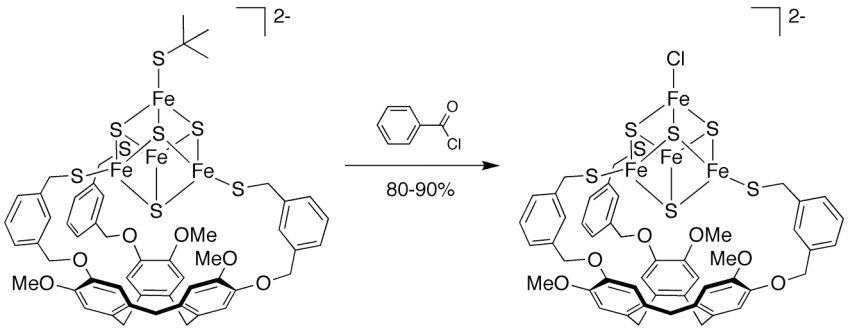

Scheme 8. Synthesis of the more reactive isomer of [Fe$_4$S$_4$(ctvS$_3$)Cl]$^{2-}$.

1.3.6. TriSH$_3$.

In 1997, Pohl *et al* reported the 3:1 site-differentiating [4Fe-4S] cluster ligand 1,3,5-triethyl-2,4,6-tris(3-sulfanylindolyl[1]methyl)benzene (TriSH$_3$, Scheme 9). Incorporating the same design principles as L(SH)$_3$, TriSH$_3$ features six substituents on a central benzene scaffold to promote an *ababab* conformation and has steric bulk on the tripod arms to force the thiol groups into the central ligand cavity.[84]

1.3.6.1. Synthesis.

Pohl *et al.* prepared TriSH$_3$ in a yield of 24% based on indole, using the same thiol protection and deprotection chemistry as used previously in the synthesis of L(SH)$_3$ (see Section 1.3.2.1).[84] TriSH$_3$ reacts with [Fe$_4$S$_4$(SEt)$_4$]$^{2-}$ to form the 3:1 site-differentiated cluster [Fe$_4$S$_4$(TriS)(SEt)]$^{2-}$. The remaining EtS$^-$ ligand can be replaced by bromide by reaction with a mild, thiourea-based oxidant, thereby activating the cluster towards substitution (Scheme 9).[84]

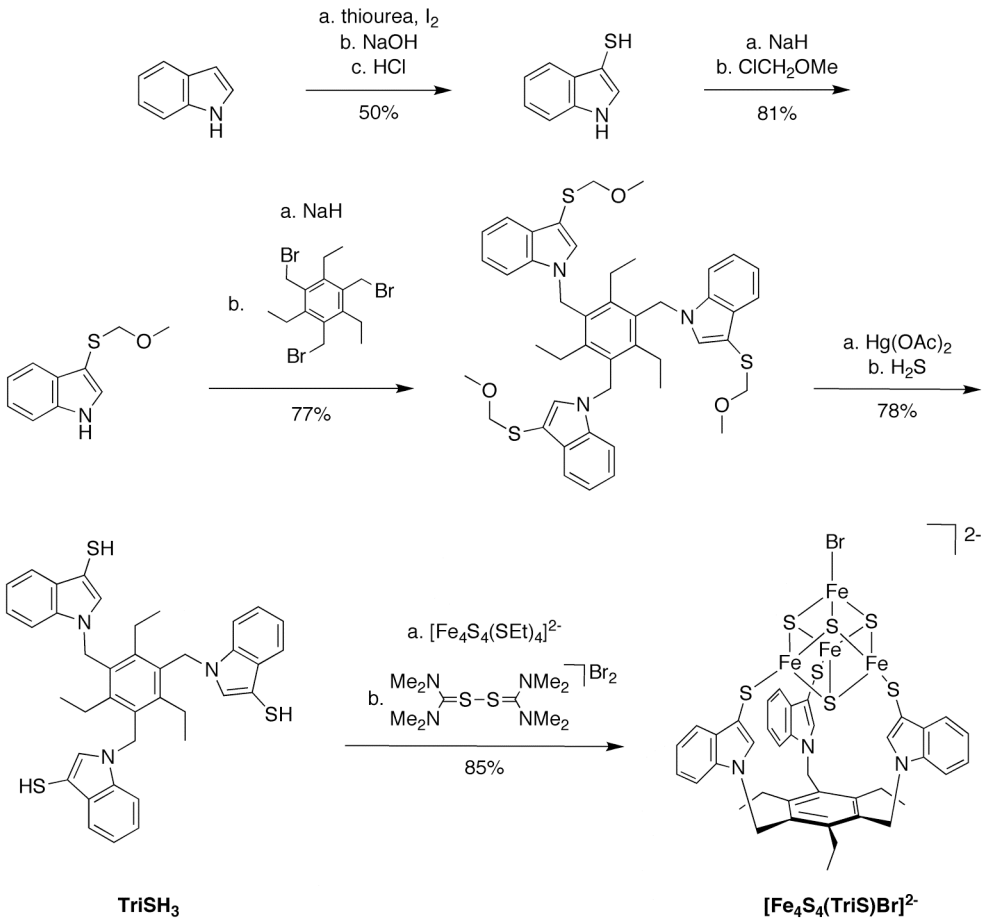

Scheme 9. Synthesis of $TriSH_3$ and $[Fe_4S_4(TriS)Br]^{2-}$.

1.3.6.2. Properties.

$[Fe_4S_4(TriS)Br]^{2-}$ reacts with NaSPh to form $[Fe_4S_4(TriS)(SPh)]^{2-}$, which has been crystallized as its PPh_4^+ salt. The $TriSH_3$ ligand retains its *ababab* conformation in the crystal structure, reflecting the higher rigidity of hexamethylene-substituted benzenes as compared to hexathioethers. Furthermore, the structure unequivocally proves the 1:1 reaction stoichiometry between ligand and cluster, making $TriSH_3$ the only alternative to $L(SH)_3$ for which such crystallographic evidence is available.[84]

The cluster $[Fe_4S_4(TriS)(SEt)]^{2-}$ does not necessarily need to be activated by thiolate-bromide exchange prior to further site-specific reactions. Tatsumi *et al.* have successfully substituted the EtS^- ligand in $[Fe_4S_4(TriS)(SEt)]^{2-}$ by direct reaction with oxygen-donor ligands.[85] The unique iron atom could also be removed to yield a [3Fe-4S] cluster.[85,86] Further studies on TriS-chelated [4Fe-4S] clusters are the subject of Chapters 2, 4, 5, and 6 of this thesis.

1.3.6.3. $HexSH_6$.

An interesting relative of the $TriSH_3$ ligand is $HexSH_6$, which is functionalized with six rather than three indole-3-thiol arms. This doubly tripodal ligand is thus preorganized to bind two [4Fe-4S] clusters at opposite sides of the central benzene ring at a well-defined distance. Indeed, reaction of $HexSH_6$ with $[Fe_4S_4(SEt)_4]^{2-}$ followed by oxidative ligand substitution resulted in the [4Fe-4S] cluster dimer $[BrFe_4S_4(HexS)Fe_4S_4Br]^{4-}$ (Scheme 11). The bromide ligands were replaced by thiophenolate, and crystal structures were obtained of both the bromide (Scheme 11) and thiophenolate cluster dimers as their PPh_4^+ salts.[87] The distance between the cluster centroids in the thiophenolate dimer is 12.83 Å, similar to the inter-cluster distance in the ferredoxin found in *Peptococcus aerogenes*.[88] This distance would be expected to preclude redox communication between the clusters, and indeed no such communication was observed by cyclic voltammetry.[87]

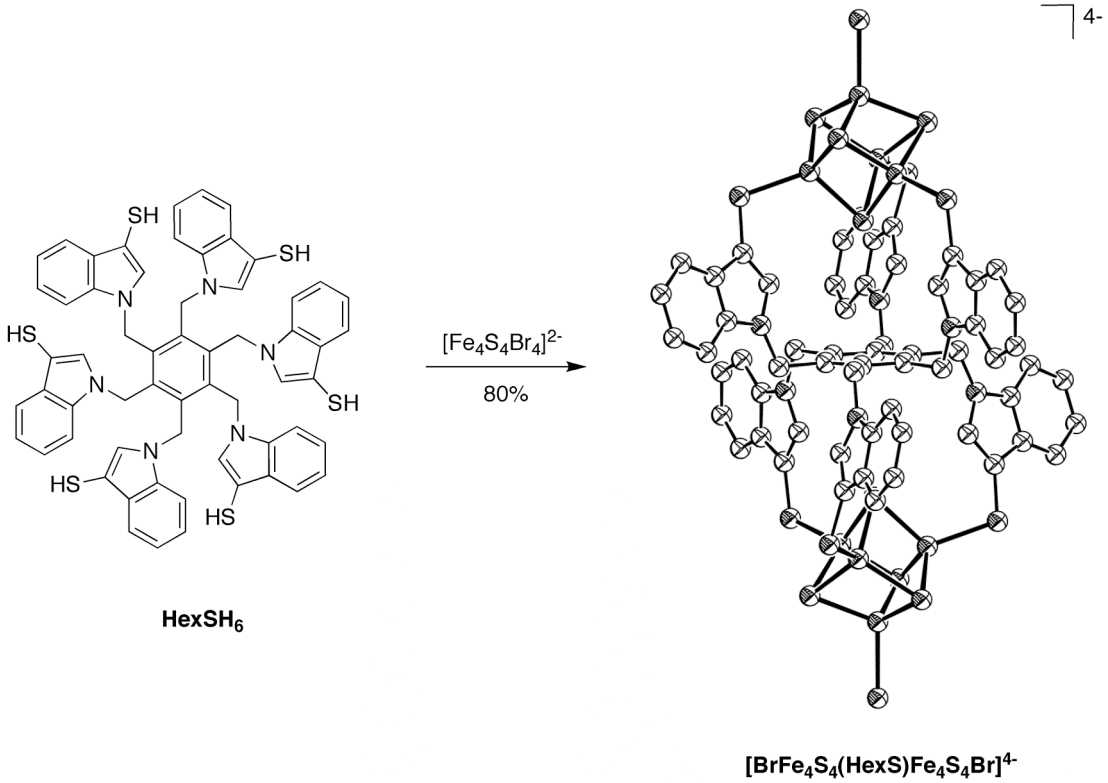

Scheme 11. Synthesis of $[BrFe_4S_4(HexS)Fe_4S_4Br]^{4-}$, shown as an ORTEP plot with ellipsoids at the 50% probability level.

1.4. Concluding remarks.

The importance of 3:1 site-differentiated [4Fe-4S] clusters has been evident since the first reports on the active-site structure of aconitase. However, the frequent new discoveries of natural 3:1 site-differentiated clusters constantly re-emphasize their significance, with the radical SAM enzyme family being the most striking recent example. Despite these rapid

developments in structural biology, biomimetic chemists have managed to keep pace, as evidenced by the recent progress in modelling the radical SAM enzyme and iron-only hydrogenase active sites. The toolbox of the biomimetic chemist currently contains five different 3:1 site-differentiated cluster systems, each one with specific properties, advantages, and disadvantages in an envisioned application. Most likely, the insight obtained from these synthetic systems will continue to make 3:1 site-differentiated [4Fe-4S] clusters a prime example of the fruitful cross-pollination between structural biology and biomimetic chemistry.

1.5. References.

[1] Venkateswara Rao, P.; Holm, R. H. *Chem. Rev.* **2004**, *104*, 527–559.
[2] Holm, R. H. *Pure Appl. Chem.* **1998**, *70*, 931–938.
[3] Stack, T. D. P.; Holm, R. H. *J. Am. Chem. Soc.* **1987**, *109*, 2546–2547.
[4] Beinert, H.; Kennedy, M. C.; Stout, C. D. *Chem. Rev.* **1996**, *96*, 2335–2373.
[5] Robbins, A. H.; Stout, C. D. *Proc. Natl. Acad. Sci. U.S.A.* **1989**, *86*, 3639–3643.
[6] Lauble, H.; Kennedy, M. C.; Beinert, H.; Stout, C. D. *Biochemistry* **1992**, *31*, 2735–2748.
[7] Dupuy, J.; Volbeda, A.; Carpentier, P.; Darnault, C.; Moulis, J.-M.; Fontecilla-Camps, J. C. *Structure* **2006**, *14*, 129–139.
[8] Jarrett, J. T. *Curr. Opin. Chem. Biol.* **2003**, *7*, 174–182.
[9] Sofia, H. J.; Chen, G.; Hetzler, B. G.; Reyes-Spindola, J. F.; Miller, N. E. *Nucleic Acids Res.* **2001**, *29*, 1097–1106.
[10] Layer, G.; Moser, J.; Heinz, D. W.; Jahn, D.; Schubert, W.-D. *EMBO J.* **2003**, *22*, 6214–6224.
[11] Berkovitch, F.; Nicolet, Y.; Wan, J. T.; Jarrett, J. T.; Drennan, C. L. *Science* **2004**, *303*, 76–79.
[12] Cosper, N. J.; Booker, S. J.; Frey, P. A.; Scott, R. A. *Biochemistry* **2000**, *39*, 15668–15673.
[13] Lepore, B. W.; Ruzicka, F. J.; Frey, P. A.; Ringe, D. *Proc. Natl. Acad. Sci. U.S.A.* **2005**, *102*, 13819–13824.
[14] Hänzelmann, P.; Schindelin, H. *Proc. Natl. Acad. Sci. U.S.A.* **2006**, *103*, 6829–6834.
[15] Crane, B. R.; Siegel, L. M.; Getzoff, E. D. *Science* **1995**, *270*, 59–67.
[16] Crane, B. R.; Siegel, L. M.; Getzoff, E. D. *Biochemistry* **1997**, *36*, 12120–12137.
[17] Schnell, R.; Sandalova, T.; Hellman, U.; Lindqvist, Y.; Schneider, G. *J. Biol. Chem.* **2005**, *280*, 27319–27328.
[18] Swamy, U.; Wang, M.; Tripathy, J. N.; Kim, S.-K.; Hirasawa, M.; Knaff, D. B.; Allen, J. P. *Biochemistry* **2005**, *44*, 16054–16063.
[19] Evans, D. J. *Coord. Chem. Rev.* **2005**, *249*, 1582–1595.
[20] Harrop, T. C.; Mascharak, P. K. *Coord. Chem. Rev.* **2005**, *249*, 3007–3024.
[21] Darnault, C.; Volbeda, A.; Kim, E. J.; Legrand, P.; Vernède, X.; Lindahl, P. A.; Fontecilla-Camps, J. C. *Nat. Struct. Biol.* **2003**, *10*, 271–279.
[22] Svetlitchnyi, V.; Dobbek, H.; Meyer-Klaucke, W.; Meins, T.; Thiele, B.; Römer, P.; Huber, R.; Meyer, O. *Proc. Natl. Acad. Sci. U.S.A.* **2004**, *101*, 446–451.
[23] Doukov, T. I.; Iverson, T. M.; Seravalli, J.; Ragsdale, S. W.; Drennan, C. L. *Science* **2002**, *298*, 567–572.
[24] Liu, X.; Ibrahim, S. K.; Tard, C.; Pickett, C. J. *Coord. Chem. Rev.* **2005**, *249*, 1641–1652.
[25] Nicolet, Y.; Cavazza, C.; Fontecilla-Camps, J. C. *J. Inorg. Biochem.* **2002**, *91*, 1–8.
[26] Peters, J. W.; Lanzilotta, W. N.; Lemon, B. J.; Seefeldt, L. C. *Science* **1998**, *282*, 1853–1858.
[27] Nicolet, Y.; Piras, C.; Legrand, P.; Hatchikian, C. E.; Fontecilla-Camps, J. C. *Structure* **1999**, *7*, 13–23.

[28] (a) Nicolet, Y.; de Lacey, A. L.; Vernède, X.; Fernandez, V. M.; Hatchikian, E. C.; Fontecilla-Camps, J. C. *J. Am. Chem. Soc.* **2001**, *123*, 1596–1601. (b) De Lacey, A. L.; Stadler, C.; Cavazza, C.; Hatchikian, E. C.; Fernandez, V. M. *J. Am. Chem. Soc.* **2000**, *122*, 11232–11233. (c) Pierik, A. J.; Hulstein, M.; Hagen, W. R.; Albracht, S. P. J. *Eur. J. Biochem.* **1998**, *258*, 572–578.
[29] Stephens, P. J.; Jollie, D. R.; Warshel, A. *Chem. Rev.* **1996**, *96*, 2491–2514.
[30] Roberts, L. M.; Lindahl, P. A. *J. Am. Chem. Soc.* **1995**, *117*, 2565–2572.
[31] Adams, M. W. *J. Biol. Chem.* **1987**, *262*, 15054–15061.
[32] Bertero, M. G.; Rothery, R. A.; Palak, M.; Hou, C.; Lim, D.; Blasco, F.; Weiner, J. H.; Strynadka, N. C. J. *Nat. Struct. Biol.* **2003**, *10*, 681–687.
[33] Jormakka, M.; Richardson, D.; Byrne, B.; Iwata, S. *Structure* **2004**, *12*, 95–104.
[34] Kloer, D. P.; Hagel, C.; Heider, J.; Schulz, G. E. *Structure* **2006**, *14*, 1377–1388.
[35] (a) Volbeda, A.; Charon, M.-H.; Piras, C.; Hatchikian, E. C.; Frey, M.; Fontecilla-Camps, J. C. *Nature* **1995**, *373*, 580–587. (b) Volbeda, A.; Garcin, E.; Piras, C.; de Lacey, A. L.; Fernandez, V. M.; Hatchikian, E. C.; Frey, M.; Fontecilla-Camps, J. C. *J. Am. Chem. Soc.* **1996**, *118*, 12989–12996. (c) Higuchi, Y.; Yagi, T.; Yasuoka, N. *Structure* **1997**, *5*, 1671–1680. (d) Higuchi, Y.; Ogata, H.; Miki, K.; Yasuoka, N.; Yagi, T. *Structure* **1999**, *7*, 549–556. (e) Garcin, E.; Vernède, X.; Hatchikian, E. C.; Volbeda, A.; Frey, M.; Fontecilla-Camps, J. C. *Structure* **1999**, *7*, 557–566. (f) Montet, Y.; Amara, P.; Volbeda, A.; Vernède, X.; Hatchikian, E. C.; Field, M. J.; Frey, M.; Fontecilla-Camps, J. C. *Nat. Struct. Biol.* **1997**, *4*, 523–526. (g) Matias, P. M.; Soares, C. M.; Saraiva, L. M.; Coelho, R.; Morais, J.; Le Gall, J.; Carrondo, M. A. *J. Biol. Inorg. Chem.* **2001**, *6*, 63–81.
[36] Sazanov, L. A.; Hinchliffe, P. *Science* **2006**, *311*, 1430–1436.
[37] Martins, B. M.; Dobbek, H.; Çinkaya, I.; Buckel, W.; Messerschmidt, A. *Proc. Natl. Acad. Sci. U.S.A.* **2004**, *101*, 15645–15649.
[38] Dobritzsch, D.; Schneider, G.; Schnakerz, K. D.; Lindqvist, Y. *EMBO J.* **2001**, *20*, 650–660.
[39] Que, L., Jr.; Anglin, J. R.; Bobrik, M. A.; Davison, A.; Holm, R. H. *J. Am. Chem. Soc.* **1974**, *96*, 6042–6048.
[40] Evans, D. J. *Inorg. Chim. Acta* **1993**, *203*, 253–256.
[41] (a) Musgrave, K. B.; Laplaza, C. E.; Holm, R. H.; Hedman, B.; Hodgson, K. O. *J. Am. Chem. Soc.* **2002**, *124*, 3083–3092. (b) Laplaza, C. E.; Holm, R. H. *J. Biol. Inorg. Chem.* **2002**, *7*, 451–460.
[42] (a) Zhou, H.-C.; Holm, R. H. *Inorg. Chem.* **2003**, *42*, 11–21. (b) Tyson, M. A.; Demadis, K. D.; Coucouvanis, D. *Inorg. Chem.* **1995**, *34*, 4519–4520. (c) Challen, P. R.; Koo, S.-M.; Dunham, W. R.; Coucouvanis, D. *J. Am. Chem. Soc.* **1990**, *112*, 2455–2456. (d) Bierbach, U.; Saak, W.; Haase, D.; Pohl, S. *Z. Naturforsch.* **1990**, *45b*, 45–52.
[43] (a) MacNicol, D. D.; Hardy, A. D. U.; Wilson, D. R. *Nature* **1977**, *266*, 611–612. (b) Hardy, A. D. U.; MacNicol, D. D.; Wilson, D. R. *J. Chem. Soc., Perkin Trans. 2* **1979**, 1011–1019.
[44] Hennrich, G.; Anslyn, E. V. *Chem. Eur. J.* **2002**, *8*, 2218–2224.
[45] Moran, J. R.; Karbach, S.; Cram, D. J. *J. Am. Chem. Soc.* **1982**, *104*, 5826–5828.
[46] Stack, T. D. P.; Holm, R. H. *J. Am. Chem. Soc.* **1988**, *110*, 2484–2494.
[47] Stack, T. D. P.; Weigel, J. A.; Holm, R. H. *Inorg. Chem.* **1990**, *29*, 3745–3760.
[48] Zhou, J.; Hu, Z.; Münck, E.; Holm, R. H. *J. Am. Chem. Soc.* **1996**, *118*, 1966–1980.
[49] Bobrik, M. A.; Que, L., Jr.; Holm, R. H. *J. Am. Chem. Soc.* **1974**, *96*, 285–287.
[50] Que, L., Jr.; Bobrik, M. A.; Ibers, J. A.; Holm, R. H. *J. Am. Chem. Soc.* **1974**, *96*, 4168–4178.
[51] Tard, C.; Liu, X.; Ibrahim, S. K.; Bruschi, M.; De Gioia, L.; Davies, S. C.; Yang, X.; Wang, L.-S.; Sawers, G.; Pickett, C. J. *Nature* **2005**, *433*, 610–613.

[52] Ciurli, S.; Carrié, M.; Weigel, J. A.; Carney, M. J.; Stack, T. D. P.; Papaefthymiou, G. C.; Holm, R. H. *J. Am. Chem. Soc.* **1990**, *112*, 2654–2664.
[53] Weigel, J. A.; Holm, R. H. *J. Am. Chem. Soc.* **1991**, *113*, 4184–4191.
[54] Weigel, J. A.; Srivastava, K. K. P.; Day, E. P.; Münck, E.; Holm, R. H. *J. Am. Chem. Soc.* **1990**, *112*, 8015–8023.
[55] Zhou, C.; Raebiger, J. W.; Segal, B. M.; Holm, R. H. *Inorg. Chim. Acta* **2000**, 300–302, 892–902.
[56] Cai, L.; Holm, R. H. *J. Am. Chem. Soc.* **1994**, *116*, 7177–7188.
[57] Zhou, C.; Cai, L.; Holm, R. H. *Inorg. Chem.* **1996**, *35*, 2767–2772.
[58] Stack, T. D. P.; Carney, M. J.; Holm, R. H. *J. Am. Chem. Soc.* **1989**, *111*, 1670–1676.
[59] Zhou, C.; Holm, R. H. *Inorg. Chem.* **1997**, *36*, 4066–4077.
[60] Zhou, J.; Holm, R. H. *J. Am. Chem. Soc.* **1995**, *117*, 11353–11354.
[61] Daley, C. J. A.; Holm, R. H. *J. Inorg. Biochem.* **2003**, *97*, 287–298.
[62] Liu, H. Y.; Scharbert, B.; Holm, R. H. *J. Am. Chem. Soc.* **1991**, *113*, 9529–9539.
[63] Sun, J.; Tessier, C.; Holm, R. H. *Inorg. Chem.* **2007**, *46*, 2691–2699.
[64] Weigel, J. A.; Holm, R. H.; Surerus, K. K.; Münck, E. *J. Am. Chem. Soc.* **1989**, *111*, 9246–9247.
[65] Robbins, A. H.; Stout, C. D. *Proteins* **1989**, *5*, 289–312.
[66] Kissinger, C. R.; Sieker, L. C.; Adman, E. T.; Jensen, L. H. *J. Mol. Biol.* **1991**, *219*, 693–715.
[67] Stout, C. D. *J. Biol. Chem.* **1993**, *268*, 25920–25927.
[68] Adman, E. T.; Siefker, L. C.; Jensen, L. H. *J. Biol. Chem.* **1976**, *251*, 3801–3806.
[69] Sweeney, W. V.; Rabinowitz, J. C. *Annu. Rev. Biochem.* **1980**, *49*, 139–161.
[70] Cai, L.; Weigel, J. A.; Holm, R. H. *J. Am. Chem. Soc.* **1993**, *115*, 9289–9290.
[71] Rao, P. V.; Bhaduri, S.; Jiang, J.; Hong, D.; Holm, R. H. *J. Am. Chem. Soc.* **2005**, *127*, 1933–1945.
[72] Krueger, R. J.; Siegel, L. M. *Biochemistry* **1982**, *21*, 2905–2909.
[73] Zhou, C.; Cai, L.; Holm, R. H. *Inorg. Chem.* **1996**, *35*, 2767–2772.
[74] Whitener, M. A.; Peng, G.; Holm, R. H. *Inorg. Chem.* **1991**, *30*, 2411–2417.
[75] Evans, D. J.; Garcia, G.; Leigh, G. J.; Newton, M. S.; Santana, M. D. *J. Chem. Soc., Dalton Trans.* **1992**, 3229–3234.
[76] Okuno, H. (Y.); Uoto, K.; Tomohiro, T.; Youinou, M.-T. *J. Chem. Soc., Dalton Trans.* **1990**, 3375–3381.
[77] Holm, R. H.; Phillips, W. D.; Averill, B. A.; Mayerle, J. J.; Herskovitz, T. *J. Am. Chem. Soc.* **1974**, *96*, 2109–2117.
[78] Barclay, J. E.; Diaz, M. I.; Evans, D. J.; Garcia, G.; Santana, M. D.; Torralba, M. C. *Inorg. Chim. Acta* **1997**, *258*, 211–219.
[79] van Strijdonck, G. P. F.; van Haare, J. A. E. H.; van der Linden, J. G. M.; Steggerda, J. J.; Nolte, R. J. M. *Inorg. Chem.* **1994**, *33*, 999–1000.
[80] van Strijdonck, G. P. F.; van Haare, J. A. E. H.; Hönen, P. J. M.; van den Schoor, R. C. G. M.; Feiters, M. C.; van der Linden, J. G. M.; Steggerda, J. J.; Nolte, R. J. M. *J. Chem. Soc., Dalton Trans.* **1997**, 449–461.
[81] Canceill, J.; Collet, A.; Gottarelli, G. *J. Am. Chem. Soc.* **1984**, *106*, 5997–6003.
[82] Feutrill, G. I.; Mirrington, R. N. *Tetrahedron Lett.* **1970**, *11*, 1327–1328.
[83] van Strijdonck, G. P. F.; ten Have, P. T. J. H.; Feiters, M. C.; van der Linden, J. G. M.; Steggerda, J. J.; Nolte, R. J. M. *Chem. Ber.* **1997**, *130*, 1151–1157.
[84] Walsdorff, C.; Saak, W.; Pohl, S. *J. Chem. Soc., Dalton Trans.* **1997**, 1857–1861.
[85] Ooike, S.; Liu, D.; Matsumoto, T.; Tatsumi, K. *Nippon Kagakkai Koen Yokoshu* **2006**, *86*, 598.
[86] Liu, D.; Ooike, S.; Matsumoto, T.; Tatsumi, K. *Nippon Kagakkai Koen Yokoshu* **2006**, *86*, 339.
[87] Walsdorff, C.; Saak, W.; Haase, D.; Pohl, S. *Chem. Commun.* **1997**, 1931–1932.

[88] Adman, E. T.; Sieker, L. C.; Jensen, L. H. *J. Biol. Chem.* **1973**, *248*, 3987–3996.

Chapter 2

A [4Fe-4S] Cluster Dimer Bridged by Bis(2,2':6',2''-Terpyridine-4'-Thiolato)iron(II)

Abstract. *The use of 2,2':6',2''-terpyridine-4'-thiol (tpySH) was explored as a bridging ligand for the formation of stable assemblies containing both [4Fe-4S] clusters and single metal ions. Reaction of tpySH (2 equiv.) with $(NH_4)_2Fe(SO_4)_2 \cdot 6H_2O$ generated the homoleptic complex $[Fe(tpySH)_2]^{2+}$, which was isolated as its PF_6^- salt. The compound could be fully deprotonated to yield neutral $[Fe(tpyS)_2]$ and the absorption spectrum is highly dependent on the protonation state. Reaction of $[Fe(tpySH)_2](PF_6)_2$ with the 3:1 site-differentiated cluster (n-$Bu_4N)_2[Fe_4S_4(TriS)(SEt)]$ yielded the first metal-bridged [4Fe-4S] cluster dimer, (n-$Bu_4N)_2[\{Fe_4S_4(TriS)(\mu\text{-}Stpy)\}_2Fe]$. Electrochemical studies indicate that the [4Fe-4S] clusters in the dimer act as independent redox units, while UV-vis spectroscopy provides strong evidence for a thioquinonoid electron distribution in the bridging $tpyS^-$ ligand. $TpyS^-$ thus acts as a directional bridging ligand between [4Fe-4S] clusters and single metal ions, thereby opening the way to the synthesis of larger, more complex assemblies.*

van der Geer, E. P. L.; van Koten, G.; Klein Gebbink, R. J. M.; Hessen, B. *Inorg. Chem.*, accepted.

2.1. Introduction.

Since the discovery of cubane-type [4Fe-4S] clusters in the 1960's, several examples of enzymes have been found which include [4Fe-4S] clusters as integral parts of the active site. Sometimes, these [4Fe-4S] clusters are themselves catalytically active, but more often, they are linked via bridging cysteine residues to a catalytically active, mono- or dimetallic subsite. For example, in the H cluster of iron-only hydrogenase, a [4Fe-4S] cluster is bound via a bridging cysteine residue to a [2Fe-2S] subsite where the actual catalysis is believed to take place.[1] Similarly, [4Fe-4S] clusters in the active sites of acetyl coenzyme A synthase/carbon monoxide dehydrogenase[2] and sulfite reductase[3] are bridged to a [2Ni-2S] subsite and a siroheme group, respectively.

Intrigued by the influence of the [4Fe-4S] cluster on the bridged, metal-containing subsite, several researchers have incorporated [4Fe-4S] clusters into active-site models. Holm and co-workers mimicked the sulfite reductase active site by binding a [4Fe-4S] cluster to siroheme analogues via bridging sulfide ions.[4] Pickett and co-workers employed the same cluster in their synthesis of a thiolate-bridged model of the iron-only hydrogenase H cluster.[5] Meanwhile, Pohl and co-workers reported the synthesis of assemblies of Ni(II) thiolates and [4Fe-4S] clusters in the context of mimicking the carbon monoxide dehydrogenase active site.[6]

In all of these biomimetic studies, the bridging ligands were chosen to reflect most closely the modeled active site architectures. However, a selective and more general bridging ligand would allow for a systematic method of forming stable complexes of [4Fe-4S] clusters and other metals. This would not only be of interest in the synthesis of new biomimetic systems but would also facilitate potential future application of [4Fe-4S] clusters as conducting or redox-active units in smart materials such as nanoelectronic devices.[7] Ideally, such a general ligand would contain two distinct metal-binding groups: one group that has a preference for strong binding to single metal ions and one thiol group for binding to [4Fe-4S] clusters.

A ligand that attractively fulfills these requirements is 2,2':6',2''-terpyridine-4'-thiol (tpySH), first reported by McEuen, Ralph, and co-workers in 2002.[8] The ligand was shown to bind Co^{2+} ions as an *N,N,N*-tridentate chelate, thereby leaving the thiol group available for binding to gold surfaces. Three years later, Constable and co-workers reported a more convenient synthesis of tpySH, and demonstrated that both in solution and the solid state, the thione tautomer of tpySH is favored over the thiol (Scheme 1).[9] Furthermore, the authors showed that after oxidation to the corresponding disulfide, tpySH can coordinate to Fe^{2+} ions to form metallomacrocyclic compounds. Inspired by these reports, we decided to attempt the use of tpySH as a bridge between Fe^{2+} ions and [4Fe-4S] clusters.

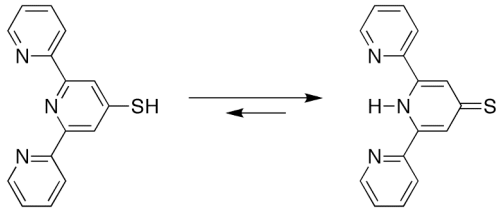

Scheme 1. Thiol and thione tautomers of tpySH.

2.2. Results and discussion.

2.2.1. Synthesis of a suitable site-differentiated [4Fe-4S] cluster system.

To study the feasibility of tpySH as bridging ligand in [4Fe-4S]-metal assemblies, a suitable [4Fe-4S] cluster was sought. The use of tripodal trithiolate ligands that coordinate to three of the iron atoms in a [4Fe-4S] cluster conveniently limits the reactivity to one specific iron site. Holm and co-workers were the first to report such a 3:1 site-differentiated [4Fe-4S] cluster, thereby using the preorganized, tripodal $L(SH)_3$ ligand (Chart 1) to chelate three of the four cluster iron atoms.[10] The synthesis of this ligand, however, is rather cumbersome, and makes use of the highly toxic chemicals chloromethyl methyl ether, $Hg(OAc)_2$, and H_2S. Alternative ligands based on cyclic polyethers,[11] triazacyclanes,[12] and cyclotriveratrylene[13] are also somewhat tedious to synthesize and their 1:1 reaction stoichiometries with [4Fe-4S] clusters were never proven through X-ray crystallography. In contrast, a tripodal ligand that is relatively simple to prepare and has a crystallographically proven capacity for site differentiation is 1,3,5-triethyl-2,4,6-tris(3-sulfanylindolyl[1]methyl)benzene ($TriSH_3$, Chart 1). In 1997, Pohl and co-workers reported this promising alternative to $L(SH)_3$ to be accessible via a five-step synthesis route.[14] We devised a modified synthesis of $TriSH_3$ that employs non-hazardous reagents and significantly improves the overall yield (Scheme 2).

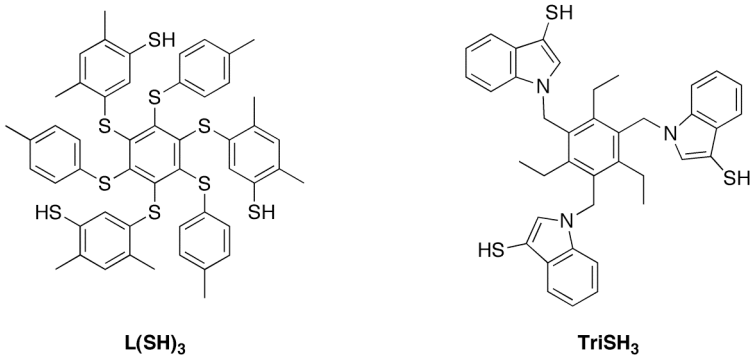

Chart 1. The tripodal $L(SH)_3$ and $TriSH_3$ ligands.

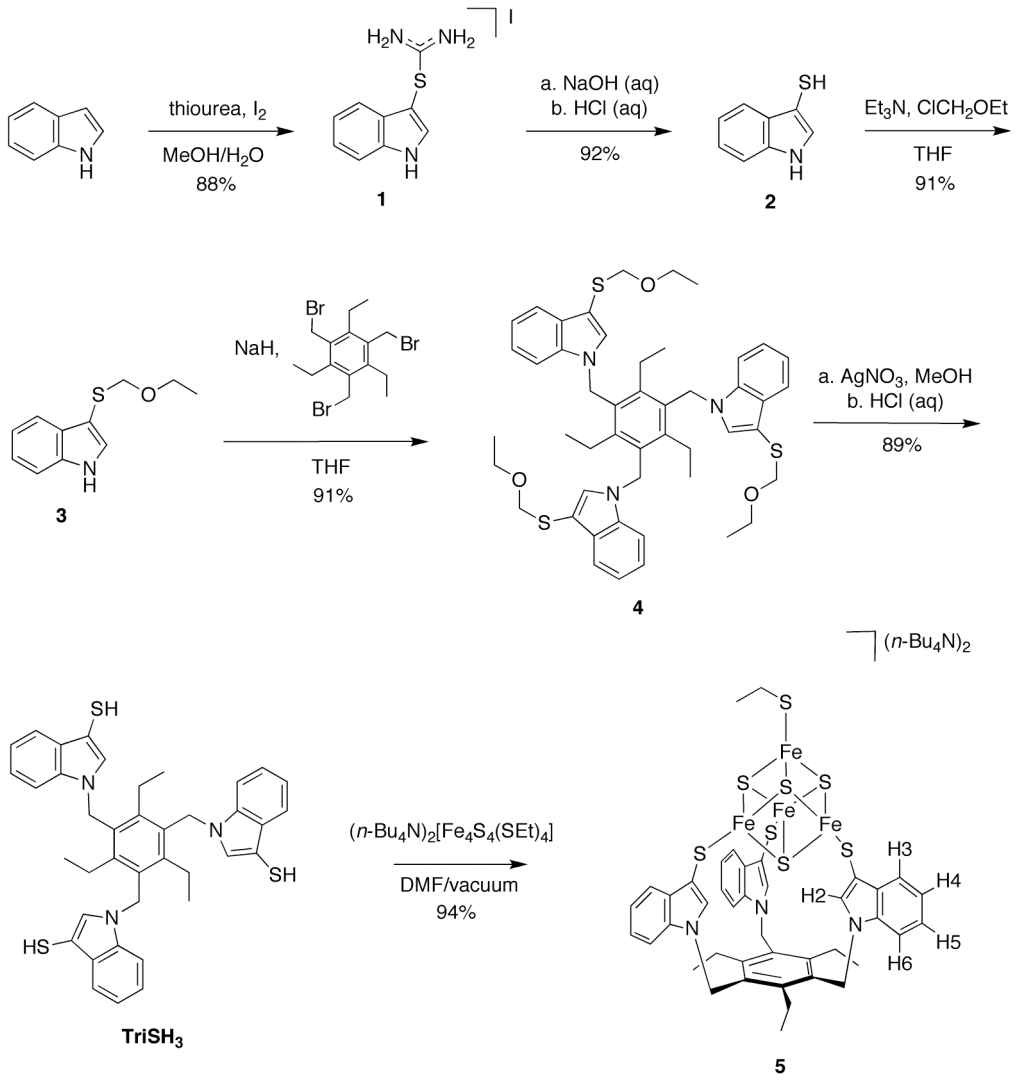

Scheme 2. Improved synthesis of $TriSH_3$ and generation of the 3:1 site-differentiated cluster $(n\text{-}Bu_4N)_2[Fe_4S_4(TriS)(SEt)]$ (**5**).

The improved synthesis begins with the two-step conversion of indole via 3-thiouroniumindole iodide (**1**) to indole-3-thiol (**2**) following literature methods[38] in an overall yield of 81%. In the subsequent thiol protection step, the use of (highly carcinogenic) chloromethyl methyl ether was circumvented by using chloromethyl ethyl ether instead, to yield 3-ethoxymethylsulfanylindole (**3**). The large difference in acidity between the thiol and indole NH groups allowed for selective thiol deprotonation by triethylamine, thus obviating the use of NaH from the original procedure.[14] Threefold nucleophilic addition of **3** to 1,3,5-tris(bromomethyl)-2,4,6-triethylbenzene[39] then yielded **4**, the ethoxymethyl-protected precursor of $TriSH_3$.

For the deprotection of **4** to yield $TriSH_3$, we devised a deprotection protocol based on the hemithioacetal cleavage method developed by Topolski.[15] First, treatment of **4** with

$AgNO_3$ in MeOH yielded a silver adduct, which is light-sensitive. Upon treatment with HCl, the adduct was converted to $TriSH_3$ in a yield of 89%.

The overall yield of $TriSH_3$ is 57% based on indole, which is more than double the yield of 24% reported in the original procedure.[14] The yield also substantially exceeds those reported for the other alternatives to $L(SH)_3$,[11-13] as well as that reported for $L(SH)_3$ itself.[16]

Reaction of $TriSH_3$ with $(n\text{-}Bu_4N)_2[Fe_4S_4(SEt)_4]$ in DMF formed the 3:1 site-differentiated cluster compound $(n\text{-}Bu_4N)_2[Fe_4S_4(TriS)(SEt)]$ (**5**) through thiol-thiolate exchange[17] (Scheme 2). Full conversion was ensured by *in vacuo* removal of the volatile EtSH coproduct. Solid **5** was then isolated in over 90% yield by means of a simple precipitation step, with elemental analyses confirming the proposed formulation.

In the ^{1}H NMR spectrum of **5**, the $TriS^{3-}$ ligand gives rise to three signals corresponding to the NCH_2 and ethyl groups, as well as four aromatic signals for the hydrogen atoms on positions 4 through 7 of the indole rings (Figure 1; for numbering, see Scheme 2). No signal is observed for the H2 protons, which are located close to the [4Fe-4S] cluster core and hence strongly experience the characteristic Fermi contact shifting expected for ligands bound to a [4Fe-4S] cluster.[18] The observation of single resonance patterns for the indolyl and ethyl groups indicates that **2** retains C_3 symmetry upon [4Fe-4S] coordination; hence, as in $(PPh_4)_2[Fe_4S_4(TriS)(SPh)]$,[14] rotation of the monodentate EtS^- ligand is fast on the NMR time scale.

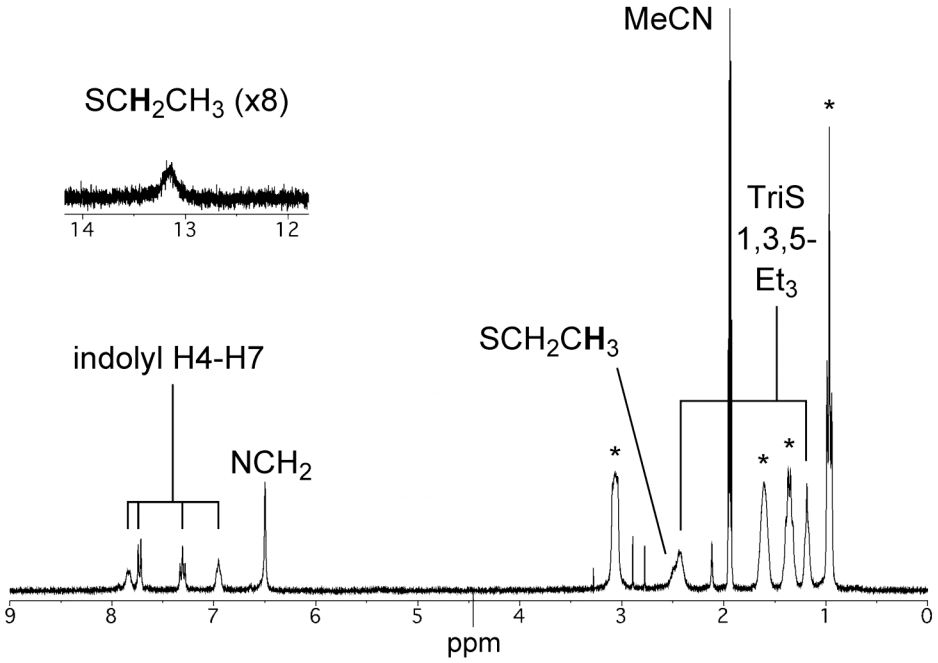

Figure 1. ^{1}H NMR spectrum of **5** in CD_3CN. $n\text{-}Bu_4N^+$ signals are marked with asterisks.

In CH_2Cl_2 solution, cluster **5** undergoes a chemically reversible 2–/3– transition, as well as a second transition to an unstable 1– state (Figure 2). The 2–/3– transition occurs at –1.27 V vs. SCE, and both i_{pc} and i_{pa} vary linearly with the square root of the scan rate. However, the peak separation is higher than expected for an electrochemically reversible process (ΔE_p = 100 mV) and increases with the scan rate, implying quasi-reversibility.

Unlike the 2–/3– transition, the 2–/1– transition at $E_{1/2}$ = –0.13 V is not fully reversible, displaying an oxidation wave that is significantly more intense than the corresponding reduction wave. Increasing the scan rate reduces the asymmetry between the waves, implying that the 1– state is unstable in solution and decomposes on the time scale of the electrochemical measurement. At more positive potentials, strictly irreversible oxidations occur.

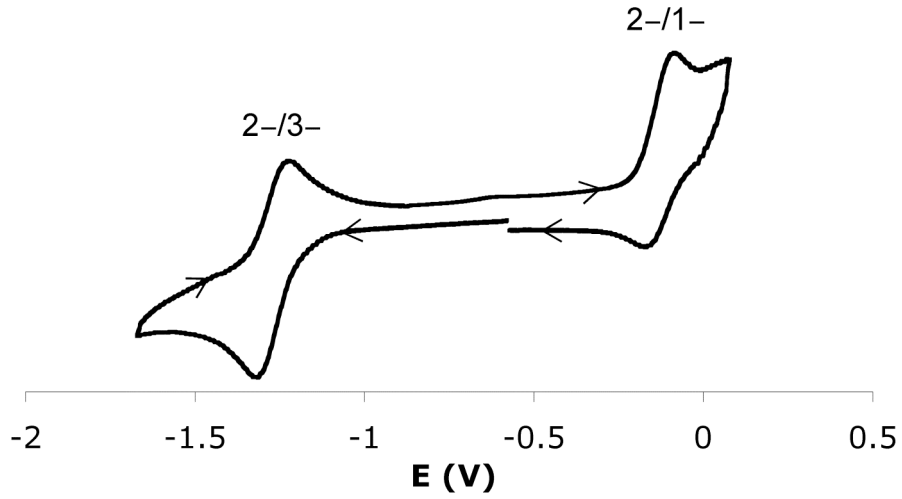

Figure 2. Cyclic voltammogram of **5** in CH_2Cl_2 (vs. SCE).

Despite the scant precedent for mass spectrometry of synthetic [4Fe-4S] clusters, a satisfactory ESI mass spectrum could be obtained for **5** under inert conditions (Figure 3). The most intense signal in the spectrum, at m/z = 527.1, represents the $[\mathbf{5} - 2(n\text{-}Bu_4N)]^{2-}$ parent ion (calculated m/z = 527.9). The isotope pattern shape for this signal agrees roughly with calculation (Figure 3, inset), although on the utilized mass spectrometer, we were unable to achieve resolutions high enough to see isotope peak separations of 0.5 m/z units. The second most intense signal (m/z = 679.3) corresponds to the adduct $[\mathbf{5} - n\text{-}Bu_4N + EtS]^{2-}$ (calculated m/z = 679.1). The mass spectrometry data for **5** constitute the second ESI-MS analysis of a 3:1 site-differentiated [4Fe-4S] cluster, preceded only by the iron-only hydrogenase H cluster mimic reported by Pickett and co-workers.[5] However, the generation of significant amounts of free EtS^- is evidence for the lability of the cluster under electrospray conditions.

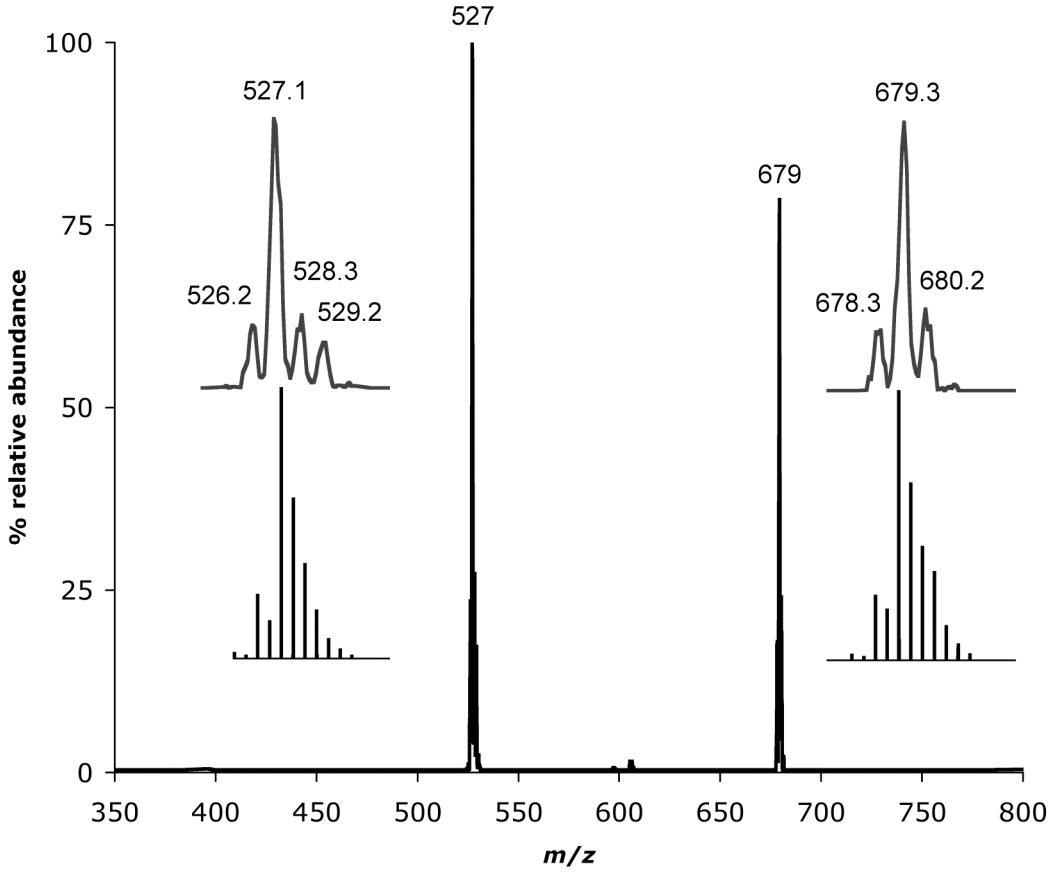

Figure 3. ESI-MS spectrum of **5**.

2.2.2. Synthesis of $[Fe(tpySH)_2](PF_6)_2$ (6).

The cation $[Fe(tpySH)_2]^{2+}$ was chosen as a convenient moiety to link to the site-differentiated [4Fe-4S] cluster since it has a high degree of symmetry and avoids potential ligand scrambling as often seen in heteroleptic tpy counterparts.[19] Possessing two thiol groups, $[Fe(tpySH)_2]^{2+}$ can potentially bind to two [4Fe-4S] clusters, thereby forming a metal-bridged [4Fe-4S] cluster dimer. Inspired by the syntheses of other 4'-R-substituted $[Fe(tpy)_2]^{2+}$ species by Slattery and co-workers,[19,20] we prepared $[Fe(tpySH)_2]^{2+}$ in one step from $(NH_4)_2Fe(SO_4)_2{\cdot}6H_2O$ and 2 equiv. of tpySH. Treatment with NH_4PF_6 subsequently afforded the PF_6^- salt $[Fe(tpySH)_2](PF_6)_2$ (**6**) in 82% yield (Scheme 3). **6** was characterized by elemental analysis, mass spectrometry, cyclic voltammetry, and ^{1}H NMR, UV-vis, and IR spectroscopy.

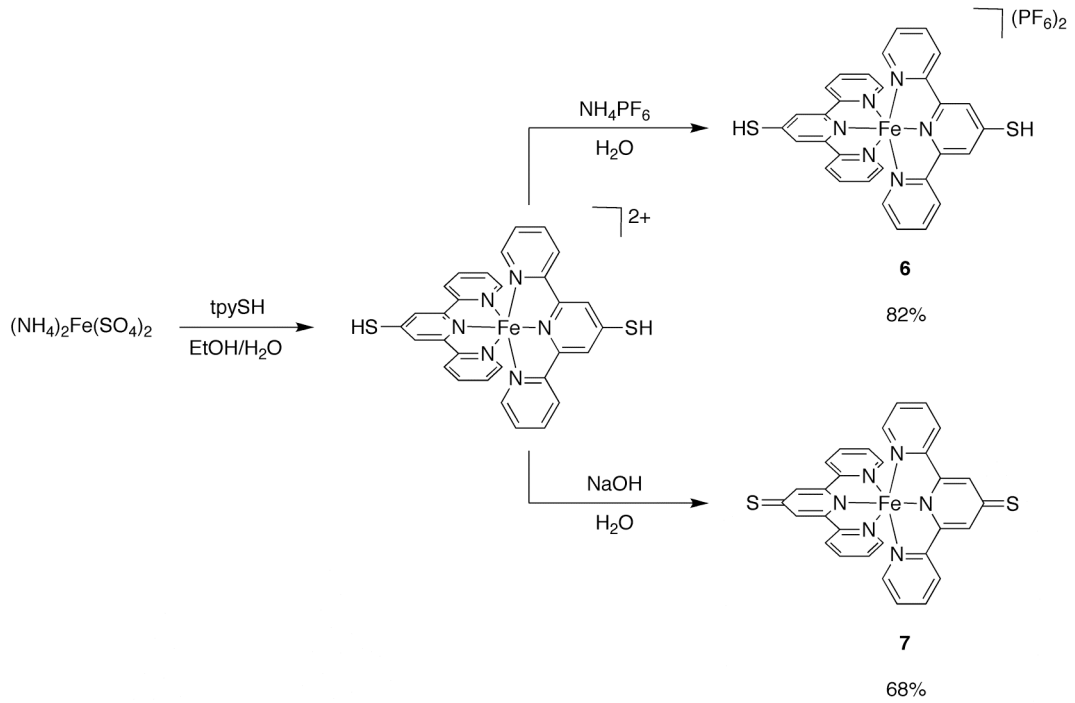

Scheme 3. Syntheses of $[Fe(tpySH)_2](PF_6)_2$ (**6**) and $[Fe(tpyS)_2]$ (**7**).

The ^{1}H NMR spectrum of **6** in CD_3CN shows a single set of tpySH signals, as would be expected for the D_{2d}-symmetric product (Figure 4). The chemical shift of the SH resonance is highly dependent on the water content of the sample, as well as on traces of acid.

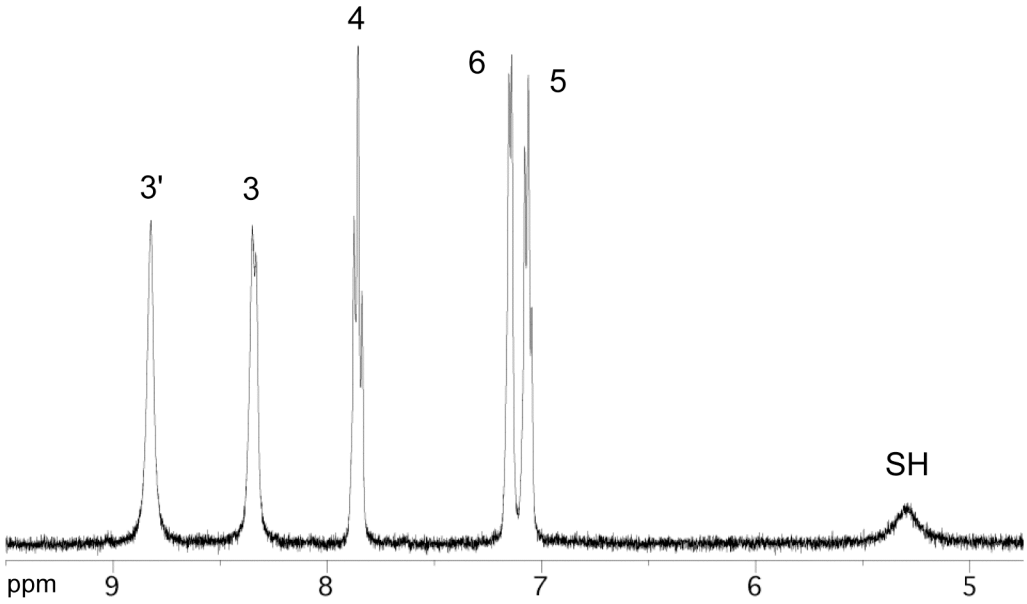

Figure 4. ^{1}H NMR spectrum of **6** in CD_3CN.

^{1}H NMR studies also showed that in CD_3CN solutions exposed to air, the thiol groups in **6** are fully oxidized within a day. A small amount of precipitate forms while the thiol signal disappears and the aromatic region of the spectrum becomes similar to that of the cyclic,

tpySStpy-bridged tetramer synthesized by Constable and co-workers.[9] Hence, the oxidation appears to yield a range of oligomeric products. This solution-phase air sensitivity has also been observed for tpySH as a free ligand.[9]

The UV-vis spectrum of **6** in MeCN (Figure 5) shows great similarity to the spectra of other 4'-substituted $[Fe(tpy)_2]^{2+}$ compounds. The lowest-energy electronic transition occurs at 564 nm, which correlates well with the 551 nm transition found in $[Fe(tpy)_2](PF_6)_2$.[21] Moreover, the 13 nm redshift of **6** as compared to the non-thiolated analogue is in agreement with the results reported by Constable[22] and Fallahpour,[23] which indicate that substitution at the 4'-position always redshifts the lowest-energy transition of a $[Fe(tpy)_2]^{2+}$ chromophore, regardless of whether the substituent is electron-donating or -accepting. Further electronic transitions in **6** occur at 317, 282, and 242 nm.

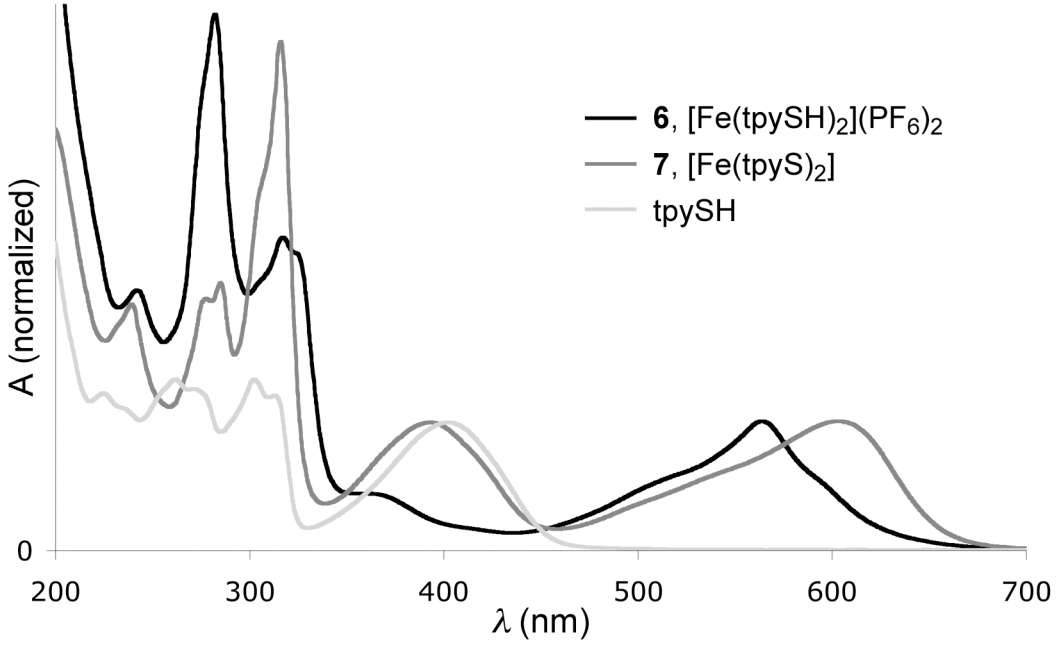

Figure 5. Normalized UV-vis spectra of **6**, **7**, and tpySH in MeCN.

In our subsequent investigation of the chemical properties of **6** in solution, we observed that deprotonation in the presence of an excess of Et_3N leads to a marked color change from purple to blue. Subsequent neutralization with aqueous HCl regenerates the purple color characteristic of **6**. In fact, the deprotonation product $[Fe(tpyS)_2]$ (**7**) could be prepared directly by reacting $(NH_4)_2Fe(SO_4)_2{\cdot}6H_2O$ with tpySH (2 equiv.) in $EtOH/H_2O$, followed by addition of aqueous NaOH (Scheme 3). Compound **7**, pure by elemental analyses, precipitated as a black powder.

The ^1H NMR spectrum of **7** in CD_2Cl_2 is similar to that of **6**, with the notable exception that a thiol signal is no longer observed (Figure 6). In contrast to **6**, compound **7** is highly unstable in solution; already within minutes from sample preparation under glovebox

conditions, the ^{1}H NMR spectrum shows the presence of a secondary species. Within a day, **7** decomposes fully, a process accompanied by the formation of a purple precipitate.

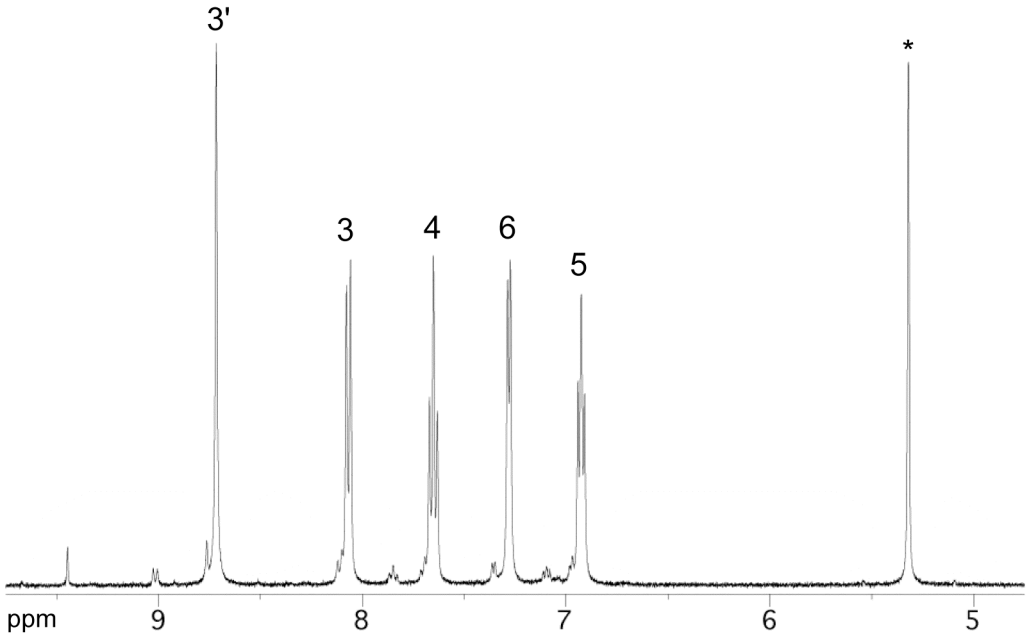

Figure 6. ^{1}H NMR spectrum of **7** in CD_2Cl_2. The asterisk denotes the residual solvent peak.

UV-vis spectroscopy confirmed the electronic absorption differences between the acid-base couple **6** and **7** (Figure 5). The lowest-energy transition in **6** experiences a redshift of 39 nm upon deprotonation and the absorption at 283 nm splits into two distinct peaks at 277 and 285 nm, thereby becoming significantly less intense than the absorption at 317 nm.

One of the most notable absorption changes, however, is the appearance of a new maximum of appreciable intensity at 394 nm. An analogous absorption is observed in the free tpySH ligand (λ_{max} = 402 nm, Figure 5) and corresponds to a π–π^* transition concentrated on the thione C–S functionality.[24] Hence, as in the free ligand, the C–S bonds in **7** have significant double-bond character, implying thioquinonoid electron distributions as shown in Scheme 3. Further evidence for this comes from IR spectroscopy, in which **7**, in contrast to **6**, shows a characteristic thione C–S stretch at 1101 cm^{-1}. This is close to the 1097 cm^{-1} absorption observed in free tpySH.

Electron distributions analogous to that in **7** have been observed in ruthenium and cobalt complexes with the oxy analogue of tpyS$^-$, tpyO$^-$,[25] as well as in compounds of pyridine-4-thiolate coordinated to ruthenium and iron.[26] However, no mention of protonation state-dependent electronic absorption changes has been made for these compounds. In fact, the only other examples that we could find of terpyridyl metal compounds with protonation state-dependent UV-vis spectra are the compounds $[M(tpy\text{-}py)_2](PF_6)_2$ (M = Ru, Os; tpy-py =

4'-(4-pyridyl)-2,2':6',2''-terpyridine) reported recently by Maestri, Credi, and co-workers.[27] In these compounds, however, the ionizable atom is located farther away from the tpy moiety as compared to the directly attached thiols group in **6**, resulting in smaller spectral sensitivities to the protonation state.

In cyclic voltammetry, compound **6** shows a reversible 2+/3+ process in MeCN at +1.12 V vs. SCE, although the peak separation of merely 38 mV suggests that the electrochemical process is complicated by adsorption effects. Slattery and co-workers observed a linear Hammett relationship between the 2+/3+ redox potential in 4'-R-substituted $[Fe(tpy)_2]^{2+}$ compounds in MeCN and the substituent σ_p value.[20] Given a σ_p value of +0.15 for the thiol group,[28] the observed potential of **6** is in excellent agreement with Slattery's imperative relation, thereby lying most closely to the potential of +1.13 V found for the non-substituted (R = H) analogue. Compound **7** was studied in CH_2Cl_2 due to its high solubility in this solvent and exhibited a reversible 2+/3+ process at +1.05 V vs. SCE. The observed peak separation of 78 mV is consistent with a quasi-reversible, one-electron transition.

2.2.3. Synthesis of a [4Fe-4S] cluster dimer bridged by 7.

Following the successful synthesis of **6**, we reacted this dithiol with **5** (2 equiv.) by means of thiol–thiolate exchange chemistry in DMF solution, forming $(n\text{-}Bu_4N)_2[\{Fe_4S_4(TriS)(\mu\text{-}Stpy)\}_2Fe]$ (**8**, Scheme 4). This [4Fe-4S] cluster dimer could be separated from the $n\text{-}Bu_4NPF_6$ byproduct by means of a slow recrystallization, resulting in a yield of 59%.

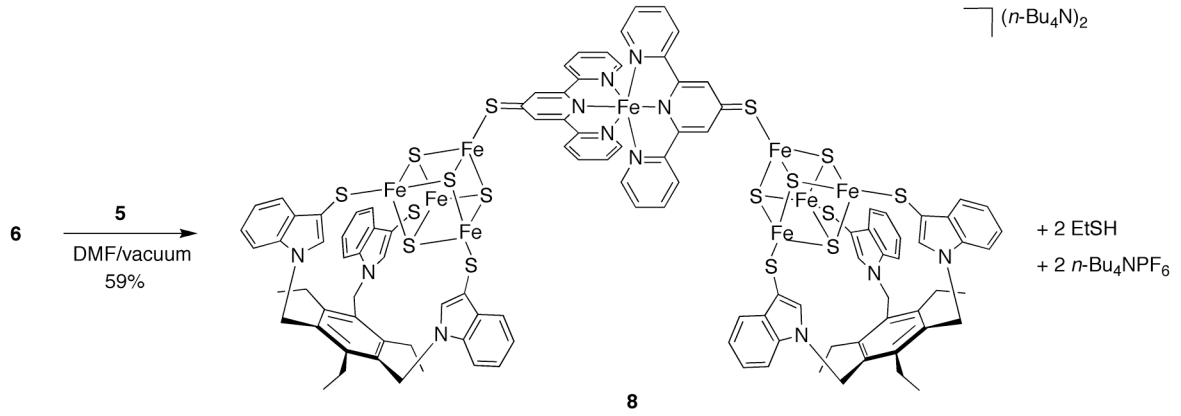

Scheme 4. Synthesis of $(n\text{-}Bu_4N)_2[\{Fe_4S_4(TriS)(\mu\text{-}Stpy)\}_2Fe]$ (**8**).

The ^1H NMR spectrum of **8** in CD_3CN clearly shows the effects of bridge formation on both the cluster and $\{Fe(tpyS)_2\}$ moieties, despite the rather low signal-to-noise ratio resulting from the poor solubility of **8** in CD_3CN (Figure 7). The indolyl H4–H7 protons resonate at chemical shifts comparable to those in **5**, while the NCH_2 signal has shifted 0.15 ppm to a higher frequency. For the $tpyS^-$ protons, substantial signal broadening is observed, as expected for ligands bound to a [4Fe-4S] cluster.[18] The most marked effect of the cluster

binding, however, is the seeming absence of the 3' signal. Similar to the likewise undetected indolyl H2 atoms (*vide supra*), the tpyS 3' hydrogen atoms in **8** are strongly contact-shifted due to their vicinity to the [4Fe-4S] cluster cores.

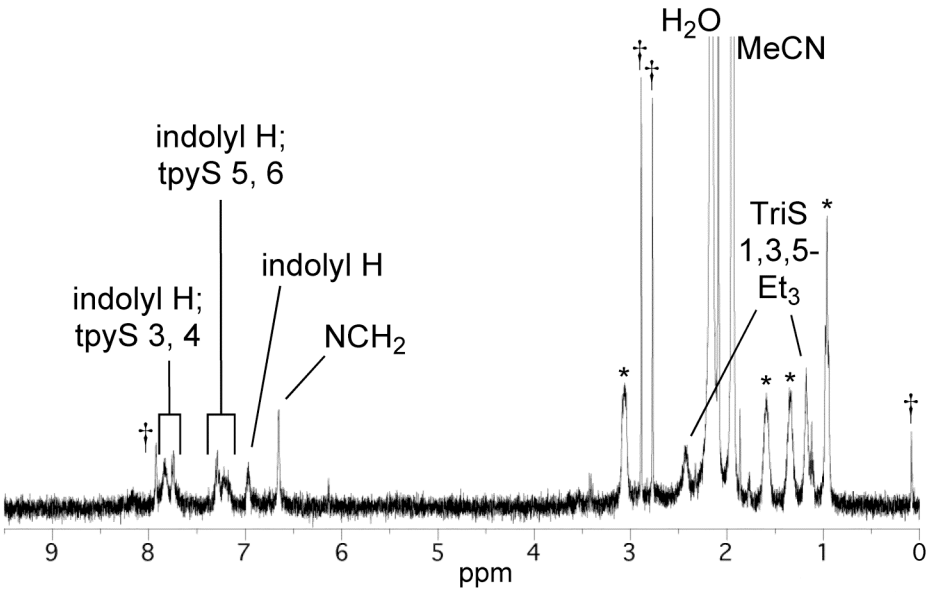

Figure 7. ^{1}H NMR spectrum of **8** in CD_3CN. *n*-Bu_4N^+ signals are marked with asterisks. DMF and silicone grease signals (marked with daggers) are probably strongly enhanced by the poor solubility of **8**.

The UV-vis spectrum of **8** approximates a linear combination of the spectra of **5** and **7** (Figure 8), implying that the [4Fe-4S] and {Fe(tpyS)$_2$} units in **8** act as rather independent chromophores. Compound **8** displays the π–π^* transition concentrated on the C–S functionality as a shoulder at 375 nm and the lowest-energy transition occurs at an energy similar to that in **7** (598 vs. 603 nm, respectively). The parallels observed between **7** and **8** indicate that the effects of [4Fe-4S] cluster coordination on the energy levels of **7** are much smaller than the effects of protonation. Hence, the thione character of the tpyS$^-$ ligand appears to be dominant in **8**, as also evidenced in IR spectroscopy by the observation of the C–S stretching frequency at 1100 cm^{-1}.

The electrochemical profile of **8** in CH_2Cl_2 is similar to that of **5**, although shifted to significantly more positive potentials (Figure 9). A chemically reversible reduction now occurs at –1.06 V vs. SCE, and, like the 2–/3– process in **5**, displays linear relationships between the square root of the scan speed and the peak currents i_{pc} and i_{pa}. The observed peak separation is 82 mV at 100 mV/s, indicating that although the overall charge of the assembly switches between 2– and 4–, the bridged [4Fe-4S] clusters essentially act as isolated redox units undergoing independent, one-electron transitions. Holm and co-workers have observed similar redox independence in a cluster dimer bridged by 1,4-benzenedithiolate and in clusters bridged by 1,3- and 1,4-benzenedimethanethiolate.[30] Analogous to the process at –1.06 V, we

assign the irreversible oxidation at E_{ox} = +0.05 V to the parallel one-electron oxidations of the [4Fe-4S] cluster units in **8**, resulting in an overall neutral assembly.

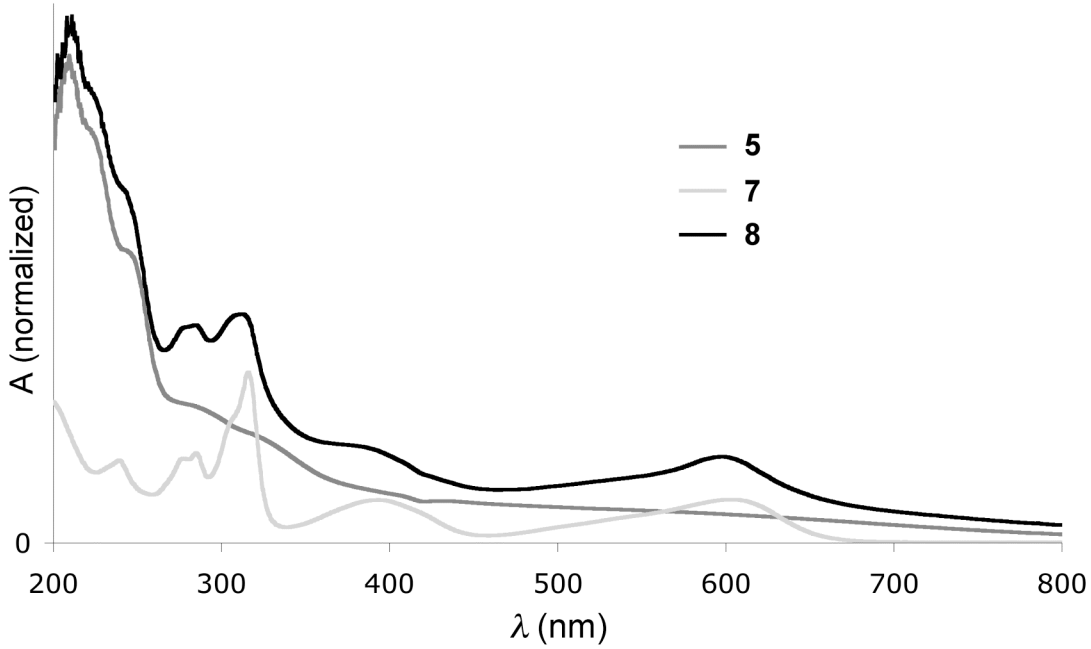

Figure 8. Normalized UV-vis spectra of **5**, **7**, and **8** in MeCN.

The positive redox potential shift of 0.21 V observed in going from **5** to **8** is comparable to the potential differences reported by Holm and co-workers between $[Fe_4S_4(LS_3)(SEt)]^{2-}$ and $[Fe_4S_4(LS_3)(L')]^{-}$, with L' a neutral pyridine or imidazole derivative.[29] The similarity reflects the fact that as in $[Fe_4S_4(LS_3)(L')]^{-}$, each [4Fe-4S] cluster in **8** is essentially mono-anionic; in other words, the formation of **8** can be seen as the substitution of EtS^{-} by the neutral ligand **7**.

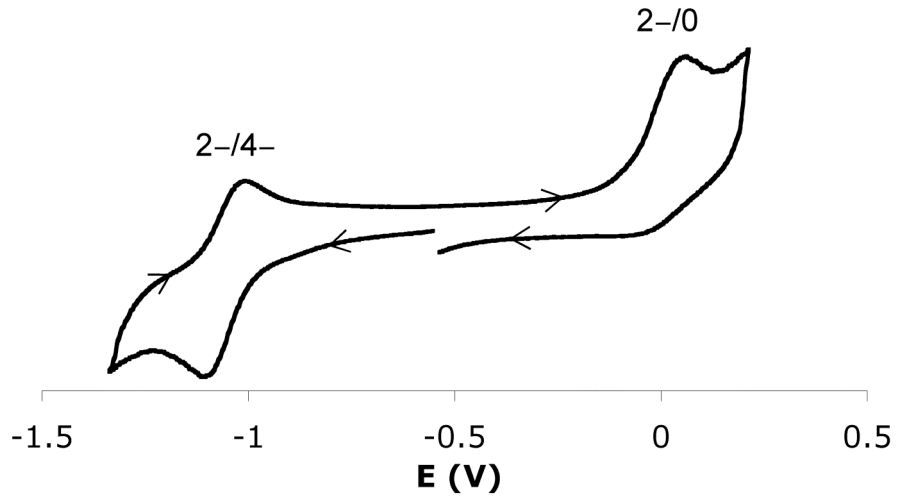

Figure 9. Cyclic voltammogram of **8** in CH_2Cl_2 (vs. SCE).

2.3. Conclusion.

The new [4Fe-4S] cluster **5** is the most easily accessible 3:1 site-differentiated cluster available thus far. Its facile, high-yielding synthesis and high purity as confirmed by spectroscopic and elemental analyses make it a most convenient starting material for more complex site-differentiated cluster systems such as **8**.

Bridged assembly **8** is the first [4Fe-4S] cluster dimer connected by a metal-containing linker. Holm and co-workers have previously reported [4Fe-4S] cluster dimers bridged by organic dithiols,[30] while the group of Pohl synthesized a dimer linked by a doubly chelating hexathiol.[31] Sulfide ions[11,30,32] and cysteine derivatives[33] have also been applied successfully as short-distance bridges in cluster dimer syntheses. Our approach employing tpySH as a directional bridging ligand has now enabled the use of a redox-active group as linking moiety between the [4Fe-4S] clusters.

Iron-containing dithiol $[Fe(tpySH)_2](PF_6)_2$, **6** represents an excellent building block in the synthesis of larger, bridged structures by virtue of its two available thiol functionalities. Furthermore, the drastic changes in electronic absorption exhibited by **6** upon deprotonation allow for the use of UV-vis spectroscopy to assess the extent of thioquinonoid electron distribution in compounds containing the $\{Fe(tpyS)_2\}$ chromophore.

Using tpySH, systematic studies of larger complexes containing both clusters and metal ions in different ratios should prove possible. Although the present study does not suggest high levels of interaction between the clusters themselves or between the clusters and the Fe^{2+} ion in **8**, the communication may be enhanced in future studies by variation of the bridging ligand or the single metal ion.

2.4. Experimental.

General. All air-sensitive compounds were handled in a glovebox or using standard Schlenk techniques. Indole, thiourea, KI, I_2, $AgNO_3$, NaH (60% dispersion in mineral oil), and NH_4PF_6 were purchased from Acros and used as received. $(NH_4)_2Fe(SO_4)_2 \cdot 6H_2O$ was purchased from Aldrich and used as received. Triethylamine (Acros) and chloromethyl ethyl ether (Aldrich) were degassed prior to use. THF and diethyl ether were distilled from Na/benzophenone, CH_2Cl_2 and DMF were distilled from CaH_2, and pentane was distilled from Na. MeCN was distilled from $KMnO_4$ and Na_2CO_3 prior to use in cyclic voltammetry.[34] Solvents for air-sensitive compounds were thoroughly degassed or flushed with N_2. ^1H and ^{13}C NMR spectra were recorded at 298 K on a Varian 400 MHz spectrometer operating at 400 and 100 MHz, respectively, or at 300 K on a Bruker AC 300 spectrometer operating at 300 and 75 MHz, respectively. Spectra were calibrated on the residual solvent peaks. Signal assignments were based on chemical shift, integral, and linewidth considerations, as well as 2D COSY ^1H NMR for **6** and **7**. Infrared spectra were recorded on a Perkin-Elmer Spectrum One FT-IR spectrometer. UV-vis spectra were recorded on a Varian Cary 50 Scan UV-visible spectrophotometer. The electrospray ionization (ESI) mass spectrum of **5** was recorded on an API 3+ triple quadrupole mass spectrometer (Sciex, Concord, Ont., Canada) equipped with a modified pneumatically assisted electrospray (IonSpray) interface.[35] The home-made front cover and

IonSpray interface ensure a gas-tight ion source. The atmospheric pressure ion source was first evacuated and then filled with dry nitrogen. N_2 was used as nebulizing gas and curtain gas. Sample preparation took place in a N_2-filled glovebox. The syringe pump used for sample introduction was also placed inside the glovebox, and a 1.6 mm o.d. 0.3 mm i.d. Teflon tube was connected between the syringe pump and the IonSpray interface. Mass spectra were recorded in negative ion mode as Q1 scans with step size 0.1 and a dwell time of 1 ms. The electrospray probe capillary voltage was set at 4.0 kV, and the cone voltage at 35 V. The ESI mass spectrum of **6** was recorded on a Micromass LC-TOF mass spectrometer by the Biomolecular Mass Spectrometry group at Utrecht University. Elemental analyses were carried out by Kolbe Mikroanalytisches Laboratorium (Mülheim an der Ruhr, Germany). Cyclic voltammograms were recorded at 100 mV/s using Pt working and counter electrodes and a Ag/AgCl reference electrode. The supporting electrolyte was 0.1 M *n*-Bu_4NClO_4 in CH_2Cl_2 for **5** and **7** and 0.1 M *n*-Bu_4NPF_6 in MeCN for **6**. Potentials were referenced to a ferrocene (Fc) internal standard. To facilitate comparison with literature values, potentials vs. a standard calomel electrode (SCE) were calculated by taking $E_{1/2}$ (Fc/Fc^+) = 0.424 V vs. SCE in CH_2Cl_2[36] and 0.379 V in MeCN.[37] Although the syntheses of 3-thiouroniumindole iodide (**1**) and indole-3-thiol (**2**) have been reported previously by Harris,[38] full experimental details and complete spectral characterizations were omitted. For convenience, we have included these data here.

3-Thiouroniumindole iodide (1). To a solution of indole (3.00 g, 25.6 mmol) and thiourea (1.95 g, 25.6 mmol) in a mixture of MeOH (80 mL) and water (20 mL) were added I_2 (6.50 g, 25.6 mmol) and KI (4.25 g, 25.6 mmol). After 3 days, the solution was concentrated to a black oil, which crystallized upon agitation. The product was washed with water and ether and recrystallized twice from acetone/diethyl ether. Yield: 7.17 g (22.5 mmol, 88%). Anal. Calcd for $C_9H_{10}IN_3S$: C, 33.87; H, 3.16; N, 13.17; S, 10.05. Found: C, 33.75; H, 3.08; N, 12.98; S, 10.07. ^{1}H NMR (DMSO-d_6): δ = 12.11 (s, broad, 1H, indolyl NH), 8.85 (s, broad, 2H, NH_2), 8.52 (s, broad, 2H, NH_2), 7.96 (d, $^3J_{H\text{-}H}$ = 2.7 Hz, 1H, indolyl H2), 7.55 (d, $^3J_{H\text{-}H}$ = 8.2 Hz, 1H, indolyl H), 7.50 (d, $^3J_{H\text{-}H}$ = 7.6 Hz, 1H, indolyl H), 7.27 (td, $^3J_{H\text{-}H}$ = 7.5 Hz, $^4J_{H\text{-}H}$ = 1.3 Hz, 1H, indolyl H), 7.21 (td, $^3J_{H\text{-}H}$ = 7.4 Hz, $^4J_{H\text{-}H}$ = 1.2 Hz, 1H, indolyl H). ^{13}C{^{1}H} NMR (DMSO-d_6): δ = 170.73 ($SC(NH_2)_2$), 136.79, 135.90, 128.26, 122.73, 121.03, 117.52, 112.77 (7 × indolyl C), 89.90 (indolyl CS). FT-IR (ATR, ν, cm^{-1}): 3288, 3250, 3132, 3090, 1689, 1637, 1607, 1457, 1425, 1412, 1342, 1284, 1237, 1127, 1042, 1008, 846, 739, 681.

Indole-3-thiol (2). A suspension of **1** (5.00 g, 15.7 mmol) in aqueous 2 M NaOH (60 mL) was heated to 100 °C for 15 min under constant stirring. After cooling to ambient temperature, the solution was filtered and aqueous 10 M HCl (12.5 mL) was added. A yellow precipitate formed, and the mixture was extracted with CH_2Cl_2 (3 × 10 mL). The combined organic extracts were dried over $MgSO_4$ and evaporated to a yellow, microcrystalline material. Yield: 2.14 g (14.4 mmol, 92%). Anal. Calcd for C_8H_7NS: C, 64.39; H, 4.73; N, 9.39; S, 21.49. Found: C, 64.27; H, 4.65; N, 9.20; S, 21.32. ^{1}H NMR (DMSO-d_6): δ = 11.25 (s, broad, 1H, NH), 7.56 (d, $^3J_{H\text{-}H}$ = 7.1 Hz, 1H, indolyl H), 7.43 (d, $^3J_{H\text{-}H}$ = 2.5 Hz, 1H, indolyl H2), 7.39 (d, $^3J_{H\text{-}H}$ = 7.1 Hz, 1H, indolyl H), 7.14 (td, $^3J_{H\text{-}H}$ = 7.2 Hz, $^4J_{H\text{-}H}$ = 1.4 Hz, 1H, indolyl H), 7.08 (td, $^3J_{H\text{-}H}$ = 7.1 Hz, $^4J_{H\text{-}H}$ = 1.1 Hz, 1H, indolyl H), 4.23 (s, broad, 1H, SH). ^{13}C{^{1}H} NMR (DMSO-d_6): δ = 136.16, 129.37, 128.83, 121.66, 119.26, 118.48, 111.76 (7 × indolyl C), 95.51 (CSH). FT-IR (ATR, ν, cm^{-1}): 3394, 3109, 3052, 2520, 1615, 1454, 1409, 1339, 1323, 1239, 1090, 1004, 930, 818, 740.

3-Ethoxymethylsulfanylindole (3). Thiol **2** (3.95 g, 26.5 mmol) was dissolved in THF (20 mL), and the resulting yellow solution cooled to 0 °C. Triethylamine (3.72 mL, 26.5 mmol) and chloromethyl ethyl ether (2.46 mL, 26.5 mmol) were subsequently added. Within minutes, a white precipitate formed, and the mixture was warmed to ambient temperature and stirred for an extra 24 h. The solution was then poured into water (40 mL) and extracted with diethyl ether (3 × 40 mL). The combined organic extracts were

washed with aqueous 1 M HCl solution (1 × 40 mL), water (1 × 40 mL), and brine (1 × 40 mL). The organic phase was dried over $MgSO_4$ and evaporated to yield a yellow oil. Yield: 4.95 g (24.0 mmol, 91%). Anal. Calcd for $C_{11}H_{13}NOS$: C, 63.74; H, 6.32; N, 6.76; S, 15.47. Found: C, 63.59; H, 6.35; N, 6.82; S, 15.38. ^{1}H NMR (300 MHz, $CDCl_3$): δ = 8.27 (s, broad 1 H, NH), 7.79–7.74 (m, 1 H, indolyl H), 7.40–7.36 (m, 1 H, indolyl H), 7.35 (d, $^3J_{H\text{-}H}$ = 2.5 Hz, 1 H, indolyl H2), 7.26–7.17 (m, 2 H, indolyl H), 4.77 (s, 2 H, SCH_2O), 3.72 (q, $^3J_{H\text{-}H}$ = 7.1 Hz, 2 H, CH_2CH_3), 1.23 (t, $^3J_{H\text{-}H}$ = 7.1 Hz, 3 H, CH_2CH_3). ^{13}C{^{1}H} NMR (75 MHz, $CDCl_3$): δ = 136.26, 129.46, 129.34, 122.71, 120.53, 119.33, 111.59 (7 × indolyl C), 105.11 (indolyl CS), 77.85 (SCH_2O), 64.12 (CH_2CH_3), 15.00 (CH_2CH_3). FT-IR (ATR, ν, cm^{-1}): 3402, 3302, 2974, 2878, 1454, 1407, 1338, 1302, 1260, 1236, 1064, 1008, 944, 833, 740, 675.

1,3,5-Triethyl-2,4,6-tris(3-ethoxymethylsulfanylindolyl[1]methyl)benzene (4). NaH (60% dispersion in mineral oil, 0.960 g, 24.0 mmol) was washed with pentane. A solution of **3** (3.96 g, 19.2 mmol) in THF (100 mL) cooled to 0 °C was then added slowly under constant stirring. After 5 min, the mixture was allowed to warm to ambient temperature and was left stirring overnight. The resulting turbid, orange solution was again cooled to 0 °C, and 1,3,5-triethyl-2,4,6-tris(bromomethyl)benzene[39] (2.60 g, 5.91 mmol) was added. A white precipitate formed immediately. The mixture was then heated to reflux for 1 h. After cooling to ambient temperature, water (150 mL) was added and the mixture was extracted with ether (3 × 75 mL). The combined organic extracts were washed with water (1 × 75 mL) and brine (1 × 75 mL), dried over $MgSO_4$, and evaporated to yield a pink solid. The product was purified over silica, using EtOAc/hexanes, 30/70 (v/v) as eluent. Yield: 4.58 g (5.58 mmol, 94%). Anal. Calcd for $C_{48}H_{57}N_3O_3S_3$: C, 70.29; H, 7.00; N, 5.12; S, 11.73. Found: C, 70.22; H, 7.08; N, 4.97; S, 11.77. ^{1}H NMR (300 MHz, acetone-d_6): δ = 7.71 (d, $^3J_{H\text{-}H}$ = 8.0 Hz, 3 H, indolyl H), 7.66 (d, $^3J_{H\text{-}H}$ = 8.3 Hz, 3 H, indolyl H), 7.29 (td, $^3J_{H\text{-}H}$ = 7.6 Hz, $^4J_{H\text{-}H}$ = 1.2 Hz, 3 H, indolyl H), 7.19 (td, $^3J_{H\text{-}H}$ = 7.5 Hz, $^4J_{H\text{-}H}$ = 1.0 Hz, 3 H, indolyl H), 6.89 (s, 3 H, indolyl H2), 5.55 (s, 6 H, NCH_2), 4.67 (s, 6 H, SCH_2O), 3.61 (q, $^3J_{H\text{-}H}$ = 7.1 Hz, 6 H, OCH_2CH_3), 2.76 (q, $^3J_{H\text{-}H}$ = 7.4 Hz, 6 H, aryl-CH_2CH_3), 1.03 (t, $^3J_{H\text{-}H}$ = 7.1 Hz, 9 H, OCH_2CH_3), 0.96 (t, $^3J_{H\text{-}H}$ = 7.6 Hz, 9 H, aryl-CH_2CH_3). ^{13}C{^{1}H} NMR (75 MHz, acetone-d_6): δ = 147.03 (aryl C), 137.95 (indolyl C), 131.98, 131.84, 131.25 (2 × indolyl C, 1 × aryl C), 123.17, 121.14, 120.27, 110.86 (4 × indolyl C), 104.59 (indolyl CS), 78.44 (SCH_2O), 64.04 (OCH_2CH_3), 44.64 (NCH_2), 24.12 (aryl CH_2CH_3), 15.57 (aryl CH_2CH_3 or OCH_2CH_3), 15.26 (aryl CH_2CH_3 or OCH_2CH_3). FT-IR (ATR, ν, cm^{-1}): 3049, 2970, 2930, 2872, 1610, 1505, 1451, 1391, 1336, 1296, 1219, 1160, 1081, 1011, 838, 738, 668.

1,3,5-Triethyl-2,4,6-tris(3-thioindolyl[1]methyl)benzene (TriSH$_3$). Protected precursor **4** (600 mg, 0.732 mmol) was suspended in a solution of $AgNO_3$ (1.24 g, 7.30 mmol) in MeOH (80 mL) and stirred vigorously for 1 h in the dark. During this time, a yellow precipitate formed, which was isolated by centrifugation and decantation of the colorless supernatant. The precipitate was then washed with MeOH (80 mL), after which aqueous 6 M HCl (40 mL) and ether (40 mL) were added. The resulting mixture was stirred vigorously in the dark for 1 h. The ether layer was removed, washed with water (3 × 60 mL) and brine (1 × 60 mL), dried over $MgSO_4$, and evaporated to yield a white solid. ^{1}H NMR revealed the presence of 0.14 eq of diethyl ether. Yield: 427 mg (0.651 mmol, 89%). The ether was removed under ultra-high vacuum conditions prior to microanalysis and further ^{1}H and ^{13}C NMR characterization. This allowed for resolution of the product methyl ^{13}C signal, which had been overlooked by Pohl and co-workers.[14] Anal. Calcd for $C_{33}H_{33}N_3S_3$: C, 72.52; H, 6.09; N, 6.51; S, 14.89. Found: C, 72.41; H, 6.15; N, 6.37; S, 14.78. ^{1}H NMR (300 MHz, $CDCl_3$): δ = 7.75 (d, $^3J_{H\text{-}H}$ = 7.6 Hz, 3 H, indolyl H), 7.48 (d, $^3J_{H\text{-}H}$ = 8.0 Hz, 3 H, indolyl H), 7.34 (td, $^3J_{H\text{-}H}$ = 7.6 Hz, $^4J_{H\text{-}H}$ = 1.2 Hz, 3 H, indolyl H), 7.26 (td, $^3J_{H\text{-}H}$ = 7.4 Hz, $^4J_{H\text{-}H}$ = 0.55 Hz, 3 H, indolyl H), 6.71 (d, $^4J_{H\text{-}H}$ = 1.4 Hz, 3 H, indolyl H2), 5.33 (s, 6 H, NCH_2), 2.90 (d, $^4J_{H\text{-}H}$ = 1.7 Hz, 3 H, SH), 2.61 (q, $^3J_{H\text{-}H}$ = 7.6 Hz, 6 H, CH_2CH_3), 0.95 (t, $^3J_{H\text{-}H}$ = 7.7 Hz, 9 H, CH_2CH_3). ^{13}C{^{1}H} NMR (75 MHz,

$CDCl_3$): δ = 146.33 (aryl C), 136.93 (indolyl C), 131.12, 130.83, 129.99 (2 × indolyl C, 1 × aryl C), 122.83, 120.76, 119.94, 109.45 (4 × indolyl C), 96.38 (indolyl CSH), 43.85 (NCH_2), 23.66 (CH_2CH_3), 15.47 (CH_2CH_3). FT-IR (ATR, ν, cm^{-1}): 3048, 2965, 2522, 1610, 1509, 1451, 1389, 1337, 1297, 1260, 1217, 1166, 1075, 1012, 928, 801, 737.

(*n*-$Bu_4N)_2[Fe_4S_4(TriS)(SEt)]$ (5). (*n*-$Bu_4N)_2[Fe_4S_4(SEt)_4]$[40] (450 mg, 0.415 mmol) was dissolved in DMF (15 mL). A solution of $TriSH_3 \cdot 0.14Et_2O$ (272 mg, 0.415 mmol) in THF (5 mL) was then added via cannula, and an immediate color change from brown to violet was observed. A periodic dynamic vacuum was applied to the stirred solution over the course of 1 h, yielding a black residue. CH_2Cl_2 (10 mL) was added, and the purple solution was filtered and concentrated to approximately 5 mL. Addition of diethyl ether (40 mL) resulted in the formation of a black precipitate, which was collected by centrifugation and dried under vacuum. ^{1}H NMR and elemental analysis revealed the presence of 0.25 eq DMF and 0.08 eq ether. Yield: 610 mg (0.390 mmol, 94%). Anal. Calcd for $C_{73}H_{113}Fe_4N_5S_8 \cdot 0.25C_3H_7NO \cdot 0.08C_4H_{10}O$: C, 56.85; H, 7.44; N, 4.70; S, 16.39. Found: C, 56.76; H, 7.37; N, 4.62; S, 16.47. The ether was removed under ultra-high vacuum conditions prior to further ^{1}H and ^{13}C NMR characterization. ^{1}H NMR (300 MHz, CD_3CN): δ = 13.14 (s, very broad, 2 H, SCH_2CH_3), 7.83 (d, broad, $^3J_{H\text{-}H}$ = 6.8 Hz, 3 H, indolyl H), 7.73 (d, $^3J_{H\text{-}H}$ = 8.2 Hz, 3 H, indolyl H), 7.31 (t, $^3J_{H\text{-}H}$ = 7.4 Hz, 3 H, indolyl H), 6.95 (t, broad, 3 H, indolyl H), 6.50 (s, broad, 6 H, NCH_2), 3.07 (t, broad, $^3J_{H\text{-}H}$ = 7.9 Hz, 16 H, *n*-Bu_4N^+ α-CH_2), 2.55-2.35 (m, broad, 9 H, SCH_2CH_3 and TriS CH_2CH_3), 1.61 (s, broad, 16 H, *n*-Bu_4N^+ β-CH_2), 1.36 (sextet, broad, $^3J_{H\text{-}H}$ = 6.5 Hz, 16 H, *n*-Bu_4N^+ γ-CH_2), 1.19 (s, broad, 9 H, TriS CH_2CH_3), 0.97 (t, $^3J_{H\text{-}H}$ = 6.9 Hz, 24 H, *n*-Bu_4N^+ CH_3). ^{13}C{^{1}H} NMR (75 MHz, CD_3CN): 146.21 (aryl C), 139.51 (indolyl C), 132.47 (aryl C), 122.26, 120.86, 120.82, 111.01 (4 × indolyl C), 60.32 (*n*-Bu_4N^+ α-C), 42.15 (TriS NCH_2), 24.80 (*n*-Bu_4N^+ β-C), 24.00 (TriS CH_2CH_3), 20.89 (*n*-Bu_4N^+ γ-C), 16.26 (TriS CH_2CH_3), 14.25 (*n*-Bu_4N^+ CH_3). The signals of the EtS^- ligand and three of the indolyl C atoms were not observed. λ_{max} (MeCN), nm: 221 sh, 243 sh, 280 sh, 316 sh. FT-IR (ATR, ν, cm^{-1}): 2959, 2871, 1454, 1380, 1335, 1295, 1246, 1204, 1170, 1150, 1010, 880, 791, 735. $E_{1/2}$ vs. Fc/Fc^+ in CH_2Cl_2 = –1.70 V (ΔE_p = 110 mV) [2–/3–], –0.56 (ΔE_p = 90 mV) [2–/1–]. $E_{1/2}$ vs. SCE in CH_2Cl_2 = –1.27 V [2–/3–], –0.13 V [2–/1–]. ESI-MS: *m*/*z* = 527.1 ($[Fe_4S_4(TriS)(SEt)]^{2-}$, calcd *m*/*z* = 527.9).

$[Fe(tpySH)_2](PF_6)_2$ (6). TpySH[9] (79.5 mg, 0.300 mmol) was stirred in EtOH (10 mL) for 15 min. A solution of $(NH_4)_2Fe(SO_4)_2 \cdot 6H_2O$ (61.0 mg, 0.156 mmol) in H_2O (10 mL) was then added dropwise, and the mixture immediately turned purple. After stirring for an additional 10 min, the mixture was filtered over Celite into a solution of NH_4PF_6 (150 mg, 0.920 mmol) in H_2O (50 mL). A purple precipitate was collected by centrifugation, washed with water (10 mL) and ether (50 mL), and dried *in vacuo*. Yield: 108 mg (0.123 mmol, 82%). Anal. Calcd for $C_{30}H_{22}F_{12}FeN_6P_2S_2$: C, 41.11; H, 2.53; N, 9.59; S, 7.32. Found: C, 41.28; H, 2.60; N, 9.58; S, 7.15. ^{1}H NMR (400 MHz, CD_3CN): δ = 8.82 (s, 4 H, H3'), 8.34 (d, $^3J_{H\text{-}H}$ = 6.4 Hz, 4 H, H3), 7.86 (t, $^3J_{H\text{-}H}$ = 7.0 Hz, 4 H, H4), 7.15 (d, $^3J_{H\text{-}H}$ = 5.2 Hz, 4 H, H6), 7.06 (t, $^3J_{H\text{-}H}$ = 6.4 Hz, 4 H, H5), 5.29 (s, broad, 2 H, SH). ^{13}C{^{1}H} NMR (100 MHz, CD_3CN): δ = 160.01, 158.64, 154.30, 139.58, 128.22, 124.49, 123.96. The signal of one remaining carbon nucleus could not be resolved. λ_{max} (MeCN), nm (ε, M^{-1} cm^{-1}): 242 (31000), 282 (64000), 317 (37000), 359 sh (6800), 564 (15000). FT-IR (ATR, ν, cm^{-1}): 3117, 2582, 1605, 1467, 1431, 1404, 1126, 907, 823, 788, 753. $E_{1/2}$ vs. Fc/Fc^+ in MeCN = +0.74 V (ΔE_p = 38 mV) [2+/3+]. $E_{1/2}$ vs. SCE in MeCN = +1.12 V [2+/3+]. ESI-MS: *m*/*z* = 293.46 ($[Fe(tpySH)_2]^{2+}$, calcd *m*/*z* = 293.54), 585.16 ([Fe(tpySH)(tpyS)]$^+$, calcd 585.06), 730.97 ({$[Fe(tpySH)_2](PF_6)$}$^+$, calcd 731.03).

$[Fe(tpyS)_2]$ (7). TpySH[9] (63.6 mg, 0.240 mmol) was stirred in EtOH (8 mL) for 15 min. A solution of $(NH_4)_2Fe(SO_4)_2 \cdot 6H_2O$ (48.7 mg, 0.124 mmol) in H_2O (8 mL) was then added dropwise, and the mixture immediately turned purple. After stirring for an additional 10 min, the mixture was filtered over Celite.

Addition of aqueous 1 M NaOH (40 mL) resulted in the precipitation of a black powder, which was collected by centrifugation, washed with H_2O (2 × 40 mL) and dried *in vacuo*. Yield: 47.7 mg (0.0816 mmol, 68%). Anal. Calcd for $C_{30}H_{20}FeN_6S_2$: C, 61.65; H, 3.45; N, 14.38; S, 10.97. Found: C, 61.54; H, 3.58; N, 14.25; S, 10.90. ^{1}H NMR (400 MHz, CD_2Cl_2): 8.72 (s, 4 H, H3'), 8.07 (d, $^3J_{H\text{-}H}$ = 8.1 Hz, 4 H, H3), 7.65 (t, $^3J_{H\text{-}H}$ = 7.7 Hz, 4 H, H4), 7.28 (d, $^3J_{H\text{-}H}$ = 5.3 Hz, 4 H, H6), 6.93 (t, $^3J_{H\text{-}H}$ = 6.5 Hz, 4 H, H5). ^{13}C{^{1}H} NMR (100 MHz, CD_2Cl_2): δ = 160.56, 155.51, 153.52, 137.52, 130.20, 126.11, 121.95. The signal of one remaining carbon nucleus could not be resolved. λ_{max} (MeCN), nm: 239, 277, 285, 316, 394, 603. Due to the instability of **7** in solution, extinction coefficients were not determined. FT-IR (ATR, ν, cm^{-1}): 1592, 1558, 1461, 1424, 1391, 1337, 1117, 1101, 1028, 1014, 836, 784, 754, 689. $E_{1/2}$ vs. Fc/Fc$^+$ in CH_2Cl_2 = +0.63 V (ΔE_p = 78 mV) [2+/3+]. $E_{1/2}$ vs. SCE in CH_2Cl_2 = +1.05 V [2+/3+].

(*n*-Bu$_4$N)$_2$[{Fe$_4$S$_4$(TriS)(μ-Stpy)}$_2$Fe] (8). A solution of **6** (20.0 mg, 0.0228 mmol) in DMF (2.5 mL) was added to a solution of **5**·0.26DMF·0.12Et$_2$O (71.6 mg, 0.0456 mmol) in DMF (2.5 mL). The mixture was stirred for 1 h and then periodically evacuated for 30 min. Overnight vapor diffusion of ether led to the precipitation of a black, amorphous product, which was collected by centrifugation and dried *in vacuo*. Elemental analysis indicated the presence of 1 eq DMF. Yield: 42.3 mg (0.0135 mmol, 59%). Anal. Calcd for $C_{140}H_{164}Fe_9N_{14}S_{16}\cdot C_3H_7NO$: C, 54.84; H, 5.50; N, 6.71; S, 16.38. Found: C, 54.45; H, 5.36; N, 6.35; S, 16.53. ^{1}H NMR (400 MHz, CD_3CN): 7.89–7.67 (m, broad, 20 H, 2 × indolyl H, tpyS H3, H4), 7.32–7.13 (m, broad, 20 H, indolyl H, tpyS H5, H6), 6.97 (s, broad, 6 H, indolyl H), 6.65 (s, 12 H, NCH_2), 3.06 (s, broad, 16 H, *n*-Bu_4N^+ α-CH_2), 2,43 (s, broad, 12 H, TriS CH_2CH$_3$), 1.59 (s, broad, 16 H, *n*-Bu_4N^+ β-CH_2), 1.34 (s, broad, 16 H, *n*-Bu_4N^+ γ-CH_2), 1.18 (s, broad, 18 H, TriS CH$_2$CH_3), 0.96 (t, $^3J_{H\text{-}H}$ = 6.6 Hz, 24 H, *n*-Bu_4N^+ CH_3). λ_{max} (MeCN), nm: 223 sh, 242 sh, 279, 285, 314, 375 (sh), 598. FT-IR (ATR, ν, cm^{-1}): 2958, 2870, 1663, 1588, 1451, 1386, 1333, 1295, 1199, 1150, 1100, 1010, 825, 786, 737. $E_{1/2}$ vs. Fc/Fc$^+$ in CH_2Cl_2 = –1.48 V (ΔE_p = 82 mV) [2–/4–]. $E_{1/2}$ vs. SCE in CH_2Cl_2 = –1.06 V [2–/4–].

2.5. References.

[1] (a) Nicolet, Y.; Piras, C.; Legrand, P.; Hatchikian, C. E.; Fontecilla-Camps, J. C. *Structure* **1999**, *7*, 13–23. (b) Peters, J. W.; Lanzilotta, W. N.; Lemon, B. J.; Seefeldt, L. C. *Science* **1998**, *282*, 1853–1858.

[2] (a) Doukov, T. I.; Iverson, T. M.; Seravalli, J.; Ragsdale, S. W.; Drennan, C. L. *Science* **2002**, *298*, 567–572. (b) Darnault, C.; Volbeda, A.; Kim, E. J.; Legrand, P.; Vernede, Z.; Lindahl, P. A.; Fontecilla-Camps, J. C. *Nat. Struct. Biol.* **2003**, *10*, 271–279.

[3] Crane, B. R.; Siegel, L. M.; Getzoff, E. D. *Science* **1995**, *270*, 59–67.

[4] (a) Cai, L.; Weigel, J. A.; Holm, R. H. *J. Am. Chem. Soc.* **1993**, *115*, 9289–9290. (b) Cai, L.; Holm, R. H. *J. Am. Chem. Soc.* **1994**, *116*, 7177–7188. (c) Zhou, C.; Cai, L.; Holm, R. H. *Inorg. Chem.* **1996**, *35*, 2767–2772.

[5] Tard, C.; Liu, X.; Ibrahim, S. K.; Bruschi, M.; De Gioia, L.; Davies, S. C.; Yang, X.; Wang, L.-S.; Sawers, G.; Pickett, C. J. *Nature* **2005**, *433*, 610–613.

[6] (a) Osterloh, F.; Saak, W.; Pohl, S. *J. Am. Chem. Soc.* **1997**, *119*, 5648–5656. (b) Osterloh, F.; Saak, W.; Haase, D.; Pohl, S. *Chem. Commun.* **1996**, 777–778.

[7] Cao, G. *Nanostructures & Nanomaterials: Synthesis, Properties & Applications*; Imperial College Press: London, the United Kingdom, 2004.

[8] Park, J.; Pasupathy, A. N.; Goldsmith, J. I.; Chang, C.; Yaish, Y.; Petta, J. R.; Rinkoski, M.; Sethna, J. P.; Abruña, H. D.; McEuen, P. L.; Ralph, D. C. *Nature* **2002**, *417*, 722–725.

[9] Constable, E. C.; Hermann, B. A.; Housecroft, C. E.; Neuburger, M.; Schaffner, S.; Scherer, L. J. *New. J. Chem.* **2005**, *29*, 1475–1481.

[10] Stack, T. D. P.; Holm, R. H. *J. Am. Chem. Soc.* **1987**, *109*, 2546–2547.
[11] Whitener, M. A.; Peng, G.; Holm, R. H. *Inorg. Chem.* **1991**, *30*, 2411–2417.
[12] Evans, D. J.; Garcia, G.; Leigh, G. J.; Newton, M. S.; Santana, M. D. *J. Chem. Soc., Dalton Trans.* **1992**, 3229–3234.
[13] (a) van Strijdonck, G. P. F.; van Haare, J. A. E. H.; van der Linden, J. G. M.; Steggerda, J. J.; Nolte, R. J. M. *Inorg. Chem.* **1994**, *33*, 999–1000. (b) van Strijdonck, G. P. F.; van Haare, J. A. E. H.; Hönen, P. J. M.; van den Schoor, R. C. G. M.; Feiters, M. C.; van der Linden, J. G. M.; Steggerda, J. J.; Nolte, R. J. M. *J. Chem. Soc., Dalton Trans.* **1997**, 449–461.
[14] Walsdorff, C.; Saak, W.; Pohl, S. *J. Chem. Soc., Dalton Trans.* **1997**, 1857–1861.
[15] Topolski, M. *J. Org. Chem.* **1995**, *60*, 5588–5594.
[16] (a) Stack, T. D. P.; Weigel, J. A.; Holm, R. H. *Inorg. Chem.* **1990**, *29*, 3745–3760. (b) Daley, C. J. A.; Holm, R. H. *J. Inorg. Biochem.* **2003**, *97*, 287–298.
[17] (a) Bobrik, M. A.; Que, L., Jr.; Holm, R. H. *J. Am. Chem. Soc.* **1974**, *96*, 285–287. (b) Que, L., Jr.; Bobrik, M. A.; Ibers, J. A.; Holm, R. H. *J. Am. Chem. Soc.* **1974**, *96*, 4168–4178.
[18] Holm, R. H.; Phillips, W. D.; Averill, B. A.; Mayerle, J. J.; Herskovitz, T. *J. Am. Chem. Soc.* **1974**, *96*, 2109–2117.
[19] Hathcock, D. J.; Stone, K.; Madden, J.; Slattery, S. J. *Inorg. Chim. Acta* **1998**, *282*, 131–135.
[20] Chambers, J.; Eaves, B.; Parker, D.; Claxton, R.; Ray, P. S.; Slattery, S. J. *Inorg. Chim. Acta* **2006**, *359*, 2400–2406.
[21] Constable, E. C.; Housecroft, C. E.; Neuburger, M.; Phillips, D.; Raithby, P. R.; Schofield, E.; Sparr, E.; Tocher, D. A.; Zehnder, M.; Zimmermann, Y. *J. Chem. Soc., Dalton Trans.* **2000**, 2219–2228.
[22] Maestri, M.; Armaroli, N.; Balzani, V.; Constable, E. C.; Cargill Thompson, A. M. W. *Inorg. Chem.* **1995**, *34*, 2759–2767.
[23] Fallahpour, R.-A.; Neuburger, M.; Zehnder, M. *New. J. Chem.* **1999**, 53–61.
[24] (a) Steer, R. P.; Ramamurthy, V. *Acc. Chem. Res.* **1988**, *21*, 380–386. (b) Maciejewski, A.; Steer, R. P. *Chem. Rev.* **1993**, *93*, 67–98.
[25] (a) Constable, E. C.; Mundwiler, S. *Polyhedron* **1999**, *18*, 2433–2444. (b) Gaspar, A. B., Muñoz, M. C.; Niel, V.; Real, J. A. *Inorg. Chem.* **2001**, *40*, 9–10.
[26] (a) Coe, B. J.; Hayat, S.; Beddoes, R. L.; Helliwell, M.; Jeffery, J. C.; Batten, S. R.; White, P. S. *J. Chem. Soc., Dalton Trans.* **1997**, 591–599. (b) Diógenes, I. C. N.; Sousa, J. R.; Carvalho, I. M. M.; Temperini, M. L. A.; Tanaka, A. A.; Moreira, I. S. *Dalton Trans.* **2003**, 2231–2236.
[27] Constable, E. C.; Housecroft, C. E.; Cargill Thompson, A.; Passaniti, P.; Silvi, S.; Maestri, M.; Credi, A. *Inorg. Chim. Acta* **2007**, *360*, 1102–1110.
[28] Hansch, C.; Leo, A.; Taft, R. W. *Chem. Rev.* **1991**, *91*, 165–195.
[29] Zhou, C.; Holm, R. H. *Inorg. Chem.* **1997**, *36*, 4066–4077.
[30] Stack, T. D. P.; Carney, M. J.; Holm, R. H. *J. Am. Chem. Soc.* **1989**, *111*, 1670–1676.
[31] Walsdorff, C.; Saak, W.; Haase, D.; Pohl, S. *Chem. Commun.* **1997**, 1931–1932.
[32] (a) Huang, J.; Mukerjee, S.; Segal, B. M.; Akashi, H.; Zhou, J.; Holm, R. H. *J. Am. Chem. Soc.* **1997**, *119*, 8662–8674. (b) Challen, P. R.; Koo, S.-M.; Dunham, W. R.; Coucouvanis, D. *J. Am. Chem. Soc.* **1990**, *112*, 2455–2456. (c) Cai, L.; Weigel, J. A.; Holm, R. H. *J. Am. Chem. Soc.* **1993**, *115*, 9289–9290. (d) Cai, L.; Holm, R. H. *J. Am. Chem. Soc.* **1994**, *116*, 7177–7188. (e) Hoveyda, H. R.; Holm, R. H. *Inorg. Chem.* **1997**, *36*, 4571–4578.
[33] Barclay, J. E.; Diaz, M. I.; Evans, D. J.; Garcia, G.; Santana, M. D.; Torralba, M. C. *Inorg. Chim. Acta* **1997**, *258*, 211–219.
[34] Cauquis, G.; Fahmy, H. M.; Pierre, G.; Elnagdi, M. H. *Electrochim. Acta* **1979**, *24*, 391–394.
[35] Bruins, A. P.; Covey, T. R.; Henion, J. D. *Anal. Chem.* **1987**, *59*, 2642–2646.

[36] Masui, M.; Sayo, H.; Tsuda, Y. *J. Chem. Soc. B* **1968**, 973–976.
[37] Kolthoff, I. M.; Thomas, F. G. *J. Phys. Chem.* **1965**, *69*, 3049–3058.
[38] Harris, R. L. N. *Tetrahedron Lett.* **1969**, 4465–4466.
[39] Vacca, A.; Nativi, C.; Cacciarini, M.; Pergoli, R.; Roelens, S. *J. Am. Chem. Soc.* **2004**, *126*, 16456–16465.
[40] Christou, G. C.; Garner, C. D. *J. Chem. Soc., Dalton Trans.* **1979**, 1093–1094.

Chapter 3

N-Substituted Indole-3-Thiolate [4Fe-4S] Clusters with a Unique and Tunable Combination of Spectral and Redox Properties

Abstract. *A series of* N-*substituted indole-3-thiols, synthesized by sequential alkylation, thiouronium salt formation, and hydrolysis, is used to generate a novel family of [4Fe-4S] clusters. The redox transitions of the clusters deviate from those of other [4Fe-4S] cluster families, with half-wave potentials lying in a range midway between those of [4Fe-4S] clusters bound by aliphatic thiolate ligands and those bound by thiophenolate-based ligands. In UV-vis spectroscopy, the new cluster family shows absorption maxima that are among the most red-shifted reported thus far in [4Fe-4S] cluster chemistry. The indole-3-thiolate ligand thus leads to a highly specific and uncommon combination of [4Fe-4S] cluster properties, which can be fine-tuned by facile derivatization at the indole nitrogen atom.*

van der Geer, E. P. L.; Li, Q.; van Koten, G.; Klein Gebbink, R. J. M.; Hessen, B. *Inorg. Chim. Acta*, in press.

3.1. Introduction.

The cuboidal [4Fe-4S] cluster is one of the most abundant and ancient protein cofactors found in Nature. Endowed with a rich redox chemistry, [4Fe-4S] clusters serve vital biological roles, including electron transport, sensing, and catalysis.[1,2] In conjunction with its importance in living systems, the synthetic accessibility of the [4Fe-4S] cluster has resulted in it being the focus of intense research since the beginning of biomimetic chemistry in the 1970s. Since then, a myriad of synthetic analogues has been prepared and analyzed, most of them in the 2– state.[3]

Some of the most interesting results in the field have been obtained utilizing tripodal ligands preorganized to chelate three of the four iron atoms in the [4Fe-4S] cluster, leaving one iron atom free to undergo site-specific substitution chemistry.[4] The first such ligand to be reported was $L(SH)_3$ (Chart 1), prepared by Holm and co-workers, and numerous 3:1 site-differentiated cluster compounds with $L(SH)_3$ have since been prepared.[3-5] However, the difficult synthesis of $L(SH)_3$ has prevented its widespread use in biomimetics and several alternatives to $L(SH)_3$ have been reported. Of these alternatives, the $TriSH_3$ ligand (Chart 1), reported by Pohl and co-workers in 1997, is arguably the most promising.[6] Not only is $TriSH_3$ the only alternative to $L(SH)_3$ for which 1:1 reaction stoichiometry with [4Fe-4S] clusters has been proven crystallographically,[6] but our recent optimization of the synthesis of $TriSH_3$ has also rendered its preparation both convenient and high-yielding.[7]

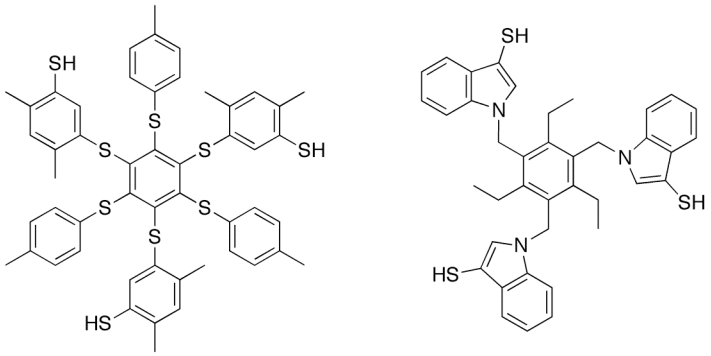

Chart 1. The tripodal ligands $L(SH)_3$ and $TriSH_3$.

The synthetic accessibility of $TriSH_3$ is based in part on the versatility of indole. Indole can not only be easily substituted at the nitrogen atom, but can also undergo regioselective electrophilic aromatic substitutions on the third position of the five-membered ring.[8] Taking advantage of this property, Harris has reported the synthesis of indole-3-thiouronium iodide using thiourea and KI_3 as oxidant. The thiouronium salt was subsequently hydrolyzed to indole-3-thiol, a thiol that is aromatic but not nearly as acidic as thiophenol.[9] Indole-3-thiol can then be further derivatized to form $TriSH_3$.[6,7]

Despite the obvious relation of $TriSH_3$ to monodentate indole-3-thiols, [4Fe-4S] clusters fully coordinated by indole-3-thiolate ligands have yet to be reported. Nevertheless, the combination of ligand aromaticity and high electron-donating ability may lead to interesting, novel properties, while *N*-substitution allows for facile derivatization. In this paper, we report the use of sequential *N*-substitution and thiouronium salt formation to synthesize new, *N*-substituted indole-3-thiols, and the application of these thiols to generate an indole-3-thiolate-based family of [4Fe-4S] clusters.

3.2. Results and discussion.

3.2.1. Synthesis of *N*-substituted indole-3-thiols 2a–2e and [4Fe-4S] clusters 3a–3e.

In order to test the general applicability of our synthetic approach to [4Fe-4S] clusters with alkyl- and aryl-substituted indole-3-thiolate ligands, we synthesized a series of five indole-3-thiols with varying *N*-substituents (Scheme 1). Unsubstituted indole-3-thiol **2a**[7,9] and its methyl-[10] and benzyl-substituted[6] analogues **2b** and **2e** have been prepared previously by Harris's method, although synthetic details for **2b** and **2e** were not reported. Two alkyl-substituted indole-3-thiols with longer aliphatic substituents (**2c** = pentyl, **2d** = decyl) were prepared analogously from the known compounds 1-pentylindole[11] and 1-decylindole.[12] The two-step yields of thiols **2b**–**2e** ranged from 40 to 63%.

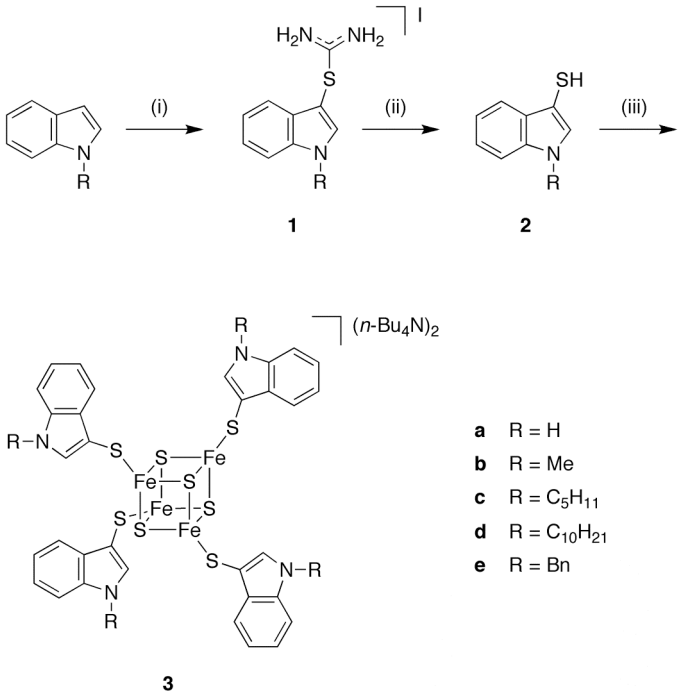

Scheme 1. Synthesis of clusters **3a**–**3e**. Conditions: (i) thiourea/KI_3 in $MeOH/H_2O$; (ii) 1. $NaOH_{(aq)}$ 2. $HCl_{(aq)}$; (iii) $(n\text{-}Bu_4N)_2[Fe_4S_4(S\text{-}t\text{-}Bu)_4]$ in DMF, vacuum.

Indole-3-thiols **2a**–**2e** were then used to generate the five new [4Fe-4S] clusters **3a**–**3e** by means of thiol exchange reactions[13,14] in DMF (Scheme 1). In each case, the formation of a deep violet color accompanied product formation. After reaction, the clusters **3a**–**3e** could be isolated easily by means of precipitation from DMF or CH_2Cl_2, with elemental analyses confirming the high purity of the products.

The physical-chemical effects of *N*-substitution are clearly manifest in the differential solubilities of clusters **3a**–**3e**. While unsubstituted cluster **3a** is insoluble in CH_2Cl_2, solubility is good for clusters **3b**–**3e**, and **3d** even shows appreciable solubility in 10:1 mixtures of ether and CH_2Cl_2. **3b**–**3e** further show good solubility in MeCN, THF, DMSO, and DMF. The decyl chains give **3d** a greasy texture, in line with the amphiphilic properties of 1-decylindole reported by Abel and co-workers.[12] Variation of the *N*-substituent in this new [4Fe-4S] cluster family thus allows effective tuning of cluster lipophilicity.

3.2.2. ^{1}H NMR spectroscopy.

The ^{1}H NMR spectra of clusters **3a**–**3e** show the characteristic contact shifting expected for ligands bound to a [4Fe-4S] cluster (Figure 1, Table 1).[15]

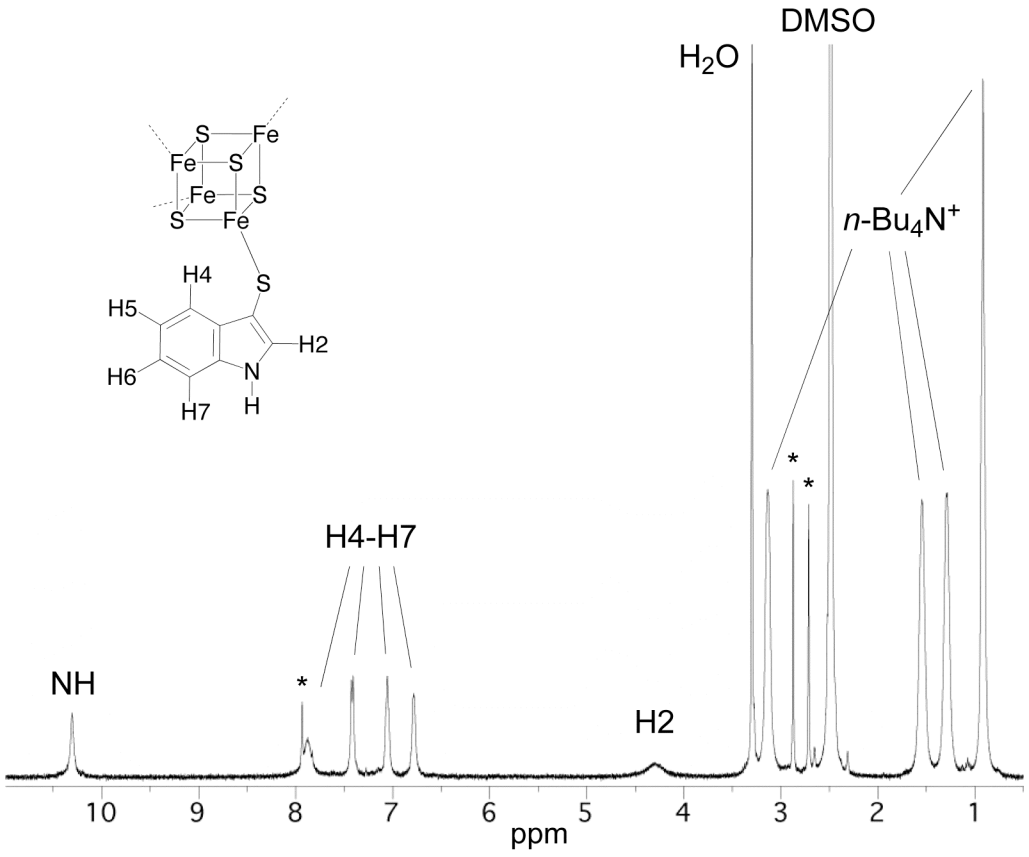

Figure 1. ^{1}H NMR spectrum of **3a** in DMSO-d_6. DMF signals are marked with asterisks.

Table 1. Contact shifts (vs. free ligands) of selected hydrogen atoms in **3a**–**3e**.

Compound	R	Contact shift, ppm		
		H2	NH	α-H
3a	H	–3.09	–0.89	n/a
3b	Me	–2.77	n/a	0.70
3c	C_5H_{11}	–2.72	n/a	0.43
3d	$C_{10}H_{21}$	–2.68	n/a	0.44
3e	Bn	–2.60	n/a	0.26

Throughout the series of clusters, the contact shifting is greatest for the indolyl H2 nucleus. This proton is bound to the ring at a position which receives delocalized positive spin density from the cluster-bound sulfur atom, and it is also the hydrogen atom closest to the cluster. Interestingly, a ^{1}H NMR signal was never observed for the analogous H2 protons of $TriSH_3$ after coordination to [4Fe-4S] clusters.[6,7]

Within the group of clusters **3a**–**3e**, the magnitude of the H2 contact shift is highest in non-alkylated cluster **3a**. *N*-methylation decreases the contact shift by more than 0.3 ppm, while extension of the alkyl chain through the pentyl to the decyl group leads to a further decrease of almost 0.1 ppm. This indicates that electron-releasing substituents on the indole nitrogen atom have a significant effect on the spin density at the H2 atom. The strongest H2 contact shift attenuation, however, is observed upon substitution with a benzyl group. The reason for this effect is unclear, but may be related to a difference in shielding of the H2 atom caused by the orientation of the benzyl group upon coordination of **2e** to a [4Fe-4S] cluster.

For the unsubstituted cluster **3a**, the contact shift of the NH proton is also negative, albeit significantly less negative than that of the H2 proton. The fact that both the NH and H2 protons are shifted to lower frequencies by contact interactions indicates the presence of same-sign spin densities at positions 1 and 2 of the indole-3-thiolate ligand. An analogous spin distribution has been found in the indole radical cation,[16] but is in contrast with thiophenolate-based systems, in which neighboring hydrogen atoms generally display opposite-sign contact shifts.[15]

While the NH protons in **3a** display a negative contact shift, the shifts of the indole substituent α protons in **3b**–**3e** are all positive. This observation parallels the results obtained by Holm and co-workers, who also observed opposite-sign contact shifts for the *para* hydrogen atom in $[Fe_4S_4(SPh)_4]^{2-}$ and the methyl protons in its *p*-tolyl analogue, $[Fe_4S_4(SC_6H_4\text{-}p\text{-}Me)_4]^{2-}$.[15] Meanwhile, the magnitudes of the α proton contact shifts follow a similar trend as that observed for the H2 protons. The methyl protons show a positive shift of 0.70 ppm, which is significantly larger than for the pentyl and decyl α methylene signals. Again, the smallest contact shift is observed for the benzyl substituent.

3.2.3. Cyclic voltammetry.

The electrochemical properties of **3b**–**3e** were studied by cyclic voltammetry in CH_2Cl_2 while, due to its insolubility in this solvent, **3a** was studied in MeCN. For comparison, a cyclic voltammogram in MeCN was also obtained for **3b** (Table 2).

Table 2. Electrochemical data for **3a**–**3e** (vs. SCE, 100 mV/s).

Compound	R	Solvent	$E_{1/2}$ [2–/3–] (V)	ΔE_p (mV)	$E_{1/2}$ [2–/1–] (V)	ΔE_p (mV)
3a	H	MeCN	–1.17	62	irreversible	n/a
3b	Me	MeCN	–1.16	98	irreversible	n/a
3b	Me	CH_2Cl_2	–1.17	75	–0.10	68
3c	C_5H_{11}	CH_2Cl_2	–1.22	84	–0.14	72
3d	$C_{10}H_{21}$	CH_2Cl_2	–1.20	110	–0.14	72
3e	Bn	CH_2Cl_2	–1.18	107	–0.12	65

Each of the clusters **3b**–**3e** undergoes a chemically reversible 2–/3– transition in CH_2Cl_2 solution (Figure 2). The peak currents vary linearly with the square root of the scan rate, as expected for an electrochemically reversible process. However, the peak separations exceed the theoretical value of 59 mV and increase with the scan rate, implying that the 2–/3– transition is quasi-reversible.

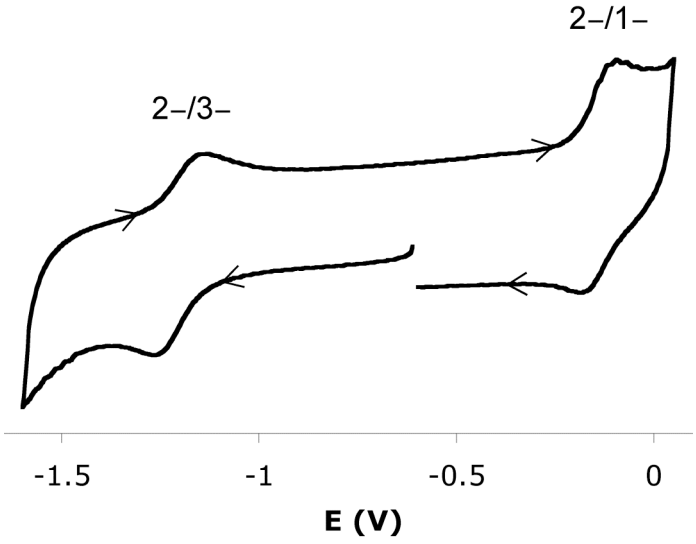

Figure 2. Cyclic voltammogram of **3d** in CH_2Cl_2 (vs. SCE, 100 mV/s).

The 2–/1– transitions, on the other hand, are not chemically reversible. Similar to the related, TriS-chelated [4Fe-4S] clusters,[7] the oxidation waves for these transitions are significantly more intense than the corresponding reduction waves, implying that the 1– state decomposes on the time scale of the cyclic voltammetry experiment. The asymmetry between the waves can be reduced by increasing the scan rate, thereby limiting the extent of decomposition.

From the redox potentials in Table 2, it is evident that the *N*-substituent has a subtle but observable effect on the electrochemical properties of **3b**–**3e**. Reduction of the pentyl- and decyl-substituted clusters **3c** and **3d** requires potentials of –1.22 and –1.20 V vs. SCE, respectively. Benzylated cluster **3e** displays the 2–/3– redox process at the slightly less negative potential of –1.18 V, while methylated cluster **3b** is the most easily reduced cluster of the series ($E_{1/2}$ = –1.17 V). A similar trend is exhibited by the 2–/1– transition.

For [4Fe-4S] clusters coordinated by *para*-substituted thiophenolates, the redox potential displays a linear dependence on the Hammett σ_p values.[17] The effect of the *N*-substituent on the redox potential of **3b**–**3e**, however, appears to be less straightforward. This is clearly exemplified by decyl-substituted compound **3d**, which displays a slightly less negative 2–/3– redox potential than **3c** despite its longer alkyl chain.

The electrochemistry of cluster **3a**, which is insoluble in CH_2Cl_2, was studied in MeCN. The cyclic voltammogram only shows reversibility for the 2–/3– process, with the 1– state apparently unstable in the presence of potentially nucleophilic solvent molecules (Figure 3). The observed peak separation for the 2–/3– redox process is close to the theoretical minimum of 59 mV, but increases with increasing scan speed, implying quasi-reversibility. Again, a linear relationship exists between the peak potentials and the square root of the scan speed.

In MeCN, methyl-substituted cluster **3b** shows similar cyclic voltammetry behavior to **3a**, despite the electron-donating ability of the methyl group. A possible explanation for this result is the fact that the NH groups in **3a** can hydrogen-bond to electron-rich solvent molecules, thereby parallelling the effects of methylation. Intramolecular N–H–S hydrogen bonds are known to lead to positive redox potential shifts in CH_2Cl_2.[18,19,20] The rigidity of the indole-3-thiolate ligand prevents such intramolecular hydrogen bonding in **3a**, leaving the NH groups free to hydrogen bond with MeCN.

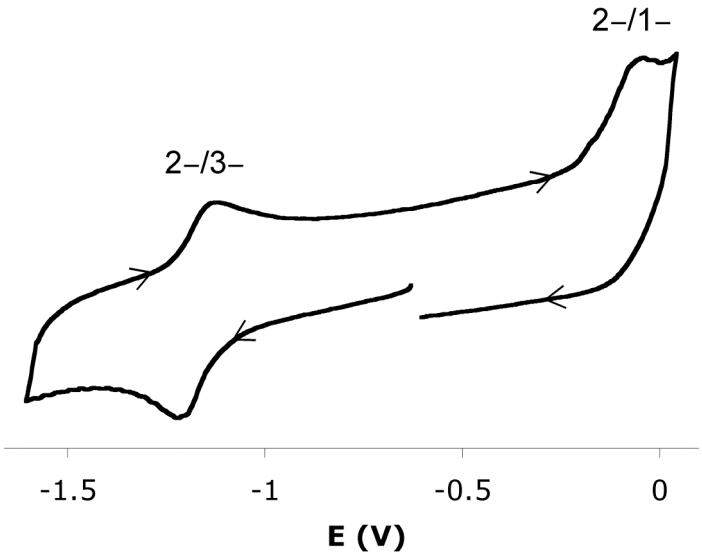

Figure 3. Cyclic voltammogram of **3a** in MeCN (vs. SCE, 100 mV/s).

In general, all the redox potentials in Table 2 are more negative than the potentials found for symmetrically substituted, thiophenolate-bound [4Fe-4S] clusters in MeCN and CH_2Cl_2, but more positive than those observed in clusters with alkylthiolate ligands.[17,21] In fact, it appears that the redox processes of indole-3-thiolate [4Fe-4S] clusters occur in an intermediate potential range deviating from the redox potentials of all other symmetrically substituted [4Fe-4S] clusters, thereby reflecting the intermediate electron-donating strength of indole-3-thiolate ligands.[7] The closest redox potential that we could find in literature for a symmetrically substituted [4Fe-4S] cluster is that of $(Me_4N)_2[Fe_4S_4(SC_6H_4\text{-}p\text{-}NMe_2)_4]$, reported by Holm and co-workers.[17] The highly electron-donating dimethylamino substituent in this cluster shifts the redox potential to approximately –1.1 V, which, however, is still substantially less negative than the redox potential of **3a**.[17]

On the other hand, the 3:1 site-differentiated cluster $(n\text{-}Bu_4N)_2[Fe_4S_4(TriS)(SC_6H_4\text{-}p\text{-}F)]$ (**4**) displays a 2–/3– redox potential of –1.19 V, close to the potentials of the related clusters **3b**–**3e**.[22] Cluster **4** is a mixed-ligand system, with one *p*-fluorothiophenolate ligand and three indole-3-thiolate binding moieties belonging to the $TriS^{3-}$ ligand. Johnson and Holm have demonstrated that in such mixed-ligand clusters, the redox properties are determined by the sum of the four, independent ligand contributions.[23] Given that the redox potential of $(n\text{-}Bu_4N)_2[Fe_4S_4(SC_6H_4\text{-}p\text{-}F)_4]$ (**5**) is –1.01 V,[22] the contribution of each indole-3-thiolate arm to the redox potential of **4** is then $((-1.19 - (0.25 \times -1.01))/3)$ V = –0.3125 V. An imaginary cluster chelated by four of such arms would thus have a redox potential of –1.25 V, more negative than the potentials observed for **3b**–**3e**. Hence, the $TriS^{3-}$ ligand appears to induce more negative redox potential shifts than non-chelating analogues. This effect possibly stems from the π electron cloud of the $TriS^{3-}$ ligand's central aryl ring, which is forced to assume a position close to the cluster core upon chelation.

The redox potentials for the 2–/1– processes in **4** and **5**, meanwhile, are –0.06 and +0.10 V, respectively.[22] Using the same reasoning as above, the contribution of each $TriS^{3-}$ indole-3-thiolate arm to the 2–/1– redox potential is then ((–0.06 – (0.25 × 0.10))/3) V = –0.028 V. A cluster chelated by four such arms would display a 2–/1– redox transition at a potential of –0.11 V, which falls in the same range as the redox potentials exhibited by **3b**–**3e**. Hence, for the 2–/1– redox process, the $TriS^{3-}$ ligand appears to behave more as the sum of three indole-3-thiolates.

3.2.4. UV-vis spectroscopy.

3a–**3e** are all intensely violet in DMF solution, and display several electronic transitions (Figure 4, Table 3).

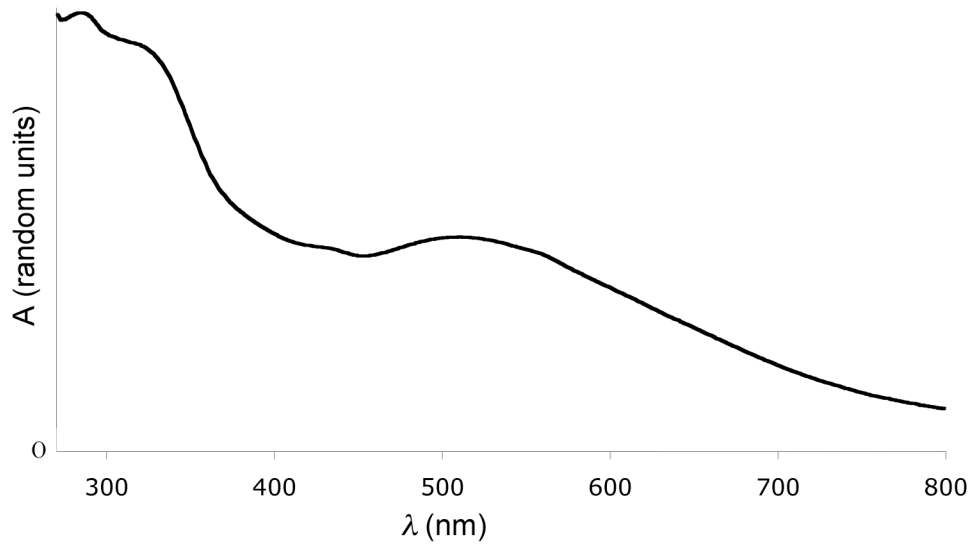

Figure 4. UV-vis spectrum of **3c** in DMF.

Table 3. Principal UV-vis absorptions of **3a**–**3e** in DMF.

Compound	R	$\lambda_{max,1}$ (nm)	$\lambda_{max,2}$ (nm)	$\lambda_{max,3}$ (nm)
3a	H	289	303*	502
3b	Me	285	304*	506
3c	C_5H_{11}	286	305*	511
3d	$C_{10}H_{21}$	287	305*	510
3e	Bn	285*	305*	500

*shoulder

All five new cluster compounds show intense absorptions between 285 and 289 nm (maxima for all clusters except **3e**) and around 304 nm (shoulders). Local maxima are also

observed between 500 and 511 nm, while additional weak features are present between 370 and 450 nm.

Transitions between 280 and 300 nm in [4Fe-4S] clusters have been assigned to charge-transfer processes from inorganic sulfide to iron 3d orbitals.[24] The energies of the corresponding transitions in the series **3a**–**3e** lie in between those generally found for clusters with purely aliphatic (297 nm and higher) and those with aromatic thiolate ligands (275 nm and lower), and are similar to that in $[Fe_4S_4(SBn)_4]^{2-}$ (approximately 286 nm).[17] Within the series **3a**–**3e**, this transition appears little affected by the indole *N*-substituent. On the other hand, *N*-substitution does to some extent affect the maxima lying between 500 and 511 nm, with significant redshifts observed upon substitution with a methyl group or with the longer pentyl and decyl chains. Benzyl-substituted cluster **3e** again behaves differently from the other clusters, displaying the least redshifted absorption. Nonetheless, even the 500 nm transition in **3e** is among the most redshifted known in [4Fe-4S] cluster chemistry. To our knowledge, **3c** even displays the most redshifted maximum in DMF solutions reported so far, approached only by the cluster $(Me_4N)_2[Fe_4S_4(SC_6H_4\text{-}p\text{-}NMe_2)_4]$ mentioned earlier (510 nm).[17] Although the exact origin of this electronic transition remains unclear, the parallel found between this cluster and **3a**–**3e** suggests that the transition is most strongly redshifted by highly electron-donating, aromatic thiolates.

3.3. Conclusion.

The thiolation of indole *via* electrophilic addition of bis(thiouronium) iodide and subsequent hydrolysis can be applied to a broad range of *N*-substituted indoles, providing convenient access to a relatively unexplored family of thiols and a corresponding family of indole-3-thiolate [4Fe-4S] clusters. The new cluster family displays several unique and distinguishing properties, including highly redshifted absorptions in the visible region and redox potentials that fall in a range deviating from all other groups of synthetic, symmetrically substituted [4Fe-4S] clusters. Their unique redox potentials make the indole-3-thiolate [4Fe-4S] clusters a valuable addition to the synthetic [4Fe-4S] clusters available for incorporation into catalysts or other functional (biomimetic) materials, in which the envisioned applications may impose strict requirements on the clusters' electrochemical properties.

Within the family of indole-3-thiolate clusters itself, facile derivatization is possible by means of substitution at the indole nitrogen atom. The current study shows that such substitution allows for fine-tuning of electrochemical, spectral, and physical properties, although the unexpected effects of *N*-benzylation indicate that the substituent effects may as yet prove difficult to predict. Apart from the fine-tuning of cluster properties, *N*-substituents may also prove useful as synthetic handles in future derivatizations.

3.4. Experimental.

General. Reactants were purchased from Acros and used as received. 1-Pentylindole and 1-decylindole were synthesized using the conditions described by Dehaen and Hassner.[25] All thiols and [4Fe-4S] clusters were handled under dry N_2 atmospheres using standard Schlenk or glovebox techniques. DMF and CH_2Cl_2 were distilled over CaH_2, while diethyl ether was distilled over Na/benzophenone. The ^{1}H NMR spectrum in Figure 2 was recorded at 298 K on a Varian spectrometer operating at 400 MHz. All other ^{1}H and ^{13}C NMR spectra were recorded at 300 K on a Bruker AC 300 spectrometer operating at 300 and 75 MHz, respectively. The spectra were calibrated on the residual solvent peaks and spectral assignments were based on chemical shift, integral, and linewidth considerations. Contact shifts were calculated vs. ^{1}H NMR shifts of the free thiols in DMSO-d_6; however, since the thiols slowly oxidized in this solvent, full spectral characterizations of the thiols were carried out in $CDCl_3$ instead. Infrared spectra were recorded on a Perkin-Elmer Spectrum One FT-IR spectrometer. UV-vis spectra were recorded on a Varian Cary 50 Scan UV-visible spectrophotometer. Elemental analyses were carried out by Kolbe Mikroanalytisches Laboratorium (Mülheim an der Ruhr, Germany). Cyclic voltammograms were recorded at 100 mV/s using Pt working and counter electrodes, a Ag/AgCl reference electrode, and 0.1 M n-Bu_4NClO_4 in CH_2Cl_2 or MeCN as supporting electrolyte. Potentials were referenced to a ferrocene (Fc) internal standard. Fc was added directly to samples of all clusters except **3d**. Here, the Fc/Fc$^+$ wave was found to overlap with irreversible, multi-electron oxidation waves, and a separate blank run with Fc was run. Potentials vs. a standard calomel electrode (SCE) were calculated by taking $E_{1/2}$ (Fc/Fc$^+$) = 0.424 V vs. SCE in CH_2Cl_2[26] and 0.379 V in MeCN.[27]

1-Methylindole-3-thiouronium iodide (1b). A solution of thiourea (0.581 g, 7.63 mmol), I_2 (1.94 g, 7.63 mmol), and KI (1.27 g, 7.63 mmol) in a 4/1 (v/v) mixture of MeOH and H_2O (30 mL) was added to 1-methylindole (1.00 g, 7.63 mmol) and stirred overnight. The solution was concentrated *in vacuo* to yield an orange, crystalline material, which was collected by filtration, washed with water and ether, and dried *in vacuo*. Yield: 2.08 g (6.24 mmol, 82%). Anal. Calcd for $C_{10}H_{12}IN_3S$: C, 36.05; H, 3.63; N, 12.61; S, 9.62. Found: C, 36.09; H, 3.58; N, 12.53; S, 9.72. ^{1}H NMR (DMSO-d_6): δ = 8.87 (s, br, 2 H, NH_2), 8.55 (s, br, 2 H, NH_2), 7.97 (s, 1 H, indolyl H2), 7.64 (d, $^3J_{H\text{-}H}$ = 8.3 Hz, 1 H, indolyl H), 7.51 (d, $^3J_{H\text{-}H}$ = 7.4 Hz, 1 H, indolyl H), 7.34 (t, $^3J_{H\text{-}H}$ = 7.6 Hz, 1 H, indolyl H), 7.25 (t, $^3J_{H\text{-}H}$ = 7.4 Hz, 1 H, indolyl H), 3.88 (s, 3 H, CH_3). ^{13}C{^{1}H} NMR (DMSO-d_6): δ = 170.71 ($C(NH_2)_2$), 139.43, 137.52, 128.72, 122.74, 121.24, 117.71, 111.16, 88.67 (8 × indolyl C), 33.27 (CH_3). FT-IR (ATR, ν, cm^{-1}): 3289, 3252, 3162, 3088, 1637, 1608, 1508, 1458, 1424, 1374, 1337, 1242, 1155, 1127, 1042, 840, 766, 745, 684.

1-Pentylindole-3-thiouronium iodide (1c). Thiourea (1.54 g, 20.2 mmol), I_2 (5.15 g, 20.3 mmol), and KI (3.37 g, 20.3 mmol) were dissolved in a 4/1 (v/v) mixture of MeOH and H_2O (150 mL). 1-Pentylindole (3.80 g, 20.3 mmol) was added after 1 h, and the dark brown solution was stirred overnight in the dark. Concentration *in vacuo* yielded a white powder, which was collected by filtration and washed with water and ether. The solid was then dissolved in acetone (10 mL), precipitated by adding ether (100 mL), collected by filtration, and dried *in vacuo*. Yield: 5.98 g (15.4 mmol, 76%). Anal. Calcd for $C_{14}H_{20}IN_3S$: C, 43.19; H, 5.18; N, 10.79; S, 8.24. Found: C, 43.08; H, 5.24; N, 10.67; S, 8.18. ^{1}H NMR (DMSO-d_6): δ = 8.69 (s, 4 H, NH_2), 8.02 (s, 1 H, indolyl H2), 7.68 (d, $^3J_{H\text{-}H}$ = 8.3 Hz, 1 H, indolyl H), 7.51 (d, $^3J_{H\text{-}H}$ = 7.7 Hz, 1 H, indolyl H), 7.33 (t, $^3J_{H\text{-}H}$ = 7.6 Hz, 1 H, indolyl H), 7.24 (t, $^3J_{H\text{-}H}$ = 7.2 Hz, 1 H, indolyl H), 4.25 (t, $^3J_{H\text{-}H}$ = 7.3 Hz, 2 H, α-CH_2), 1.83 (quintet, $^3J_{H\text{-}H}$ = 6.9 Hz, 2 H, β-CH_2), 1.38–1.27 (m, 4 H, CH_2), 0.87 (t, $^3J_{H\text{-}H}$ = 6.9 Hz, 3 H, CH_3). ^{13}C{^{1}H} NMR (DMSO-d_6): δ = 170.54 ($C(NH_2)_2$), 138.25, 136.77, 128.69, 122.61, 121.07, 117.76, 111.17, 88.85 (8 × indolyl C), 46.19, 29.02, 28.18, 21.63 (4 × CH_2), 13.71 (CH_3).

FT-IR (ATR, ν, cm^{-1}): 3309, 3248, 3078, 2930, 2870, 1637, 1610, 1507, 1456, 1425, 1224, 1181, 1042, 1010, 837, 743, 727, 678.

1-Decylindole-3-thiouronium iodide (1d). Thiourea (1.55 g, 20.4 mmol), I_2 (5.15 g, 20.3 mmol), and KI (3.37 g, 20.3 mmol) were dissolved in a 4/1 (v/v) mixture of MeOH and H_2O (150 mL). 1-Decylindole (5.22 g, 20.3 mmol) was added after 1 h, and the dark brown solution was stirred overnight in the dark. Concentration *in vacuo* yielded a yellow solid, which was collected by filtration and washed with water and ether. The solid was then dissolved in acetone (10 mL), precipitated by adding hexane (100 mL), collected by filtration, and dried *in vacuo*. Yield: 7.20 g (15.7 mmol, 77%). Anal. Calcd for $C_{19}H_{30}IN_3S$: C, 49.67; H, 6.58; N, 9.15; S, 6.98. Found: C, 49.58; H, 6.59; N, 9.11; S, 7.03. ^{1}H NMR (DMSO-d_6): δ = 8.69 (s, 4 H, NH_2), 8.01 (s, 1 H, indolyl H2), 7.67 (d, $^3J_{H\text{-}H}$ = 8.0 Hz, 1 H, indolyl H), 7.51 (d, $^3J_{H\text{-}H}$ = 7.4 Hz, 1 H, indolyl H), 7.32 (t, $^3J_{H\text{-}H}$ = 7.6 Hz, 1 H, indolyl H), 7.24 (t, $^3J_{H\text{-}H}$ = 7.0 Hz, 1 H, indolyl H), 4.24 (t, $^3J_{H\text{-}H}$ = 7.1 Hz, 2 H, α-CH_2), 1.81 (quintet, $^3J_{H\text{-}H}$ = 4.8 Hz, 2 H, β-CH_2), 1.33–1.19 (m, br, 14 H, CH_2), 0.85 (t, $^3J_{H\text{-}H}$ = 6.7 Hz, 3 H, CH_3). $^{13}C\{^1H\}$ NMR (DMSO-d_6): δ = 170.51 ($C(NH_2)_2$), 138.25, 136.77, 128.69, 122.61, 121.07, 117.76, 111.18, 88.86 (8 × indolyl C), 46.21, 31.12, 29.30, 28.76, 28.75, 28.49, 28.47, 26.00, 21.92 (9 × CH_2), 13.80 (CH_3). FT-IR (ATR, ν, cm^{-1}): 3307, 3250, 3082, 2919, 2849, 1637, 1608, 1507, 1458, 1428, 1393, 1227, 1167, 1044, 1012, 836, 740, 721, 683.

1-Benzylindole-3-thiouronium iodide (1e). To a solution of 1-benzylindole[28] (1.762 g, 8.50 mmol) in a 19/1 (v/v) mixture of MeOH and H_2O (20 mL) were added thiourea (0.647 g, 8.50 mmol), I_2 (2.157 g, 8.50 mmol), and KI (1.411 g, 8.50 mmol). The mixture was stirred overnight and evaporated to dryness. To the dark brown residue were added H_2O (30 mL) and ether (30 mL). Swirling led to the formation of a yellow powder, which was collected by filtration, washed with water and ether, and dried *in vacuo*. Yield: 1.969 g (4.81 mmol, 57%). Anal. Calcd for $C_{16}H_{16}IN_3S$: C, 46.95; H, 3.94; N, 10.27; S, 7.83. Found: C, 46.84; H, 3.87; N, 10.18; S, 7.91. ^{1}H NMR (DMSO-d_6): δ = 8.77 (s, br, 4 H, NH_2), 8.18 (s, 1 H, indolyl H2), 7.61 (d, $^3J_{H\text{-}H}$ = 7.1 Hz, 1 H, indolyl H), 7.52 (d, $^3J_{H\text{-}H}$ = 7.0 Hz, 1 H, indolyl H), 7.38–7.20 (m, 7 H, indolyl and phenyl H), 5.52 (s, 2 H, CH_2). $^{13}C\{^1H\}$ NMR (DMSO-d_6): δ = 170.49 ($C(NH_2)_2$), 138.88 (indolyl C), 136.93, 136.88, 129.02, 128.62 (2 × indolyl C and 2 × phenyl C), 127.69, 127.47 (2 × phenyl C), 122.96, 121.44, 118.02, 111.68, 89.77 (5 × indolyl C), 49.89 (CH_2). FT-IR (ATR, ν, cm^{-1}): 3303, 3250, 3084, 1636, 1609, 1503, 1459, 1427, 1388, 1343, 1250, 1200, 1157, 1081, 1046, 1012, 980, 908, 840, 732, 696.

1-Methylindole-3-thiol (2b). A suspension of **1b** (2.082 g, 6.25 mmol) in aqueous NaOH (1 M, 25 mL) was heated to 90 °C for 10 min. After cooling to ambient temperature, aqueous HCl (2 M, 12.5 mL) was added, and the solution extracted with ether (3 × 15 mL). The ether was evaporated *in vacuo* and the residue was distilled to yield a colorless oil. Yield: 0.782 g (4.79 mmol, 77%). Anal. Calcd for C_9H_9NS: C, 66.22; H, 5.56; N, 8.58; S, 19.64. Found: C, 66.08; H, 5.51; N, 8.52; S, 19.70. ^{1}H NMR ($CDCl_3$): δ = 7.73 (d, $^3J_{H\text{-}H}$ = 8.3 Hz, 1 H, indolyl H), 7.35–7.19 (m, 3 H, indolyl H), 7.15 (s, 1 H, indolyl H2), 3.77 (s, 3 H, CH_3), 2.89 (s, 1 H, SH). $^{13}C\{^1H\}$ NMR ($CDCl_3$): 137.21, 133.21, 130.66, 122.45, 120.11, 119.52, 109.58, 95.37 (8 × indolyl C), 33.05 (CH_3). FT-IR (ATR, ν, cm^{-1}): 3108, 3050, 2942, 2518, 1613, 1514, 1481, 1461, 1421, 1357, 1333, 1317, 1240, 1154, 1128, 1110, 1010, 926, 806, 735.

1-Pentylindole-3-thiol (2c). A suspension of **1c** (2.04 g, 5.24 mmol) in aqueous NaOH (1 M, 25 mL) was heated to 100 °C for 15 min. The resulting solution was cooled to ambient temperature and filtered. Addition of aqueous HCl (1 M, 25 mL) led to the separation of a yellow oil. The mixture was extracted with ether (3 × 10 mL), the combined organic extracts were dried over $MgSO_4$, and the ether was removed *in vacuo*. The residue was distilled *in vacuo* to yield a colorless oil. Yield: 0.606 g (2.76 mmol, 53%). Anal. Calcd for $C_{13}H_{17}NS$: C, 71.18; H, 7.81; N, 6.39; S, 14.62. Found: C, 71.11; H, 7.88; N, 6.32; S, 14.54. ^{1}H

NMR ($CDCl_3$): δ = 7.73 (d, $^3J_{H\text{-}H}$ = 8.1 Hz, 1 H, indolyl H), 7.34 (d, $^3J_{H\text{-}H}$ = 8.2 Hz, 1 H, indolyl H), 7.28–7.17 (m, 3 H, indolyl H), 4.08 (t, $^3J_{H\text{-}H}$ = 7.1 Hz, 2 H, α-CH_2), 2.88 (s, 1 H, SH), 1.83 (quintet, $^3J_{H\text{-}H}$ = 7.3 Hz, 2 H, β-CH_2), 1.40–1.26 (m, 4 H, CH_2), 0.89 (t, $^3J_{H\text{-}H}$ = 6.9 Hz, 3 H, CH_3). $^{13}C\{^1H\}$ NMR ($CDCl_3$): 136.55, 132.26, 130.76, 122.29, 120.04, 119.62, 109.79, 95.30 (8 × indolyl C), 46.70, 30.05, 29.21, 22.45 (4 × CH_2), 14.06 (CH_3). FT-IR (ATR, ν, cm^{-1}): 3054, 2956, 2929, 2871, 2525, 1612, 1512, 1480, 1460, 1388, 1349, 1317, 1235, 1171, 1155, 1011, 926, 804, 736.

1-Decylindole-3-thiol (2d). A suspension of **1d** (1.84 g, 4.00 mmol) in aqueous NaOH (1 M, 30 mL) was heated to 90 °C for 15 min. The resulting solution was cooled to ambient temperature, filtered, and washed with ether (5 mL). Addition of aqueous HCl (2 M, 15 mL) led to the separation of a yellow oil. The mixture was extracted with ether (3 × 10 mL), the combined organic extracts were dried over $MgSO_4$, and concentrated *in vacuo* to yield a yellow oil. Yield: 0.813 g (2.81 mmol, 70%). Anal. Calcd for $C_{18}H_{27}NS$: C, 74.68; H, 9.40; N, 4.84; S, 11.08. Found: C, 74.81; H, 9.33; N, 4.92; S, 11.13. ^1H NMR ($CDCl_3$): δ = 7.72 (d, $^3J_{H\text{-}H}$ = 7.6 Hz, 1 H, indolyl H), 7.33 (d, $^3J_{H\text{-}H}$ = 8.2 Hz, 1 H, indolyl H), 7.28–7.18 (m, 3 H, indolyl H), 4.08 (t, $^3J_{H\text{-}H}$ = 7.1 Hz, 2 H, α-CH_2), 2.87 (d, $^4J_{H\text{-}H}$ = 1.4 Hz, 1 H, SH), 1.82 (quintet, $^3J_{H\text{-}H}$ = 7.2 Hz, 2 H, β-CH_2), 1.35–1.23 (m, br, 14 H, CH_2), 0.88 (t, $^3J_{H\text{-}H}$ = 6.7 Hz, 3 H, CH_3). $^{13}C\{^1H\}$ NMR ($CDCl_3$): 136.56, 132.24, 130.75, 122.29, 120.02, 119.62, 109.78, 95.30 (8 × indolyl C), 46.70, 32.01, 30.34, 29.66, 29.62, 29.41, 29.36, 27.09, 22.82 (9 × CH_2), 14.24 (CH_3). FT-IR (ATR, ν, cm^{-1}): 3056, 2923, 2853, 2528, 1612, 1512, 1480, 1460, 1389, 1350, 1318, 1234, 1165, 1012, 927, 803, 737.

1-Benzylindole-3-thiol (2e). A suspension of **1e** (0.600 g, 1.47 mmol) in aqueous NaOH (1 M, 20 mL) was heated to 100 °C for 15 min. The resulting solution was filtered and cooled to ambient temperature. Aqueous HCl (2 M, 10 mL) was added, leading to the formation of white needles. The mixture was extracted with ether (3 × 20 mL), after which the combined organic extracts were dried over $MgSO_4$ and concentrated *in vacuo* to an off-white powder. Yield: 0.315 g (1.32 mmol, 90%). Anal. Calcd for $C_{15}H_{13}NS$: C, 75.28; H, 5.47; N, 5.85; S, 13.40. Found: C, 75.16; H, 5.41; N, 5.92; S, 13.36. ^1H NMR ($CDCl_3$): δ = 7.82–7.78 (m, 1 H, indolyl H), 7.39–7.25 (m, 8 H, indolyl and phenyl H), 7.19–7.16 (m, 1 H, indolyl H2), 5.32 (s, 2 H, CH_2), 3.06 (s, br, 1 H, SH). $^{13}C\{^1H\}$ NMR ($CDCl_3$): 137.01, 132.46, 130.86 (3 × indolyl C), 129.02, 128.01, 127.10, 127.00 (4 × phenyl C), 122.68, 120.39, 119.67, 110.09, 96.44 (5 × indolyl C), 50.40 (CH_2). FT-IR (ATR, ν, cm^{-1}): 3030, 2530, 1610, 1571, 1515, 1494, 1479, 1461, 1452, 1440, 1352, 1336, 1318, 1254, 1199, 1170, 1075, 1009, 923, 803, 738, 729, 694.

(*n*-$Bu_4N)_2[Fe_4S_4(S\text{-}3\text{-}C_8H_6N)_4]$ (3a). To a mixture of (*n*-$Bu_4N)_2[Fe_4S_4(S\text{-}t\text{-}Bu)_4]$[29] (0.100 g, 0.0838 mmol) and indole-3-thiol[7,9] (63 mg, 0.42 mmol) was added DMF (7 mL). The mixture was stirred overnight to yield a dark violet solution, which was concentrated *in vacuo*. Addition of ether (60 mL) led to the formation of a fine black precipitate, which was collected by centrifugation, washed with ether, and dried *in vacuo*. ^1H NMR revealed the presence of 1.0 eq DMF. Yield: 0.115 g (0.0765 mmol, 91%). The product was further dried under ultra-high vacuum before elemental analysis, but 0.2 eq DMF remained. Anal. Calcd for $C_{64}H_{96}Fe_4N_6S_8 \cdot 0.2C_3H_7NO$: C, 53.73; H, 6.80; N, 6.01; S, 17.76. Found: C, 53.71; H, 6.77; N, 5.95; S, 17.75. ^1H NMR (DMSO-d_6): δ = 10.35 (s, br, 4 H, NH), 7.89 (s, br, 4 H, indolyl H), 7.43 (d, $^3J_{H\text{-}H}$ = 7.6 Hz, 4 H, indolyl H), 7.07 (t, br, $^3J_{H\text{-}H}$ = 6.4 Hz, 4 H, indolyl H), 6.81 (s, br, 4 H, indolyl H), 4.34 (s, very br, 4 H, indolyl H2), 3.16 (t, $^3J_{H\text{-}H}$ = 8.4 Hz, 16 H, *n*-Bu_4N^+ α-CH_2), 1.56 (quintet, br, $^3J_{H\text{-}H}$ = 7.7 Hz, 16 H, *n*-Bu_4N^+ β-CH_2), 1.30 (sextet, $^3J_{H\text{-}H}$ = 7.1 Hz, 16 H, *n*-Bu_4N^+ γ-CH_2), 0.93 (t, $^3J_{H\text{-}H}$ = 7.3 Hz, 24 H, *n*-Bu_4N^+ CH_3). λ_{max} (DMF, nm): 289, 303 (shoulder), 502. $E_{1/2}$ vs. Fc/Fc^+ in MeCN = –1.55 V (ΔE_p = 62 mV) [2–/3–]. $E_{1/2}$ vs. SCE in MeCN = –1.17 V [2–/3–].

(n-$Bu_4N)_2[Fe_4S_4(S\text{-}3\text{-}C_8H_5N\text{-}1\text{-}CH_3)_4]$ (3b). To a solution of (n-$Bu_4N)_2[Fe_4S_4(S\text{-}t\text{-}Bu)_4]$[29] (0.129 g, 0.108 mmol) in DMF (5 mL) was added **2b** (0.088 g, 0.54 mmol). A periodic vacuum was applied to the stirred solution for 2 h, during which a color change from dark green to dark violet was observed. The solution was concentrated *in vacuo*. Addition of ether (40 mL) led to the formation of a fine black precipitate, which was collected by centrifugation, washed with ether, and dried *in vacuo*. Yield: 0.123 g (0.0828 mmol, 77%). Anal. Calcd for $C_{68}H_{104}Fe_4N_6S_8$: C, 54.98; H, 7.06; N, 5.66; S, 17.27. Found: C, 55.12; H, 7.02; N, 5.54; S, 17.20. ^{1}H NMR (DMSO-d_6): δ = 8.00 (s, br, 4 H, indolyl H), 7.45 (d, $^3J_{H\text{-}H}$ = 8.1 Hz, 4 H, indolyl H), 7.16 (t, br, $^3J_{H\text{-}H}$ = 6.8 Hz, 4 H, indolyl H), 6.81 (d, br, $^3J_{H\text{-}H}$ = 5.1 Hz, 4 H, indolyl H), 4.66 (s, very br, 4 H, indolyl H2), 4.45 (s, 12 H, NCH_3), 3.15 (t, $^3J_{H\text{-}H}$ = 7.7 Hz, 16 H, n-Bu_4N^+ α-CH_2), 1.57 (quintet, br, 16 H, n-Bu_4N^+ β-CH_2), 1.31 (sextet, $^3J_{H\text{-}H}$ = 6.9 Hz, 16 H, n-Bu_4N^+ γ-CH_2), 0.93 (t, $^3J_{H\text{-}H}$ = 7.1 Hz, 24 H, n-Bu_4N^+ CH_3). λ_{max} (DMF, nm): 285, 304 (shoulder), 506. $E_{1/2}$ vs. Fc in MeCN = –1.54 V (ΔE_p = 98 mV) [2–/3–]. $E_{1/2}$ vs. SCE in MeCN = –1.16 V [2–/3–]. $E_{1/2}$ vs. Fc/Fc^+ in CH_2Cl_2 = –1.59 V (ΔE_p = 75 mV) [2–/3–], –0.53 V (ΔE_p = 68 mV) [2–/1–]. $E_{1/2}$ vs. SCE in CH_2Cl_2 = –1.17 V [2–/3–], –0.10 V [2–/1–].

(n-$Bu_4N)_2[Fe_4S_4(S\text{-}3\text{-}C_8H_5N\text{-}1\text{-}C_5H_{11})_4]$ (3c). A solution of (n-$Bu_4N)_2[Fe_4S_4(S\text{-}t\text{-}Bu)_4]$[29] (0.0650 g, 0.0545 mmol) and **2c** (0.0538 g, 0.245 mmol) in DMF (5 mL) was stirred overnight, after which the DMF was removed *in vacuo*. The sticky black residue was dissolved in CH_2Cl_2 (10 mL) and filtered. Ether (60 mL) was added and a sticky, black product was collected by centrifugation, washed with ether, and dried under ultra-high vacuum. Yield: 0.0629 g (0.0368 mmol, 68%). Anal. Calcd for $C_{84}H_{136}Fe_4N_6S_8$: C, 59.00; H, 8.02; N, 4.91; S, 15.00. Found: C, 58.87; H, 7.91; N, 4.88; S, 14.96. ^{1}H NMR (DMSO-d_6): δ = 7.98 (s, br, 4 H, indolyl H), 7.48 (d, $^3J_{H\text{-}H}$ = 7.4 Hz, 4 H, indolyl H), 7.13 (t, br, $^3J_{H\text{-}H}$ = 5.8 Hz, 4 H, indolyl H), 6.79 (d, br, $^3J_{H\text{-}H}$ = 4.7 Hz, 4 H, indolyl H), 4.76 (s, very br, 4 H, indolyl H2), 4.56 (s, br, 8 H, pentyl α-CH_2), 3.16 (t, $^3J_{H\text{-}H}$ = 8.2 Hz, 16 H, n-Bu_4N^+ α-CH_2), 1.70 (s, 8 H, pentyl β-CH_2), 1.54 (quintet, br, $^3J_{H\text{-}H}$ = 7.7 Hz, 16 H, n-Bu_4N^+ β-CH_2), 1.31 (sextet, $^3J_{H\text{-}H}$ = 7.3 Hz, 16 H, n-Bu_4N^+ γ-CH_2), 1.23 (s, br, 16 H, pentyl CH_2), 0.93 (t, $^3J_{H\text{-}H}$ = 7.3 Hz, 24 H, n-Bu_4N^+ CH_3), 0.80 (t, br, 12 H, pentyl CH_3). λ_{max} (DMF, nm): 286, 305 (shoulder), 511. $E_{1/2}$ vs. Fc/Fc^+ in CH_2Cl_2 = –1.64 V (ΔE_p = 84 mV) [2–/3–], –0.56 V (ΔE_p = 72 mV) [2–/1–]. $E_{1/2}$ vs. SCE in CH_2Cl_2 = –1.22 V [2–/3–], –0.14 V [2–/1–].

(n-$Bu_4N)_2[Fe_4S_4(S\text{-}3\text{-}C_8H_5N\text{-}1\text{-}C_{10}H_{21})_4]$ (3d). To a solution of (n-$Bu_4N)_2[Fe_4S_4(S\text{-}t\text{-}Bu)_4]$[29] (0.148 g, 0.124 mmol) in DMF (10 mL) was added **2d** (0.162 g, 0.560 mmol). A periodic vacuum was applied to the stirred solution for 4 h, during which a color change from dark green to dark violet was observed. After a further 16 h of stirring, the DMF was removed *in vacuo*. The resulting sticky black residue was dissolved in CH_2Cl_2 (10 mL) and filtered. The solution was then concentrated *in vacuo* to 5 mL, ether was added (60 mL), and the mixture kept at –20 °C for several h. A fine black powder was collected by centrifugation, washed twice with ether, and dried *in vacuo*. ^{1}H NMR revealed the presence of 1 eq ether. Yield: 0.211 g (0.102 mmol, 82%). The ether was removed from the product under ultra-high vacuum prior to further analyses. Anal. Calcd for $C_{104}H_{176}Fe_4N_6S_8$: C, 62.76; H, 8.91; N, 4.22; S, 12.89. Found: C, 62.64; H, 8.97; N, 4.18; S, 12.76. ^{1}H NMR (DMSO-d_6): δ = 7.96 (s, br, 4 H, indolyl H), 7.48 (d, $^3J_{H\text{-}H}$ = 7.9 Hz, 4 H, indolyl H), 7.12 (t, br, $^3J_{H\text{-}H}$ = 6.7 Hz, 4 H, indolyl H), 6.80 (s, br, 4 H, indolyl H), 4.80 (s, very br, 4 H, indolyl H2), 4.57 (s, br, 8 H, decyl α-CH_2), 3.16 (t, $^3J_{H\text{-}H}$ = 8.3 Hz, 16 H, n-Bu_4N^+ α-CH_2), 1.70 (s, 8 H, decyl β-CH_2), 1.54 (t, br, $^3J_{H\text{-}H}$ = 7.7 Hz, 16 H, n-Bu_4N^+ β-CH_2), 1.31 (sextet, $^3J_{H\text{-}H}$ = 7.3 Hz, 16 H, n-Bu_4N^+ γ-CH_2), 1.19 (s, br, 56 H, decyl CH_2), 0.93 (t, $^3J_{H\text{-}H}$ = 7.4 Hz, 24 H, n-Bu_4N^+ CH_3), 0.83 (t, $^3J_{H\text{-}H}$ = 6.5 Hz, 12 H, decyl CH_3). λ_{max} (DMF, nm): 287, 305 (shoulder), 510. $E_{1/2}$ vs. Fc/Fc^+ in CH_2Cl_2 = –1.63 V (ΔE_p = 110 mV) [2–/3–], –0.56 V (ΔE_p = 72 mV) [2–/1–]. $E_{1/2}$ vs. SCE in CH_2Cl_2 = –1.20 V [2–/3–], –0.14 V [2–/1–].

(n-$Bu_4N)_2[Fe_4S_4(S\text{-}3\text{-}C_8H_5N\text{-}1\text{-}Bn)_4]$ (3e). To a solution of (n-$Bu_4N)_2[Fe_4S_4(S$-t-$Bu)_4]$[29] (0.161 g, 0.135 mmol) in DMF (10 mL) was added **2e** (0.162 g, 0.677 mmol). A periodic vacuum was applied to the stirred solution for 5 h, during which a color change from dark green to dark violet was observed. The solution was concentrated *in vacuo*. Addition of ether (40 mL) led to the formation of a fine black precipitate, which was collected by centrifugation, washed with ether, and dried in vacuo. Yield: 0.242 g (0.135 mmol, quant.). Anal. Calcd for $C_{92}H_{120}Fe_4N_6S_8$: C, 61.74; H, 6.76; N, 4.70; S, 14.33. Found: C, 61.82; H, 6.73; N, 4.59; S, 14.37. ^{1}H NMR (DMSO-d_6): δ = 7.98 (s, br, 4 H, indolyl H), 7.45 (d, $^3J_{H\text{-}H}$ = 7.9 Hz, 4 H, indolyl H), 7.36–7.00 (m, 24 H, indolyl and phenyl H), 6.80 (s, br, 4 H, indolyl H), 5.66 (s, br, 8 H, NCH_2), 5.03 (s, very br, 4 H, indolyl H2) 3.16 (t, $^3J_{H\text{-}H}$ = 7.9 Hz, 16 H, n-Bu_4N^+ α-CH_2), 1.56 (quintet, br, 16 H, n-Bu_4N^+ β-CH_2), 1.30 (sextet, $^3J_{H\text{-}H}$ = 7.1 Hz, 16 H, n-Bu_4N^+ γ-CH_2), 0.93 (t, $^3J_{H\text{-}H}$ = 7.4 Hz, 24 H, n-Bu_4N^+ CH_3). λ_{max} (DMF, nm): 285 (shoulder), 305 (shoulder), 500. $E_{1/2}$ vs. Fc/Fc$^+$ in CH_2Cl_2 = –1.60 V (ΔE_p = 107 mV) [2–/3–], –0.54 V (ΔE_p = 65 mV) [2–/1–]. $E_{1/2}$ vs. SCE in CH_2Cl_2 = –1.18 V [2–/3–], –0.12 V [2–/1–].

3.5. References.

[1] Beinert, H.; Holm, R. H.; Münck, E. *Science* **1997**, *277*, 653–659.
[2] Johnson, M. K. *Curr. Opin. Chem. Biol.* **1998**, *2*, 173–181.
[3] Venkateswara Rao, P.; Holm, R. H. *Chem. Rev.* **2004**, *104*, 527–559.
[4] Holm, R. H. *Pure Appl. Chem.* **1998**, *70*, 931–938.
[5] Stack, T. D. P.; Holm, R. H. *J. Am. Chem. Soc.* **1987**, *109*, 2546–2547.
[6] Walsdorff, C.; Saak, W.; Pohl, S. *J. Chem. Soc., Dalton Trans.* **1997**, 1857–1861.
[7] van der Geer, E. P. L.; van Koten, G.; Klein Gebbink, R. J. M.; Hessen, B. *Inorg. Chem.*, accepted (Chapter 2 of this thesis).
[8] Sundberg, R. J. *Indoles*; Katritzky, A. R.; Meth-Cohn, O.; Rees, C. S., Eds.; Best Synthetic Methods; Academic Press Limited: London, the United Kingdom, 1996; pp 105–118.
[9] Harris, R. L. N. *Tetrahedron Lett.* **1969**, 4465–4466.
[10] Schultz, A. G.; Fu, W. Y.; Lucci, R. D.; Kurr, B. G.; Lo, K. M.; Boxer, M. *J. Am. Chem. Soc.* **1978**, *100*, 2140–2149.
[11] Barco, A.; Benetti, S.; Pollini, G. P.; Baraldi, P. G. *Synthesis* **1976**, 124–125.
[12] Abel, E.; Fedders, M. F.; Gokel, G. W. *J. Am. Chem. Soc.* **1995**, *117*, 1265–1270.
[13] Bobrik, M. A.; Que, L., Jr.; Holm, R. H. *J. Am. Chem. Soc.* **1974**, *96*, 285–287.
[14] Que, L., Jr.; Bobrik, M. A.; Ibers, J. A.; Holm, R. H. *J. Am. Chem. Soc.* **1974**, *96*, 4168–4178.
[15] Holm, R. H.; Phillips, W. D.; Averill, B. A.; Mayerle, J. J.; Herskovitz, T. *J. Am. Chem. Soc.* **1974**, *96*, 2109–2117.
[16] Walden, S. E.; Wheeler, R. A. *J. Phys. Chem.* **1996**, *100*, 1530–1535.
[17] DePamphilis, B. V.; Averill, B. A.; Herskovitz, T.; Que, L., Jr.; Holm, R. H. *J. Am. Chem. Soc.* **1974**, *96*, 4159–4167.
[18] Ueyama, N.; Terakawa, T.; Nakata, M.; Nakamura, A. *J. Am. Chem. Soc.* **1983**, *105*, 7098–7102.
[19] Ueyama, N.; Kajiwara, A.; Terakawa, T.; Ueno, S.; Nakamura, A. *Inorg. Chem.* **1985**, *24*, 4700–4704.
[20] Ohno, R.; Ueyama, N.; Nakamura, A. *Inorg. Chem.* **1991**, *30*, 4887–4891.
[21] Blonk, H. L.; Kievit, O.; Roth, E. K.-H.; Jordanov, J.; van der Linden, J. G. M.; Steggerda, J. J. *Inorg. Chem.* **1991**, *30*, 3231–3234.
[22] van der Geer, E. P. L.; van Koten, G.; Klein Gebbink, R. J. M.; Hessen, B., to be submitted (Chapter 4 of this thesis).
[23] Johnson, R. W.; Holm, R. H. *J. Am. Chem. Soc.* **1978**, *100*, 5338–5344.
[24] Aizman, A.; Case, D. A. *J. Am. Chem. Soc.* **1982**, *104*, 3269–3279.
[25] Dehaen, W.; Hassner, A. *J. Org. Chem.* **1991**, *56*, 896–900.

[26] Masui, M.; Sayo, H.; Tsuda, Y. *J. Chem. Soc. B* **1968**, 973–976.
[27] Kolthoff, I. M.; Thomas, F. G. *J. Phys. Chem.* **1965**, *69*, 3049–3058.
[28] Heaney, H.; Ley, S. V. *Org. Synth. Coll. Vol.* **1988**, *6*, 104.
[29] Christou, G. C.; Garner, C. D. *J. Chem. Soc., Dalton Trans.* **1979**, 1093–1094.

Chapter 4

3:1 Site-Differentiated [4Fe-4S] Clusters: Visualizing Ligand Substitutions by ^{19}F NMR and Synthesis of a [4Fe-4S]-Ruthenium Assembly

Abstract. *Three new chelated, 3:1 site-differentiated [4Fe-4S] clusters were prepared by substitutions of the EtS^- ligand in (*n-$Bu_4N)_2[Fe_4S_4(TriS)(SEt)]$ (**1**). The successful substitution with ethyl (*R*)-cysteinate proves that full and clean conversions are possible with aliphatic thiols, without the need for prior activation of the unique iron site. Reaction with* p-FC_6H_4SH *appeared to yield pure (*n-$Bu_4N)_2[Fe_4S_4(TriS)(SC_6H_4$-p-$F)]$, *but ^{19}F NMR revealed the presence of two minor impurities stemming from partial and complete decoordination of the $TriS^{3-}$ ligand. Thus, in exchange reactions with (substituted) thiophenols, the preference for reaction at the unique iron site in **1** is strong, but not absolute. The pyridine-functionalized cluster (*n-$Bu_4N)_2[Fe_4S_4(TriS)(S$-4-py$)]$ *is the most conveniently accessible 3:1 site-differentiated cluster with a site for bridging interactions with other metal ions. Reaction of this cluster with a ruthenium porphyrin resulted in the isolation of the first [4Fe-4S]-Ru assembly.*

van der Geer, E. P. L.; van Koten, G.; Klein Gebbink, R. J. M.; Hessen, B., to be submitted.

4.1. Introduction.

Cubane-type [4Fe-4S] clusters play crucial roles in many proteins, serving catalytic, sensing, and electron-transport roles.[1] For [4Fe-4S] clusters present in the active sites of enzymes, three of the four iron atoms are often coordinated by cysteine residues, while the fourth iron atom is either linked to another metal ion *via* a bridging cysteine (examples being iron-only hydrogenase[2] and acetyl coenzyme A synthase/carbon monoxide dehydrogenase)[3] or coordinated by a non-cysteine ligand (as in aconitase).[4] The incorporation of similarly 3:1 site-differentiated clusters into synthetic active-site models can provide valuable insight into the mechanisms of action of these enzymes.[5,6] Holm and co-workers were the first to report a synthetic 3:1 site-differentiated [4Fe-4S] cluster, making use of the tripodal $L(SH)_3$ ligand (Chart 1).[7] The vast number of site-specific ligand substitutions that have since been reported on clusters chelated by LS_3^{3-} have provided a wealth of insight into both synthetic and natural [4Fe-4S] clusters.[5]

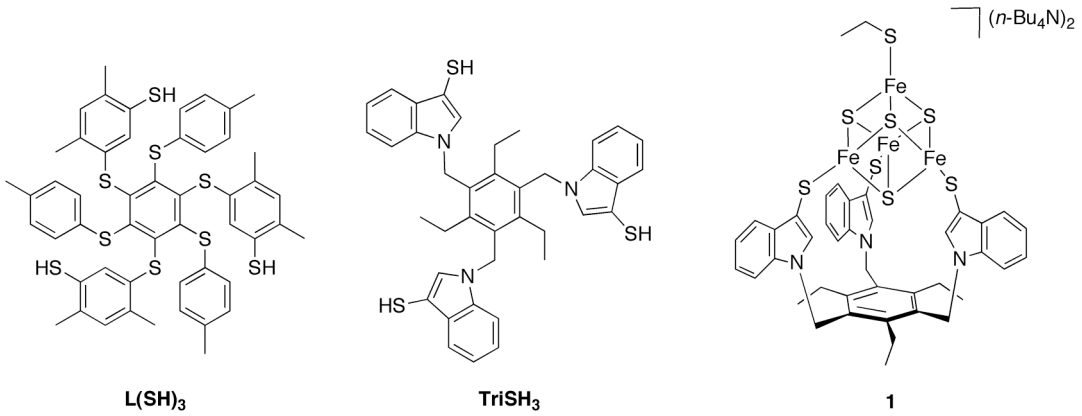

Chart 1. $L(SH)_3$, $TriSH_3$, and the 3:1 site-differentiated cluster $(n\text{-}Bu_4N)_2[Fe_4S_4(TriS)(SEt)]$ (**1**).

Since the original reports of the $L(SH)_3$ ligand, several other, site-differentiating ligands for [4Fe-4S] clusters have been synthesized.[8] One of the alternatives is the trithiol $TriSH_3$ (Chart 1), first reported by Pohl and co-workers in 1997.[9] Our recent modification and optimization of the synthesis of $TriSH_3$, which circumvent the use of highly toxic reagents and result in an overall yield substantially exceeding those reported for the other ligands, arguably makes $TriSH_3$ one of the most conveniently accessible, 3:1 site-differentiating [4Fe-4S] cluster ligands reported to date.[10] Furthermore, the derived cluster $(n\text{-}Bu_4N)_2[Fe_4S_4(TriS)(SEt)]$ (**1**, Chart 1) is a reliable starting material in site-differentiated [4Fe-4S] cluster chemistry, since it is one of the few 3:1 site-differentiated clusters that is pure by both spectroscopic and microanalytical criteria.[8b,8d,9] In order to gain more insight into the behavior and synthetic versatility of **1** in ligand exchange reactions, we have studied the reaction of **1** with three different thiols: the biologically relevant, aliphatic thiol ethyl (*R*)-cysteinate, the ^{19}F NMR probe ligand *p*-fluorothiophenol ($p\text{-}FC_6H_4SH$), and the potentially bridging thiol 4-thiopyridine (4-pySH).

4.2. Results and discussion.

4.2.1. Ligand substitutions.

Reaction of cluster **1** with the monothiols EtCysSH, *p*-FC_6H_4SH, and 4-pySH in DMF yielded the three new clusters **2**, **3**, and **4**, respectively, in high yields (Scheme 1). The reactions were driven to completion by removal of the volatile EtSH coproduct. As was the case for **1**, microanalytical figures of the new clusters were consistently in good agreement with the proposed formulations.

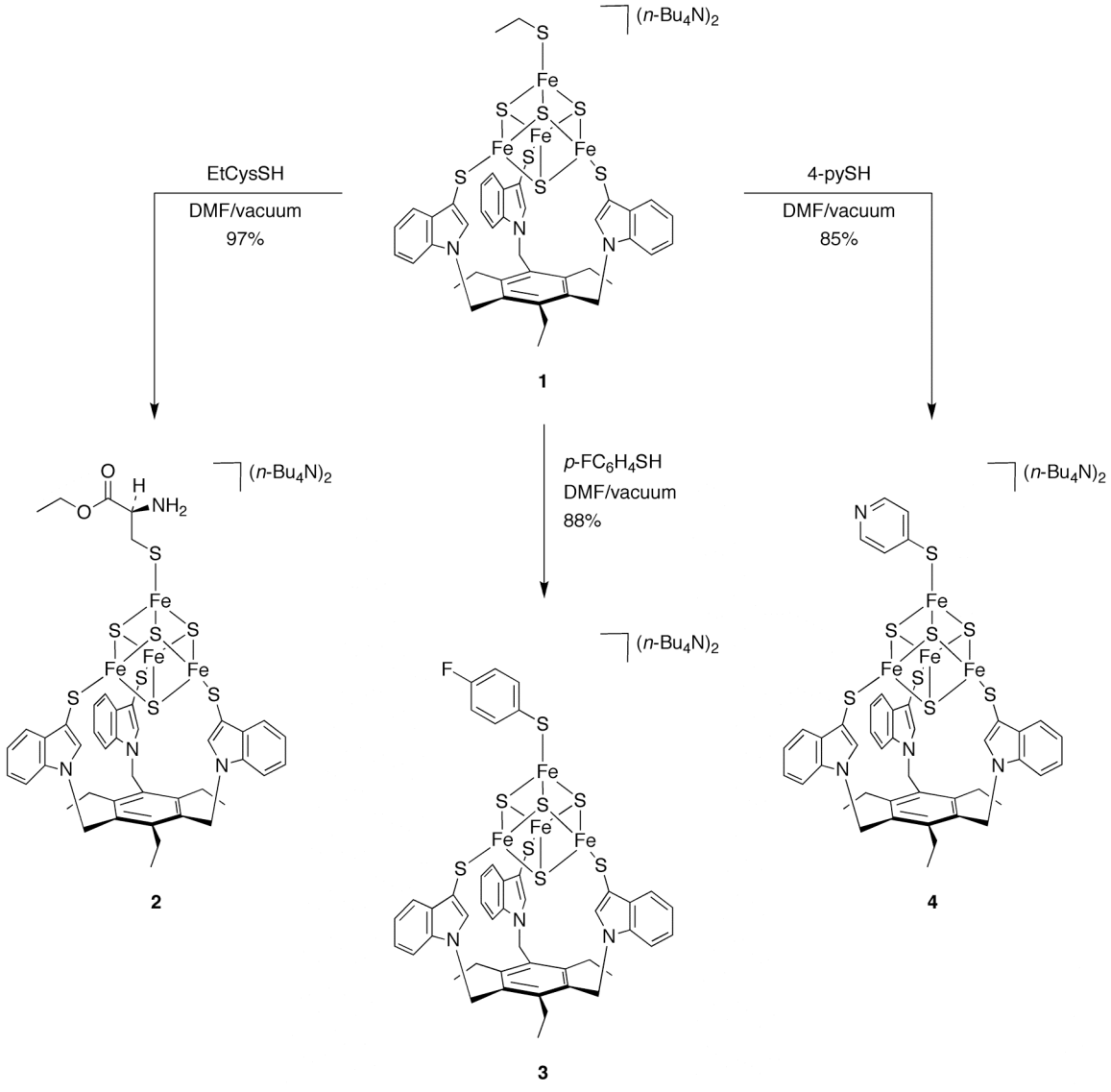

Scheme 1. Synthesis of 3:1 site-differentiated [4Fe-4S] clusters **2**–**4**.

The substitutions of the EtS^- ligand by *p*-FC_6H_4SH and 4-pySH to form **3** and **4**, respectively, reflect the thermodynamically favorable binding of more acidic, aromatic thiols over less acidic, aliphatic thiols. In previously reported 3:1 site-differentiated systems,

substitutions at the unique coordination sites were often preceded by activation steps, in which the monodentate thiolates were substituted for chloride or bromide ligands.[7,8a,9,11] The successful synthesis of **2** demonstrates that removal of the volatile EtSH coproduct is sufficient to drive the reaction between **1** and EtCysSH to completion, despite the comparable acidities of the incoming and departing thiols.

4.2.2. Electrochemistry.

Similar to the parent cluster **1**, the new clusters **2**–**4** all show chemically reversible 2–/3– redox processes and transitions to an unstable 1– state; the cyclic voltammogram of **3** is shown in Figure 1. The observed peak separations for the 2–/3– processes all exceed the theoretical value of 59 mV, but the peak currents i_{pc} and i_{pa} do display linear dependence on the square root of the scan speed. Hence, the 2–/3– processes are electrochemically quasi-reversible.

For the 2–/1– processes, the oxidation peaks are more intense than the reduction peaks. The intensity difference can be minimized by increasing the scan speed; thus, the 1– states of clusters **2**–**4** are unstable and decompose on the time scale of the cyclic voltammetry experiment.

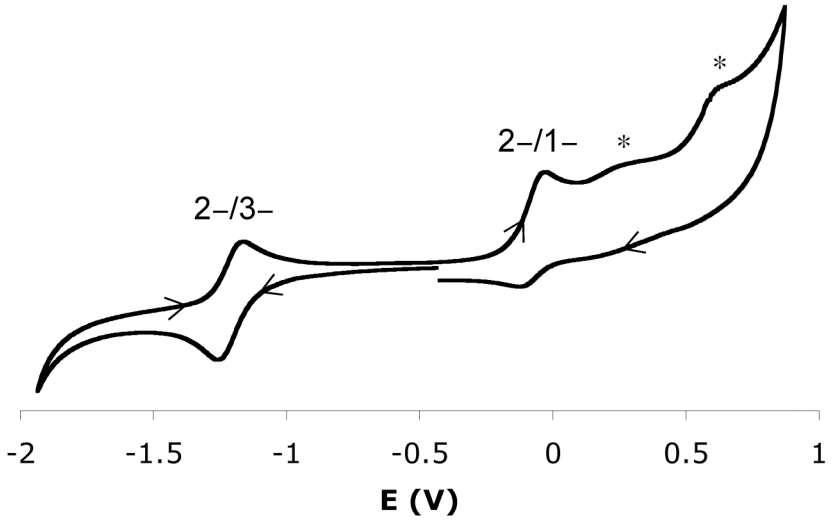

Figure 1. Cyclic voltammogram of **3** in CH_2Cl_2 (vs. SCE). Asterisks denote irreversible oxidations beyond the 1– state.

Table 1 summarizes the redox potentials of clusters **1**–**4** together with those of (n-$Bu_4N)_2[Fe_4S_4(SC_6H_4$-p-$F)_4]$ (**5**). In general, the redox potentials of clusters **1**–**4** reflect the intermediate electron-donating strength of the indole-3-thiol derivative $TriSH_3$. We have previously observed that related, symmetrically substituted indole-3-thiolate [4Fe-4S] clusters

also display redox transitions in a potential range that is intermediate between those of clusters with all-aromatic and all-aliphatic thiolate ligands.[12]

Table 1. Redox properties of clusters **1**–**5**.

Compound	Ligand set	$E_{1/2}$[2–/3–], V vs. SCE	$E_{1/2}$[2–/1–], V vs. SCE
1	$TriS^{3-}$, EtS^-	–1.27[a]	–0.13[a]
2	$TriS^{3-}$, $EtCysS^-$	–1.24	[b]
3	$TriS^{3-}$, *p*-$FC_6H_4S^-$	–1.19	–0.06
4	$TriS^{3-}$, 4-pyS^-	–1.13	0.00
5	4 × *p*-$FC_6H_4S^-$	–1.01	+0.10

[a] data taken from reference 10 [b] not determined; overlapping oxidations

Substitution of the EtS^- ligand in **1** has readily observable effects on the 2–/3– and 2–/1– transitions. Replacement by $EtCysS^-$ induces a small, positive potential shift, in agreement with the results obtained by Holm and co-workers using a cysteine derivative.[13] As expected,[14,15] larger potential shifts are observed upon substitution with the aromatic ligands *p*-FC_6H_4SH and 4-pySH. The largest shift is seen in 4-pySH-substituted **4**, reflecting the stronger electron-withdrawing properties of the 4-pyridyl as compared to the *p*-fluorophenyl group.[16] Unfortunately, we have not been able to protonate the pyridyl group by reactions with mild acids without also destroying the [4Fe-4S] cluster core.

Johnson and Holm have demonstrated that in mixed-ligand clusters, the redox properties are determined by the sum of four independent ligand contributions.[17] Using cluster **1**, the contributions of each indole-3-thiolate arm in $TriS^{3-}$ have been determined to be –0.3125 V and –0.028 V for the 2–/3– and 2–/1– processes, respectively.[12] Comparison between the redox properties of cluster **3** and its symmetrically substituted analogue **5** now allows for an independent verification of this approach. Indeed, the 2–/3– and 2–/1– potentials measured for **3** are identical to the sums of one *p*-$FC_6H_4S^-$ contribution and three contributions from $TriS^{3-}$ (one for each indole-3-thiolate arm).

4.2.3. ^{1}H NMR spectroscopy.

Similar to **1**, the clusters **2**–**4** all show three ^{1}H NMR signals corresponding to the NCH_2 and ethyl groups in $TriS^{3-}$, as well as four aromatic signals for the hydrogen atoms on positions 4 through 7 of the indolyl groups (see Figure 2 for the ^{1}H NMR spectrum of **4**). No signal is observed for the H2 protons owing to their close proximity to the [4Fe-4S] cluster core and the consequent strong Fermi contact shifting characteristic of ligands bound to a [4Fe-4S] cluster.[18] The nature of the unique ligand in clusters **1**–**4** has a small to negligible effect on all observed $TriS^{3-}$ signals except for that belonging to the NCH_2 group. In going from **1** to **4**, the NCH_2 signal shifts 0.09 ppm to higher frequency, indicating that the NCH_2

resonance may prove useful in monitoring site-specific substitution reactions in **1** and its derivatives.

The monodentate ligands in **2**–**4** show the expected characteristics for contact-shifted, aromatic and aliphatic thiolate ligands.[18] In both **3** and **4**, the hydrogen atoms *ortho* to the coordinated sulfur atom experience strong signal broadening and shifting to lower frequency, while the *meta* hydrogen atoms are shifted to higher frequency. In **2**, the signals for the α proton and the diastereotopic SCH_2 protons are both broadened and shifted to higher frequency, with the SCH_2 group being most strongly affected.

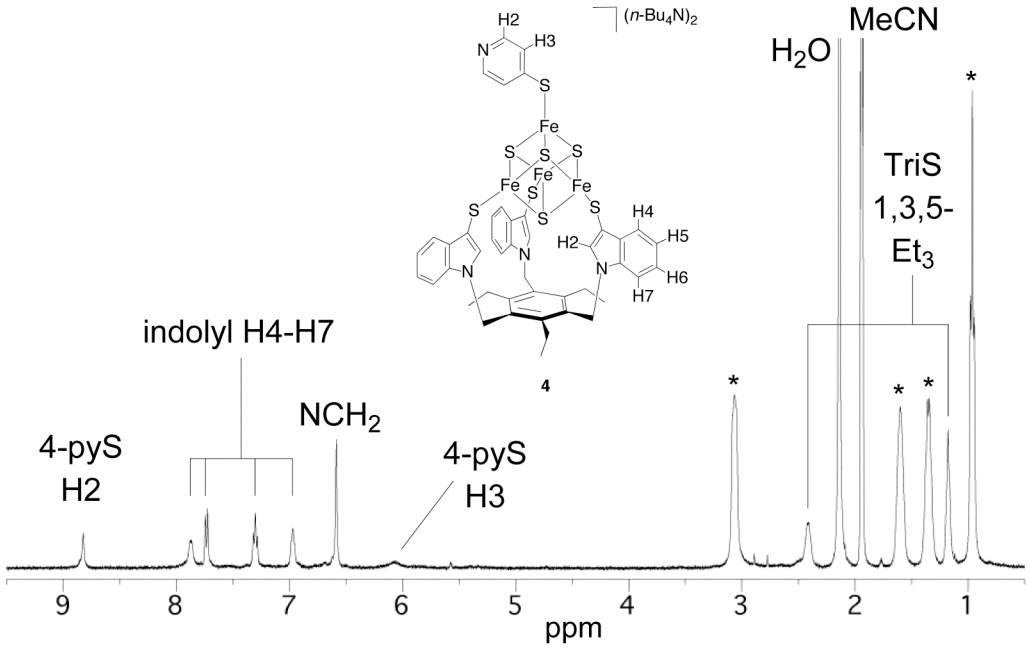

Figure 2. ^{1}H NMR spectrum of **4** in CD_3CN. *n*-Bu_4N^+ signals are marked with asterisks.

4.2.4. ^{19}F NMR spectroscopy.

^{19}F NMR has been applied in iron-sulfur cluster chemistry using the ligands *p*-$FC_6H_4S^-$ and *p*-$CF_3C_6H_4S^-$, relying on the large contact shift experienced by *para* substituents on cluster-coordinated thiophenolates[9,18,19] for their use as ^{19}F NMR probe molecules. All but one of these studies used ^{19}F NMR in order to distinguish clusters differing in iron and sulfur content.[20] The only application of ^{19}F NMR in the analysis of [4Fe-4S] clusters differing in ligand environment was reported by Hoveyda and Holm in their study of the self-condensation equilibrium of $(n\text{-}Pr_4N)_2[Fe_4S_4(SH)_4]$.[21]

As expected, the homo-substituted cluster **5** displays a single, somewhat broadened ^{19}F NMR resonance in CD_3CN, located at 45.67 ppm. Interestingly, ^{19}F NMR spectra of isolated **3** never showed a single resonance as would be expected for a pure compound. Instead, all the synthesized batches of **3** consistently displayed a major product signal at 45.27 ppm as well as minor, yet readily observable signals at 45.36 and 45.66 ppm in CD_3CN (Figure 3). Thus,

synthetic batches of **3** also appear to contain **5**, as well as a third species **3'**, which we propose to be a [4Fe-4S] cluster with two coordinated p-$FC_6H_4S^-$ ligands (*vide infra*).

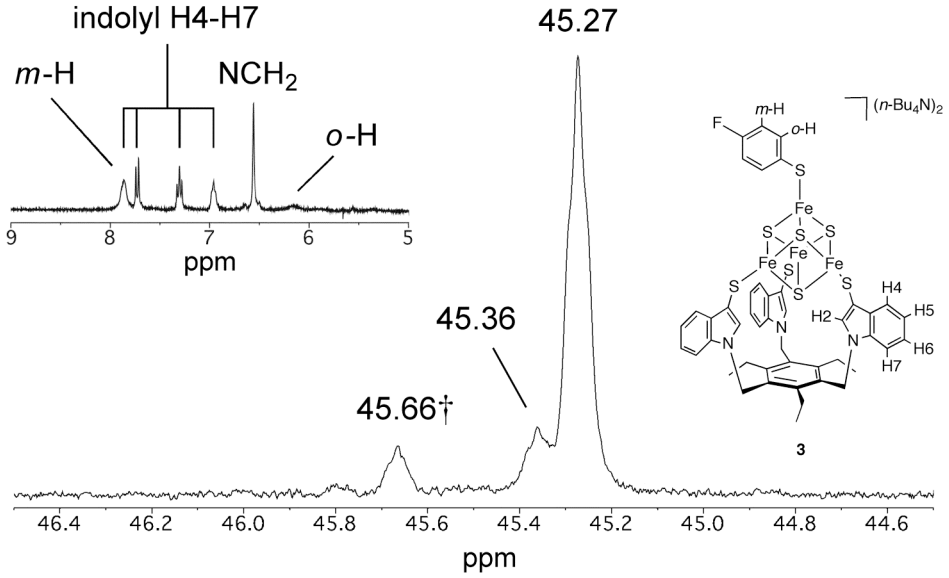

Figure 3. ^{19}F NMR spectrum of **3** in CD_3CN, showing the main product signal as well as the signals of two impurities. The dagger marks the signal assigned to **5**. Inset: aromatic region of the ^1H NMR spectrum of **3**.

^{19}F NMR spectra of **3** in DMSO-d_6 and DMF also showed a minor signal at practically the same chemical shift as measured for **5** (δ = 45.66 and 45.67 ppm, respectively). Comparison to the ^{19}F NMR spectra of p-FC_6H_4SH in the three solvents further demonstrated that none of the species observed in **3** correspond to free p-FC_6H_4SH. Table 2 summarizes the ^{19}F isotropic shifts in **3** and **5**, defined as the change in chemical shift that the ^{19}F nucleus undergoes upon deprotonation of p-FC_6H_4SH followed by coordination to the [4Fe-4S] cluster.[18]

Table 2. ^{19}F NMR shifts of **3**, **3'**, **5**, and p-FC_6H_4SH in different solvents.

Solvent	**δ(p-FC_6H_4SH) (ppm)**	**Isotropic shift (ppm)**		
		3	**3'**	**5**
DMF[a]	44.96	–0.22	+0.05	+0.38
CD_3CN	45.32	–0.05	+0.04	+0.35
DMSO-d_6	44.43	+0.62	[b]	+1.06

[a] In DMF solution, **3** also displays a sharp signal at 30.15 ppm. [b] Not resolved.

The ability to detect and distinguish easily between **3**, **3'**, and **5** by ^{19}F NMR highlights the great potential for the use of p-FC_6H_4SH as a ^{19}F NMR probe molecule in analyzing different coordination environments in [4Fe-4S] clusters. When Hoveyda and Holm used ^{19}F NMR to distinguish between the clusters $(n\text{-}Pr_4N)_2[Fe_4S_4(SH)_m(SC_6H_4\text{-}p\text{-}CF_3)_n]$, a contact

shift difference ($\Delta\sigma$) of 0.16 ppm was observed between the monosubstituted (m = 3, n = 1) and fully substituted (m = 0, n = 4) clusters.[21] In our work with p-$FC_6H_4S^-$, the analogous $\Delta\sigma$ is much higher in all three solvents, most likely due to the direct positioning of the fluorine atom on the aromatic ring.

Results obtained using p-$FC_6H_4S^-$ as a ^{19}F NMR probe ligand can most likely be extrapolated to other thiophenolate-containing clusters without p-fluorine substituents. Comparison between the cyclic voltammetry data for **5** and those reported for $[Fe_4S_4(SPh)_4]^{2-}$ shows that the potential for the 2–/3– process is only 0.03 V more positive for **5**, while the difference in potential for the 2–/1– process is merely 0.01 V.[22] Furthermore, the pK_a values of p-FC_6H_4SH and C_6H_5SH are the same (6.62 and 6.6, respectively),[23] indicating that clusters with p-$FC_6H_4S^-$ and p-$C_6H_5S^-$ ligands will show similar thiol-thiolate exchange behavior.

The generation of **5** in the synthesis of **3** may be explained by the relatively high acidity of p-FC_6H_4SH as compared to the conjugate acids of not only the EtS^- ligand, but also the indole-3-thiolate arms of the coordinated $TriS^{3-}$ tripod. This acidity could lead to a reduced ability to discriminate between the chelated and non-chelated subsites in **1**. Hence, p-FC_6H_4SH might not only be able to react with **1**, but also with the already substituted cluster **3**, sequentially displacing its three indole-3-thiolate ligands to ultimately generate cluster **5**. This reaction would proceed through two intermediates containing two and three coordinated p-$FC_6H_4S^-$ ligands, respectively, which should show ^{19}F NMR shifts somewhere between those of **3** and **5**. We propose **3'** to be a species containing two coordinated p-$FC_6H_4S^-$ ligands, since the species containing three p-$FC_6H_4S^-$ ligands should be especially susceptible to substitution of the remaining coordinated indole-3-thiolate ligand due to the lack of chelate stabilization.

The effects of imperfect site specificity have been observed before by Nolte and co-workers in their cyclotriveratrylene trithiolate-chelated clusters.[8c,d] For the other 3:1 site-differentiated cluster systems, ^{19}F NMR may also prove valuable in assessing the regioselectivity of ligand substitutions, especially since even the binding of the thiophenolate-based LS_3^{3-} ligand is known to be dynamic.[24]

A ^{19}F NMR titration of **1** with p-FC_6H_4SH provided further insight into the substitution process (Figure 4). When 0.6 equiv. of p-FC_6H_4SH are added to **1**, only a small amount of **3'** is formed, while the formation of **5** is negligible. As the amount of p-FC_6H_4SH is increased sequentially to 0.8 and 1.0 equiv., the ratio of **5** in the product increases until its signal is approximately as strong as that of **3'**. Addition of larger amounts of p-FC_6H_4SH not only leads to increased formation of **5**, but also the appearance of new signals at 46.00 and 49.23 ppm.

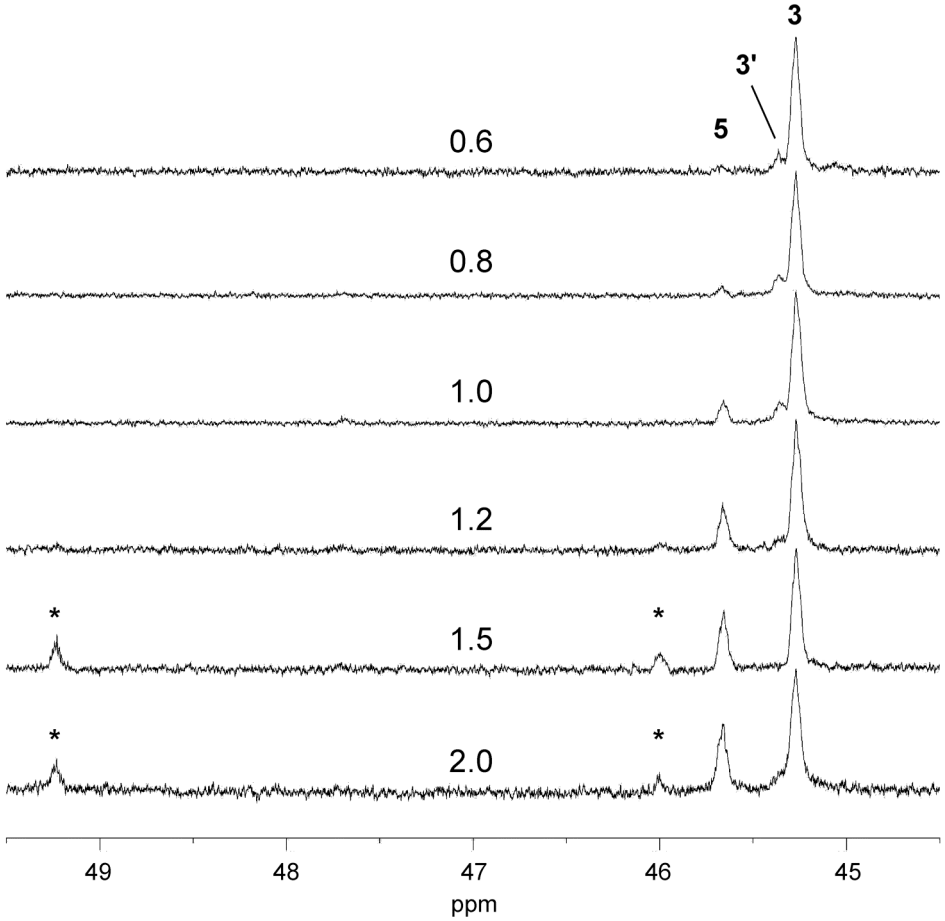

Figure 4. ^{19}F NMR titration of **1** with *p*-FC_6H_4SH. The spectra are labeled with the number of equiv. of *p*-FC_6H_4SH added. *p*-$FC_6H_4S^-$-containing decomposition products are marked with asterisks.

The species resonating at 46.00 and 49.23 ppm probably arise from the decomposition of $TriS^{3-}$-chelated [4Fe-4S] clusters. Despite an increasing concentration of ^{19}F nuclei, the signal-to-noise ratio in the NMR titration decreases as the amount of *p*-FC_6H_4SH is increased from 1 to 2 equiv., suggesting the formation of paramagnetic decomposition products. Furthermore, if excess *p*-FC_6H_4SH would solely lead to formation of **5** from **3** *via* **3'** and a negligible amount of **3'** remains at the end of the reaction, then the molar ratio of **5** to **3** after addition of 2 equiv of *p*-FC_6H_4SH should be 1:2. In the ^{19}F NMR titration, this ratio is much higher (the observed 1:2 integral ratio corresponds to a 2:1 molar ratio), implying that the $TriS^{3-}$-chelated clusters have also reacted in ways beside simple ligand exchange. If 1 equiv. of *p*-FC_6H_4SH is added to **5**, the signals are not observed, indicating that **5** is stable in the presence of excess *p*-FC_6H_4SH. When performing site-specific substitutions on $TriS^{3-}$-chelated systems using a thiol with a comparable or higher acidity as compared to $TriSH_3$, it deserves recommendation to keep the concentration of the substituting thiol low to minimize side product formation.

In light of the ^{19}F NMR results, the choice of 4-pySH as a potentially bridging unit between $TriS^{3-}$-chelated clusters and single metal ions is extra attractive. With a pK_a of 8.83,[25]

4-pySH in its tautomeric thione form is significantly less acidic than *p*-FC_6H_4SH, and the reaction with **1** to form **4** is hence expected to proceed in an even more site-specific manner.

4.2.5. A [4Fe-4S]-Ru assembly.

Following the successful synthesis of **4**, we employed the coordination ability of the pendant pyridyl group in a bridge-forming reaction with a ruthenium porphyrin, forming a hetero-multimetallic complex as also proposed for Pd and Pt complexes of 4-pySH.[26] Holm and co-workers have previously employed 4-pySH as a linker between a [4Fe-4S] cluster and *N*,*N*,*O*,*O*-chelated iron(II) complexes in the context of mimicking the active site of sulfite reductase.[15] The pyridine-iron(II) bonds in the bridged assemblies were found to be labile in solution, with bridge formation constants of 790–920 M^{-1}. Thus, the 4-pySH ligand seemed unsuitable for forming stable [4Fe-4S]-Fe assemblies. However, in contrast to iron-pyridine complexes, complexes of pyridines with ruthenium are, in general, kinetically stable. Furthermore, the incorporation of ruthenium into [4Fe-4S] cluster-based molecules and materials may generate interesting interplays between the two metal centers. Ruthenium compounds are widely applied as (photo)redox catalysts,[27] and the recent incorporation of ruthenium photosensitizers and catalysts in biologically inspired materials demonstrates the great potential of ruthenium in biomimetic chemistry.[28]

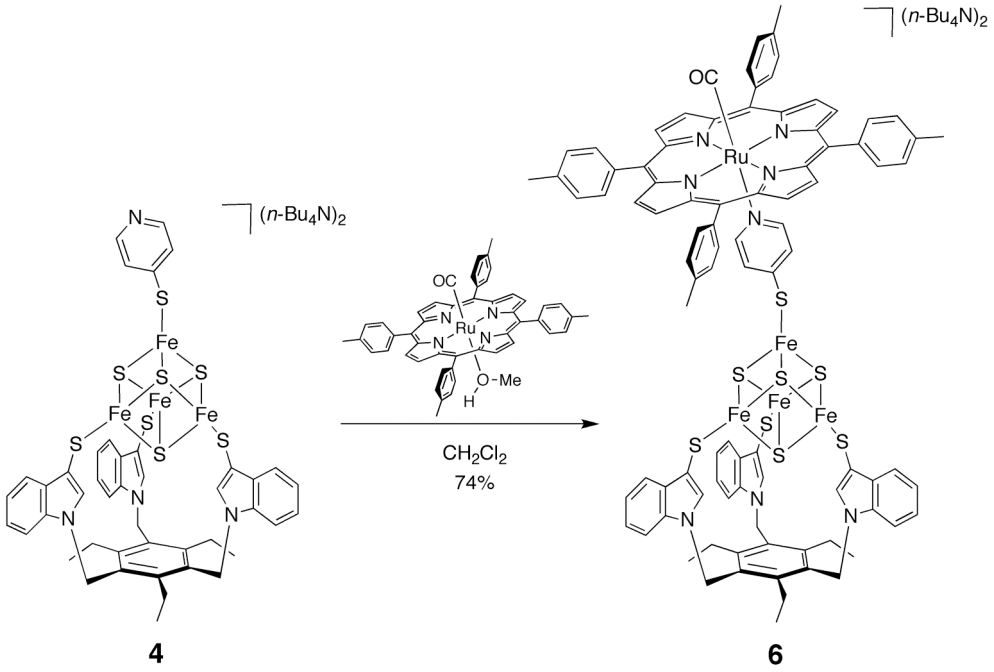

Scheme 2. Synthesis of $(n\text{-}Bu_4N)_2[Fe_4S_4(TriS)(\mu\text{-}\{S\text{-}4\text{-}py\})Ru(TTP)(CO)]$ (**6**).

The bridged compound $(n\text{-}Bu_4N)_2[Fe_4S_4(TriS)(\mu\text{-}\{S\text{-}4\text{-}py\})Ru(TTP)(CO)]$ (**6**) was synthesized by reacting **4** with a slight excess of [Ru(TTP)(CO)(MeOH)] (TTP = 5,10,15,20-tetra(*p*-tolyl)porphyrinato dianion) in CH_2Cl_2 (Scheme 2). Addition of diethyl ether led to the

precipitation of the bridged product in a yield of 74%, with elemental analyses confirming the proposed formulation.

Compound **6** shows a strong and isolated carbonyl stretch absorption at 1937 cm^{-1} (Figure 5). In the related, pyridine-bound compound [Ru(TTP)(CO)(C_5H_5N)] (**7**),[29] the analogous stretching frequency is slightly higher (1940 cm^{-1}). The electron-donating properties of the cluster-bound thiolate group,[16] which also affect the ruthenium porphyrin redox potential (*vide infra*), weaken the π acidity of the pyridine ligand in **6** as compared to **7**. This then results in slightly stronger back-bonding to the carbonyl ligand, since there is direct competition between the π^* orbitals of the pyridine and carbonyl ligands for the electron density in the filled dπ orbitals.[30]

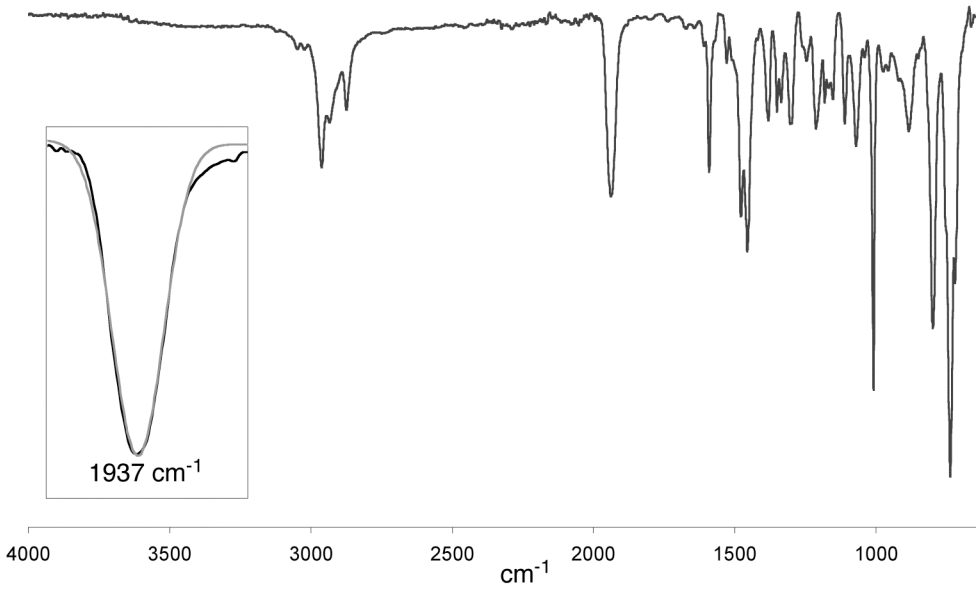

Figure 5. IR spectrum of **6**. Inset: CO stretching frequency as measured (black) and reconstructed with a Gaussian function (gray).

McCleverty and co-workers have reported similar small shifts of the CO stretching frequency depending on the nature of ligand L in the related system [Ru(TPP)(CO)(L)] (TPP = 5,10,15,20-tetraphenylporphyrinato dianion).[31] In contrast, Pizzotti and co-workers recently studied the same metalloporphyrin with substituted stilbazoles as axial ligands, but reported that the nature of the substituent has no effect on the CO stretching frequency.[32] This led the authors to suggest that the effects of altered axial σ donation and π acidity in ruthenium porphyrins largely cancel out, with any net charge movement dissipating into the porphyrin ring system rather than affecting the *trans* ligand. Together with McCleverty's results, the small but observable difference of 3 cm^{-1} that we have found between **6** and **7** indicates that the absence of an effect on CO in Pizzotti's systems may be mainly due to the modest changes in electron donating strength brought about by the substituents on the stilbazole, rather than an inherent insensitivity of the ruthenium porphyrin system to axial substitution effects.

^{1}H NMR studies of compounds **4**, **6**, and **7** in CD_2Cl_2 provided further evidence for the formation of a [4Fe-4S]-Ru assembly (Table 3).

Table 3. ^{1}H NMR signals of **4**, **6**, and **7** in CD_2Cl_2.

		δ (ppm)		
Signal		**4**	**6**	**7**
porphyrin	*β*-H	n/a	8.60	8.64
	tolyl H		8.06	8.10
			8.01–7.86[a] 7.53[b]	7.92
				7.55, 7.50
	tolyl CH_3		2.67	2.68
$TriS^{3-}$	indolyl H	7.95	8.01–7.86[a] 7.60	n/a
		7.65	7.28	
		7.29	6.93	
		6.95		
	NCH_2	6.57	6.55	
	1,3,5-Et_3	2.40	2.32	
		1.15	1.11	
n-Bu_4N^+		3.10	2.91	n/a
		1.70	1.51	
		1.43	1.22	
		0.96	0.76	
4-pyS^-		8.77	[c]	n/a
		5.93		
C_5H_5N		n/a	n/a	6.13
				5.23
				0.88

[a] overlapping porphyrin and $TriS^{3-}$ signals [b] double intensity [c] not detected

In going from **4** to **6**, the isolated $TriS^{3-}$ resonances shift to slightly lower frequencies. Interestingly, the *n*-Bu_4N^+ signals shift more strongly, suggesting ion pair formation. Unfortunately, assignment of the H2 and H3 signals of the bridging 4-pyS^- ligand in **6** proved difficult. In **4**, the (very broad) H3 signal is located at 5.93 ppm. Shielding by the porphyrin macrocycle in **6** should shift this resonance to a lower frequency, but we did not detect any signals between 3.68 and 6.55 ppm aside from the residual solvent peak. In **7**, the pyridine H2

signal is located at 0.88 ppm. The analogous 4-pyS^- resonance in **6** should be contact-shifted to higher frequency, probably leading to overlap with the broad *n*-Bu_4N^+ signals.

In cyclic voltammetry, **6** shows three distinct redox processes: a reversible transition at –1.11 V (ΔE_p = 76 mV), an irreversible oxidation at $E_{1/2}$ = +0.01 V, and an irreversible reduction at E_{red} = –1.75 V (Figure 6).

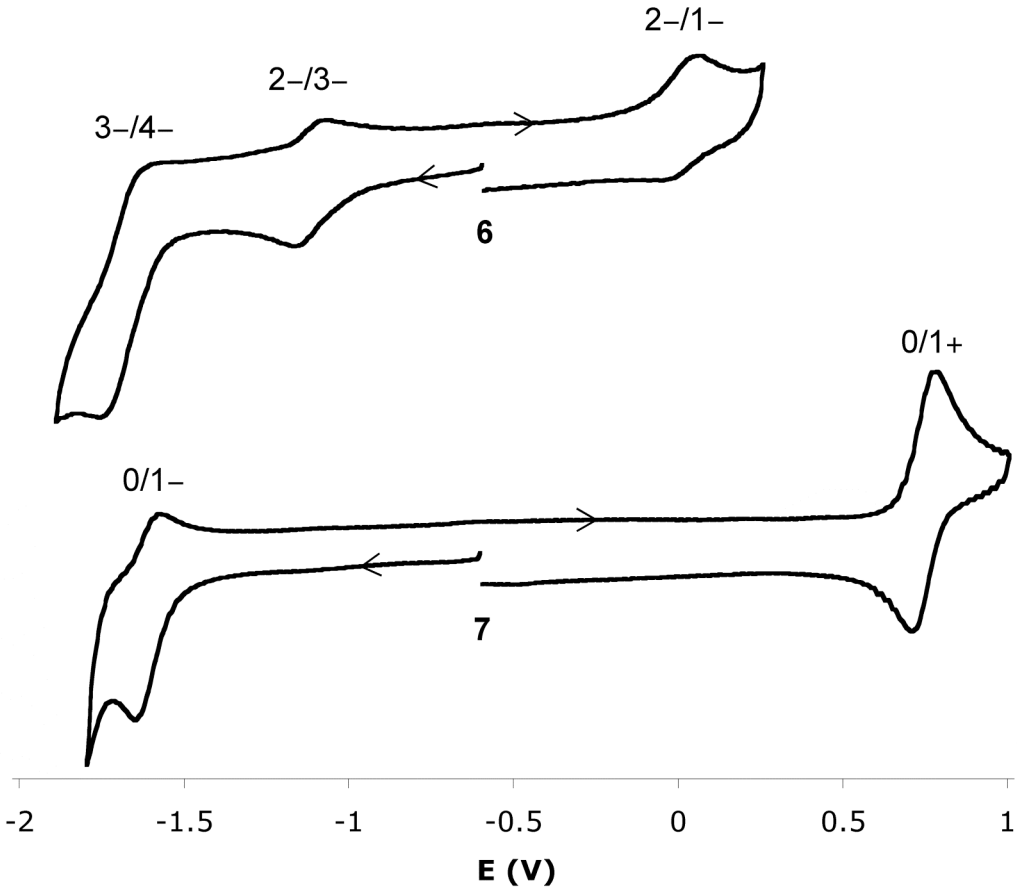

Figure 6. Cyclic voltammograms of **6** (top) and **7** (bottom) in CH_2Cl_2 (vs. SCE).

The reversible process at –1.11 V corresponds to the cluster-centered 2–/3– transition. Compared to the non-bridged compound **4**, the redox potential has shifted only slightly (+0.02 V), indicating that binding of the ruthenium porphyrin to the pendant pyridyl group does not markedly alter the cluster's redox properties. The small difference is in agreement with the +0.01 V potential shift observed by Holm and co-workers upon coordination of the neutral, *N*,*N*,*O*,*O*-chelated Fe^{2+} complexes to the pyridyl group in $[Fe_4S_4(LS_3)(S\text{-}4\text{-}py)]^{2-}$.[15] For the irreversible 2–/1– cluster-centered oxidation in **6**, the potential shift is also +0.01 V.

The third redox process occurs at E_{red} = –1.75 V and is assigned to a reduction of the porphyrin ring.[31] The irreversibility of this process may be due to its proximity to the limit of the experiment's electrochemical window. Compared to ruthenium porphyrin **7**, where the porphyrin-centered reduction occurs reversibly at $E_{1/2}$ = –1.61 V, this transition is strongly

anodically shifted. Thus, while IR spectroscopy had already indicated that some of the electron density donated by the cluster-bound thiolate group in **6** is transferred to the carbonyl ligand (*vide supra*), a significant portion is also dissipated into the porphyrin ring.[31] The extra electron density in the porphyrin ring is also reflected by the slightly lower frequency of the *β* hydrogen ^{1}H NMR signal in **6** as compared to **7** (8.60 vs. 8.65 ppm).

Holm and co-workers attributed the modest effects of Fe^{2+} coordination on the redox properties of $[Fe_4S_4(LS_3)(S\text{-}4\text{-}py)]^{2-}$ to the fact that only one cluster ligand is modified as well as the appreciable distance at which this modification takes place.[15] However, we have observed large shifts in the redox properties of $TriS^{3-}$-chelated [4Fe-4S] clusters upon binding to a Fe^{2+} ion *via* 2,2':6':2"-terpyridine-4'-thiol (tpySH), despite the cluster-metal distance being similar to that in **6**.[10] Hence, the effect of a bridged metal ion on a [4Fe-4S] cluster also depends on the nature and, most significantly, the overall charge of the metal species (including the bridging ligand) to which the cluster is being linked.

The UV-vis spectrum of **6** approximates a linear combination of the spectra of **4** and **7** (Figure 9). There is no increased absorption around 356 nm (where the C–S centered π-π* transition of 1*H*-pyridine-4-thione occurs in CH_2Cl_2 solution), indicating that the C–S bond in the 4-pyS^- ligand retains full single-bond character upon formation of **6**. Furthermore, a negligible difference is observed between the locations of the Soret bands in **6** (414 nm) and **7** (413 nm), and the Q-band regions are also virtually identical. In other compounds of the type [Ru(P)(CO)(L)] (with P a porphyrin macrocycle), similar insensitivities of the Soret and Q bands on the nature of L have been reported.[31,32, 33] Hence, 4-pySH can function as a linker between ruthenium compounds and [4Fe-4S] clusters without significantly affecting the properties of either moiety.

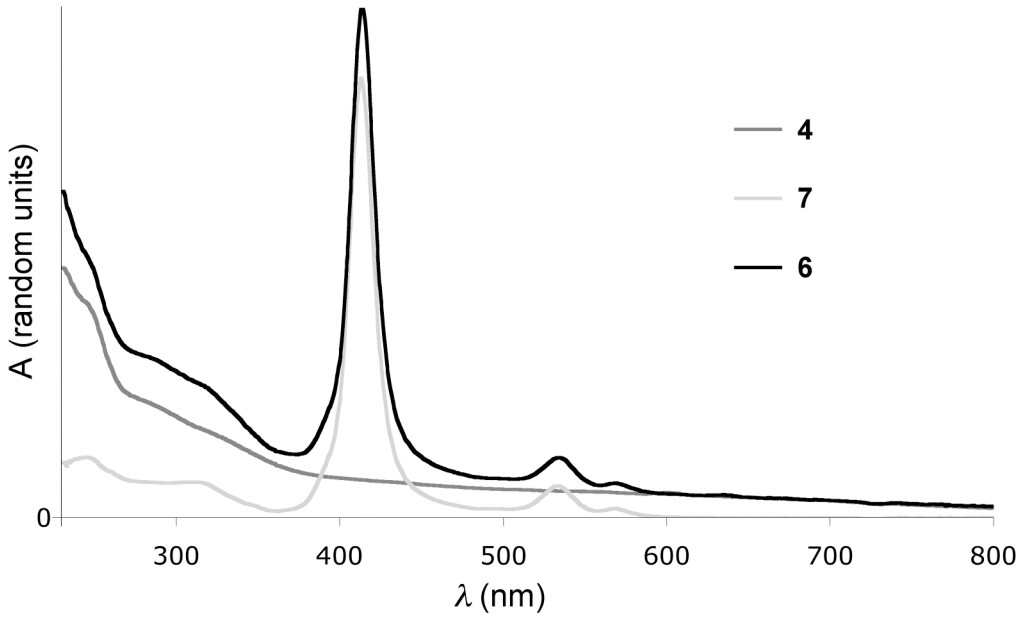

Figure 7. UV-vis spectra of **4**, **6**, and **7** in CH_2Cl_2.

4.3. Conclusion.

By virtue of its ability to undergo site-specific substitutions with both aliphatic and aromatic thiols, cluster **1** is a versatile starting compound for the synthesis of a wide variety of 3:1 site-differentiated [4Fe-4S] clusters. However, the fact that some substitution takes place at the $TriS^{3-}$-chelated positions in **1** upon reaction with *p*-FC_6H_4SH indicates that care should be taken when employing **1** in ligand exchange reactions with relatively acidic aromatic thiols. In such cases, prior activation of **1** by exchange of the EtS^- ligand for Cl^- or Br^- may be preferred.

The attractively simple 4-pySH ligand has proven to be capable of effectively linking a [4Fe-4S] cluster to a ruthenium porphyrin. It may prove equally possible to form stable, bridged assemblies with (photo)catalytic ruthenium compounds, *en route* to novel, bio-inspired redox catalysts.

4.4. Experimental.

General methods. ^1H and ^{13}C NMR spectra were recorded at 298 K on a Varian 400 MHz spectrometer operating at 400 and 100 MHz, respectively, or at 300 K on a Bruker AC 300 spectrometer operating at 300 and 75 MHz, respectively. Spectra were calibrated on the residual solvent peaks and assignments were based on chemical shift, integral, and linewidth considerations. ^{19}F NMR spectra were recorded at 298 K on the Varian 400 MHz spectrometer operating at 376 MHz and referenced to a C_6F_6 internal standard. Infrared spectra were recorded on a Perkin-Elmer Spectrum One FT-IR spectrometer. UV-vis spectra were recorded on a Varian Cary 50 Scan UV-visible spectrophotometer. Elemental analyses were carried out by Kolbe Mikroanalytisches Laboratorium (Mülheim an der Ruhr, Germany). Cyclic voltammograms were recorded at 100 mV/s using Pt working and counter electrodes, a Ag/AgCl reference electrode, and 0.1 M *n*-Bu_4NClO_4 in CH_2Cl_2 as supporting electrolyte. Potentials were referenced to a ferrocene (Fc) internal standard. Fc was added directly to all samples except **5**. Here, the Fc/Fc^+ wave was found to overlap with irreversible, multielectron oxidation waves and the cyclic voltammogram was calibrated against a separate run with Fc. Potentials vs. a standard calomel electrode (SCE) were calculated by taking $E_{1/2}$ (Fc/Fc^+) = +0.424 V vs. SCE.[34] The electrospray mass spectrum was recorded on an API 3+ triple quadrupole mass spectrometer (Sciex, Concord, Ont., Canada) equipped with a modified pneumatically assisted electrospray (IonSpray) interface.[35] The home-made front cover and IonSpray interface ensure a gas-tight ion source. The atmospheric pressure ion source was first evacuated and then filled with dry nitrogen. N_2 was used as nebulizing gas and curtain gas. Sample preparation took place in a N_2-filled glovebox. The syringe pump used for sample introduction was also placed inside the glovebox, and a 1.6 mm o.d. 0.3 mm i.d. Teflon tube was connected between the syringe pump and the IonSpray interface. Mass spectra were recorded in negative ion mode as Q1 scans with step size 0.1 and a dwell time of 1 ms. The electrospray probe capillary voltage was set at 4.0 kV, and the cone voltage at 40 V.

All air-sensitive compounds were handled in a glovebox or using standard Schlenk techniques. Ethyl (*R*)-cysteinate hydrochloride was purchased from Acros, neutralized with Na_2CO_3 in H_2O, extracted with ether, and distilled to yield pure ethyl (*R*)-cysteinate (EtCysSH). 4-Pyridinethiol was purchased from Acros and recrystallized from toluene to give pure 1*H*-pyridine-4-thione;[36] the abbreviation 4-pySH is used for both tautomers. *p*-FC_6H_4SH (Acros) was degassed prior to use. [Ru(TTP)(CO)(MeOH)] (TTP = 5,10,15,20-

tetra(*p*-tolyl)porphyrinato dianion) was synthesized according to the method described by Simonneaux and co-workers.[37] DMF and CH_2Cl_2 were distilled from CaH_2 and diethyl ether was distilled from Na/benzophenone. Solvents for air-sensitive compounds were thoroughly degassed or flushed with N_2 before use.

(*n*-Bu_4N)$_2$[Fe_4S_4(TriS)(SCysEt)] (2). A solution of EtCysSH (10.5 mg, 70.4 μmol) in DMF (1 mL) was added to a solution of **1**·0.06DMF[10] (99.0 mg, 64.1 μmol) in DMF (5 mL). The mixture was stirred under periodic vacuum for 3 h and evaporated to dryness. The residue was dissolved in CH_2Cl_2 (5 mL) and filtered. Addition of ether (40 mL) yielded a black precipitate, which was collected by centrifugation, washed with ether, and dried *in vacuo*. Yield: 101 mg (62.1 μmol, 97%). Anal. Calcd for $C_{76}H_{118}Fe_4N_6O_2S_8$: C, 56.08; H, 7.31; N, 5.16; S, 15.76. Found: C, 55.87; H, 7.24; N, 4.99; S, 15.70. ^{1}H NMR (300 MHz, CD_3CN): δ = 15.41 (s, very broad, 1 H, SCH_2), 14.37 (s, very broad, 1 H, SCH_2), 7.86 (d, broad, $^3J_{H\text{-}H}$ = 5.8 Hz, 3 H, indolyl H), 7.73 (d, $^3J_{H\text{-}H}$ = 8.3 Hz, 3 H, indolyl H), 7.32 (t, $^3J_{H\text{-}H}$ = 7.8 Hz, 3 H, indolyl H), 6.95 (t, broad, $^3J_{H\text{-}H}$ = 6.6 Hz, 3 H, indolyl H), 6.51 (s, 6 H, NCH_2), 5.53 (s, very broad, 1 H, EtCysS α-H), 4.24 (s, broad, 2 H, EtCysS CH_2CH$_3$), 3.06 (t, broad, $^3J_{H\text{-}H}$ = 8.0 Hz, 16 H, *n*-Bu_4N^+ α-CH_2), 2.42 (s, broad, 6 H, TriS CH_2CH$_3$), 1.60 (s, broad, 16 H, *n*-Bu_4N^+ β-CH_2), 1.43–1.26 (m, 19 H, EtCysS CH_2CH_3 and *n*-Bu_4N^+ γ-CH_2), 1.18 (s, broad, 9 H, TriS CH_2CH_3), 0.97 (t, $^3J_{H\text{-}H}$ = 7.1 Hz, 24 H, *n*-Bu_4N^+ CH_3). We were unable to locate the NH_2 resonance. λ_{max} (CH_2Cl_2), nm: 249 sh, 282 sh, 322 sh. FT-IR (ATR, ν, cm^{-1}): 2959, 2872, 1733, 1606, 1454, 1380, 1334, 1295, 1203, 1169, 1151, 1010, 881, 736. $E_{1/2}$ vs. Fc/Fc$^+$ in CH_2Cl_2 = –1.66 V (ΔE_p = 210 mV) [2–/3–]. $E_{1/2}$ vs. SCE in CH_2Cl_2 = –1.24 V [2–/3–].

(*n*-Bu_4N)$_2$[Fe_4S_4(TriS)(SC$_6$H$_4$-*p*-F)] (3). An 82.05 mM stock solution of *p*-FC_6H_4SH in DMF (390 μL, 32.0 μmol) was added to a solution of **1**·0.25DMF·0.08Et_2O[10] (50.0 mg, 32.0 μmol) in DMF (10 mL). The solution was stirred for 1 h, after which dynamic vacuum was applied periodically for 3 h to yield a sticky, black residue. This was dried *in vacuo* for 2 h and subsequently dissolved in CH_2Cl_2 (5 mL). The purple solution was filtered and diethyl ether (40 mL) was added. A black precipitate was collected by centrifugation, washed with diethyl ether, and dried *in vacuo*. Yield: 45 mg (28 μmol, 88%). Anal. Calcd for $C_{77}H_{112}FFe_4N_5S_8$: C, 57.56; H, 7.03; N, 4.36; S, 15.97. Found: C, 57.38; H, 6.88; N, 4.41; S, 16.11. ^{1}H NMR (300 MHz, CD_3CN): δ = 7.86 (s, broad, 5 H, indolyl H and *p*-FC_6H_4S *m*-H), 7.73 (d, $^3J_{H\text{-}H}$ = 8.0 Hz, 3 H, indolyl H), 7.30 (t, $^3J_{H\text{-}H}$ = 7.4 Hz, 3 H, indolyl H), 6.96 (t, broad, 3 H, indolyl H), 6.56 (s, broad, 6 H, NCH_2), 6.16 (s, broad, 2 H, *p*-FC_6H_4S *o*-H), 3.07 (t, broad, $^3J_{H\text{-}H}$ = 7.1 Hz, 16 H, *n*-Bu_4N^+ α-CH_2), 2.41 (d, broad, $^3J_{H\text{-}H}$ = 6.1 Hz, 6 H, TriS CH_2CH$_3$), 1.61 (s, broad, 16 H, *n*-Bu_4N^+ β-CH_2), 1.36 (sextet, broad, $^3J_{H\text{-}H}$ = 6.6 Hz, 16 H, *n*-Bu_4N^+ γ-CH_2), 1.18 (s, broad, 9 H, TriS CH_2CH_3), 0.97 (t, $^3J_{H\text{-}H}$ = 6.9 Hz, 24 H, *n*-Bu_4N^+ CH_3). $^{13}C\{^1H\}$ NMR (75 MHz, CD_3CN): δ = 157.13 (*p*-FC_6H_4S), 146.18 (aryl C), 139.49 (indolyl C), 132.47 (aryl C), 122.34, 120.88, 120.80 (3 × indolyl C), 111.99, 111.40 (2 × *p*-FC_6H_4S), 111.00 (indolyl C), 60.27 (*n*-Bu_4N^+ α-C), 42.05 (TriS NCH_2), 24.84 (*n*-Bu_4N^+ β-C), 23.98 (TriS CH_2CH$_3$), 20.95 (*n*-Bu_4N^+ γ-C), 16.23 (TriS CH_2CH_3), 14.24 (*n*-Bu_4N^+ CH_3). The resonances for three of the indolyl and one of the *p*-$FC_6H_4S^-$ C atoms were not observed. ^{19}F NMR (CD_3CN): δ = 45.27 ppm. Minor signals observed in the ^{19}F NMR spectrum at 45.66 and 45.36 ppm are discussed in the text. λ_{max} (CH_2Cl_2), nm: 247 sh, 285 sh, 319 sh. FT-IR (ATR, ν, cm^{-1}): 2959, 2872, 1582, 1480, 1455, 1380, 1335, 1295, 1207, 1152, 1082, 1010, 880, 821, 736. $E_{1/2}$ vs. Fc/Fc$^+$ in CH_2Cl_2 = –1.61 V (ΔE_p = 90 mV) [2–/3–], –0.48 (ΔE_p = 110 mV) [2–/1–]. $E_{1/2}$ vs. SCE in CH_2Cl_2 = –1.19 V [2–/3–], –0.06 V [2–/1–].

(*n*-Bu_4N)$_2$[Fe_4S_4(TriS)(S-4-py)] (4). A solution of 4-pySH (7.7 mg, 69 μmol) in DMF (2 mL) was added to a solution of **1**·0.09DMF[10] (107 mg, 69.2 μmol) in DMF (8 mL). The mixture was stirred under periodic vacuum for 4 h, resulting in a color change from purple to purple-brown, and evaporated to dryness. The

residue was dissolved in CH_2Cl_2 (10 mL) and filtered, after which ether (50 mL) was added. A black powder was collected by centrifugation, washed with ether (50 mL), and dried *in vacuo*. Yield: 93.9 mg (59.1 μmol, 85%). Anal. Calcd for $C_{76}H_{112}Fe_4N_6S_8$: C, 57.42; H, 7.10; N, 5.29; S, 16.14. Found: C, 57.30; H, 7.04; N, 5.22; S, 16.12. ^{1}H NMR (400 MHz, CD_3CN): δ = 8.82 (s, broad, 2 H, 4-pyS H2), 7.87 (s, broad, 3 H, indolyl H), 7.73 (d, $^3J_{H\text{-}H}$ = 8.5 Hz, 3 H, indolyl H), 7.30 (t, $^3J_{H\text{-}H}$ = 7.4 Hz, 3 H, indolyl H), 6.97 (t, broad, 3 H, indolyl H), 6.59 (s, 6 H, NCH_2), 6.07 (s, very broad, 2 H, 4-pyS H3), 3.06 (t, broad, 16 H, *n*-Bu_4N^+ *α*-CH_2), 2.42 (s, broad, 6 H, TriS CH_2CH$_3$), 1.60 (s, broad, 16 H, *n*-Bu_4N^+ *β*-CH_2), 1.35 (sextet, broad, $^3J_{H\text{-}H}$ = 6.3 Hz, 16 H, *n*-Bu_4N^+ *γ*-CH_2), 1.18 (t, broad, 9 H, TriS CH_2CH_3), 0.96 (t, $^3J_{H\text{-}H}$ = 6.7 Hz, 24 H, *n*-Bu_4N^+ CH_3). λ_{max} (CH_2Cl_2), nm: 244 sh, 280 sh, 317 sh. FT-IR (ATR, ν, cm^{-1}): 2958, 2871, 1568, 1452, 1379, 1335, 1294, 1203, 1009, 879, 805, 735, 704. $E_{1/2}$ vs. Fc/Fc$^+$ in CH_2Cl_2 = –1.56 V (ΔE_p = 62 mV) [2–/3–], –0.43 V (ΔE_p = 113 mV) [2–/1–]. $E_{1/2}$ vs. SCE in CH_2Cl_2 = –1.13 V [2–/3–], 0.00 V [2–/1–].

(*n*-$Bu_4N)_2[Fe_4S_4(SC_6H_4$-*p*-F)$_4$] (5). To a solution of (*n*-$Bu_4N)_2[Fe_4S_4$(S-*t*-Bu)$_4$][38] (50 mg, 42 μmol) in DMF (5 mL) was added *p*-FC_6H_4SH (22.3 μl, 210 μmol). The mixture was stirred for 30 min, after which dynamic vacuum was applied for 80 min. The solution was concentrated to approximately 2 mL by gently heating under vacuum and diethyl ether (40 mL) was added. A brown precipitate was collected by filtration, redissolved in CH_3CN, filtered, and evaporated to a black powder. Yield: 57 mg (42 μmol, 100%). Anal. Calcd for $C_{56}H_{88}F_4Fe_4N_2S_8$: C, 50.00; H, 6.59; N, 2.08; S, 19.07. Found: C, 49.83; H, 6.65; N, 1.99; S, 19.16. ^{1}H NMR (300 MHz, CD_3CN): δ = 7.87 (d, broad, $^3J_{H\text{-}H}$ = 8.3 Hz, 8 H, *m*-H), 5.90 (s, broad, 8 H, *o*-H), 3.08 (t, broad, $^3J_{H\text{-}H}$ = 8.4 Hz, 16 H, *n*-Bu_4N^+ *α*-CH_2), 1.61 (quintet, broad, $^3J_{H\text{-}H}$ = 7.8 Hz, 16 H, *n*-Bu_4N^+ *β*-CH_2), 1.36 (sextet, $^3J_{H\text{-}H}$ = 7.3 Hz, 16 H, *n*-Bu_4N^+ *γ*-CH_2), 0.97 (t, $^3J_{H\text{-}H}$ = 7.3 Hz, 24 H, *n*-Bu_4N^+ CH_3). ^{13}C{^{1}H} NMR (75 MHz, DMSO-d_6): δ = 162.46, 110.79, 110.51 (3 × *p*-FC_6H_4S), 57.68 (*n*-Bu_4N^+ *α*-C), 23.13 (*n*-Bu_4N^+ *β*-C), 19.34 (*n*-Bu_4N^+ *γ*-C), 13.57 (*n*-Bu_4N^+ CH_3). The signal of one C atom in *p*-FC_6H_4S was not observed. ^{19}F NMR (CD_3CN): δ = 45.67 ppm. λ_{max} (CH_2Cl_2), nm: 293 sh, 446. FT-IR (ATR, ν, cm^{-1}): 2961, 2933, 2874, 1584, 1480, 1379, 1220, 1154, 1083, 1014, 883, 818, 738. $E_{1/2}$ vs. Fc/Fc$^+$ in CH_2Cl_2 = –1.43 V (ΔE_p = 100 mV) [2–/3–], –0.33 V (ΔE_p = 90 mV) [2–/1–]. $E_{1/2}$ vs. SCE in CH_2Cl_2 = –1.01 V [2–/3–], +0.10 V [2–/1–]. ESI-MS: *m*/*z* = 430.0 ([$Fe_4S_4(SC_6H_4$-*p*-F)$_4$]$^{2-}$, calcd *m*/*z* = 429.8).

(*n*-$Bu_4N)_2[Fe_4S_4$(TriS)(μ-{S-4-py})Ru(TTP)(CO)] (6). CH_2Cl_2 (7 mL) was added to a mixture of **4** (33.0 mg, 20.8 μmol) and [Ru(TTP)(CO)(MeOH)] (18.0 mg, 21.7 μmol). The resulting brown solution was stirred for 30 min, after which ether (40 mL) was added. A brown product was collected by centrifugation and dried *in vacuo*. Yield: 36.8 mg (15.4 μmol, 74%). Anal. Calcd for $C_{125}H_{148}Fe_4N_{10}ORuS_8$: C, 62.88; H, 6.25; N, 5.87; S, 10.74. Found: C, 62.73; H, 6.18; N, 5.75; S, 10.80. ^{1}H NMR (400 MHz, CD_2Cl_2): δ = 8.60 (s, 8 H, porphyrin *β*-H), 8.06 (d, $^3J_{H\text{-}H}$ = 7.8 Hz, 4 H, tolyl H), 8.01–7.86 (m, 7 H, tolyl and indolyl H), 7.60 (d, $^3J_{H\text{-}H}$ = 8.1 Hz, 3 H, indolyl H), 7.53 (d, $^3J_{H\text{-}H}$ = 6.5 Hz, 8 H, tolyl H), 7.28 (t, broad, $^3J_{H\text{-}H}$ = 6.3 Hz, 3 H, indolyl H), 6.93 (s, broad, 3 H, indolyl H), 6.55 (s, 6 H, NCH_2), 2.91 (s, broad, 16 H, *n*-Bu_4N^+ *α*-CH_2), 2.67 (s, 12 H, tolyl CH_3), 2.32 (s, broad, 6 H, TriS CH_2CH$_3$), 1.51 (s, broad, 16 H, *n*-Bu_4N^+ *β*-CH_2), 1.22 (s, broad, 16 H, *n*-Bu_4N^+ *γ*-CH_2), 1.11 (s, broad, 9 H, TriS CH_2CH_3), 0.76 (s, broad, 24 H, *n*-Bu_4N^+ CH_3). We were unable to locate the 4-pyS resonances. λ_{max} (CH_2Cl_2), nm: 247 sh, 286 sh, 313 sh, 414, 534, 569. FT-IR (ATR, ν, cm^{-1}): 2961, 2873, 1937, 1590, 1478, 1456, 1380, 1303, 1212, 1110, 1070, 1008, 799, 737. $E_{1/2}$ vs. Fc/Fc$^+$ in CH_2Cl_2 = –1.54 V (ΔE_p = 76 mV) [2–/3–], –0.42 V (ΔE_p = 110 mV) [2–/1–]. $E_{1/2}$ vs. SCE in CH_2Cl_2 = –1.11 V [2–/3–], +0.01 V [2–/1–].

[Ru(TTP)(CO)(C_5H_5N)] (7). The phosphorescence spectrum of this compound has been reported elsewhere.[29] For convenience, we describe here its preparation and full characterization. Pyridine (3.7 μL, 46 μmol) was added to a solution of [Ru(TTP)(CO)(MeOH)] (30.4 mg, 36.6 μmol) in CH_2Cl_2 (10 mL) and

the mixture was stirred for 1 h in the dark. Hexane (10 mL) was added and the solution was concentrated to approximately 3 mL. After 3 h at –30 °C, a microcrystalline product was collected by centrifugation and dried *in vacuo*. Yield: 28.5 mg (32.5 μmol, 89%). Anal. Calcd for $C_{54}H_{41}N_5ORu$: C, 73.95; H, 4.71; N, 7.99. Found: C, 74.20; H, 4.71; N, 7.85. ^{1}H NMR (400 MHz, CD_2Cl_2): δ = 8.64 (s, 8 H, *β*-H), 8.10 (d, $^3J_{H\text{-}H}$ = 7.2 Hz, 4 H, tolyl H), 7.92 (d, $^3J_{H\text{-}H}$ = 7.9 Hz, 4 H, tolyl H), 7.55 (d, $^3J_{H\text{-}H}$ = 7.4 Hz, 4 H, tolyl H), 7.50 (d, $^3J_{H\text{-}H}$ = 8.0 Hz, 4 H, tolyl H), 6.13 (t, $^3J_{H\text{-}H}$ = 7.1 Hz, 1 H, C_5H_5N *p*-H), 5.23 (t, $^3J_{H\text{-}H}$ = 6.3 Hz, 2 H, C_5H_5N *m*-H), 2.68 (s, 12 H, CH_3), 0.88 (d, $^3J_{H\text{-}H}$ = 7.0 Hz, 2 H, C_5H_5N *o*-H). $^{13}C\{^1H\}$ NMR (100 MHz, CD_2Cl_2): δ = 180.93 (CO), 144.38, 144.24, 140.14, 137.60, 135.09, 134.71, 134.53, 132.23, 127.85, 127.60, 122.19, 122.08 (12 × TPP and C_5H_5N C), 21.76 (CH_3). λ_{max} (CH_2Cl_2), nm: 310, 413, 533, 569. FT-IR (ATR, ν, cm^{-1}): 3021, 2920, 2854, 1940, 1602, 1527, 1444, 1349, 1304, 1212, 1181, 1107, 1071, 1006, 792, 756, 715, 691. $E_{1/2}$ vs. Fc/Fc^+ in CH_2Cl_2 = –2.03 V (ΔE_p = 77 mV) [0/1–], 0.32 V (ΔE_p = 66 mV) [0/1+]. $E_{1/2}$ vs. SCE in CH_2Cl_2 = –1.61 V [0/1–], 0.74 V [0/1+].

^{19}F NMR titration. DMF solutions of **1** (5.0 mM) and *p*-FC_6H_4SH (9.9 mM) were mixed in varying ratios to yield 600 μL samples. The solutions were stirred for 2 h under periodic vacuum, evaporated and dried *in vacuo*, and finally dissolved and measured in CD_3CN.

4.5. References.

[1] (a) Beinert, H.; Holm, R. H.; Münck, E. *Science* **1997**, *277*, 653–659. (b) Johnson, M. K. *Curr. Opin. Chem. Biol.* **1998**, *2*, 173–181.

[2] (a) Nicolet, Y.; Piras, C.; Legrand, P.; Hatchikian, C. E.; Fontecilla-Camps, J. C. *Structure* **1999**, *7*, 13–23. (b) Peters, J. W.; Lanzilotta, W. N.; Lemon, B. J.; Seefeldt, L. C. *Science* **1998**, *282*, 1853–1858.

[3] (a) Doukov, T. I.; Iverson, T. M.; Seravalli, J.; Ragsdale, S. W.; Drennan, C. L. *Science* **2002**, *298*, 567–572. (b) Darnault, C.; Volbeda, A.; Kim, E. J.; Legrand, P.; Vernede, Z.; Lindahl, P. A.; Fontecilla-Camps, J. C. *Nat. Struct. Biol.* **2003**, *10*, 271–279.

[4] (a) Beinert, H.; Kennedy, M. C.; Stout, D. C. *Chem. Rev.* **1996**, *96*, 2335–2373. (b) Dupuy, J.; Volbeda, A.; Carpentier, P.; Darnault, C.; Moulis, J.-M.; Fontecilla-Camps, J. C. *Structure* **2006**, *14*, 129–139.

[5] (a) Holm, R. H. *Pure Appl. Chem.* **1998**, *70*, 931–938. (b) Venkateswara Rao, P.; Holm, R. H. *Chem. Rev.* **2004**, *104*, 527–559.

[6] Tard, C.; Liu, X.; Ibrahim, S. K.; Bruschi, M.; De Gioia, L.; Davies, S. C.; Yang, X.; Wang, L.-S.; Sawers, G.; Pickett, C. J. *Nature* **2005**, *433*, 610–613.

[7] Stack, T. D. P.; Holm, R. H. *J. Am. Chem. Soc.* **1987**, *109*, 2546–2547.

[8] (a) Whitener, M. A.; Peng, G.; Holm, R. H. *Inorg. Chem.* **1991**, *30*, 2411–2417. (b) Evans, D. J.; Garcia, G.; Leigh, G. J.; Newton, M. S.; Santana, M. D. *J. Chem. Soc., Dalton Trans.* **1992**, 3229–3234. (c) van Strijdonck, G. P. F.; van Haare, J. A. E. H.; van der Linden, J. G. M.; Steggerda, J. J.; Nolte, R. J. M. *Inorg. Chem.* **1994**, *33*, 999–1000. (d) van Strijdonck, G. P. F.; van Haare, J. A. E. H.; Hönen, P. J. M.; van den Schoor, R. C. G. M.; Feiters, M. C.; van der Linden, J. G. M.; Steggerda, J. J.; Nolte, R. J. M. *J. Chem. Soc., Dalton Trans.* **1997**, 449–461.

[9] Walsdorff, C.; Saak, W.; Pohl, S. *J. Chem. Soc., Dalton Trans.* **1997**, 1857–1861.

[10] van der Geer, E. P. L.; van Koten, G.; Klein Gebbink, R. J. M.; Hessen, B. *Inorg. Chem.*, accepted (Chapter 2 of this thesis).

[11] Stack, T. D. P.; Weigel, J. A.; Holm, R. H. *Inorg. Chem.* **1990**, *29*, 3745–3760.

[12] van der Geer, E. P. L.; Li, Q.; van Koten, G.; Klein Gebbink, R. J. M.; Hessen, B. *Inorg. Chim. Acta*, in press (Chapter 3 of this thesis).

[13] Que, L., Jr.; Anglin, J. R.; Bobrik, M. A.; Davison, A.; Holm, R. H. *J. Am. Chem. Soc.* **1974**, *96*, 6042–6048.

[14] DePamphilis, B. V.; Averill, B. A.; Herskovitz, T.; Que, L., Jr.; Holm, R. H. *J. Am. Chem. Soc.* **1974**, *96*, 4159–4167.
[15] Liu, H. Y.; Scharbert, B.; Holm, R. H. *J. Am. Chem. Soc.* **1991**, *113*, 9529–9539.
[16] Hansch, C.; Leo, A.; Taft, R. W. *Chem. Rev.* **1991**, *91*, 165–195, and references therein.
[17] Johnson, R. W.; Holm, R. H. *J. Am. Chem. Soc.* **1978**, *100*, 5338–5344.
[18] Holm, R. H.; Phillips, W. D.; Averill, B. A.; Mayerle, J. J.; Herskovitz, T. *J. Am. Chem. Soc.* **1974**, *96*, 2109–2117.
[19] Ciurli, S.; Carrié, M.; Weigel, J. A.; Carney, M. J.; Stack, T. D. P.; Papaefthymiou, G. C.; Holm, R. H. *J. Am. Chem. Soc.* **1990**, *112*, 2654–2664.
[20] For representative examples, see: (a) Wong, G. B.; Kurtz, D. M., Jr.; Holm, R. H.; Mortenson, L. E.; Upchurch, R. G. *J. Am. Chem. Soc.* **1979**, *101*, 3078–3090. (b) Mascharak, P. K.; Smith, M. C.; Armstrong, W. H.; Burgess, B. K.; Holm, R. H. *Proc. Nat. Acad. Sci. USA* **1982**, *79*, 7056–7060. (c) Stevens, W. C.; Kurtz, D. M., Jr. *Inorg. Chem.* **1985**, *24*, 3444–3449.
[21] Hoveyda, H. R.; Holm, R. H. *Inorg. Chem.* **1997**, *36*, 4571–4578.
[22] Blonk, H. L.; Kievit, O.; Roth, E. K.-H.; Jordanov, J.; van der Linden, J. G. M.; Steggerda, J. J. *Inorg. Chem.* **1991**, *30*, 3231–3234.
[23] (a) DeCollo, T. V.; Lees, W. J. *J. Org. Chem.* **2001**, *66*, 4244–4249. (b) Alborz, M.; Douglas, K. T.; Said, F. M. *J. Chem. Soc., Perkin Trans. II* **1982**, 1467–1470.
[24] Zhou, C.; Holm, R. H. *Inorg. Chem.* **1997**, *36*, 4066–4077.
[25] Albert, A.; Barlin, G. B. *J. Chem. Soc.* **1959**, 2384–2396.
[26] Chuchuryukin, A. V.; Chase, P. A.; Mills, A. M.; Lutz, M.; Spek, A. L.; van Klink, G. P. M.; van Koten, G. *Inorg. Chem.* **2006**, *45*, 2045–2054.
[27] Trost, B. M.; Frederiksen, M. U.; Rudd, M. T. *Angew. Chem., Int. Ed.* **2005**, *44*, 6630–6666.
[28] For representative examples, see: (a) Rauchfuss, T. B. *Science* **2007**, *316*, 585–587. (b) Na, Y.; Pan, J.; Wang, M.; Sun, L. *Inorg. Chem.* **2007**, *46*, 3813–3815. (c) Ekström, J.; Abrahamsson, M.; Olson, C.; Bergquist, J.; Kaynak, F. B.; Eriksson, L.; Sun, L.; Becker, H.-C.; Åkermark, B.; Hammarström, L.; Ott, S. *Dalton Trans.* **2006**, 4599–4606. (c) Justice, A. K.; Linck, R. C.; Rauchfuss, T. B.; Wilson, S. R. *J. Am. Chem. Soc.* **2004**, *126*, 13214–13215. (d) Konduri, R.; Ye, H.; MacDonnell, F. M.; Serroni, S.; Campagna, S.; Rajeshwar, K. *Angew. Chem., Int. Ed.* **2002**, *41*, 3185–3187.
[29] Chichak, K.; Branda, N. R. *Chem. Commun.* **1999**, 523–524.
[30] Cheng, R.-J.; Lin, S.-H.; Mo, H.-M. *Organometallics* **1997**, *16*, 2121–2126.
[31] McCleverty, J. A.; Navas Badiola, J. A.; Ward, M. D. *J. Chem. Soc., Dalton Trans.* **1994**, 2415–2421.
[32] Annoni, E.; Pizzotti, M.; Ugo, R.; Quici, S.; Morotti, T.; Casati, N.; Macchi, P. *Inorg. Chim. Acta* **2006**, *359*, 3029–3041.
[33] (a) Levine, L. M. A.; Holten, D. *J. Phys. Chem.* **1988**, *92*, 714–720. (b) Tait, C. D.; Holten, D.; Barley, M. H.; Dolphin, D.; James, B. R. *J. Am. Chem. Soc.* **1985**, *107*, 1930–1934. (c) Kadish, K. M.; Chang, D. *Inorg. Chem.* **1982**, *21*, 3614–3618. (d) Kadish, K. M.; Leggett, D. J.; Chang, D. *Inorg. Chem.* **1982**, *21*, 3618–3622.
[34] Masui, M.; Sayo, H.; Tsuda, Y. *J. Chem. Soc. B* **1968**, 973–976.
[35] Bruins, A. P.; Covey, T. R.; Henion, J. D. *Anal. Chem.* **1987**, *59*, 2642–2646.
[36] Stoyanov, S.; Petkov, I.; Antonov, L.; Stoyanova, T.; Karagiannidis, P.; Aslanidis, P. *Can. J. Chem.* **1990**, *68*, 1482–1489.
[37] Poriel, C.; Ferrand, Y.; Juillard, S.; Le Maux, P.; Simonneaux, G. *Tetrahedron* **2004**, *60*, 145–158.
[38] Christou, G. C.; Garner, C. D. *J. Chem. Soc., Dalton Trans.* **1979**, 1093–1094.

Chapter 5

Effects of the Chelating [4Fe-4S] Ligand on a Model for the Iron-Only Hydrogenase H Cluster

Abstract. *A new stuctural model of the H cluster of iron-only hydrogenase is presented. The mimic is closely related to the only other reported H cluster model encompassing both [4Fe-4S] and di-iron subunits, but contains a 3:1 site-differentiated cluster with an alternative chelating ligand and different redox properties. The modification of the [4Fe-4S] cluster results in a stronger bridge between the [4Fe-4S] cluster and di-iron moieties. Furthermore, the moieties show substantial redox coupling, as also observed in the Fe-only hydrogenase from* Desulfovibrio desulfuricans*.*

van der Geer, E. P. L.; Panday, D.; van Koten, G.; Klein Gebbink, R. J. M.; Hessen, B., to be submitted.

5.1. Introduction.

In recent years, the enzyme iron-only hydrogenase has been the focus of intense theoretical[1] and synthetic[2] modelling efforts. The research appeal springs partially from the industrial interest in dihydrogen fuel cells, but also from a more fundamental, mechanistic, and structural interest in how iron-only hydrogenase is able to catalyze the reversible redox chemistry of dihydrogen. The active site (H cluster) features a [4Fe-4S] cluster bridged *via* a cysteinyl sulfur atom to the proximal iron atom (Fe_p) of a di-iron subsite (Chart 1). Fe_p is, in turn, bridged to the subsite's distal iron atom Fe_d by a low-molecular weight cofactor, probably 1,3-propanedithiolate or di(thiolatomethyl)amine. In addition to the empty (or aquated) coordination site on Fe_d that is the presumed site of proton reduction and dihydrogen binding, the remaining coordination positions in the di-iron subunit are occupied by carbonyl and cyanide ligands.[3]

Most H cluster models synthesized thus far have focused on the di-iron subsite, owing to the presumed location of the catalytic cycle on Fe_d.[2] However, the incorporation of [4Fe-4S] clusters into models for cluster-containing active sites can lead to important new mechanistic insights.[4] Recently, Pickett and co-workers have incorporated a [4Fe-4S] cluster into the first and only full H cluster mimic (**1**, Chart 1) and demonstrated that the model is capable of electrocatalyzing proton reduction. **1** was further found to possess complex electrochemical properties in MeCN, involving the ability to undergo intramolecular charge transfers leading to cleavage of the [4Fe-4S]–S–Fe_p bridge.[5]

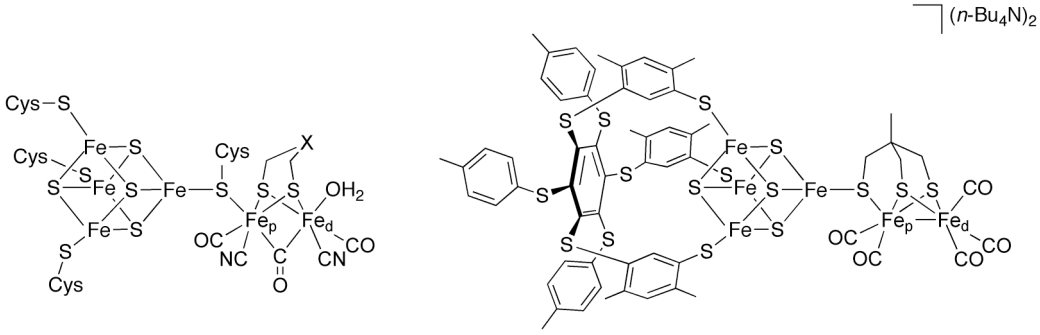

Chart 1. Schematic representation of the iron-only hydrogenase H cluster (left)[3] and the structure of its recently reported mimic (**1**, right).[5]

The [4Fe-4S] cluster in **1** is chelated by the tripodal LS_3^{3-} ligand, which effectively blocks three of the four coordination positions of a [4Fe-4S] cluster and leaves one iron atom available for site-specific modification.[6] Recently, we have explored the chemistry of the cluster $(n\text{-}Bu_4N)_2[Fe_4S_4(TriS)(SEt)]$ (**2**, Chart 2), which is chelated by the alternative $TriS^{3-}$ ligand (Chart 2).[7] In general, $TriS^{3-}$-chelated clusters display redox transitions at more negative potentials than LS_3^{3-}-chelated analogues.[8] Especially when the electrochemical properties of an active-site model are paramount in understanding its structure and function,

modifying the properties of a constituent [4Fe-4S] cluster may have revealing consequences for the behavior of the mimic as a whole. Hence, we decided to employ **2** in the synthesis of a $TriS^{3-}$ analogue of H cluster model **1** and explore the spectroscopic and (electro)chemical consequences of the ligand modification.

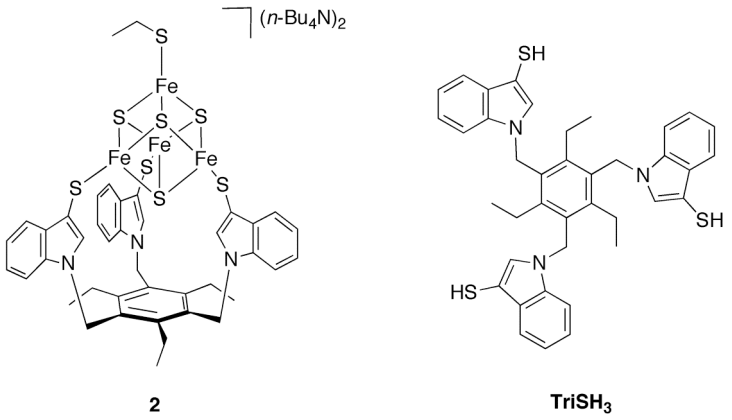

Chart 2. $(n\text{-}Bu_4N)_2[Fe_4S_4(TriS)(SEt)]$ (**2**) and $TriSH_3$.

5.2. Results and discussion.

5.2.1. Synthesis.

The reported synthesis of iron-only hydrogenase mimic **1** involved separate preparations of the [4Fe-4S] cluster and di-iron subsite units, which were then combined in a final coupling step to yield the full mimic.[5] In this procedure, the synthesis of the di-iron subsite required two flash chromatographic purifications under inert conditions. In an attempt to simplify the envisioned synthesis of our $TriS^{3-}$-chelated analogue, we conceived a less convergent but more efficient route building on the 3:1 site-differentiated [4Fe-4S] cluster (Scheme 1).

The trithiol 1,1,1-tris(mercaptomethyl)ethane (LH_3) was first coordinated to cluster **2** by means of a thiol-thiolate exchange reaction[9] in DMF. A threefold excess of LH_3 was used to minimize the potential formation of bridged cluster compounds. Nonetheless, evaporation of the reaction mixture resulted in a product that was not fully soluble in CH_2Cl_2, indicating that some oligomer formation had occurred. These oligomeric species could be removed by means of a filtration step, and precipitation with diethyl ether then yielded the product $(n\text{-}Bu_4N)_2[Fe_4S_4(TriS)(LH_2)]$ (**3**) in a good yield of 82%.

Precursor **3** was then converted into H cluster mimic $(n\text{-}Bu_4N)_2[Fe_4S_4(TriS)\{(L)Fe_2(CO)_5\}]$ (**4**) in 55% yield by reaction with a stoichiometric amount of $[Fe_3(CO)_{12}]$ in MeCN. Elemental analysis results were consistent with the proposed formulation.[10]

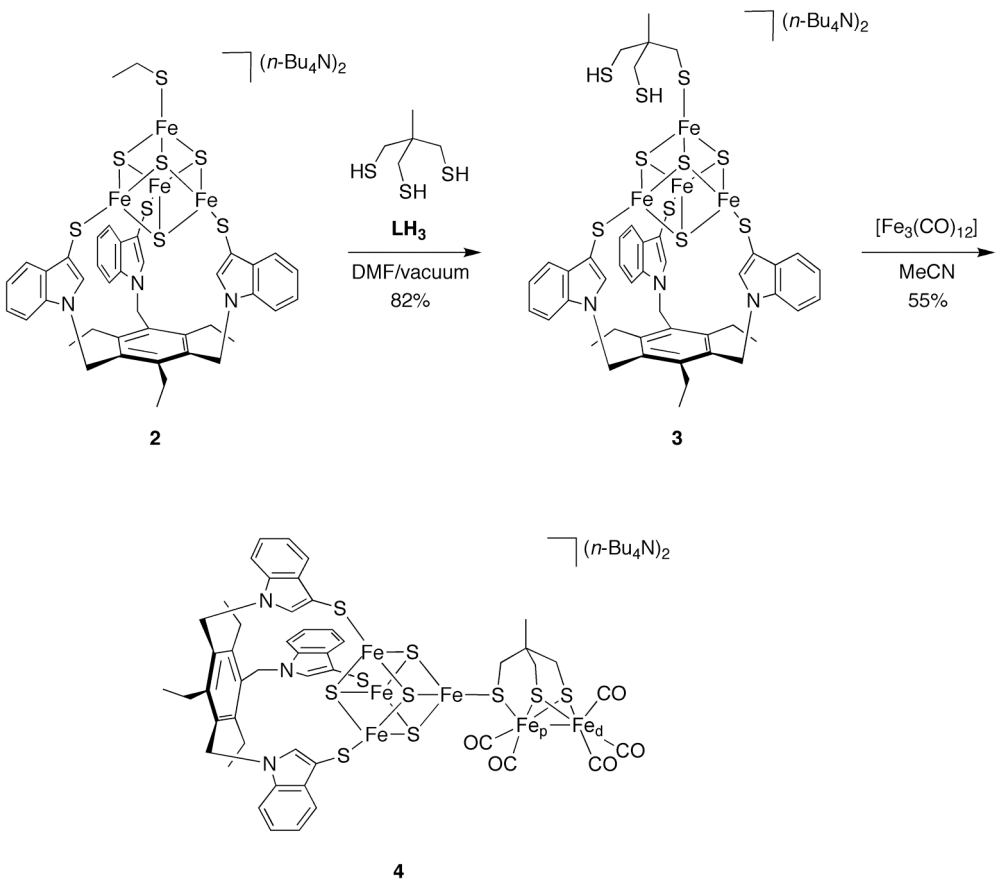

Scheme 1. Synthesis of H cluster mimic **4**.

5.2.2. ^{1}H NMR spectroscopy.

The ^{1}H NMR spectrum of **4** in CD_3CN shows all the expected $TriS^{3-}$ signals at chemical shifts comparable to those in **3**,[8] indicating that the $TriS^{3-}$ ligand is barely influenced by the modification at the non-chelated iron site (Figure 1, Table 1). On the other hand, the signals of the EtS^- ligand in **3** have been replaced by three singlets at 3.61, 3.43, and 1.81 ppm, as well as a very broad signal at 13.03 ppm. The broadness of this latter signal and its shift to a high frequency are characteristic of hydrogen atoms experiencing strong contact shifting by a [4Fe-4S] cluster; hence, this signal can be assigned to the cluster-bound thiolatomethyl hydrogen atoms (H_c) of LH_2^-. The signal at 1.81 ppm is assigned to the methyl hydrogen atoms (H_a) of LH_2^-. The methylene hydrogen atoms of the non-coordinating arms of LH_2^- are enantiotopic and should thus give rise to separate signals H_b and H'_b. Most likely, these correspond to the peaks observed at 3.61 and 3.41 ppm, although we are unable to explain the difference in lineshape for these two signals. Unfortunately, we were unable to detect a signal for the free SH protons. By comparing the observed resonances to the spectrum of free LH_3 in CD_3CN, the present signal assignment was found to lead to reasonable contact shift magnitudes (Table 1).[11]

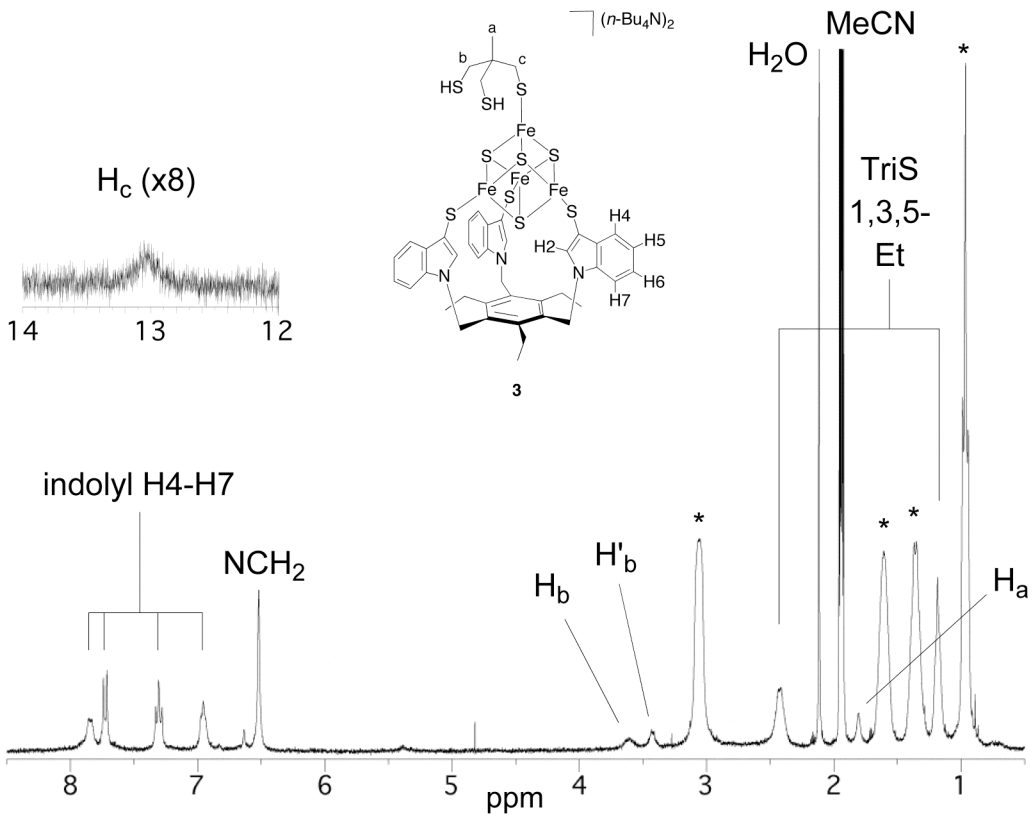

Figure 1. ^{1}H NMR spectrum of (n-Bu$_4$N)$_2$[Fe$_4$S$_4$(TriS)(LH$_2$)] (**3**) in CD$_3$CN. n-Bu$_4$N$^+$ signals are marked with asterisks.

Table 1. Selected ^{1}H NMR data for **3**.

Ligand	Signal	δ (ppm)	Contact shift (ppm)*
TriS^{3-}	indolyl H4–H7	7.84, 7.73, 7.31, 6.95	
	NCH_2	6.52	
	1,3,5-Et$_3$	2.43, 1.18	
LH_2^-	H_c	13.03	10.44
	H_b	3.61	1.02
	H'_b	3.43	0.84
	H_a	1.81	0.20

*calculated with respect to the free ligand in the same solvent (CD$_3$CN)

The ^{1}H NMR spectrum of **4**, measured in DMSO-d_6 due to the compound's limited solubility in CD$_3$CN, clearly demonstrates the effects of di-iron subsite binding (Figure 2). Spectral evidence for the L^{3-} ligand is not clearly present. The observed aromatic signals are significantly broader than those in the precursor cluster **3**, rendering signal assignment difficult. Unfortunately, comparison of the ^{1}H NMR spectrum of **4** to that of **1** is not possible as the ^{1}H NMR characterization of the latter model has not been reported, save for a broad

signal at 5.84 ppm assigned to the bridging CH_2S^- group.[12] The absence of L^{3-} signals in the ^1H NMR spectrum of **4** is unexpected and suggests that a significant amount of spin density resides on the di-iron subsite, resulting in strong contact shifting of the L^{3-} hydrogen atoms. Such a situation could arise if there is a high degree of coupling between the di-iron subsite and the [4Fe-4S] cluster, essentially forming one large redox unit as also suggested by cyclic voltammetry (*vide infra*). Recent EPR studies on the oxidized and CO-inhibited forms of *Desulfovibrio desulfuricans* iron-only hydrogenase have indicated that the spin density in this enzyme is similarly delocalized over the entire H cluster.[13]

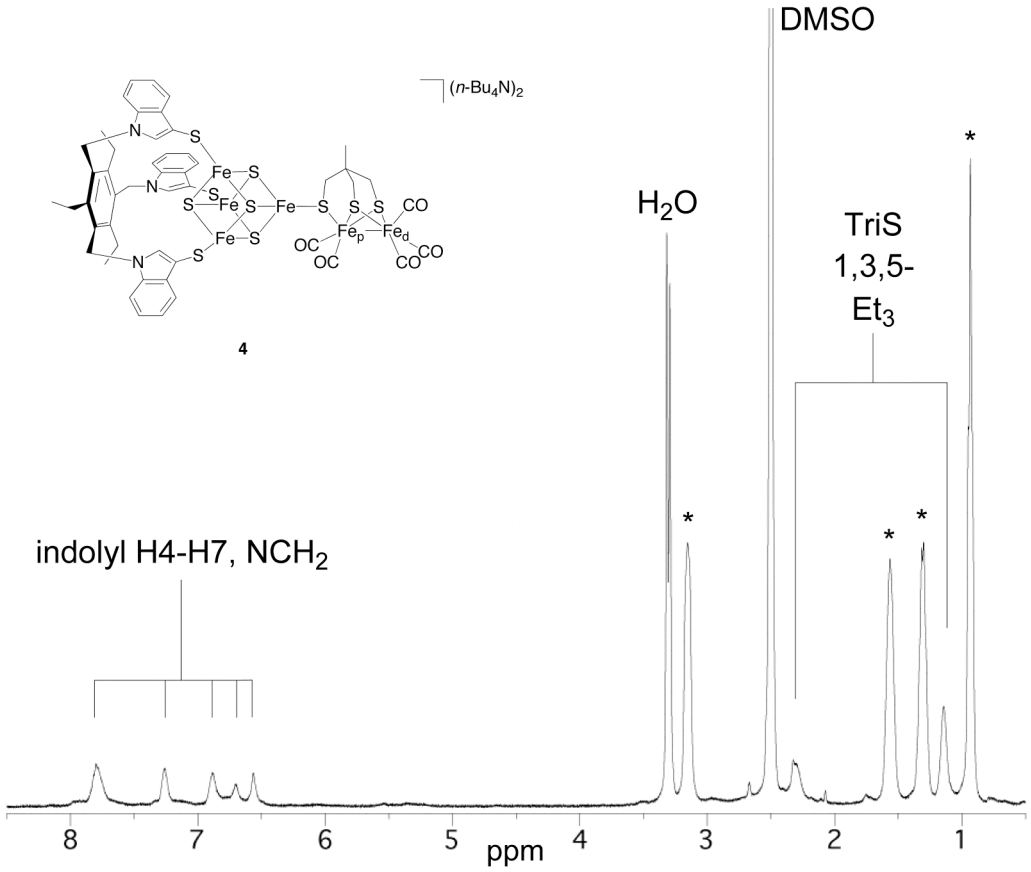

Figure 2. ^1H NMR spectrum of H cluster mimic **4** in DMSO-d_6. n-Bu_4N^+ signals are marked with asterisks.

5.2.3. Electrochemistry.

In MeCN, **3** shows a reversible 2–/3– transition at –1.51 V vs. Fc/Fc^+, which is close to the redox potential of –1.53 V observed for the analogous transition in **2** (Figure 3). The similarity is expected, given the fact that the conversion of **2** to **3** involves a substitution of the EtS^- ligand for another aliphatic thiolate of comparable electron-donating ability. To our surprise, however, the cyclic voltammogram of mimic **4** is also highly similar and displays the 2–/3– transition at –1.54 V (Figure 3). A secondary (irreversible) redox process in the form of a weak shoulder around –1.45 V may be the result of a slight impurity.

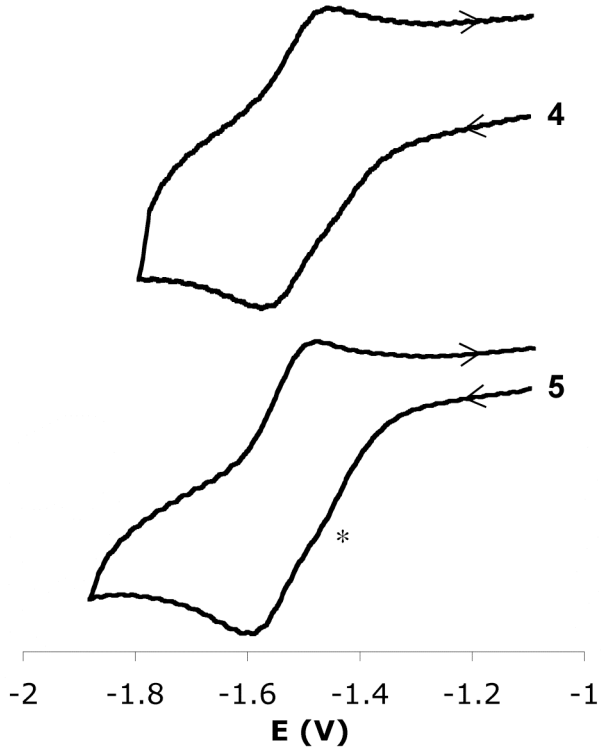

Figure 3. Cyclic voltammograms of **3** (top) and **4** (bottom) in MeCN (vs. Fc/Fc^+, 100 mV/s). The shoulder in the cyclic voltammogram of **4** is marked with an asterisk.

In cyclic voltammetry of **1**, Pickett and co-workers clearly observed two distinct redox processes. The authors hypothesized that the first reduction of the [4Fe-4S] cluster at –1.41 V[14] (process I), observed as a shoulder of the main signal at low scan rates, was followed by an intramolecular charge transfer to the di-iron subsite, with a concomitant opening of the [4Fe-4S]–S–Fe_p bridge (Scheme 2). The second reduction of the [4Fe-4S] cluster (process II) then occurred at a potential similar to that of the parent compound (n-$Bu_4N)_2[Fe_4S_4(LS_3)(SEt)]$ (–1.50 V and –1.52 V,[14] respectively). Higher scan speeds led to supression of the intermolecular charge transfer, and hence to an increase in the intensity of the signal for process I as compared to that of process II.[5]

In **4**, the scan rate was found to have no influence on the shape of the cyclic voltammogram. Repeated cyclic voltammetry over ten cycles also had no effect on **4**, in contrast to **1**, for which repeated cycling proved necessary to establish equilibrium.

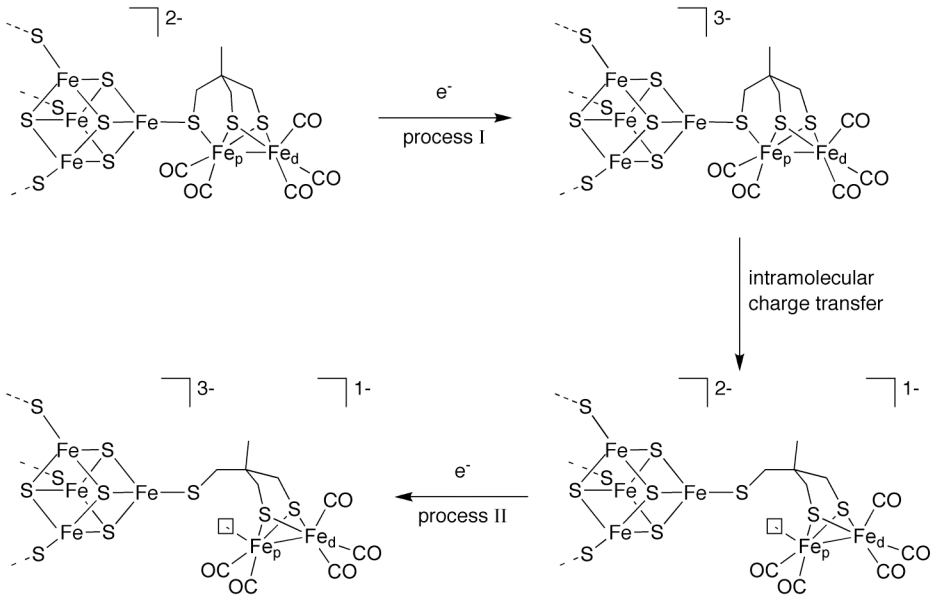

Scheme 2. Mechanism proposed by Pickett and co-workers for the electrochemistry of **1**. The backbone of the LS_3^{3-} ligand has been omitted for clarity.

The differences observed between the cyclic voltammograms of **1** and **4** indicate that the nature of the chelating [4Fe-4S] ligand has a substantial effect on the electrochemistry of the two mimics.[15] It appears that the [4Fe-4S] and di-iron subunits in **4** are strongly coupled to form a single redox system, as also suggested by ^{1}H NMR (*vide supra*) and as observed in the *Desulfovibrio desulfuricans* Fe-only hydrogenase.[13] The redox potential of –1.54 V for the [2–/3–] process can then be rationalized on the basis of the potentials of the respective subunits: **3** is reduced at –1.51 V while the di-iron subsite, if the [4Fe-4S] cluster is replaced by a methyl or benzyl group, requires the more negative potentials of –1.76 and –1.74 V, respectively.[16,17] Furthermore, the apparent greater stability of the [4Fe-4S]–S–Fe_p bridge in **4** as compared to **1**, and hence the absence of process I in the cyclic voltammogram of **4**, can be explained by the stronger electron-donating ability of the $TriS^{3-}$ as compared to the LS_3^{3-} ligand. The resultant increased electron density in the [4Fe-4S] cluster leads to a greater Lewis basicity for the bridging sulfur atom, and hence to a stronger bridging interaction. This is supported by the fact that **4** shows CO stretching frequencies at 2028 and 1954 cm^{-1}, substantially lower than the analogous signals in the IR spectrum of **1** (2035 and 1970 cm^{-1}), respectively.

5.2.4. Electrocatalytic proton reduction.

In order to facilitate comparison of the performance of mimic **4** with that of **1** in electrocatalytic proton reduction, **4** was applied as a catalyst under identical conditions;[5] that is, using a vitreous carbon working electrode and 2,6-dimethylpyridinium tetrafluoroborate (DMPT) as proton source.[18] Unfortunately, solutions of **4** are unstable in the presence of excess DMPT, as manifested by a color change from purple to brown and the formation of a

black precipitate. Since the [4Fe-4S] cluster is electron-richer in **4** than in **1** and contains a more basic chelating trithiolate, a more acute acid sensitivity for **4** is not unexpected.

Without **4**, a 15 mM solution of DMPT exhibits a strong reduction wave at –1.99 V. In order to minimize cluster decomposition, the electrocatalytic run was performed on a 15 mM solution of DMPT immediately after addition of 0.1 equiv. of **4**. The DMPT reduction wave was consequently shifted from –1.99 V in the uncatalyzed run to –1.93 V, but also became significantly less intense (Figure 5). Generally, the main evidence that electrocatalysis is occurring is not a potential shift but an increase in the reduction or oxidation peak current;[19] a likely cause for the peak decrease observed here is electrode surface fouling as a result of the decomposition of **4**. The shift in the E_{red} of DMPT provides tentative support for electrocatalytic activity by **4**, but confirmation will depend on finding a novel proton source in the presence of which mimic **4** is sufficiently stable.

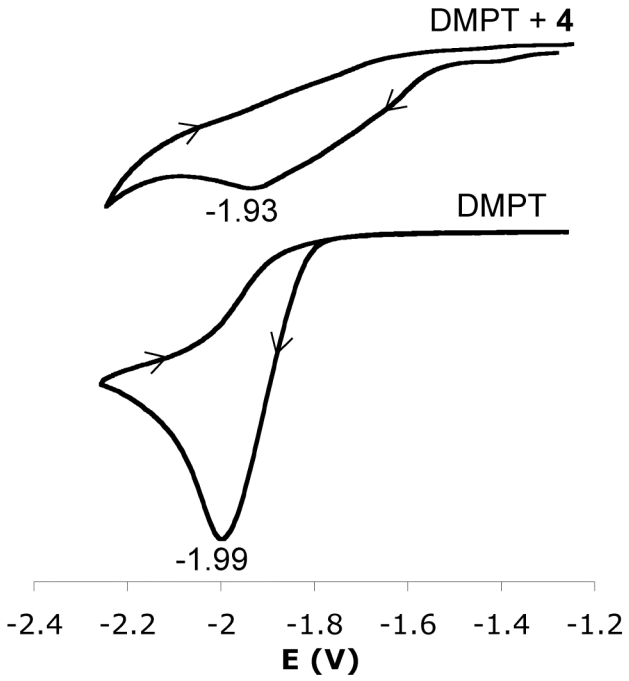

Figure 5. Cyclic voltammograms of DMPT in MeCN, in the absence (bottom) and presence (top) of H cluster mimic **4** (vs. Fc/Fc^+, 100 mV/s).

5.3. Conclusion.

The choice of tripodal ligand used to chelate three of the four cluster iron atoms in an active-site model can have profound consequences on the model's (electro)chemical properties, and hence on its behavior as a biomimic. Despite the structural similarity between **1** and **4**, the two hydrogenase H cluster mimics display different electrochemical properties, and indicate that only **4** reproduces the strong interaction between the [4Fe-4S] and di-iron redox units observed in the *Desulfovibrio desulfuricans* H cluster. This may, to some extent,

be the result of a stronger [4Fe-4S]–S–Fe_p bridge in **4**, for which no bridge lability such as in **1** was observed. Future comparisons of biomimics chelated by $TriS^{3-}$ and LS_3^{3-} may help to further unravel the effect of the chelating ligand on the mimic as a whole, and help to apply this knowledge in choosing the 3:1 site-differentiated [4Fe-4S] cluster to be incorporated into a biomimetic design.

5.4. Experimental.

General methods. ^{1}H NMR spectra were recorded at 298 K on a Varian 400 MHz or a Bruker AC 300 spectrometer. Spectra were calibrated on the residual solvent peaks, and assignments were based on chemical shift, integral, and linewidth considerations. Infrared spectra were recorded on a Perkin-Elmer Spectrum One FT-IR spectrometer. UV-Vis spectra were recorded on a Varian Cary 50 Scan UV-Visible spectrophotometer. Elemental analyses were carried out by Kolbe Mikroanalytisches Laboratorium (Mülheim an der Ruhr, Germany). Cyclic voltammograms were recorded using a vitreous carbon working electrode, a Pt counter electrode, and a water-free Ag/AgCl reference electrode (0.45 M *n*-Bu_4NBF_4 and 0.05 M *n*-Bu_4NCl in CH_2Cl_2). The supporting electrolyte was 0.1 M *n*-Bu_4NClO_4. Potentials were referenced to a ferrocene (Fc) internal standard.

Air-sensitive compounds were handled in a glovebox or using standard Schlenk techniques. [$Fe_3(CO)_{12}$] was purchased from Acros and used as received. 1,1,1-Tris(mercaptomethyl)ethane (LH_3) was synthesized according to a literature procedure.[20] 2,6-Dimethylpyridinium tetrafluoroborate was synthesized by treatment of 2,6-lutidine with aqueous HCl, followed by an anion exchange with $AgBF_4$. DMF and CH_2Cl_2 were distilled from CaH_2 and diethyl ether was distilled from Na/benzophenone. MeCN for cyclic voltammetry was distilled from $KMnO_4$ and Na_2CO_3.[21] Solvents for air-sensitive compounds were thoroughly degassed or flushed with N_2 before use.

(*n*-$Bu_4N)_2[Fe_4S_4(TriS)(LH_2)]$ (3). (*n*-$Bu_4N)_2[Fe_4S_4(TriS)(SEt)]\cdot 0.25DMF\cdot 0.08Et_2O$[8] (117 mg, 0.0748 mmol) and LH_3 (37.8 mg, 0.225 mmol) were dissolved in DMF (7 mL). The resulting solution was treated with periodic vacuum for 6 h and then evaporated to dryness. The residue was dissolved in CH_2Cl_2 (5 mL) and filtered to remove some insoluble black material. After addition of ether (40 mL), a black precipitate was collected by centrifugation. The product was redissolved in CH_2Cl_2 (5 mL), again precipitated by adding ether (40 mL), collected by centrifugation, and dried *in vacuo*. Yield: 101 mg (0.0613 mmol, 82%). Anal. Calcd for $C_{76}H_{119}Fe_4N_5S_{10}$: C, 55.43; H, 7.28; N, 4.25; S, 19.47. Found: C, 55.32; H, 7.21; N, 4.22; S, 19.59. ^{1}H NMR (300 MHz, CD_3CN): δ = 13.03 (s, very broad, 2 H, Fe-SCH_2), 7.84 (d, broad, $^3J_{H\text{-}H}$ = 5.9 Hz, 3 H, indolyl H), 7.73 (d, $^3J_{H\text{-}H}$ = 8.3 Hz, 3 H, indolyl H), 7.31 (t, $^3J_{H\text{-}H}$ = 7.5 Hz, 3 H, indolyl H), 6.95 (t, broad, 3 H, indolyl H), 6.52 (s, 6 H, NCH_2), 3.61 (s, broad, 2 H, CH_2SH), 3.43 (s, broad, 2 H, CH_2SH), 3.06 (s, broad, 16 H, *n*-Bu_4N^+ α-CH_2), 2.43 (s, broad, 6 H, TriS CH_2CH_3), 1.81 (s, 2 H, $(CH_2)_3CCH_3$), 1.61 (s, broad, 16 H, *n*-Bu_4N^+ β-CH_2), 1.36 (sextet, broad, 16 H, *n*-Bu_4N^+ γ-CH_2), 1.18 (t, broad, 9 H, TriS CH_2CH_3), 0.97 (t, $^3J_{H\text{-}H}$ = 6.5 Hz, 24 H, *n*-Bu_4N^+ CH_3). We were unable to locate the SH resonance. $\lambda_{max}(CH_2Cl_2)$, nm: 250 sh, 286 sh, 324 sh. FT-IR (ATR, ν, cm^{-1}): 2958, 2871, 1454, 1379, 1335, 1295, 1203, 1170, 1150, 1010, 881, 735. $E_{1/2}$ vs. Fc/Fc^+ in MeCN = –1.51 V (ΔE_p = 100 mV) [2–/3].

(*n*-$Bu_4N)_2[Fe_4S_4(TriS)\{(L)Fe_2(CO)_5\}]$ (4). Compound **3** (48.1 mg, 0.0292 mmol) and [$Fe_3(CO)_{12}$] (9.8 mg, 0.019 mmol) were dissolved in MeCN (8 mL) and stirred in the dark overnight. The clear solution was concentrated to approximately 4 mL and diethyl ether (40 mL) was added. A black precipitate was collected by centrifugation and dried *in vacuo*. Yield: 30.6 mg (0.0161 mmol, 55%). Anal. Calcd for

$C_{81}H_{117}Fe_6N_5O_5S_{10}$: C, 51.30; H, 6.22; N, 3.69; S, 16.91. Found: C, 51.06; H, 6.30; N, 3.77; S, 16.68. ^{1}H NMR (400 MHz, DMSO-d_6): δ = 7.87–7.70 (m, 6 H), 7.26 (s, 3 H), 6.95–6.48 (m, 9 H), 3.15 (t, 16 H, *n*-Bu_4N^+ α-CH_2), 2.30 (s, 6 H, TriS CH_2CH$_3$), 1.56 (s, 16 H, *n*-Bu_4N^+ β-CH_2), 1.31 (sextet, $^3J_{H\text{-}H}$ = 6.2 Hz, 16 H, *n*-Bu_4N^+ γ-CH_2), 1.14 (s, 9 H, TriS CH_2CH_3), 0.93 (t, $^3J_{H\text{-}H}$ = 6.0 Hz, 24 H, *n*-Bu_4N^+ CH_3). All the observed signals were broad. $\lambda_{max}(CH_2Cl_2)$, nm: 249 sh, 283 sh, 325 sh. FT-IR (ATR, ν, cm^{-1}): 2959, 2871, 2028, 1953, 1453, 1379, 1334, 1294, 1202, 1151, 1010, 878, 735. $E_{1/2}$ vs. Fc/Fc$^+$ in MeCN = –1.54 V (ΔE_p = 110 mV) [2–/3].

5.5. References.

[1] For reviews, see: (a) Armstrong, F. A. *Curr. Opin. Chem. Biol.* **2004**, *8*, 133–140. (b) Bruschi, M.; Zampella, G.; Fantucci, P.; De Gioia, L. *Coord. Chem. Rev.* **2005**, *249*, 1620–1640. (c) Georgakaki, I. P.; Thomson, L. M.; Lyon, E. J.; Hall, M. B.; Darensbourg, M. Y. *Coord. Chem. Rev.* **2003**, *238–239*, 255–266. (d) Bertini, L.; Bruschi, M.; De Gioia, L.; Fantucci, P.; Greco, C. *Top. Curr. Chem.* **2007**, *268*, 1–46.

[2] For reviews, see: (a) Liu, X.; Ibrahim, S. K.; Tard, C.; Pickett, C. J. *Coord. Chem. Rev.* **2005**, *249*, 1641–1652. (b) Evans, D. J.; Pickett, C. J. *Chem. Soc. Rev.* **2003**, *32*, 268–275. (c) Darensbourg, M. Y.; Lyon, E. J.; Zhao, X.; Georgakaki, I. P. *Proc. Natl. Acad. Sci. U.S.A.* **2003**, *100*, 3683–3688. (d) Capon, J.-F.; Gloaguen, F.; Schollhammer, P.; Talarmin, J. *Coord. Chem. Rev.* **2005**, *249*, 1664–1676. For more recent representative examples, see: (e) Justice, A. K.; Zampella, G.; De Gioia, L.; Rauchfuss, T. B.; van der Vlugt, J. I.; Wilson, S. R. *Inorg. Chem.* **2007**, *46*, 1655–1664. (f) Liu, T.; Darensbourg, M. Y. *J. Am. Chem. Soc.* **2007**, *129*, 7008–7009. (g) Adam, F. I.; Hogarth, G.; Richards, I.; Sanchez, B. E. *Dalton Trans.* **2007**, *24*, 2495–2498. (h) Morvan, D.; Capon, J.-F.; Gloaguen, F.; Le Goff, A.; Marchivie, M.; Michaud, F.; Schollhammer, P.; Talarmin, J.; Yaouanc, J.-J.; Pichon, R.; Kervarec, N. *Organometallics* **2007**, *26*, 2042–2052. (i) Song, L.-C.; Yin, B.-S.; Li, Y.-L.; Zhao, L.-Q.; Ge, J.-H.; Yang, Z.-Y.; Hu, Q.-M. *Organometallics* **2007**, *26*, 4921–4929. (j) Jiang, S.; Liu, J.; Shi, Y.; Wang, Z.; Åkermark, B.; Sun, L. *Dalton Trans.* **2007**, 896–902. (k) Gao, W.; Ekström, J.; Liu, J.; Chen, C.; Eriksson, L.; Weng, L.; Åkermark, B.; Sun, L. *Inorg. Chem.* **2007**, *46*, 1981–1991. (k) Schwartz, L.; Ekström, J.; Lomoth, R.; Ott, S. *Chem. Commun.* **2006**, 4206–4208. (l) Schwartz, L.; Eilers, G.; Eriksson, L.; Gogoll, A.; Lomoth, R.; Ott, S. *Chem. Commun.* **2006**, 520–522. (m) Dong, W.; Wang, M.; Liu, X.; Jin, K.; Li, G.; Wang, F.; Sun, L. *Chem. Commun.* **2006**, 305–307. (n) Ezzaher, S.; Capon, J.-F.; Gloaguen, F.; Petillon, F. Y.; Schollhammer, P.; Talarmin, J.; Pichon, R.; Kervarec, N. *Inorg. Chem.* **2007**, *46*, 3426–3428. (o) Aguirre de Carcer, I.; DiPasquale, A.; Rheingold, A. L.; Heinekey, D. M. *Inorg. Chem.* **2006**, *45*, 8000–8002.

[3] (a) Nicolet, Y.; Piras, C.; Legrand, P.; Hatchikian, C. E.; Fontecilla-Camps, J. C. *Structure* **1999**, *7*, 13–23. (b) Peters, J. W.; Lanzilotta, W. N.; Lemon, B. J.; Seefeldt, L. C. *Science* **1998**, *282*, 1853–1858. (c) Nicolet, Y.; Cavazza, C.; Fontecilla-Camps, J. C. *J. Inorg. Biochem.* **2002**, *91*, 1–8.

[4] (a) Holm, R. H. *Pure Appl. Chem.* **1998**, *70*, 931–938. (b) Venkateswara Rao, P.; Holm, R. H. *Chem. Rev.* **2004**, *104*, 527–559.

[5] Tard, C.; Liu, X.; Ibrahim, S. K.; Bruschi, M.; De Gioia, L.; Davies, S. C.; Yang, X.; Wang, L.-S.; Sawers, G.; Pickett, C. J. *Nature* **2005**, *433*, 610–613.

[6] Stack, T. D. P.; Holm, R. H. *J. Am. Chem. Soc.* **1987**, *109*, 2546–2547.

[7] Walsdorff, C.; Saak, W.; Pohl, S. *J. Chem. Soc., Dalton Trans.* **1997**, 1857–1861.

[8] van der Geer, E. P. L.; van Koten, G.; Klein Gebbink, R. J. M.; Hessen, B. *Inorg. Chem.*, accepted (Chapter 2 of this thesis).

[9] (a) Bobrik, M. A.; Que, L., Jr.; Holm, R. H. *J. Am. Chem. Soc.* **1974**, *96*, 285–287. (b) Que, L., Jr.; Bobrik, M. A.; Ibers, J. A.; Holm, R. H. *J. Am. Chem. Soc.* **1974**, *96*, 4168–4178.

[10] The difference between the calculated and observed values for sulfur was 0.31%, as opposed to the 1.72% discrepancy found for mimic **1**.

[11] Holm, R. H.; Phillips, W. D.; Averill, B. A.; Mayerle, J. J.; Herskovitz, T. *J. Am. Chem. Soc.* **1974,** *96*, 2109–2117.
[12] Broad features of low intensity are also observed around 5.4 ppm in **4**. We are hesitant to assign this signal analogously since [4Fe-4S] cluster-coordinated CH_2S^- groups, including that in the precursor compound **3** (see Table 1), almost invariably exhibit contact shifts of at least 8 ppm (see reference 11).
[13] Silakov, A.; Reijerse, E. J.; Albracht, S. P. J.; Hatchikian, E. C.; Lubitz, W. *J. Am. Chem. Soc.* **2007**, *129*, 11447–11458.
[14] The original values were reported vs. a Ag/AgCl electrode. Using this same electrode, we found $E_{1/2}$ (Fc/Fc^+) = 0.54 V vs. Ag/AgCl and used this value to calculate potentials vs. Fc/Fc^+.
[15] The mechanism proposed for **1** cannot hold true for **4**, since in this mechanism, process II occurs only after process I has occurred. Even if the slight shoulder observed in the cyclic voltammogram were evidence for process I, the redox wave for process II could not then be more intense.
[16] Razavet, M.; Davies, S. C.; Hughes, D. L.; Barclay, J. E.; Evans, D. J.; Fairhurst, S. A.; Liu, X.; Pickett, C. J. *Dalton Trans.* **2003**, 586–595.
[17] The original values were reported vs. the standard calomel electrode (SCE); the values vs. Fc/Fc^+ quoted here were calculated using $E_{1/2}$ (Fc/Fc^+) = 0.379 V vs. SCE in MeCN. Kolthoff, I. M.; Thomas, F. G. *J. Phys. Chem.* **1965**, *69*, 3049–3058.
[18] The proton source was erronously referred to as the 4,6-dimethylpyridinium cation in reference 5. Tard, C.: personal communication 2007.
[19] Felton, G. A. N.; Glass, R. S.; Lichtenberger, D. L.; Evans, D. H. *Inorg. Chem.* **2006**, *45*, 9181–9184.
[20] Kolomyjec, C.; Whelan, J.; Bosnich, B. *Inorg. Chem.* **1983**, *22*, 2343–2345.
[21] Cauquis, G.; Fahmy, H. M.; Pierre, G.; Elnagdi, M. H. *Electrochim. Acta* **1979**, *24*, 391–394.

Chapter 6

A 3:1 Site-Differentiated [4Fe-4S] Cluster Immobilized on a Self-Assembled Monolayer

Abstract. *A 3:1 site-differentiated [4Fe-4S] cluster is immobilized on a thiol-functionalized self-assembled layer on Au(111) by thiol-thiolate exchange chemistry. Fe 2*p *signals observed in X-ray photoelectron spectroscopy support the presence of [4Fe-4S] clusters at the SAM surface; further evidence comes from the detection of* n-Bu_4N^+ *and cluster-derived species by secondary-ion mass spectrometry. The immobilizing interaction is sufficiently strong to allow the study of [4Fe-4S] clusters at solid-liquid interfaces.*

van der Geer, E. P. L.; van den Brom, C. R.; Arfaoui, I. E.; Houssiau, L.; Rudolf, P.; van Koten, G.; Klein Gebbink, R. J. M.; Hessen, B., manuscript in preparation.

6.1. Introduction.

The widespread use Nature makes of cubane-type [4Fe-4S] clusters to mediate electron transfer in redox enzymes has led to detailed studies of synthetic analogues in solution.[1] On the other hand, studies of synthetic [4Fe-4S] clusters at solid surfaces are rare. Pickett and co-workers have immobilized [4Fe-4S] clusters by trapping them in an ionic polymer matrix on an electrode, demonstrating that the electrostatic interactions with the polymer have a large effect on the cluster redox potential.[2] In a later study, [4Fe-4S] clusters were immobilized by electropolymerization. Although the molecular nature of the clusters was lost, the technique elegantly created polyferredoxin-like materials.[3]

Nonetheless, no strategy has yet been reported for the immobilization of [4Fe-4S] clusters onto solid surfaces in such a way that their molecular nature is preserved and each cluster is in a well-defined but readily variable environment. In an attempt to fill this void in [4Fe-4S] cluster chemistry, we report herein the first immobilization of synthetic [4Fe-4S] clusters on alkanethiol self-assembled monolayers (SAMs)[4] on Au(111) surfaces.

6.2. Results and discussion.

6.2.1. Immobilization strategy: the [4Fe-4S] cluster.

In order for both the structure and the environment of immobilized clusters to remain well-defined, the immobilizing interaction should be unambiguous and strong enough to resist work-up conditions. Each iron atom in a synthetic or natural [4Fe-4S] cluster is usually coordinated by a thiolate ligand, which can be exchanged for other thiolates by means of thiol-thiolate exchange chemistry.[5] By utilizing a SAM functionalized with surface thiol groups, thiol-thiolate exchange could immobilize a dissolved [4Fe-4S] cluster onto a SAM surface by a strong coordination bond.

For the binding mode to be unambiguous, each cluster should be able to bind to the surface in one way only. This can be achieved by using a 3:1 site-differentiated cluster such as $(n\text{-Bu}_4\text{N})_2[\text{Fe}_4\text{S}_4(\text{TriS})(\text{SEt})]$ (**1**, Chart 1), the synthesis of which we have recently optimized.[6] In this cluster, the [4Fe-4S] core is bound to the chelating, tripodal TriS^{3-} ligand (Chart 1), which blocks ligand exchanges at all but one of the iron sites. Only the unique iron atom is available for binding to the thiol-functionalized SAM surface.[7]

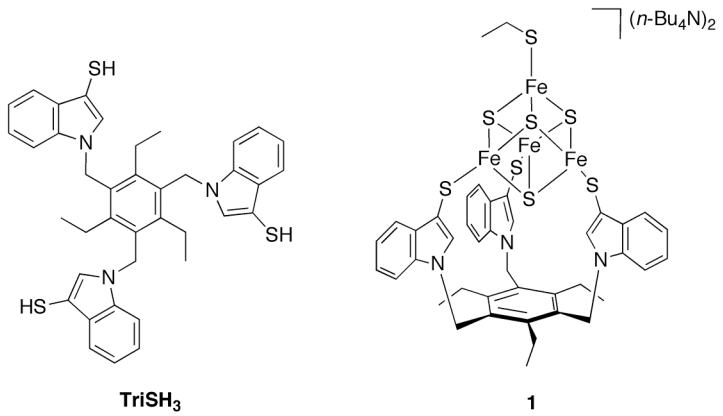

Chart 1. The tripodal $TriSH_3$ ligand and the 3:1 site-differentiated cluster $(n\text{-}Bu_4N)_2[Fe_4S_4(TriS)(SEt)]$ (**1**).

In order to facilitate X-ray photoelectron spectroscopy (XPS) analysis of immobilized [4Fe-4S] cluster samples, we first performed XPS measurements of **1** drop-cast on Al foil from THF (Figure 1 and Table 1).

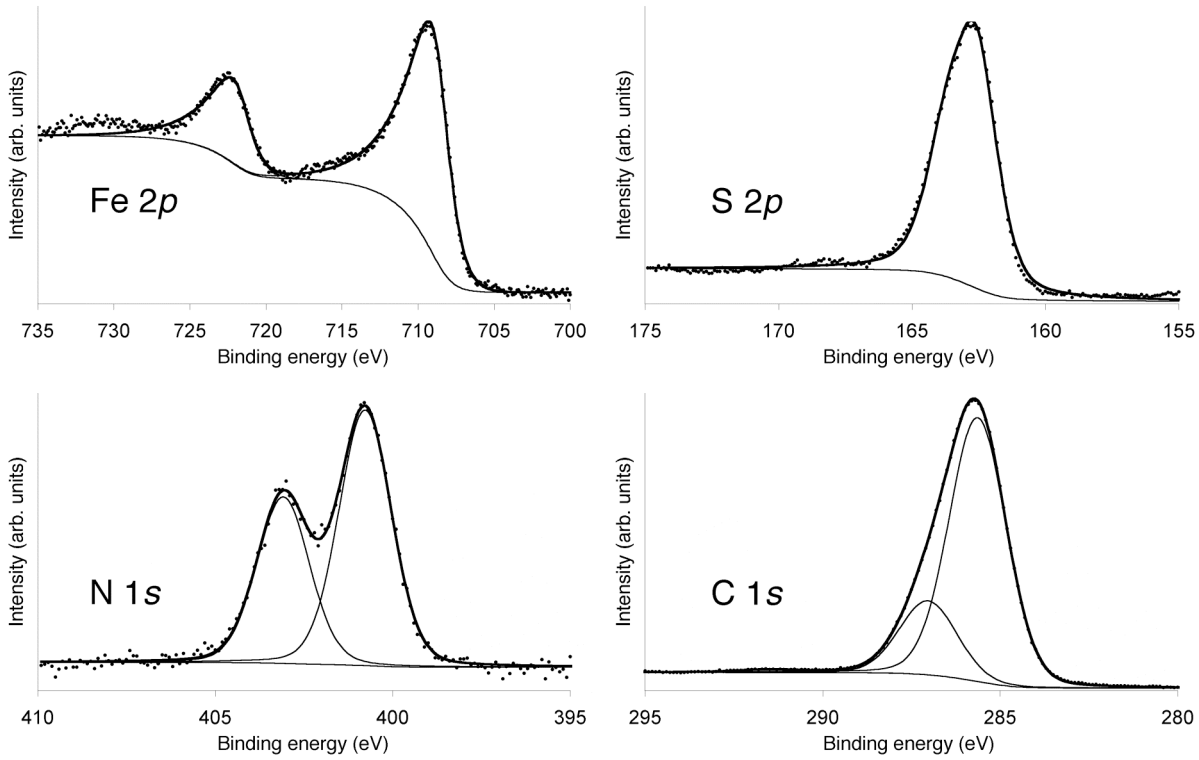

Figure 1. X-ray photoemission spectra of the Fe 2*p*, S 2*p*, N 1*s*, and C 1*s* core level regions of **1** drop-cast on Al foil.

Table 1. Binding energies (BE) of selected core levels in **1** drop-cast on Al foil.

			Stoichiometry	
	BE (eV)	**FWHM[a] (eV)**	**Found**	**Calculated**
Fe $2p_{1/2}$	721.0	1.51	3.3	4
Fe $2p_{3/2}$	707.9	1.51		
S $2p_{3/2}$	161.4	1.82	8[b]	8
N1 1*s*	399.6	1.74	3.3	3
N2 1*s*	401.9[b]	1.74	2.2	2
C1 1*s*	284.4	1.89	67.8	
C2 1*s*	285.8	1.89	19.0	73
C3 1*s* [c]	290.3	1.89	0.6	

[a]or Losev parameter *a* for Fe $2p$[8] [b]used as reference values [c]shake-up signal

The data does not indicate the presence of more than one iron species in **1**, despite the fact that **1** contains both $TriS^{3-}$- and ethanethiolate-coordinated iron atoms. In contrast, the broadness of the S 2*p* doublet suggests independent contributions from the different types of sulfur atoms in **1**, although fits of the signal with more than one doublet did not converge to realistic intensity ratios. The carbon signal could be reproduced well using three peaks, including a signal assigned to shake-up effects. The N 1*s* peaks at 401.9 and 399.6 eV converged to an intensity ratio of 2 : 3.1, in excellent agreement with their assignment as the *n*-Bu_4N^+ and $TriS^{3-}$ nitrogen atoms, respectively. In general, the stoichiometry of **1** determined from XPS is reasonable, although the intensities of the carbon and nitrogen signals are rather higher than expected.

To confirm the insensitivity of the Fe 2*p* signals to the nature of the coordinating thiolate, we also analyzed the related, symmetrically substituted cluster (*n*-$Bu_4N)_2[Fe_4S_4(SEt)_4]$[9] (**2**, Chart 2) and its *N*-decylindole-3-thiolate counterpart (*n*-$Bu_4N)_2[Fe_4S_4(S\text{-}3\text{-}C_8H_5N\text{-}1\text{-}C_{10}H_{21})_4]$[10] (**3**, Chart 2). The Fe $2p_{1/2}$ and $2p_{3/2}$ binding energies in **2** were determined to be 721.1 and 708.0 eV, respectively; those in **3** were 721.2 and 708.1 eV, respectively. The negligible differences prove that the iron atoms in **1** should be indistinguishable by XPS. In all three clusters, the Fe $2p_{3/2}$ binding energies are relatively close to that of pyrite (FeS_2, 707.4 eV)[11] but lower than the value reported by Holm and co-workers for (*n*-$Pr_4N)_2[Fe_4S_4(SEt)_4]$ (710.4 eV).[12] Most likely, a difference in the utilized reference standards is responsible for the anomaly.

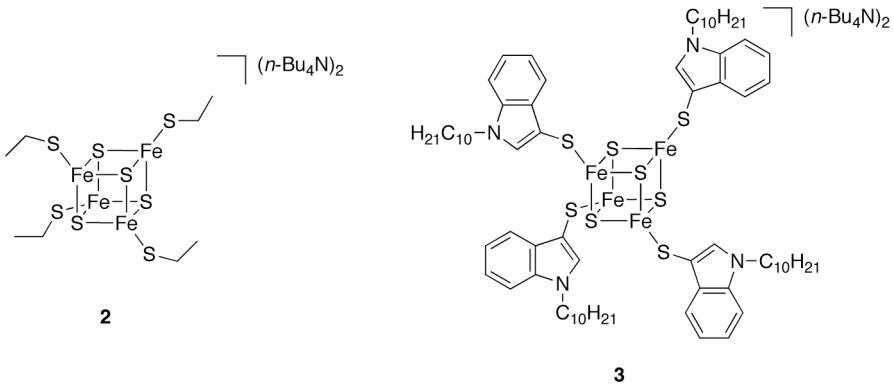

Chart 2. $(n\text{-}Bu_4N)_2[Fe_4S_4(SEt)_4]$ (**2**) and $(n\text{-}Bu_4N)_2[Fe_4S_4(S\text{-}3\text{-}C_8H_5N\text{-}1\text{-}C_{10}H_{21})_4]$ (**3**).

6.2.2. Immobilization strategy: a thiol-functionalized SAM.

In practice, the simplest conceivable SAM with surface thiol groups is one consisting of an α,ω-alkanedithiol on a Au(111) surface. However, the dense packing of surface thiol groups in such a SAM might hinder reactions of the thiol groups with dissolved clusters. In contrast, using a mixed SAM consisting of 1-decanethiol and the slightly longer 1,12-dodecanedithiol creates a surface of protruding thiol groups with more space to react with **1** (Scheme 1).

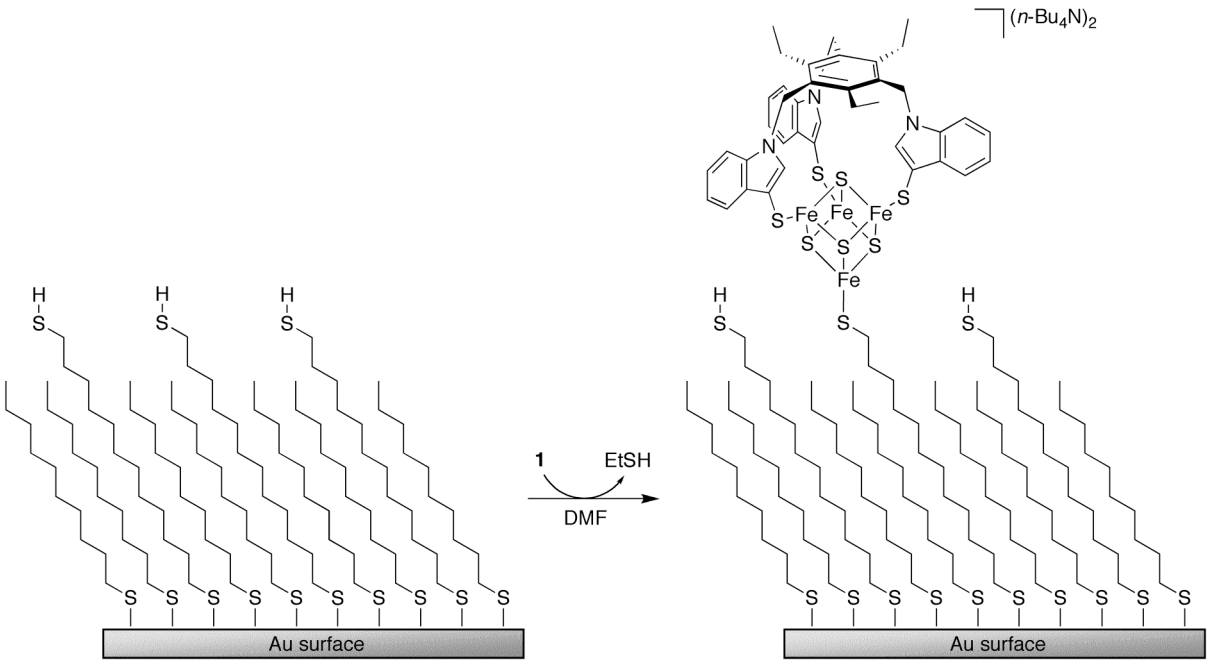

Scheme 1. The immobilization of **1** on a mixed SAM with surface thiol groups.

The mixed SAMs were synthesized on Au(111) on mica from ethanol solutions containing the mono- and dithiols in a 9:1 ratio. XPS results for the SAM are summarized in Figure 2 and Table 2.

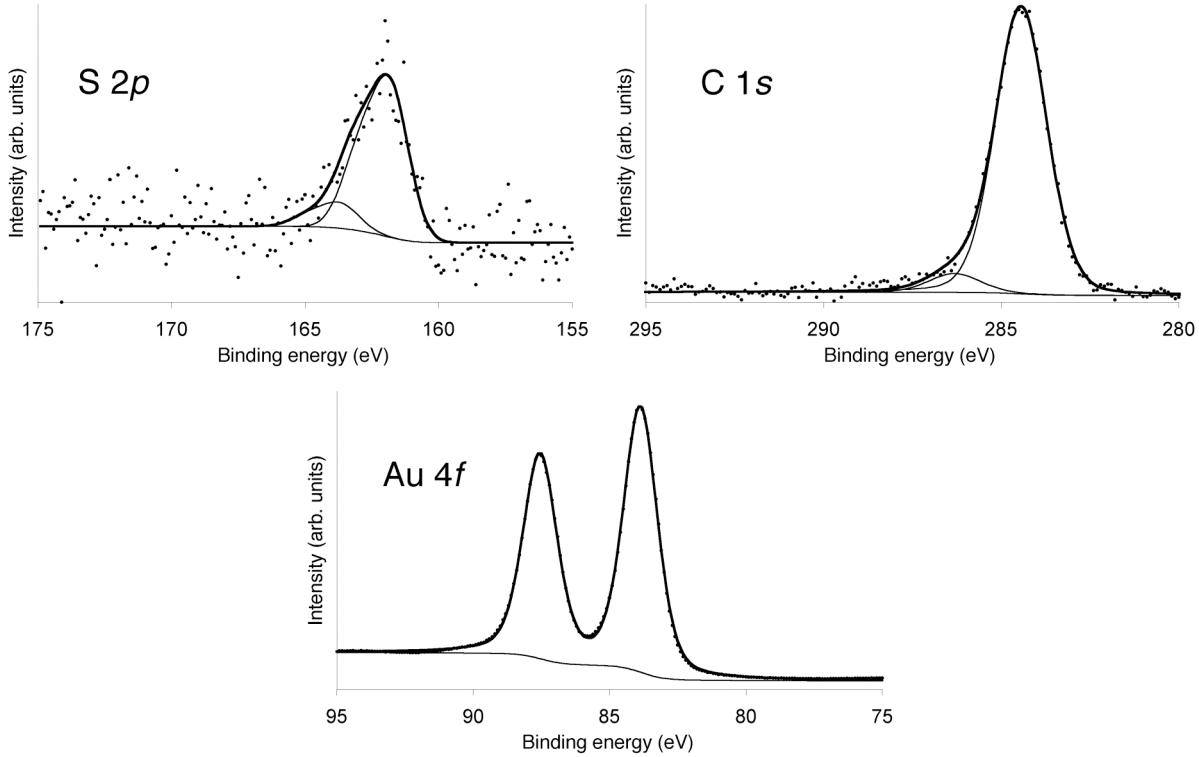

Figure 2. X-ray photoemission spectra of the S 2*p*, C 1*s*, and Au 4*f* core level regions of the mixed monothiol/dithiol SAM on Au(111) on mica.

Table 2. Binding energies (BE) of selected core levels in the mixed monothiol/dithiol SAM on Au(111) on mica.

			Stoichiometry	
	BE (eV)	**FWHM (eV)**	**Found**	**Calculated**
S1 $2p_{3/2}$	161.7	1.59	10.1	10
S2 $2p_{3/2}$	163.6	1.59	1[a]	1
C1 1*s*	284.4	1.71	101.3	91
C2 1*s*	286.2	1.71	8.1	11
Au $4f_{7/2}$	83.8[a,b]	1.48		

[a]used as reference values [b]splitting = 3.67 eV

The S 2*p* region contains two overlapping signals: a major doublet at 161.7 eV corresponding to surface-bound thiol groups and a minor doublet at 163.6 eV corresponding to unbound thiol groups at the SAM surface (and possibly also products of radiation damage).[13] After correcting the intensity of the signal at 161.7 eV for attenuation (see section 6.6), the ratio between the two signals is 10.1 to 1. This corresponds to a monothiol:dithiol ratio of 9.1 to 1, in excellent agreement with the ratio of the two species in solution.

The C 1*s* region can also be modeled as arising from two overlapping signals: one for sulfur-bound methylene carbon atoms at 286.2 eV and one for the remaining carbon atoms at 284.4 eV.[14] The ratio between these sulfur-bound and non-sulfur-bound carbon atoms was found to be somewhat too low. Possibly, the peak fitting underrepresented the sulfur-bound carbon signal, but the fact that the overall carbon signal intensity is also too high suggests that some carbon contamination has taken place.

6.2.3. Immobilization studies.

The mixed SAM was functionalized with [4Fe-4S] clusters by reaction with **1** in DMF, followed by washing in CH_2Cl_2 and spin-drying to remove unbound cluster. Subsequent XPS analysis of the mixed SAM clearly revealed Fe $2p_{1/2}$ and $2p_{3/2}$ signals at 723.1 and 710.3 eV, respectively (Figure 3 and Table 3). Probably because of differences in the utilized reference signals, these binding energies are higher than the values found for **1** drop-cast on Al foil. The Fe $2p_{3/2}$ binding energy is now close to that reported by Holm and co-workers for $(n\text{-}Pr_4N)_2[Fe_4S_4(SEt)_4]$ (*vide supra*).[12]

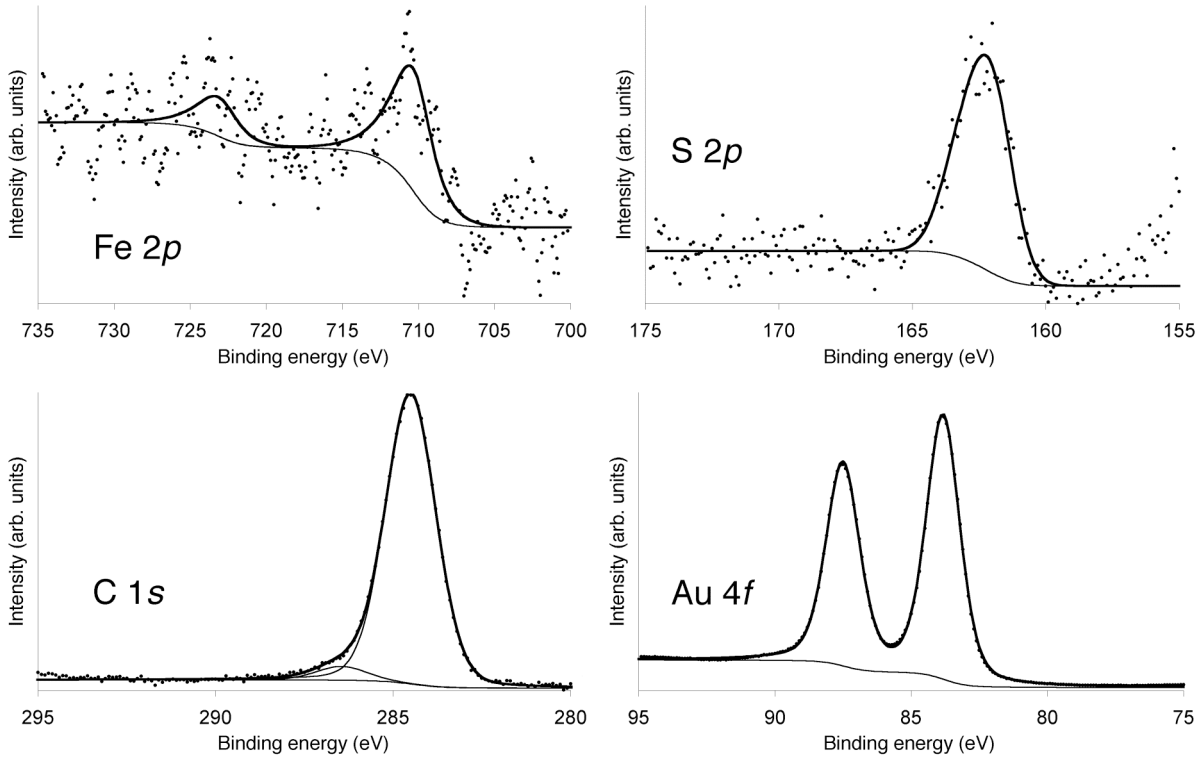

Figure 3. X-ray photoemission spectra of the Fe 2*p*, S 2*p*, C 1*s*, and Au 4*f* core level regions of the mixed monothiol/dithiol SAM treated with cluster **1**. The Fe 2*p* data is given as a moving average over 5 points.

Table 3. Binding energies (BE) of selected core levels in the mixed monothiol/dithiol SAM treated with **1**.

			Stoichiometry		
	BE (eV)	**FWHM[a] (eV)**	**Found**	**Found[b]**	**Calculated[b]**
Fe $2p_{1/2}$	723.1	1.02	1[c]		
Fe $2p_{3/2}$	710.3	1.02			
S $2p_{3/2}$	162.0	1.81	34.3	11	11
C1 1*s*	284.5	1.67	578.5	189.0	102
C2 1*s*	286.4	1.67			
Au $4f_{7/2}$	83.8[c,d]	1.46			

[a]or Losev parameter *a* for Fe $2p$[8] [b]SAM only [c]used as reference values [d]splitting = 3.67 eV

As in the XPS analysis of **1**, the sulfur signal could only be fitted realistically with a single doublet. After correcting for contributions from immobilized clusters, the carbon and sulfur signals were corrected for attenuation disregarding any potential attenuation by cluster species. The ratio of clusters to surface thiol groups was then approximately 1:3, indicating that one in three surface thiol groups were functionalized with [4Fe-4S] clusters. The high carbon-to-sulfur ratio is again suggestive of carbon contamination.

Time-of-flight secondary-ion mass spectrometry (ToF-SIMS)[15] provided further support for [4Fe-4S] cluster immobilization. As expected,[16] $Au_mS_nH_p^-$ species dominate the negative-ion spectrum (Figure 4), while a weak, SAM-derived $C_{10}H_{22}S^-$ signal is observed at m/z = 174.14 (calculated m/z = 174.14). Signals at m/z = 87.93 and 119.89 indicate the presence of FeS^- (calculated m/z = 87.91) and FeS_2^- (calculated m/z = 119.88), respectively. Furthermore, a signal at m/z = 147.01 can be assigned to the indolyl species $C_8H_5NS^-$ (calculated m/z = 147.01), a fragmentation product of the $TriS^{3-}$ ligand.

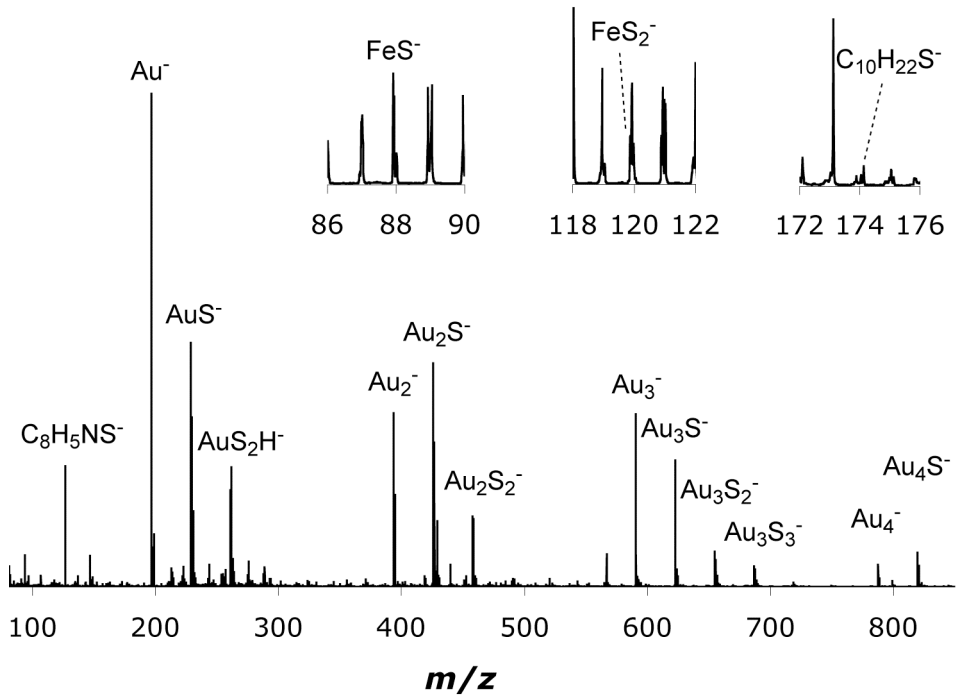

Figure 4. Negative time-of-flight secondary ion mass spectrum of the mixed monothiol/dithiol SAM treated with cluster **1**. Insets: cluster- and SAM-derived signals at 40× magnification.

The XPS N 1*s* signal had been too weak to allow for analysis and assignment as the nitrogen atom in *n*-Bu_4N^+. On the other hand, positive-ion ToF-SIMS (Figure 5) shows a strong signal at m/z = 242.30 corresponding to *n*-Bu_4N^+ (calculated m/z = 242.28). Further, a clear Fe^+ signal is observed at m/z = 55.94 (calculated m/z = 55.93).

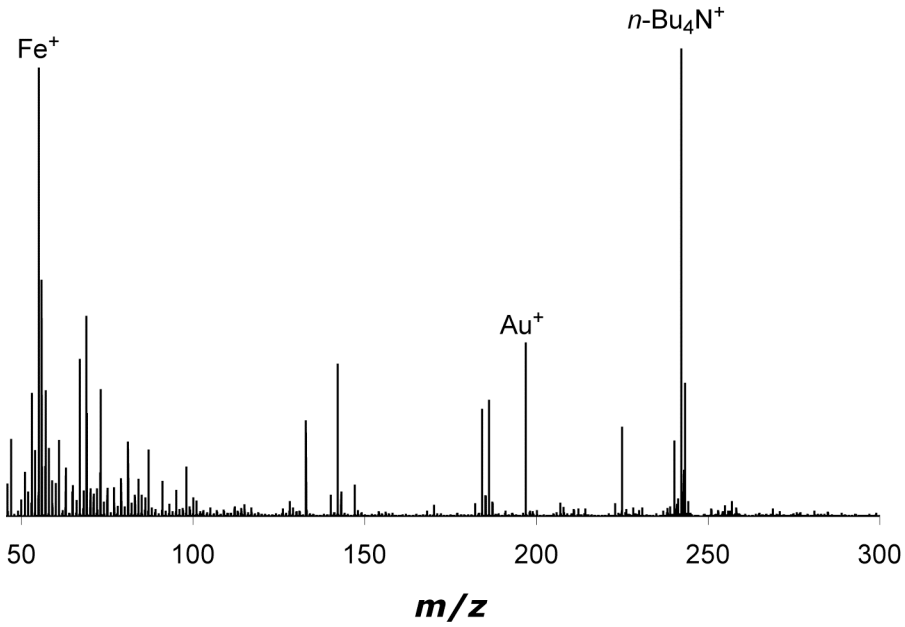

Figure 5. Positive time-of-flight secondary ion mass spectrum of the mixed monothiol/dithiol SAM treated with cluster **1**.

6.3. Conclusion.

The Fe 2*p* XPS signals from the [4Fe-4S] cluster-treated SAM samples, together with the observation of cluster and ligand fragments and the *n*-Bu_4N^+ counterion in ToF-SIMS, provide strong evidence that cluster **1** has been immobilized on the mixed SAM samples. Although the exact binding mode of the cluster to the surface has not yet been elucidated, the interaction with the surface is strong enough to resist washing. Hence, we are currently investigating the behavior of the [4Fe-4S] clusters at solid-liquid interfaces.

6.4. Experimental.

General. All glassware was treated with basic piranha solution (volume H_2O : NH_3(aq, conc.) : H_2O_2 (aq, conc.) = 5:1:1) at 70 °C and rinsed with milli-Q grade H_2O before use. Tools used for handling SAM samples were cleaned by sonication in acetone and toluene, respectively. All solvents were of p.a. quality. 1-Decanethiol was purchased from Aldrich.

Preparation of self-assembled monolayers. 6 mM stock solutions of 1-decanethiol and 1,12-dodecanedithiol[17] in EtOH were prepared directly before use and mixed and diluted to yield a solution containing 0.9 mM 1-decanethiol and 0.1 mM 1,12-dodecanedithiol. The Au(111) on mica was prepared by evaporation of gold (99.99%) onto freshly cleaved mica (2.54×5.08 cm) in a home-built, fully automated thermal evaporator, until a thickness of 150 nm had been achieved. The gold substrates were cut into pieces of about 10×5 mm and flame-annealed for 30 s with an H_2 flame directly before immersion into the thiol solution. After leaving the gold substrates in the solutions in the dark for 24 h, they were carefully washed for 30 s in ethanol, toluene, and 2-propanol, respectively, and spin-dried.

Immobilization of [4Fe-4S] clusters. SAM samples were placed in 0.1 mM solutions of (*n*-$Bu_4N)_2[Fe_4S_4(TriS)(SEt)]$ in DMF. After 10 min, the samples were carefully washed in DMF (30 s) and CH_2Cl_2 (30 s) and immediately spin-dried.

X-ray photoelectron spectroscopy (XPS). XPS spectra were recorded on an SSX-100 spectrometer (Surface Science Instruments, United Kingdom) equipped with a hemispherical analyzer and installed in an ultra-high vacuum chamber with an operating pressure of $2–3\times10^{-13}$ bar. Spectra were obtained using monochromatic Al K_α radiation ($h\nu$ = 1486.6 eV) with a spot size of 600 μm, a resolution of 1.50 eV, an analyzer step size of 0.1 eV, and a take-off angle of 53°. Acquisition times were limited to a maximum of 30 min on any one location to minimize radiation damage; the N 1*s* or S 2*p* level was compared at the beginning and the end of each measurement to assess if any gross damage had occurred. The binding energy of the Au $4f_{7/2}$ level (83.8 eV)[11] was used as a reference for the SAM samples. For the drop-cast samples on Al, the N 1*s* level of the *n*-Bu_4N^+ was used as reference and set to 401.9 eV.[18]

Prior to analysis, spectra obtained at different locations on a single sample were compared and, if sufficiently similar, added to obtain better signal-to-noise ratios. The spectra were then analyzed by mathematical reconstruction using Winspec, a least-squares fitting program developed at the Laboratoire Interdisciplinaire de Spectroscopie Electronique, Facultés Universitaires Notre-Dame de la Paix, Namur, Belgium. Each region of interest was fitted using a Shirley background[19] and a minimal number of pure Gaussian or mixed Gaussian/Lorentzian peak functions necessary to reproduce the S, N, C, and Au regions of the spectrum.[20] For the S 2*p* doublet, the spin-orbit coupling constant and intensity ratios were fixed at

1.18 eV and 0.52, respectively. If a region was fitted using more than one signal, the Gaussian/Lorentzian mixing ratios and the peak widths were coupled. The Fe signals were fitted using pairs of Losev singlets with coupled Losev parameters *a* and *b*.[8]

Elemental compositions of the samples were determined from integrated signal intensities of peaks, corrected for the sensitivity factors using data tabulated for the employed spectrometer. For the SAM samples, corrections were applied for the attenuation of buried SAM atom signals by atoms located closer to the SAM surface (see Section 6.6). The XPS characterizations of **1**, $(n\text{-}Bu_4N)_2[Fe_4S_4(SEt)_4]$[21] (**2**) and $(n\text{-}Bu_4N)_2[Fe_4S_4(S\text{-}3\text{-}C_8H_5N\text{-}1\text{-}C_{10}H_{21})_4]$[10] (**3**) were performed on samples drop-cast from THF onto Al (99.99 %) foil. The Al foil was first cleaned with soap, followed by rinsing with milli-Q grade H_2O and sonication in acetone and toluene.

Time-of-flight Secondary Ion Mass Spectrometry (ToF-SIMS). The ToF-SIMS spectra were recorded at the Laboratoire Interdisciplinaire de Spectroscopie Electronique of the Facultés Universitaires Notre-Dame de la Paix, Namur, Belgium on a TOF-SIMS IV spectometer manufactured by IONTOF GmbH (Münster, Germany). A primary ion beam of 25 keV Ga^+ ions was applied at an incidence angle of 45°. The beam was pulsed at a frequency of 10 kHz with a pulsed current of 1 pA. The mass resolution M/δM was 7000 in both positive and negative polarities. The analyzed area measured 100×100 μm^2. The total ion fluence was typically 10^{12} ions/cm^2. Secondary ions were extracted with an extractor voltage of 2 kV.

6.5. Appendix: Attenuation correction in a mixed monothiol/dithiol SAM.

In XPS analyses of SAMs, the photoelectron response from atoms buried under the surface is attenuated by scattering effects from overlying layers. To correct for this attenuation, Whitesides *et al.* have studied the attenuation lengths λ of photoelectrons in SAMs, with λ defined as the thickness of material required to attenuate the generated flux of electrons by a factor 1/e.[22] If the experimentally measured signal intensity of a layer of an element *X* under study is $I_e(X)$, and $I_i(X)$ is the signal were it not attenuated by overlying layers, then λ relates the two variables according to:

(1)
$$I_e(X) = I_i(X)e^{\frac{-\rho d}{\lambda \cos\theta}}$$

Here, *d* is the thickness of the layer overlying the atoms under study and θ is the take-off angle, defined as the angle between the surface normal and the analyzer axis. ρ is the density of the overlying layer, relative to a solid layer (ρ = 1). In contrast to I_e, I_i can be used to calculate the elemental composition of the sample under investigation.

In a mixed monothiol/dithiol SAM, three different depths with respect to the outermost surface define the structure of the sample (Figure 6).

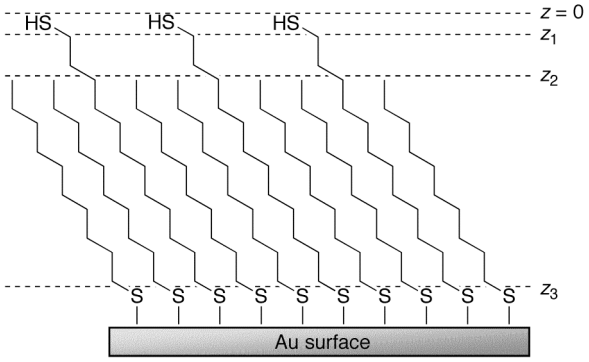

Figure 6. Layers relevant to attenuation in a mixed monothiol/dithiol SAM.

z_1 is the thickness of the surface thiol layer, z_2 is the thickness of the entire protruding layer, and z_3 is the thickness of the SAM without the gold-bound sulfur atoms. Of the two sulfur signals, only the one arising from the gold-bound sulfur layer is attenuated. For convenience, we assume that the attenuating effects of the protruding thiol and methylene groups are the same and that the entire protruding layer $0 < z < z_2$ has a uniform density ρ. I_e for the gold-bound sulfur signal can then be expressed as:

(2)
$$I_e(S) = I_i(S)e^{\frac{-\rho z_2}{\lambda\cos\theta}}e^{\frac{-(z_3-z_2)}{\lambda\cos\theta}} = I_i(S)e^{\frac{(1-\rho)z_2-z_3}{\lambda\cos\theta}}$$

For carbon, generation and attenuation of photoelectrons occur in the same layer. $I_e(C)$ in such a layer, if not attenuated by any overlying layers, can be expressed as:[23]

(3)
$$I_e(C) = \int_0^z \rho(z)I_0(C)e^{\frac{-\rho(z)z}{\lambda\cos\theta}}dz$$

Here, $I_0(C)$ is the intrinsic intensity per unit thickness. For the mixed SAM, $I_e(C)$ is the sum of contributions from the carbon atoms in the protruding ($z_1 < z < z_2$) and the buried ($z_2 < z < z_3$) layers:

(4)
$$I_e(C) = e^{\frac{-\rho z_1}{\lambda\cos\theta}}\int_{z_1}^{z_2}\rho I_0(C)e^{\frac{-\rho(z-z_1)}{\lambda\cos\theta}}dz + e^{\frac{-\rho z_2}{\lambda\cos\theta}}\int_{z_2}^{z_3}I_0(C)e^{\frac{-(z-z_2)}{\lambda\cos\theta}}dz$$

The factors preceding the integrals correct for the attenuation by overlying layers. Evaluation of the integrals gives:

(5)
$$I_e(C) = I_0(C)\lambda\cos\theta(e^{\frac{-\rho z_1}{\lambda\cos\theta}} - e^{\frac{(1-\rho)z_2-z_3}{\lambda\cos\theta}})$$

$I_0(C)$ can be expressed in terms of $I_i(C)$ using:

(6)
$$I_i(C) = \int_0^{z_3} \rho(z) I_0(C) dz = \int_{z_1}^{z_2} \rho I_0(C) dz + \int_{z_2}^{z_3} I_0(C) dz$$

Evaluation of the integrals leads to:

(7)
$$I_0(C) = \frac{I_i(C)}{z_3 - \rho z_1 - (1-\rho) z_2}$$

Finally, substitution of equation 7 in equation 5 gives:

(8)
$$I_e(C) = I_i(C) \frac{\lambda \cos\theta}{z_3 - \rho z_1 - (1-\rho) z_2} \left(e^{\frac{-\rho z_1}{\lambda \cos\theta}} - e^{\frac{(1-\rho) z_2 - z_3}{\lambda \cos\theta}} \right)$$

Equation 8 holds true if all the carbon atoms are treated collectively, but the carbon signal can also be split into contributions from sulfur- and non-sulfur-bound methylene groups. The carbon atoms bound to the protruding thiol groups are only attenuated by those thiol groups. For every protruding thiol-bound carbon atom, there are $1/\rho$ carbon atoms attached to gold-bound sulfur atoms. The expression for their attenuation is the same as that of the gold-bound sulfur atoms, corrected for the fact that the attenuating layer above them is less thick by the thickness d_0 of one methylene or thiol layer. The experimental intensity $I_e(C_S)$ of the sulfur-bound carbon signal can then be expressed as a sum:

(9)
$$I_e(C_S) = \frac{\rho}{\rho + 1} I_i(C_S) e^{\frac{-\rho z_1}{\lambda \cos\theta}} + \frac{1}{\rho + 1} I_i(C_S) e^{\frac{(1-\rho) z_2 - z_3 + d_0}{\lambda \cos\theta}}$$

For the remaining carbon atoms, the intrinsic intensity $I_e(C_C)$ becomes:

(10)
$$I_e(C_C) = I_i(C_C) \frac{\lambda \cos\theta}{z_3 - \rho z_1 - (1-\rho) z_2 - (1+\rho) d_0} \left(e^{\frac{-\rho (z_1 + d_0)}{\lambda \cos\theta}} - e^{\frac{(1-\rho) z_2 - z_3 + d_0}{\lambda \cos\theta}} \right)$$

In order to use equations 2, 9, and 10 for calculating the stoichiometry of the mixed SAM, the values of ρ, d_0, and λ must be known. For d_0, we have employed the value reported by Porter and co-workers[24] for alkanethiolate SAMs on gold (1.1 Å) and assumed the same value for the surface thiol groups; the error possibly arising from this assumption is minimal. λ was calculated using the empirical formula reported by Whitesides and co-workers:[22a]

(11)
$$\lambda = 0.31 (E_K)^{0.67}$$

Here, E_K is the kinetic energy of the photoelectron signal.

For ρ, we assumed a value of 0.1, reflecting the ratio of monothiol and dithiol in the solution from which the mixed SAM was obtained. Equation 2 then yields the intrinsic intensity of the gold-bound sulfur signal, which can be compared to the intrinsic intensity of the (unattenuated) surface thiol groups. The comparison gives a corrected value for ρ which can be re-entered in equation 2. Performing this process iteratively leads to convergence of ρ at the practically unchanged value of 0.099, supporting our initial assumption.

6.6. References.

[1] (a) Beinert, H.; Holm, R. H.; Münck, E. *Science* **1997**, *277*, 653–659. (b) Johnson, M. K. *Curr. Opin. Chem. Biol.* **1998**, *2*, 173–181. (c) Venkateswara Rao, P.; Holm, R. H. *Chem. Rev.* **2004**, *104*, 527–559.

[2] Moutet, J.-C.; Pickett, C. J. *J. Chem. Soc., Chem. Commun.* **1989**, 188-190.

[3] Pickett, C. J.; Ibrahim, S. K.; Hughes, D. L. *Faraday Discuss.* **2000**, *116*, 235-244.

[4] (a) Love, J. C.; Estroff, L. A.; Kriebel, J. K.; Nuzzo, R. G.; Whitesides, G. M. *Chem. Rev.* **2005**, *105*, 1103–1169. (b) Chen, D.; Li, J. *Surf. Sci. Rep.* **2006**, *61*, 445–463.

[5] (a) Bobrik, M. A.; Que, L., Jr.; Holm, R. H. *J. Am. Chem. Soc.* **1974**, *96*, 285–287. (b) Que, L., Jr.; Bobrik, M. A.; Ibers, J. A.; Holm, R. H. *J. Am. Chem. Soc.* **1974**, *96*, 4168–4178.

[6] van der Geer, E. P. L.; van Koten, G.; Klein Gebbink, R. J. M.; Hessen, B. *Inorg. Chem.*, accepted (Chapter 2 of this thesis).

[7] Walsdorff, C.; Saak, W.; Pohl, S. *J. Chem. Soc., Dalton Trans.* **1997**, 1857–1861.

[8] Losev, A. *Surf. Interface Anal.* **1989**, *14*, 845–849.

[9] Christou, G. C.; Garner, C. D. *J. Chem. Soc., Dalton Trans.* **1979**, 1093–1094.

[10] van der Geer, E. P. L.; Li, Q.; van Koten, G.; Klein Gebbink, R. J. M.; Hessen, B. *Inorg. Chim. Acta*, in press (Chapter 3 of this thesis).

[11] Wagner, C. D.; Riggs, W. M.; Davis, L. E.; Moulder, J. F. *Handbook of X-ray Photoelectron Spectroscopy*; Muilenberg, G. E., Ed.; Perkin-Elmer Corporation: Eden Prairie, USA, 1979.

[12] Holm, R. H.; Averill, B. A.; Herskovitz, T.; Frankel, R. B.; Gray, H. B.; Siiman, O.; Grunthaner, F. J. *J. Am. Chem. Soc.* **1974**, *96*, 2644–2646.

[13] (a) Laibinis, P. E.; Whitesides, G. M.; Allara, D. L.; Tao, Y.-T.; Parikh, A. N.; Nuzzo, R. G. *J. Am. Chem. Soc.* **1991**, *113*, 7152–7167. (b) Castner, D. G.; Hinds, K.; Grainger, D. W. *Langmuir* **1996**, *12*, 5083–5086. (c) Ishida, T.; Choi, N. *Langmuir* **1999**, *15*, 6799–6806.

[14] Mendoza, S. M.; Arfaoui, I.; Zanarini, S.; Paolucci, F.; Rudolf, P. *Langmuir* **2007**, *23*, 582–588.

[15] Van Vaeck, L.; Adriaens, A.; Gijbels, R. *Mass Spectrom. Rev.* **1999**, *18*, 1–47.

[16] (a) Graham, D. J.; Price, D. D.; Ratner, B. D. *Langmuir* **2002**, *18*, 1518–1527. (b) Gillen, G.; Bennett, J.; Tarlov, M. J.; Burgess, D. R. F., Jr. *Anal. Chem.* **1994**, *66*, 2170–2174. (c) Tarlov, M. J.; Newman, J. G. *Langmuir* **1992**, *8*, 1398–1405.

[17] Akkerman, H. B.; Blom, P. W. M.; de Leeuw, D. M.; de Boer, B. *Nature* **2006**, *441*, 69–72.

[18] A large majority of literature values for the N 1*s* binding energy in *n*-Bu_4N^+ fall between 401.4 and 402.4 eV, with an average value of 401.9 eV. (a) Gniewek, A.; Trzeciak, A. M.; Ziółkowski, J. J.; Kępiński, L.; Wrzyszcz, J.; Tylus, W. *J. Catal.* **2005**, *229*, 332–343. (b) Yang, P.; Cao, Y.; Hu, J.-C.; Dai, W.-L.; Fan, K.-N. *Appl. Catal., A* **2003**, *241*, 363-373. (c) Liu, S.-G.; Liu, Y.-Q.; Zhu, D.-B. *Synth. Met.* **1997**, *89*, 187–191. (d) Wenkin, M.; Devillers, M.; Tinant, B.; Declercq, J.-P. *Inorg. Chim. Acta* **1997**, *258*, 113–118. (e) Liu, S.-G.; Liu, Y.-Q.; Liu, S.-H.; Zhu, D.-B. *Synth. Met.* **1995**, *74*, 137–143. (f) Anderson, J. E.; Gregory, T. P.; Net, G.; Bayón, J. C. *J. Chem. Soc., Dalton Trans.* **1992**, 487–495. (g) Bayón, J. C.; Net, G.; Esteban,

P.; Rasmussen, P. G.; Bergstrom, D. F. *Inorg. Chem.* **1991**, *30*, 4771–4777. (h) Sieklucka, B.; Dziembaj, R.; Witkowski, S. *Inorg. Chim. Acta* **1991**, *187*, 5–8. (i) Mialki, W. S.; Stiefel, E. I.; Bruce, A. E.; Walton, R. A. *Inorg. Chem.* **1981**, *20*, 1614–1616.

[19] Shirley, D. A. *Phys. Rev. B* **1972**, *5*, 4709–4714.

[20] Briggs, D.; Seah, M. P. (eds.); *Practical Surface Analysis, by Auger and X-Ray Photoelectron Spectroscopy*; John Wiley & Sons, Chichester (1983).

[21] Christou, G. C.; Garner, C. D. *J. Chem. Soc., Dalton Trans.* **1979**, 1093–1094.

[22] (a) Laibinis, P. E.; Bain, C. D.; Whitesides, G. M. *J. Phys. Chem.* **1991**, *95*, 7017–7021. (b) Bain, C. D.; Whitesides, G. M. *J. Phys. Chem.* **1989**, *93*, 1670–1673.

[23] van den Brom, C. R., PhD thesis, Rijksuniversiteit Groningen, Groningen, the Netherlands, available *via* http://irs.ub.rug.nl/ppn/292186150

[24] Porter, M. D.; Bright, T. B.; Allara, D. L.; Chidsey, C. E. D. *J. Am. Chem. Soc.* **1987**, *109*, 3559–3568.

Appendix 1

Synthesis and Crystal Structures of tpySAc and $[FeCl_3(tpySAc)]\cdot MeCN$ (tpySAc = 4'-Acetylthio-2,2':6',2''-Terpyridine)

The new ligand 4'-acetylthio-2,2':6',2''-terpyridine (tpySAc) can be prepared in high yield from 4'-chloro-2,2':6',2''-terpyridine and thioacetic acid. Reaction with $FeCl_3$ yields the compound $[FeCl_3(tpySAc)]\cdot MeCN$. Crystal structures of both ligand and complex are presented.

van der Geer, E. P. L.; Gagliardo, M.; Lutz, M.; Spek, A. L.; van Klink, G. P. M.; van Koten, G.; Klein Gebbink, R. J. M.; Hessen, B., manuscript in preparation.

A1.1. Introduction.

2,2':6',2''-Terpyridine (tpy) and its derivatives are one of the most commonly applied ligand systems in coordination chemistry. The ligand's popularity is due to its structural utility in supramolecular chemistry,[1] the interesting photochemical properties exhibited by compounds of Ru, Ir, and Pt with tpy,[2,3] and the fact that $[M(tpy)_2]^{n+}$ compounds lack the stereoisomerism that can complicate the chemistry of their 2,2'-bipyridine counterparts.[3] Recently, McEuen, Ralph, and co-workers have synthesized the tpy derivative 2,2':6',2''-terpyridine-4'-thiol (tpySH) and used the complex $[Co(tpySH)_2]^{2+}$ in gold surface-binding studies.[4] Constable and coworkers used the oxidized ligand tpySStpy to synthesize the cyclic compound $[Fe_4(tpySStpy)_4](BF_4)_8$.[5] Here, we report the synthesis and crystal structures of the acetyl-protected tpySH analogue 4'-acetylthio-2,2':6',2''-terpyridine (tpySAc) and the Fe^{3+} complex $[FeCl_3(tpySAc)]\cdot MeCN$.

A1.2. Results and discussion.

Synthesis of the ligand tpySAc proceeds smoothly in one step from 4'-chloro-2,2':6',2''-terpyridine (tpyCl) by means of a nucleophilic substitution reaction with excess thioacetic acid in THF (Scheme 1). In an attempt to increase the nucleophilicity of the thioacetic acid, the reaction was also conducted in the presence of base. However, no reaction was found to occur under these conditions, indicating that the substitution only takes place after the tpyCl is protonated by thioacetic acid, thereby activating it towards nucleophilic substitution.

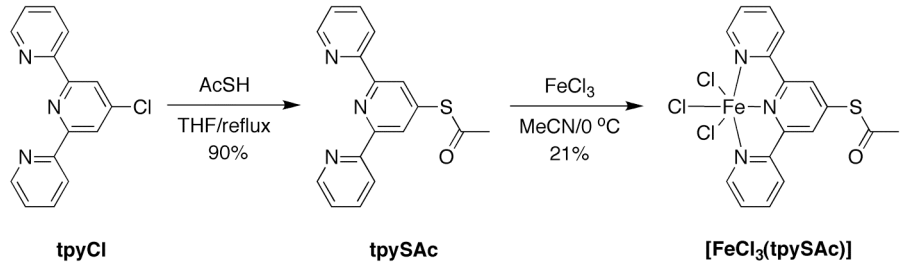

Scheme 1. Synthesis of tpySAc and $[FeCl_3(tpySAc)]$.

A crystal structure obtained of the tpySAc ligand after crystallization from CH_2Cl_2 clearly shows the positioning of the thioacetyl sulfur atom on the 4' position of the central pyridine ring (Figure 1). The two S–C bonds are comparable in length (1.7705(14) and 1.7874(16) Å for the S–terpy and S–acyl bonds, respectively) and fall within the normal range for S–C single bonds. Together with the short C–O distance of 1.199(2) Å, this indicates that, as would be expected for a thioester,[6] the thioacetyl double bond is localized on the acyl group. The pyridine rings, furthermore, are nearly coplanar (with deviations of 1.2° between neighboring rings) and adopt an *anti*,*anti* conformation in the absence of a coordinating metal ion.

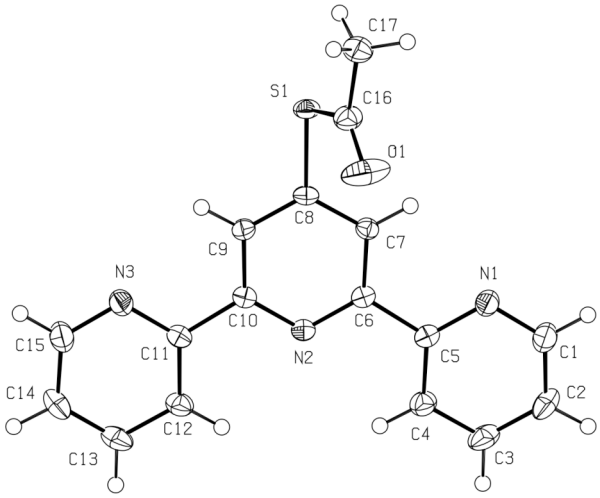

Figure 1. ORTEP plot of tpySAc, showing ellipsoids at the 50% probability level.

Cotton and co-workers synthesized the complex [$FeCl_3$(tpy)] by mixing MeCN solutions of $FeCl_3$ and tpy at 40 to 50 °C.[7] However, reaction of $FeCl_3$ with tpySAc under these conditions immediately yields (substituted) $[Fe(tpy)_2]^{2+}$ chromophores, as indicated by the formation of a purple color. Reasoning that lower temperatures might be needed to ensure inertness of the Fe–Cl bonds towards substitution, and thus obtain the kinetic, mono-substituted product rather than thermodynamically favored, di-substituted products, subsequent reactions were conducted without extra heating. Although the reaction behaved identically at ambient temperature, reaction between tpySAc and $FeCl_3$ at 0 °C produced microcrystalline [$FeCl_3$(tpySAc)], albeit in low yield (21%, Scheme 1). At –30 °C, the reaction was slow enough to generate single crystals suitable for X-ray diffraction studies.

The crystal structure of [$FeCl_3$(tpySAc)] (Figure 2) shows that the compound crystallizes as a solvate with one molecule of MeCN per formula unit. The thioacetyl functionality has remained intact upon coordination to the Fe^{3+} ion, which has adopted a distorted octahedral coordination geometry. The N–Fe–N angles are essentially the same as those found in [$FeCl_3$(tpy)],[7] and reflect the steric constraints imposed by the meridional *N*,*N*,*N*-binding of tpySAc. Geometrical constraints also force the N2 atom to be bound to the iron atom at a distance of 2.112(3) Å, significantly shorter than the other two Fe–N distances (2.138(3) and 2.143(3) Å).

The three Fe–Cl bonds in [$FeCl_3$(tpySAc)]·MeCN are significantly asymmetrical. Cl1, the chloride ligand *trans* to the N2 atom, is bound closest to the iron atom (2.2680(10) Å), indicating that the structural *trans*-effect[8] of the tpySAc N2 atom is smaller than that of chloride.[7] Compared to the Fe–Cl1 bond, the bonds to the other two chloride ligands Cl2 and Cl3 are both longer but also appreciably unequal in length (2.3670(8) vs. 2.3393(9) Å, respectively). A similar discrepancy between the mutually-*trans* Fe–Cl distances has been observed in [$FeCl_3$(tpy)]·MeCN, where it was attributed to the fact that only the chloride

ligand bound at a greater distance was involved in short-distance (<2.8 Å) C–H···Cl–Fe contacts.[7] In [FeCl$_3$(tpySAc)]·MeCN, both Cl2 and Cl3 have short C–H···Cl–Fe contacts, but Cl2 has three while Cl3 has only one. Thus, the discrepancy in the Fe–Cl distances in [FeCl$_3$(tpySAc)]·MeCN also appears to originate from a difference in the number of C–H···Cl–Fe interactions.

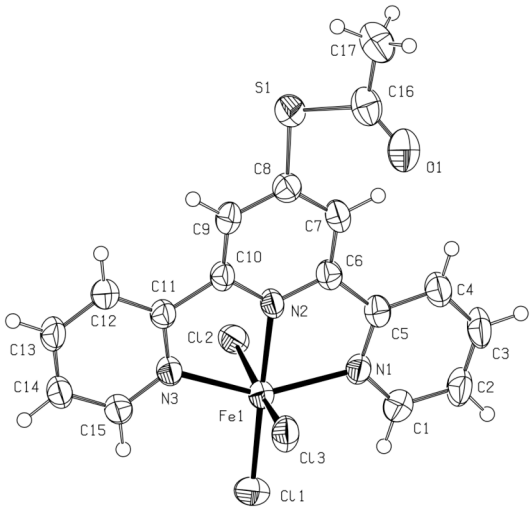

Figure 2. ORTEP plot of [FeCl$_3$(tpySAc)]·MeCN, showing ellipsoids at the 50% probability level. The MeCN molecule has been omitted for clarity.

The crystals of [FeCl$_3$(tpySAc)]·MeCN had been grown at –30 °C to prevent conversion to thermodynamically more favorable [Fe(tpy)$_2$]$^{2+}$ derivatives, but even at this temperature, the isolated kinetic product was found to slowly turn purple in the mother liquor. Due to this instability, we could not obtain reliable microanalysis data for [FeCl$_3$(tpySAc)], in agreement with the difficulties experienced by Cotton and co-workers in their microanalyses of complexes of FeCl$_3$ with *N*-donor ligands.[7] Furthermore, [FeCl$_3$(tpySAc)] showed appreciable O_2 sensitivity, with exposure to air quickly resulting in a color change from yellow-orange to brown.

In subsequent reactions, [FeCl$_3$(tpySAc)] was found to be highly unstable. Rather than forming [Fe(tpy)(tpySAc)]$^{2+}$, reaction of [FeCl$_3$(tpySAc)] with tpy yielded complex mixtures devoid of both thioacetyl and thiol groups, suggesting modification or substitution of the thioacetyl functionality. Comparable results were obtained using [FeCl$_3$(tpy)] and tpySAc as alternative starting materials. Possibly, the synthetic difficulties stem from the reduction of Fe^{3+} to Fe^{2+} which accompanies the coordination of a second terpyridyl ligand to [FeCl$_3$(tpy)] or [FeCl$_3$(tpySAc)]. The electron involved in this reduction may come from the coordinating tpySH or tpySAc ligand, thereby leading to destructive follow-up reactions concentrated at the 4' substituent. We are currently researching ways to circumvent this problem, including the use of different metals and chemical reducing agents.

A1.3. Experimental.

General methods. ^{1}H and ^{13}C NMR spectra were recorded at 298 K on a Varian 400 MHz spectrometer operating at 400 and 100 MHz, respectively. The spectra were calibrated on the residual solvent peaks, and spectral assignments were based on chemical shift, integral, and linewidth considerations. Infrared spectra were recorded on a Perkin-Elmer Spectrum One FT-IR spectrometer. Elemental analyses were carried out by Kolbe Mikroanalytisches Laboratorium (Mülheim an der Ruhr, Germany).

4'-Acetylthio-2,2':6',2''-terpyridine (tpySAc). Thioacetic acid (Aldrich, 0.47 mL, 6.6 mmol) was added to a suspension of 4'-chloro-2,2':6',2''-terpyridine[9] (174 mg, 0.651 mmol) in THF (20 mL). The mixture was then refluxed for 24 h, during which time it became yellow and turbid. More thioacetic acid (0.47 mL, 6.6 mmol) was added, and refluxing was continued for another 24 h. After cooling to ambient temperature, the mixture was evaporated to a yellow powder. CH_2Cl_2 (40 mL) and H_2O (40 mL) were added, and the two layers were separated in a separatory funnel. The organic layer was washed with sat. aq. $NaHCO_3$ (3 × 40 mL), dried over $MgSO_4$, and evaporated to a crystalline yellow material. The product was dried in vacuo. Yield: 180 mg (586 mmol, 90%). Anal. Calcd for $C_{17}H_{13}N_3OS$: C, 66.43; H, 4.26; N, 13.67. Found: C, 66.53; H, 4.22; N, 13.63. ^{1}H NMR (400 MHz, CD_3CN): δ = 8.70 (d, $^{3}J_{H\text{-}H}$ = 4.7 Hz, 2H, H6), 8.66 (d, $^{3}J_{H\text{-}H}$ = 8.0 Hz, 2H, H3), 8.50 (s, 2H, H3'), 7.97 (td, $^{3}J_{H\text{-}H}$ = 7.7 Hz, $^{4}J_{H\text{-}H}$ = 1.7 Hz, 2H, H4), 7.47–7.43 (m, 2H, H5), 2.51 (s, 3H, CH_3). $^{13}C\{^{1}H\}$ NMR (100 MHz, $CDCl_3$): δ = 191.67 (CO), 156.15, 155.62, 149.35, 140.84, 137.08, 125.41, 124.22, 121.52 (8 × pyridyl C), 30.84 (CH_3). FT-IR (ATR, ν, cm^{-1}): 3054, 2920, 2851, 1715, 1557, 1466, 1387, 1265, 1116, 1092, 891, 792, 745, 735, 680, 656. Crystals suitable for X-ray diffraction studies were obtained by slow evaporation of a solution of tpySAc in CH_2Cl_2.

[$FeCl_3$(tpySAc)]·MeCN. An ice-cooled solution of tpySAc (0.100 g, 0.325 mmol) in MeCN (25 mL) was added to an ice-cooled solution of $FeCl_3$ (53 mg, 0.33 mmol) in MeCN (2 mL). The solution turned red and was allowed to warm to ambient temperature. After 1 h, yellow needles were collected by centrifugation, washed with cold MeCN (2 × 3 mL) and ether (20 mL), and dried *in vacuo*. Yield: 32 mg (0.068 mmol, 21%). Anal. Calcd for $C_{17}H_{13}Cl_3FeN_3OS$: C, 43.48; H, 2.79; N, 8.95; S, 6.83. Found: C, 44.20; H, 2.70; N, 10.06; S, 4.51. FT-IR (ATR, ν, cm^{-1}): 3675, 2988, 2902, 1732, 1592, 1477, 1416, 1249, 1066, 1057, 1022, 947, 887, 824, 789, 750, 729, 656. Crystals suitable for X-ray diffraction were grown by adding a solution of tpySAc (9.5 mg, 0.031 mmol) to a solution of $FeCl_3$ (5.0 mg, 0.031 mmol) at –30 °C. After 3 days at –30 °C, several yellow crystals large enough for X-ray diffraction studies had formed. IR spectroscopy showed these crystals to be identical to the product obtained in the preparative synthesis.

Crystal structure determinations of tpySAc and [$FeCl_3$(tpySAc)]·MeCN. X-ray intensities were measured on a Nonius Kappa CCD diffractometer with rotating anode (graphite monochromator, λ = 0.71073 Å) at a temperature of 150 K. The structures were solved with Direct Methods (program SHELXS-97[10] for tpySAc and program SIR-97[11] for [$FeCl_3$(tpySAc)]·MeCN). Refinement was performed with SHELXL-97[12] against F^2 of all reflections. Non-hydrogen atoms were refined freely with anisotropic displacement parameters. All hydrogen atoms were located in difference Fourier maps and refined with a riding model. Geometry calculations, illustrations, and checking for higher symmetry was performed with the PLATON program.[13]

Further details about the crystal structure determinations are given in Table 1.

Table 1. Crystallographic data for tpySAc and [FeCl$_3$(tpySAc)]·MeCN.

	tpySAc	**[FeCl$_3$(tpySAc)]·MeCN**
formula	$C_{17}H_{13}N_3OS$	$C_{17}H_{13}Cl_3FeN_3OS{\cdot}CH_3CN$
fw	307.36	510.62
crystal color	yellowish	yellow
crystal size (mm^3)	0.60 × 0.24 × 0.21	0.32 × 0.03 × 0.03
crystal system	monoclinic	monoclinic
space group	C2/c (no. 15)	P2$_1$/c (no. 14)
a (Å)	26.2152(9)	10.8110(2)
b (Å)	11.5679(7)	14.4621(3)
c (Å)	9.9155(3)	14.8134(3)
β (°)	100.232(5)	109.2131(10)
V (Å^3)	2959.1(2)	2187.07(8)
Z	8	4
D_x (g/cm^3)	1.380	1.551
μ (mm^{-1})	0.224	1.170
abs. corr. method	multi-scan	multi-scan
abs. corr. range	0.86 – 0.95	0.93 – 0.97
$(\sin\theta/\lambda)_{max}$ (Å^{-1})	0.65	0.58
refl. (meas./unique)	27128 / 3403	19545 / 3595
obs. refl. (I>2σ(I))	2740	2395
param./restraints	200 / 0	264 / 0
R1/wR2 (I>2σ(I))	0.0356 / 0.0909	0.0354 / 0.0748
R1/wR2 (all refl.)	0.0502 / 0.0981	0.0670 / 0.0868
S	1.027	1.058
$\rho_{min/max}$ (e/Å^3)	–0.25 / 0.31	–0.29 / 0.27

A1.4. References.

[1] (a) Constable, E. C. *Chem. Soc. Rev.* **2007**, *36*, 246–253. (b) Andres, P. R.; Schubert, U. S. *Adv. Mater.* **2004**, *16*, 1043–1068. (c) Hofmeier, H.; Schubert, U. S. *Chem. Soc. Rev.* **2004**, *33*, 373–399.
[2] (a) McMillin, D. R.; Moore, J. J. *Coord. Chem. Rev.* **2002**, *229*, 113–121. (b) Grätzel, M. *J. Photochem. Photobiol.* **2004**, *A164*, 3–14.
[3] Baranoff, E.; Collin, J.-P.; Flamigni, L.; Sauvage, J.-P. *Chem. Soc. Rev.* **2004**, *33*, 147–155.
[4] Park, J.; Pasupathy, A. N.; Goldsmith, J. I.; Chang, C.; Yaish, Y.; Petta, J. R.; Rinkoski, M.; Sethna, J. P.; Abruña, H. D.; McEuen, P. L.; Ralph, D. C. *Nature* **2002**, *417*, 722–725.
[5] Constable, E. C.; Hermann, B. A.; Housecroft, C. E.; Neuburger, M.; Schaffner, S.; Scherer, L. J. *New. J. Chem.* **2005**, *29*, 1475–1481.

[6] (a) Jios, J. L.; Kirin, S. I.; Weyhermüller, T.; Metzler-Nolte, N.; Della Védova, C. O. *J. Mol Struct.* **2006**, *825*, 53–59. (b) Erben, M. F.; Boese, R.; Della Védova, C. O.; Oberhammer, H.; Willner, H. *J. Org. Chem.* **2006**, *71*, 616–622.
[7] Cotton, S. A.; Franckevicius, V.; Fawcett, J. *Polyhedron* **2002**, *21*, 2055–2061.
[8] Coe, B. J.; Glenwright, S. J. *Coord. Chem. Rev.* **2000**, *203*, 5–80.
[9] Constable, E. C.; Ward, M. D. *J. Chem. Soc., Dalton Trans.* **1990**, 1405–1409.
[10] Sheldrick, G. M. *SHELXS-97. Program for crystal structure solution*; Universität Göttingen: Göttingen, Germany, 1997.
[11] Altomare, A.; Burla, M. C.; Camalli, M.; Cascarano, G. L.; Giacovazzo, C.; Guagliardi, A.; Moliterni, A. G. G.; Polidori, G.; Spagna, R. *J. Appl. Cryst.* **1999**, *32*, 115–119.
[12] Sheldrick, G. M. *SHELXL-97. Program for crystal structure refinement*; Universität Göttingen: Göttingen, Germany, 1997.
[13] Spek, A. L. *J. Appl. Cryst.* **2003**, *36*, 7–13.

Appendix 2

Crystal Structures of Three Indole-3-Thiouronium Salts

*Indole-3-thiouronium nitrate crystallizes as a strongly hydrogen-bonded, Y-type complex. In indole-3-thiouronium iodide, the hydrogen bonding interactions are visibly weaker. Hydrogen bonding in indole-3-*N,N,N',N'*-tetramethylthiouronium nitrate is restricted to the indole NH group. A multipole refinement of this third structure reveals single C–S bonds and partial double bonding in the N–C–N group.*

Lutz, M.; Spek, A. L.; van der Geer, E. P. L.; van Koten, G.; Klein Gebbink, R. J. M. *Acta Cryst.* **2008**, *C64*, o87–o90.

Lutz, M.; Spek, A. L.; van der Geer, E. P. L.; van Koten, G.; Klein Gebbink, R. J. M. *Acta Cryst.* **2008**, *E64*, o194.

Lutz, M.; Spek, A. L.; van der Geer, E. P. L.; van Koten, G.; Klein Gebbink, R. J. M. *Acta Cryst.* **2008**, *E64*, o195.

A2.1. Introduction.

Thiourea derivatives have found widespread application in molecular recognition and supramolecular chemistry, largely due to their hydrogen-bonding complementarity with carboxylate groups.[1] Of all thiourea derivatives, positively-charged thiouronium salts may be among the strongest anion receptors due to their increased acidity and the electrostatic stabilization of the anion-receptor complex.[2] Recently, we have demonstrated that *N*-substituted indole-3-thiouronium salts are readily available from indole by nucleophilic substitution at the nitrogen atom followed by electrophilic aromatic substitution with thiourea.[3] In order to gain more insight into the hydrogen-bonding properties of indole-3-thiouronium salts, we have obtained crystal structures of indole-3-thiouronium nitrate (**1**), indole-3-thiouronium iodide (**2**) and indole-3-*N,N,N′,N′*-tetramethylthiouronium nitrate (**3**) (Chart 1).

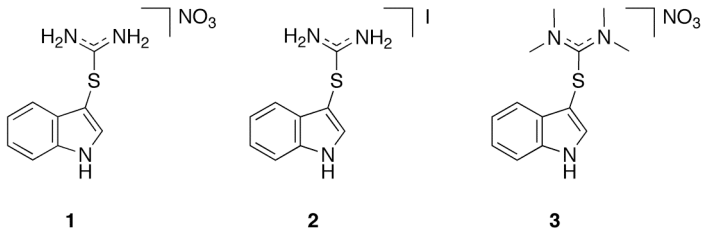

Chart 1. Structures of thiouronium salts **1**–**3**.

A2.2. Results and discussion.

The crystal structure of **1** (Figure 1) exhibits normal bond distances and angles. The thiouronium group is planar, with the C—N bond lengths of 1.3076(19) and 1.3162(19) Å indicating a significant degree of double-bond character, while the C—S bond length of 1.7566(15) Å lies in the range expected for a single bond. Distances and angles similar to the thiouronium group in **1** have been reported for the benzylthiouronium cation.[4] Reflecting the resulting hindered rotation about the C—N bonds, solution-phase ^{1}H NMR shows separate signals for the thiouronium hydrogen atoms *cis* and *trans* to sulfur at room temperature. The least-squares plane of the thiouronium moiety forms an interplanar angle of 88.62(6)° with respect to the least-squares plane of the indole group. A thermal motion analysis using the THMA11 program[5] results in a low weighted *R* value ($R = [(\Sigma\ (w\Delta U)^2) / (\Sigma\ (wU_{obs})^2)]^{1/2}$) of 0.084, indicating that the molecule behaves as a rigid body in the solid state.

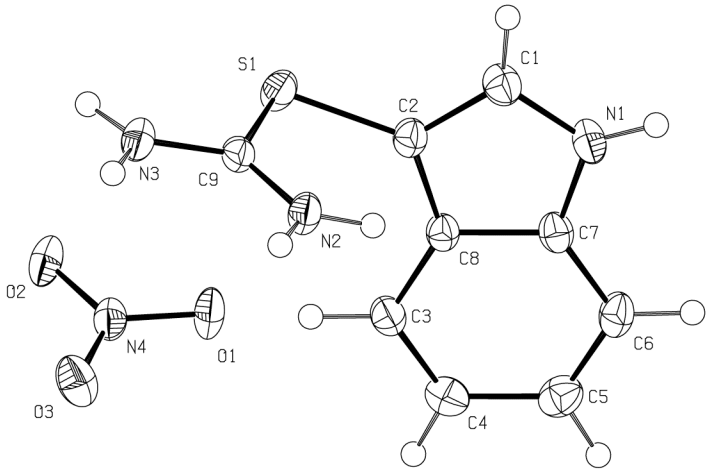

Figure 1. ORTEP plot of **1**, showing ellipsoids at the 50% probability level. Hydrogen atoms are shown as small spheres of arbitrary radius.

Hydrogen bonding between the nitrate anion and the thiouronium hydrogen atoms *trans* to sulfur results in a Y-type complex as often seen in thiourea-carboxylate recognition.[6] In fact, all NH groups act as hydrogen bond donors with nitrate oxygen atoms as acceptors. O1 and O2 each accept two hydrogen bonds while O3 accepts only one. This hydrogen bonding scheme results in a two-dimensional network in the *ab* plane (Figure 2).

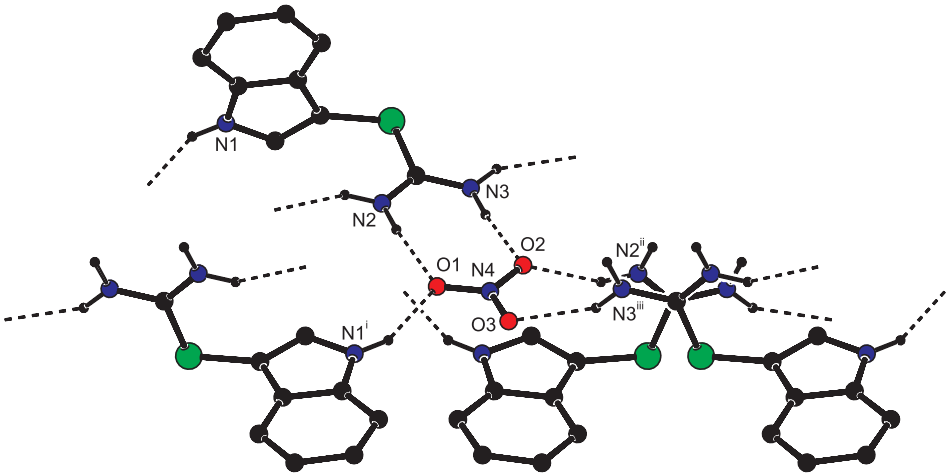

Figure 2. Hydrogen bonding scheme in **1** viewed along the crystallographic *b* axis. CH hydrogen atoms have been omitted for clarity. Symmetry operations i: 1 – x, 0.5 + y, 0.5 – z; ii: 0.5 + x, y, 0.5 – z; iii: 2 – x, 0.5 + y, 0.5 – z.

The indole ring systems form parallel, centrosymmetric dimers with an average ring···ring distance of 3.449(2) Å via π stacking interactions (Figure 3). These interactions connect the two-dimensional hydrogen bonded layers.

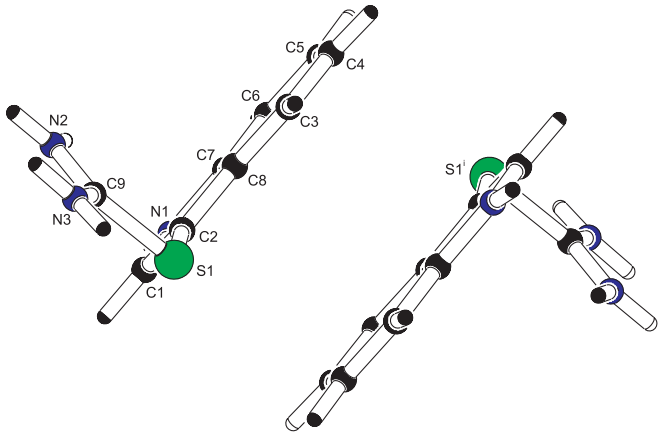

Figure 3. π stacking interactions between the indole ring systems in **1** viewed along the crystallographic *a* axis. Symmetry operation i: 1 – x, 1 – y, –z.

The molecular geometry of the cation in iodide salt **2** is very similar to that in the nitrate analogue **1** (Figure 4). The C—N distances of 1.306 (2) and 1.317 (2) Å again indicate significant double bond character while the C—S distance of 1.7533 (19) Å indicates a single bond. As in **1**, the cation consists of two, planar indole and thiouronium moieties, which are perpendicular to each other with an angle of 89.87(8)° between the corresponding least squares planes. The weighted R value resulting from a thermal motion analysis using the program THMA11[5] is 0.106, slightly higher than in **1**.

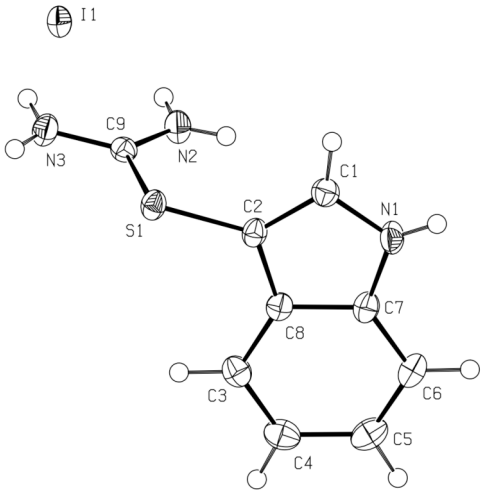

Figure 4. ORTEP plot of **2**, showing ellipsoids at the 50% probability level. Hydrogen atoms are shown as small spheres of arbitrary radius.

The iodide anion in **2** is surrounded by five N—H groups acting as hydrogen bond donors (Figure 5), which results in a three-dimensional hydrogen bonded network. The H···I distances of 2.76(3) to 2.97(2) Å are in the same range as found for other N—H···I hydrogen bonds in the Cambridge Structural Database (CSD),[7] where we calculate an average H···I distance of

2.80 Å. In general, N—H···I hydrogen bonds are relatively weak; the average hydrogen bonded intermolecular N···I distance is 3.65 Å in the CSD, which is not shorter than the sum of the van der Waals radii of nitrogen (1.55 Å) and iodine (1.98 Å).

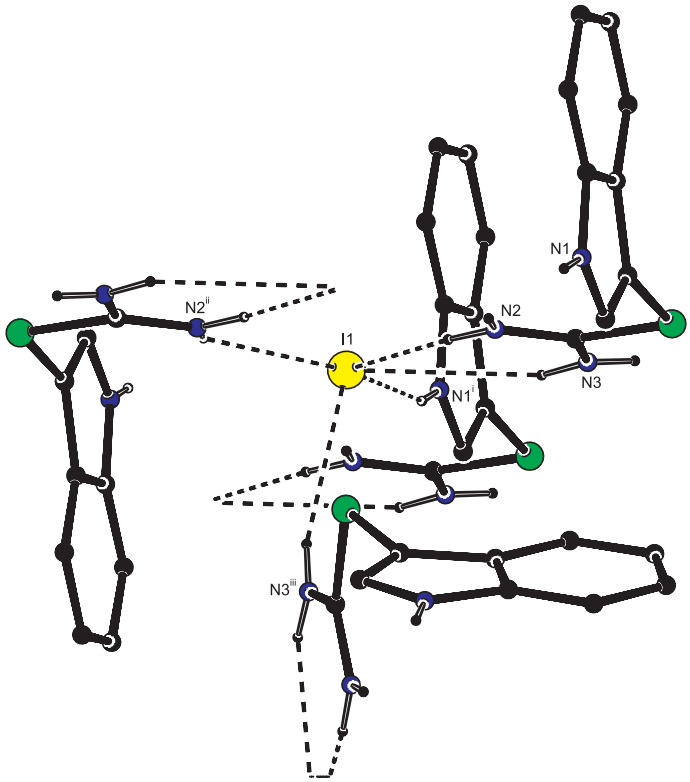

Figure 5. Hydrogen bonding of the iodide anion in **2**. CH hydrogen atoms have been omitted for clarity. Symmetry operations i: 1 + x, y, z; ii: 1 – x, 1 – y, –z; iii: x, 0.5 – y, z – 0.5.

In addition to the N—H···I hydrogen bonds, there are weak intermolecular C—H···π interactions between H1 and indole's six-membered ring (Figure 6). The distance of H1 to the least squares plane of the six-membered ring is 2.83 (2) Å and the distance to the ring's center of gravity is 2.91 (2) Å. According to the classification formulated by Malone *et al.*[8] this is a Type I C—H···π interaction.

In the crystal structure of **3** (Figure 7), the C9—N distances are 1.3291(4) and 1.3355(4) Å, again indicative of significant double-bond character. However, the bonds are longer than the 1.306(2) to 1.317(2) Å bonds in the non-methylated thiouronium salts **1** and **2**. The corresponding C—N bond lengths in urea[9] and *N*,*N*,*N*′,*N*′-tetramethylurea[10] are 1.343(13) and 1.3706(13) Å, respectively. Unfortunately, the bond lengths cannot be compared to those in the corresponding thiourea derivatives as free thiourea undergoes ferroelectric phase transitions[11] and the crystal structure of *N*,*N*,*N*′,*N*′-tetramethylthiourea is not available in the literature.

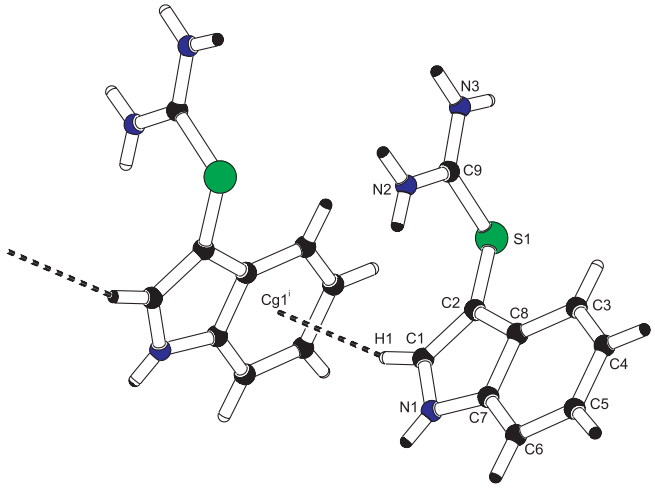

Figure 6. C—H···π interaction in **2** viewed along the crystallographic *b* axis. Symmetry operation i: x, 0.5 – y, z – 0.5.

Due to the permethylation of the thiouronium group, the cation in **3** has only one N—H hydrogen bond donor. O1 of the nitrate anion accepts the hydrogen bond to form an isolated cation-anion-pair with graph set descriptor D.[12] The NH_2 derivatives **1** and **2** each have five hydrogen bond donors and form polymeric two- and three-dimensional networks, respectively. The density of **3** (1.388 g/cm^3) is consequently lower than the densities of **1** and **2** (1.513 and 1.819 g/cm^3, respectively).

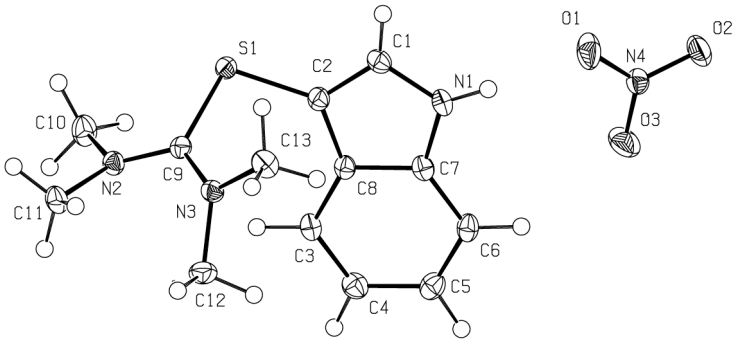

Figure 7. ORTEP plot of **3** after multipole refinement, showing ellipsoids at the 50% probability level. Hydrogen atoms are shown as small spheres of arbitrary radius.

The indole ring systems in **3** form centrosymmetric, parallel dimers (Figure 8). The intermolecular distance of S1i (i: 1 − x, 1 − y, 1 − z) with the least squares plane of the indole ring is 3.43323(6) Å. Despite this relatively short distance, we do not assume π stacking interactions because the indole systems are not on top of each other. The intermolecular distance between the centers of gravity of the 5-membered rings is consequently very long (4.5681(2) Å).

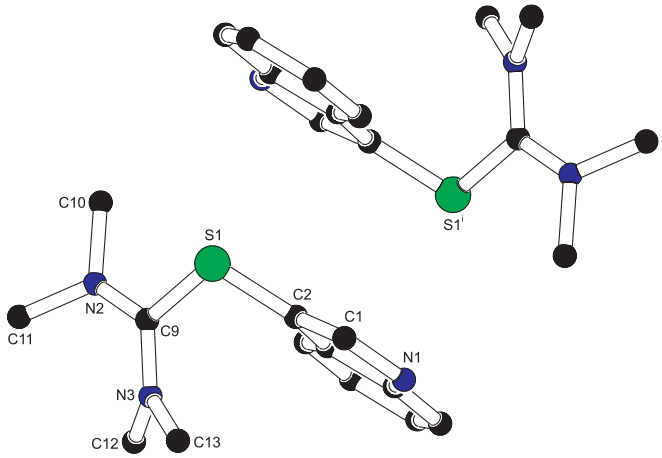

Figure 8. Centrosymmetric dimer of the indole systems in **3** viewed along the crystallographic [1,1,0] direction. Hydrogen atoms and nitrate anions have been omitted for clarity. Symmetry operation i: 1 – *x*, 1 – *y*, 1 – *z*.

Searching the CSD revealed 38 entries of thiouronium and 4 entries of *N*,*N*,*N*′,*N*′-tetramethylthiouronium compounds of which 12 are drawn with a S=C9 double bond.[13] 20 entries have a C9=N double bond and consequently a positive charge on a nitrogen atom,[14] nine entries have the positive charge delocalized over the N—C—N group,[15] and one entry has no bond order indication. Solution-phase ^{1}H and ^{13}C NMR studies show only one signal for the methyl groups in **3** at room temperature. To investigate the bonding situation of the thiouronium group we performed a high-resolution diffraction experiment of **3** followed by a multipole refinement of the structure.

A topological analysis of the cation shows that the Laplacian at the bond critical points of the C9—N bonds have highest magnitudes of −26.33 (7) and −26.02 (7) e Å^{-5}, respectively. Because the Laplacian at the bond critical point is a measure for the bond strength,[16] this analysis clearly shows that these are the strongest bonds in the cations. The negative sign of the values indicates covalent bonding. A quantum chemical study of urea gives a value of −1.15 au (corresponding to −27.71 e Å^{-5}) for the Laplacian at the bond critical point of the C—N single bond.[17] In an experimental study, Zavodnik *et al.* determined a value of −27.34 e Å^{-5}.[18] We can therefore conclude that the bond strengths of the C—N bonds in **3** and in urea are very similar.

The Laplacians at the bond critical points of the C—S bonds of −4.918(19) and −5.008(19) e Å^{-5} are very similar to the C—S single bonds of the dipeptide DL-alanylmethionine with values of −4.9 and −4.7 e Å^{-5}.[19] The C—S bonds in **3** are thus best described as single bonds.

The net charges of the atoms derived from the monopole populations indicate a negative charge concentration on the carbon atoms of the four methyl groups. As expected, the positive

charges are distributed over the hydrogen atoms. Adding these charges gives a negative charge of −0.51 for the nitrate anion and, due to the applied electroneutrality constrain, +0.51 for the cation.

A thermal motion analysis using the program THMA11[5] results in a low weighted R value of 0.093, indicating that the molecule behaves as a rigid body in the solid state at 110 K. The value can be decreased if the thiouronium moiety is treated as an independent rigid body with the S1—C9 bond as rotation axis resulting in R = 0.065. This analysis additionally supports the description of S1—C9 as a single bond allowing free rotation.

A2.3. Conclusion.

The current study shows that the hydrogen bonding in Y-type complex indole-3-thiouronium nitrate can be effectively tailored by changing the counterion to iodide (reduction of hydrogen bonding strength) or thiouronium permethylation (constriction of hydrogen bonding donor ability to the indole NH atom). The ease with which the ionic thiouronium and *N*,*N*,*N*′,*N*′-tetramethylthiouronium groups can be introduced into indole and its (*N*-substituted) derivatives may facilite the application of indole-3-thiouronium salts in (bio)molecular recognition, supramolecular chemistry, and crystal engineering.

A2.4. Experimental.

General methods. Reactants were purchased from Acros and used as received. ^{1}H and ^{13}C NMR spectra were recorded at 300 K on a Bruker AC 300 spectrometer operating at 300 and 75 MHz, respectively. The spectra were calibrated on the residual solvent peaks, and spectral assignments were based on chemical shift, integral, and linewidth considerations. Infrared spectra were recorded on a Perkin-Elmer Spectrum One FT-IR spectrometer. Elemental analyses were carried out by Kolbe Mikroanalytisches Laboratorium (Mülheim an der Ruhr, Germany). X-ray intensities were measured on a Nonius Kappa CCD diffractometer with rotating anode (graphite monochromator, λ = 0.71073 Å) at a temperature of 150 K. Further crystallographic details are given in Table 1.

Indole-3-thiouronium iodide (2). This compound was prepared as described in literature,[20,21] and crystallized by diethyl ether vapor diffusion into an acetone solution.

Data collection: *COLLECT*;[22] cell refinement: *PEAKREF*;[23] data reduction: *EVAL14*[24] and *SADABS*;[25] program used to solve structure: *SHELXS97*;[26] program used to refine structure: *SHELXL97*;[27] molecular graphics: *PLATON*.[28]

Indole-3-thiouronium nitrate (1). To a solution of **2** (0.100 g, 0.313 mmol) in EtOH (10 mL) was added $AgNO_3$ (0.0532 g, 0.313 mmol). The solution was stirred for 1 h, filtered to remove AgCl, and concentrated to approximately 3 mL. Ether (60 mL) was added, and after 48 h, white needles were collected by centrifugation, washed with ether, and dried *in vacuo*. Yield: 0.0738 g (0.290 mmol, 93%). Anal. Calcd for $C_9H_{10}N_4O_3S$: C, 42.51; H, 3.96; N, 22.03; S, 12.61. Found: C, 42.32; H, 4.08; N, 21.92; S, 12.73. The ^{1}H NMR spectrum was identical to that of indole-3-thiouronium iodide.[21] FT-IR (ATR, ν,

cm^{-1}): 3335, 3264, 3122, 1662, 1640, 1498, 1423, 1388, 1308, 1237, 1218, 1128, 1104, 1065, 1049, 1006, 816, 744. Crystals suitable for X-ray diffraction studies were obtained by ether vapor diffusion into an EtOH solution of the product.

Data collection: *COLLECT*;[22] cell refinement: *HKL2000*;[29] data reduction: *HKL2000*;[29] program used to solve structure: *SHELXS97*;[26] program used to refine structure: *SHELXL97*;[27] molecular graphics: *PLATON*.[28]

Indole-3-*N,N,N',N'*-tetramethylthiouronium iodide. To a solution of indole (0.600 g, 5.12 mmol) and *N,N,N',N'*-tetramethylthiourea (0.677 g, 5.12 mmol) in a 4/1 (v/v) mixture of MeOH and H_2O (20 mL) were added I_2 (1.30 g, 5.12 mmol) and KI (0.850 g, 5.12 mmol). The mixture was stirred overnight and then evaporated to dryness. The residue was washed with water and ether, yielding a dark yellow powder. Yield: 1.67 g (4.45 mmol, 87%). Anal. Calcd for $C_{13}H_{18}IN_3S$: C, 41.61; H, 4.83; N, 11.20; S, 8.54. Found: C, 41.53; H, 4.78; N, 11.15; S, 8.65. ^{1}H NMR (DMSO-d_6): δ = 12.00 (s, br, 1H, NH), 7.99 (d, $^3J_{H\text{-}H}$ = 2.7 Hz, 1H, indolyl 2-H), 7.53 (d, $^3J_{H\text{-}H}$ = 7.9 Hz, 1H, indolyl H), 7.43 (d, $^3J_{H\text{-}H}$ = 7.9 Hz, 1H, indolyl H), 7.26 (td, $^3J_{H\text{-}H}$ = 7.6 Hz, $^4J_{H\text{-}H}$ = 1.2 Hz, 1H, indolyl H), 7.18 (t, $^3J_{H\text{-}H}$ = 7.4 Hz, 1H, indolyl H), 3.14 (s, 12 H, CH_3). ^{13}C{^{1}H} NMR (DMSO-d_6): δ = 174.76 ($C(NMe_2)_2$), 136.25, 132.65, 126.97, 122.77, 121.02, 117.28, 112.75, 94.54 (8 × indolyl C), 43.58 (CH_3). FT-IR (ATR, ν, cm^{-1}): 3136, 3099, 1600, 1498, 1455, 1413, 1380, 1340, 1256, 1235, 1166, 1100, 1006, 874, 758, 751, 691.

Indole-3-*N,N,N',N'*-tetramethylthiouronium nitrate (3). To a solution of $AgNO_3$ (0.0453 g, 0.266 mmol) in EtOH (10 mL) was added indole-3-*N,N,N',N'*-tetramethylthiouronium iodide (0.100 g, 0.266 mmol). The mixture was refluxed for 1 h and then filtered to remove AgCl. The resulting cream-colored solution was concentrated *in vacuo*. Ether was added overnight by vapor diffusion. Colorless crystals formed which proved to be suitable for X-ray diffraction studies. The crystals remaining after X-ray analysis were filtered, washed with ether, and dried *in vacuo*. Yield: 0.0667 g (2.15 mmol, 81%). Anal. Calcd for $C_{13}H_{18}N_4O_3S$: C, 50.31; H, 5.85; N, 18.05; S, 10.33. Found: C, 50.46; H, 5.80; N, 18.15; S, 10.25. The ^{1}H NMR spectrum was identical to that of the starting compound. FT-IR (ATR, ν, cm^{-1}): 3100, 2927, 1599, 1502, 1456, 1362, 1324, 1256, 1238, 1208, 1166, 1112, 1101, 1059, 1042, 1009, 876, 830, 784, 760, 748.

Data collection: *COLLECT*;[22] cell refinement: *PEAKREF*;[23] data reduction: *EVAL15*;[30] *SADABS*;[25] program used to solve structure: *SHELXS97*;[26] program used to refine structure: XD;[31] molecular graphics: XD[31] and *PLATON*.[28]

Table 1. Crystallographic data for **1**, **2**, and **3**.

	1	**2**	**3**
formula	$C_9H_{10}N_3S{\cdot}NO_3$	$C_9H_{10}N_3S{\cdot}I$	$C_{13}H_{18}N_3S{\cdot}NO_3$
fw	254.27	319.16	310.37
crystal color	colorless	colorless	colorless
crystal size (mm^3)	0.30 × 0.24 × 0.06	0.30 × 0.30 × 0.30	0.36 × 0.24 × 0.24
crystal system	orthorhombic	monoclinic	orthorhomic
space group	Pbca	$P2_1/c$	Pbca
a (Å)	12.0524(2)	10.5098(2)	12.46443(1)
b (Å)	8.7395(1)	10.6264(3)	11.02991(7)
c (Å)	21.1893(3)	10.6951(4)	21.60929(4)
β	90°	102.648(2)°	90°
V ($Å^3$)	2231.91(5)	1165.46(6)	2970.88(2)
Z	8	4	8
F_{000}	1056	616	1312
D_x (g/cm^3)	1.513	1.819	1.388
λ (Å)	0.71073	0.71073	0.71073
θ	1.0°–27.5°	2.0°–27.5°	1.9°–45.0°
μ (mm^{-1})	0.29	2.89	0.23
abs. corr. method	none	multi-scan	multi-scan
refl. (meas./unique)	32180 / 2563	15531 / 2668	247693 / 12242
obs. refl. ($I>2\sigma(I)$)	2120	2470	9924
R_{int}	0.048	0.033	0.034
θ_{max}	27.5°	27.5°	45.0°
parameters	194	167	570
$R[F^2 > 2\sigma(F^2)]$	0.032	0.018	0.020
$wR(F^2)$	0.089	0.045	0.011
S	1.04	1.09	2.03
$\rho_{min/max}$ ($e/Å^3$)	–0.23 / 0.26	–0.53 / 0.50	–0.29 / 0.34

A2.5. References.

[1] For reviews, see: (a) Takemoto, Y. *Org. Biomol. Chem.* **2005**, *3*, 4299–4306. (b) Fitzmaurice, R. J.; Kyne, G. M.; Douheret, D.; Kilburn, J. D. *J. Chem. Soc., Perkin Trans. 1* **2002**, 841–864. (c) Schmidtchen, F. P.; Berger, M. *Chem. Rev.* **1997**, *97*, 1609–1646. For recent examples, see: (d) Pfeffer, F. M.; Kruger, P. E.; Gunnlaugsson, T. *Org. Biomol. Chem.* **2007**, *5*, 1894–1902. (e) Jordan, B. J.; Pollier, M. A.; Miller, L. A.; Tiernan, C.; Clavier, G.; Audebert, P.; Rotello, V. M. *Org. Lett.* **2007**, *9*, 2835–2838. (f) Jose, D. A.; Singh, A.; Das, A.; Ganguly, B. *Tetrahedron Lett.* **2007**, *48*, 3695–3698. (g) Amendola, V.; Esteban-Gómez, D.; Fabbrizzi, L.; Licchelli, M.; Monzani, E.; Sancenón, F. *Inorg. Chem.* **2005**, *44*, 8690–8698. (h) Ragusa, A.; Rossi, S.; Hayes, J. M.; Stein, M.; Kilburn, J. D. *Chem. Eur. J.* **2005**, *11*, 5674–5688. (i) Wu, J.-L.; He, Y.-B.; Wei, L.-H.; Liu, S.-Y.; Meng, L.-Z.; Hu, L. *Supramol. Chem.* **2004**, *16*, 353–359. (j) Nie, L.; Li, Z.; Han, J.; Zhang, X.; Yang, R.; Liu, W.-X.; Wu, F.-Y.; Xie, J.-W.; Zhao, Y.-F.; Jiang, Y.-B. *J. Org. Chem.* **2004**, *69*, 6449–6454. (k) Jiménez Blanco, J. L.; Bootello, P.; Ortiz Mellet, C.; Gutiérrez Gallego, R.; García Fernández, J. M. *Chem. Commun.* **2004**, 92–93.

[2] Esteban Gómez, D.; Fabbrizzi, L.; Lichelli, M.; Monzani, E. *Org. Biomol. Chem.* **2005**, *3*, 1495–1500.

[3] van der Geer, E. P. L.; Li, Q.; van Koten, G.; Klein Gebbink, R. J. M.; Hessen, B. *Inorg. Chim. Acta*, in press (Chapter 3 of this thesis).

[4] Ng, S. W. *Acta Cryst.* **1995**, *C51*, 1143–1144.

[5] Schomaker, V.; Trueblood, K. N. *Acta Cryst.* **1998**, *B54*, 507–514.

[6] Costero, A. M.; Gaviña, P.; Rodríguez-Muñiz, G. M.; Gil, S. *Tetrahedron* **2007**, *63*, 7899–7905, and references therein.

[7] Allen, F. H. *Acta Cryst.* **2002**, *B58*, 380–388.

[8] Malone, J. F.; Murray, C. M.; Charlton, M. H.; Docherty, R.; Lavery, A. J. *J. Chem. Soc. Faraday Trans.* **1997**, *93*, 3429–3436.

[9] Zavodnik, V.; Stash, A.; Tsirelson, V.; de Vries, R.; Feil, D. *Acta Cryst.* **1999**, *B55*, 45–54.

[10] Frampton, C. S.; Parkes, K. E. B. *Acta Cryst.* **1996**, *C52*, 3246–3248.

[11] Takahashi, I.; Onodera, A.; Shiozaki, Y. *Acta Cryst.* **1990**, *B46*, 661–664.

[12] Etter, M. C. *Acc. Chem. Res.* **1990**, *23*, 120–126.

[13] see, for example: Abashev, G. G.; Vlasova, R. M.; Kartenko, N. F.; Kuzmin, A. M.; Rozhdestvenskaya, I. V.; Semkin, V. N.; Usov, O. A.; Russkikh, V. S. *Acta Cryst.* **1987**, *C43*, 1108–1112.

[14] see, for example: Garner, P.; Anderson, J. T.; Dey, S.; Youngs, W. J.; Galat, K. *J. Org. Chem.* **1998**, *63*, 5732–5733.

[15] Ishii, Y.; Matsunaka, K.; Sakaguchi, S. *J. Am. Chem. Soc.* **2000**, *122*, 7390–7391.

[16] Bader, R. F. W. *Atoms in Molecules: A Quantum Theory*; Oxford University Press: Oxford, the United Kingdom, 1990.

[17] Gatti, C.; Saunders, V. R.; Roetti, C. *J. Chem. Phys.* **1994**, *101*, 10686–10696.

[18] Zavodnik, V.; Stash, A.; Tsirelson, V.; de Vries, R.; Feil, D. *Acta Cryst.* **1999**, *B55*, 45–54.

[19] Guillot, R.; Muzet, N.; Dahaoui, S.; Lecomte, C.; Jelsch, C. *Acta Cryst.***2001**, *B57*, 567–578.

[20] Harris, R. L. N. *Tetrahedron Lett.* **1969**, 4465–4466.

[21] van der Geer, E. P. L.; van Koten, G.; Klein Gebbink, R. J. M.; Hessen, B. *Inorg. Chem.*, accepted (Chapter 2 of this thesis).

[22] *COLLECT data collection software*; Nonius B.V.: Delft, The Netherlands, 1999.

[23] Schreurs, A. M. M. *PEAKREF*; Utrecht University: Utrecht, The Netherlands, 2005.

[24] Duisenberg, A. J. M.; Kroon-Batenburg, L. M. J.; Schreurs, A. M. M. *J. Appl. Cryst.* **2003**, *36*, 220–229.

[25] Sheldrick, G. M. *SADABS*; Universität Göttingen: Göttingen, Germany, 2002.

[26] Sheldrick, G. M. *SHELXS-97. Program for crystal structure solution*; Universität Göttingen: Göttingen, Germany, 1997.

[27] Sheldrick, G. M. *SHELXL-97*. *Program for crystal structure refinement*; Universität Göttingen: Göttingen, Germany, 1997.
[28] Spek, A. L. *J. Appl. Cryst.* **2003**, *36*, 7–13.
[29] Otwinowski, Z.; Minor, W. *Macromolecular Crystallography, Part A*; Carter, C. W., Jr.; Sweet, R. M., Eds.; Methods in Enzymology; Academic Press Limited: London, the United Kingdom, 1997; pp 307-326.
[30] Xian, X.; Schreurs, A. M. M.; Kroon-Batenburg, L. M. J. *Acta Cryst.* **2006**, *A62*, s92.
[31] Koritsanszky, T.; Howard, S. T.; Richter, T.; Macchi, P.; Volkov, A.; Gatti, C.; Mallinson, P. R.; Farrugia, L.; Su, Z.; Hansen, N. K.; *XD - a computer program package for multipole refinement and topological analysis of charge densities from diffraction data*; Freie Universität Berlin: Berlin, Germany, 2003.

Summary and Perspective

[4Fe-4S] clusters are one of Nature's most ubiquitous cofactors, playing vital roles in protein structure stabilization, electron transport, catalysis, and sensing.[1] When an enzyme features a [4Fe-4S] cluster in the active site, the coordination environment of the cluster is *3:1 site-differentiated*, meaning that the ligand or residue coordinated to one of the four iron atoms is markedly different from those coordinated to the other three iron atoms. Examples include aconitase, in which one of the four iron atoms is the site of substrate binding,[2] and iron-only hydrogenase, in which the unique iron atom is linked to a diiron subsite *via* a bridging cysteinyl thiolate.[3]

As an introduction into the field, **Chapter 1** of this thesis provides a comprehensive overview of natural and synthetic [4Fe-4S] clusters with 3:1 site-differentiated coordination environments. X-ray crystallography has revealed the presence of 3:1 site-differentiated [4Fe-4S] clusters in a large and growing number of natural enzymes, with the family of radical *S*-adenosylmethionine enzymes being the most exciting recent addition. In many cases, the additional discoveries pose immediate new questions and scientific challenges, underlining the limited current insight and understanding of biological 3:1 site differentiated [4Fe-4S] clusters in particular and catalytic iron-sulfur sites in general. One method of unraveling the (bio)chemistry of these intriguing metallosites is the synthetic analogue approach, in which synthetic [4Fe-4S] clusters are prepared, studied, and compared to their biological counterparts.[4] 3:1 site differentiation in these synthetic clusters is usually achieved by the use of tripodal trithiolate ligands, which chelate three of the four iron sites, leaving one iron atom free for further modification. The nature of the tripodal ligand fundamentally affects the properties of the [4Fe-4S] cluster and has specific advantages as well as disadvantages for a given application.

The most promising 3:1 site-differentiating [4Fe-4S] cluster ligand is arguably the $TriSH_3$ trithiol, reported by Pohl *et al.* in 1997 (Chart 1).[5] Unfortunately, the reported synthesis of $TriSH_3$ employs hazardous thiol protection and deprotection chemistry. In an effort to provide more convenient acccess to synthetic, 3:1 site-differentiated [4Fe-4S] clusters, **Chapter 2** of this thesis presents a new synthetic route to $TriSH_3$. In this route, indole-3-thiol is protected using chloromethyl ethyl ether rather than its carcinogenic counterpart chloromethyl methyl ether. The masked thiol groups are later deprotected using $AgNO_3$ and HCl instead of the conventional deprotection reagents $Hg(OAc)_2$ and H_2S. Not only does the new route avoid the use of highly toxic reagents, but it also results in an overall yield that is more than double that in the original procedure.

The reaction of $TriSH_3$ with $(n\text{-}Bu_4N)_2[Fe_4S_4(SEt)_4]$ in DMF yields the 3:1 site-differentiated cluster $(n\text{-}Bu_4N)_2[Fe_4S_4(TriS)(SEt)]$, with full conversion being ensured by

removal of the volatile EtSH coproduct. The new cluster displays good solubility and excellent purity as confirmed by spectroscopic, microanalytical, and electrochemical characterizations.

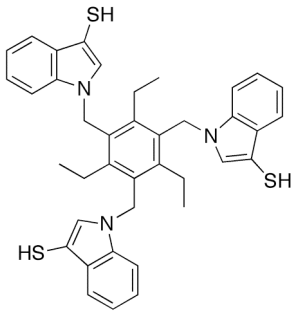

Chart 1. The tripodal $TriSH_3$ ligand.

Chapter 2 further illustrates the synthetic versatility of $(n\text{-}Bu_4N)_2[Fe_4S_4(TriS)(SEt)]$ by describing its reaction with the new thiol-functionalized Fe(II) compound $[Fe(tpySH)_2](PF_6)_2$ (tpySH = 2,2':6',2''-terpyridine-4'-thiol). The product is the first [4Fe-4S] cluster dimer to be linked by a metal-containing bridge (Chart 2). In cyclic voltammetry at 100 mV/s, the dimer undergoes a single cluster-centered transition with a peak separation of 82 mV, demonstrating that the [4Fe-4S] clusters in the dimer act as independent redox units. In UV-vis spectroscopy, the dimer displays a 375 nm absorption corresponding to a π–π^* transition centered on the $tpyS^-$ C–S functionality, indicative of a thioquinonoid electron distribution in the bridging $\{Fe(tpyS)_2\}$ moiety.

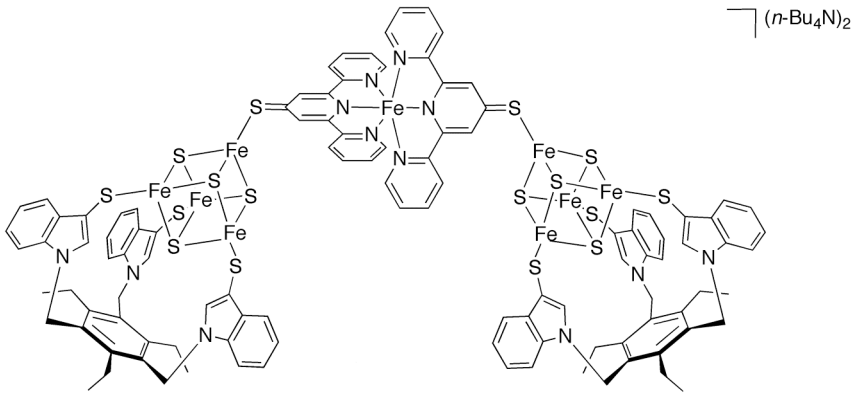

Chart 2. The [4Fe-4S] cluster dimer $(n\text{-}Bu_4N)_2[\{Fe_4S_4(TriS)(\mu\text{-}Stpy)\}_2Fe]$.

The $TriSH_3$ ligand contains three indolyl-3-thiol arms preorganized to bind a [4Fe-4S] cluster in a central cavity. Despite the vast number of known, symmetrically substituted clusters of the type $[Fe_4S_4(SR)_4]^{2-}$, no synthetic clusters fully coordinated by monodentate ligands based on indole-3-thiol have yet been reported. **Chapter 3** of this thesis addresses this gap in [4Fe-4S] cluster chemistry by presenting the synthesis of a series of symmetrically substituted [4Fe-4S] clusters with *N*-substituted indole-3-thiolate ligands (Scheme 1). The

new cluster family undergoes 2–/3– redox transitions at potentials between –1.17 and –1.22 V vs. the standard calomel electrode (SCE) in CH_2Cl_2, depending on the nature of the *N*-substituent. These redox potentials fall in between the potential ranges in which clusters fully coordinated by all-aliphatic and all-aromatic thiolates generally display redox transitions, emphasizing the intermediate electron-donating properties of indole-3-thiolates. In DMF solution, the indole-3-thiolate clusters show a lowest-energy electronic transition between 500 nm for the pentyl- and 511 nm for the benzylindole-3-thiolate [4Fe-4S] cluster. These transitions are among the most redshifted known in [4Fe-4S] cluster chemistry.

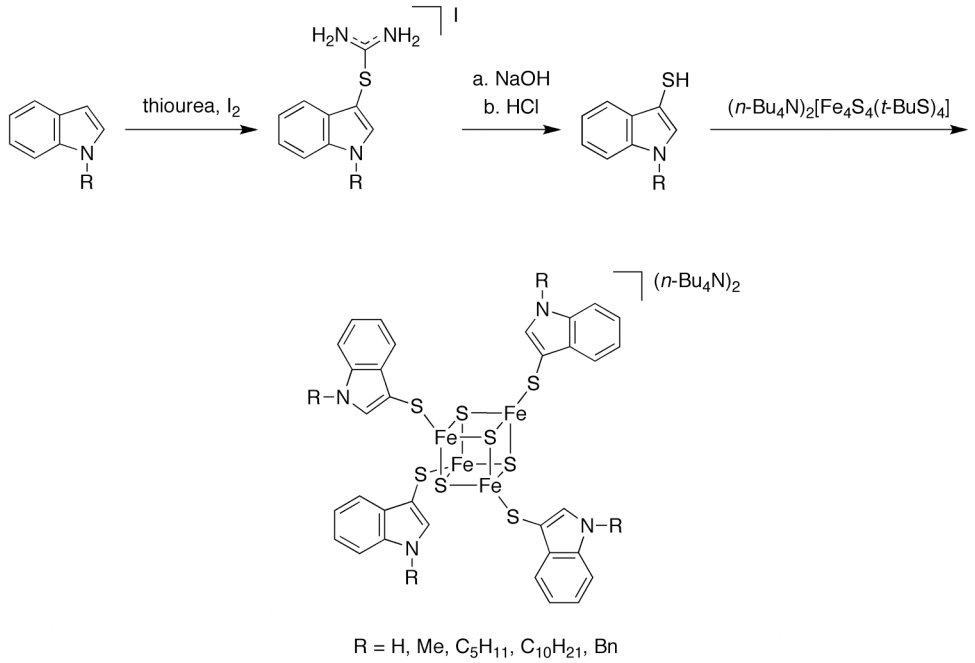

Scheme 1. Synthesis of a series of [4Fe-4S] clusters with *N*-substituted indole-3-thiolate ligands.

Chapter 4 further explores and expands the chemistry of $TriS^{3-}$-chelated [4Fe-4S] clusters by studying the reaction of $(n\text{-}Bu_4N)_2[Fe_4S_4(TriS)(SEt)]$ with three different thiols. Reaction with ethyl cysteinate (EtCysSH) proceeds cleanly to yield analytically pure $(n\text{-}Bu_4N)_2[Fe_4S_4(TriS)(SCysEt)]$, demonstrating that $(n\text{-}Bu_4N)_2[Fe_4S_4(TriS)(SEt)]$ can undergo site-specific ligand exchanges with aliphatic thiols without prior activation of the unique iron site. Reaction with 4-pyridinethiol results in a 3:1 site-differentiated [4Fe-4S] cluster with a pendant pyridyl group. This group can subsequently react with the ruthenium porphyrin [Ru(TTP)(CO)(MeOH)] (TTP = 5,10,15,20-tetra(*p*-tolyl)porphyrinato dianion) to form the first [4Fe-4S]-Ru assembly (Scheme 2). In CD_2Cl_2, the ^1H NMR signals of both the cluster and porphyrin moieties are affected by the formation of the bridged assembly. The largest shifts, however, are experienced by the $n\text{-}Bu_4N^+$ counterion, indicating ion-pairing. In cyclic voltammetry, the [4Fe-4S] cluster is little affected by the binding of the ruthenium porphyrin: the cluster-centered 2–/3– transition occurs at –1.13 and –1.11 V vs. SCE in CH_2Cl_2 for the starting cluster and the resulting assembly, respectively. The ruthenium porphyrin is electrochemically more sensitive to the nature of its axial substituent. Compared to the TTP

reduction in its unsubstituted pyridine-bound analogue ($E_{1/2}$ = –1.61 V vs. SCE), the TTP reduction in the assembly is strongly anodically shifted (E_{red} = –1.75 V vs. SCE). Furthermore, the carbonyl stretch frequency in the assembly is slightly lower (1937 vs. 1940 cm^{-1}), reflecting the electron donation by the cluster-bound thiolate group.

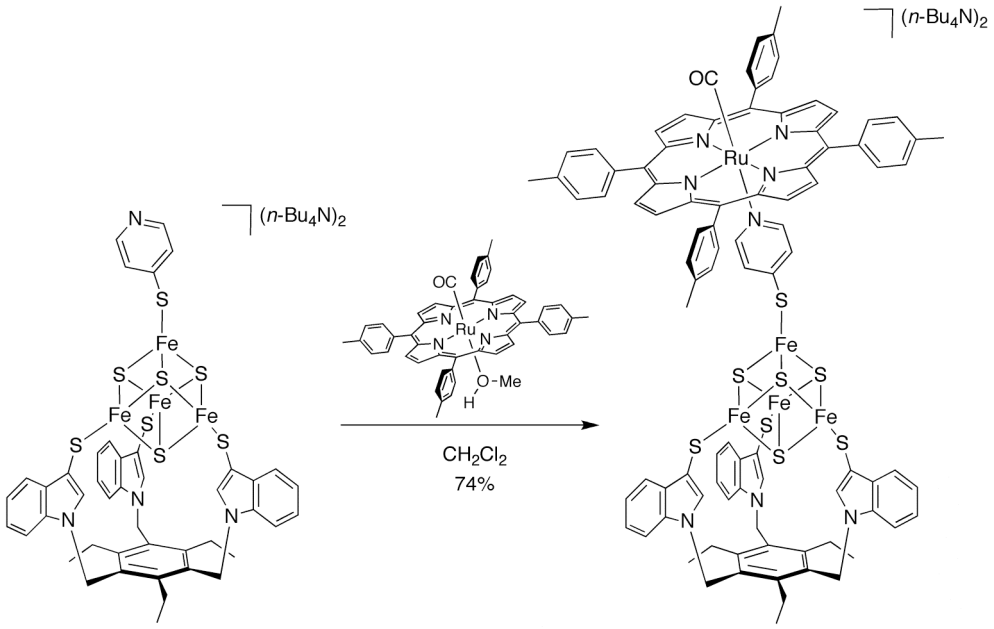

Scheme 2. Synthesis of a [4Fe-4S]-Ru assembly.

The third reaction presented in **Chapter 4** is that between $(n\text{-}Bu_4N)_2[Fe_4S_4(TriS)(SEt)]$ and *p*-fluorothiophenol, which forms the compound $(n\text{-}Bu_4N)_2[Fe_4S_4(TriS)(SC_6H_4\text{-}p\text{-}F)]$. Although all other spectroscopic and elemental analyses suggest a fully site-specific substitution, ^{19}F NMR indicates the formation of minor side products stemming from decoordination of $TriS^{3-}$ arms. The sensitivity of the ^{19}F resonance to the coordination environment demonstrates the benefits of using ^{19}F NMR in conjunction with a suitable, fluorinated reporter ligand to study the substitution behavior of [4Fe-4S] clusters.

Chapter 5 describes the most biomimetically relevant application of a $TriS^{3-}$-chelated cluster by presenting a new model for the active site of iron-only hydrogenase (Chart 3). The model is the $TriS^{3-}$ analogue of an earlier, LS_3^{3-}-based model reported by Pickett and co-workers[6] and the change in tripodal ligand has a profound impact on the properties of the mimic as a whole. Whereas the labile bridge between the [4Fe-4S] and diiron moieties in Pickett's model is broken upon reduction, resulting in the observation of two interdependent reductions in cyclic voltammetry, the bridge in the $TriS^{3-}$-chelated model remains intact. The only observed reduction occurs at –1.54 V vs. the ferrocene/ferrocinium couple in MeCN, close to the analogous redox potential in the absence of the iron-carbonyl moiety (–1.51 V). Together with the strong contact shifting observed in the bridging ligand, the absence of a cathodic shift upon introduction of the iron-carbonyl moiety implies that the [4Fe-4S] and diiron redox entities are strongly coupled, as also observed in the natural enzyme.[7]

Unfortunately, the new mimic is unstable in the presence of 2,6-dimethylpyridinium cations, hampering investigations of the model's activity in electrocatalytic proton reduction.

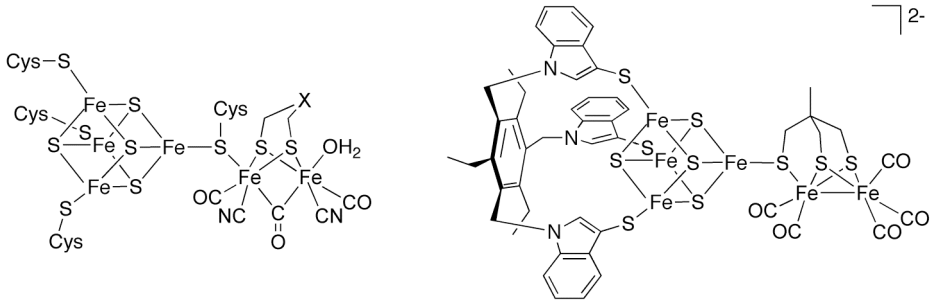

Chart 3. Schematic representation of the active site of iron-only hydrogenase (left, X = CH_2 or NH) and a $TriS^{3-}$-chelated active-site mimic (right).

The results described in Chapters 2–5, and indeed almost all [4Fe-4S] cluster studies reported thus far, deal with clusters in solution. In contrast, **Chapter 6** of this thesis describes the immobilization of [4Fe-4S] clusters on self-assembled monolayers (SAMs), a first step towards studies of [4Fe-4S] clusters at controlled solid-liquid interfaces. To effect the immobilization, $(n\text{-}Bu_4N)_2[Fe_4S_4(TriS)(SEt)]$ reacts with a mixed SAM consisting of 1-decanethiol and 1,12-dodecanedithiol on Au(111). Ligand exchange between the surface thiol groups and the EtS^- ligand results in an immobilizing interaction strong enough to resist extensive washing (Scheme 3). X-ray photoelectron spectroscopy (XPS) show the presence of an iron species at the SAM surface while time-of-flight secondary ion mass spectrometry (ToF-SIMS) detects fragments originating from both the [4Fe-4S] cluster core and the $TriS^{3-}$ ligand.

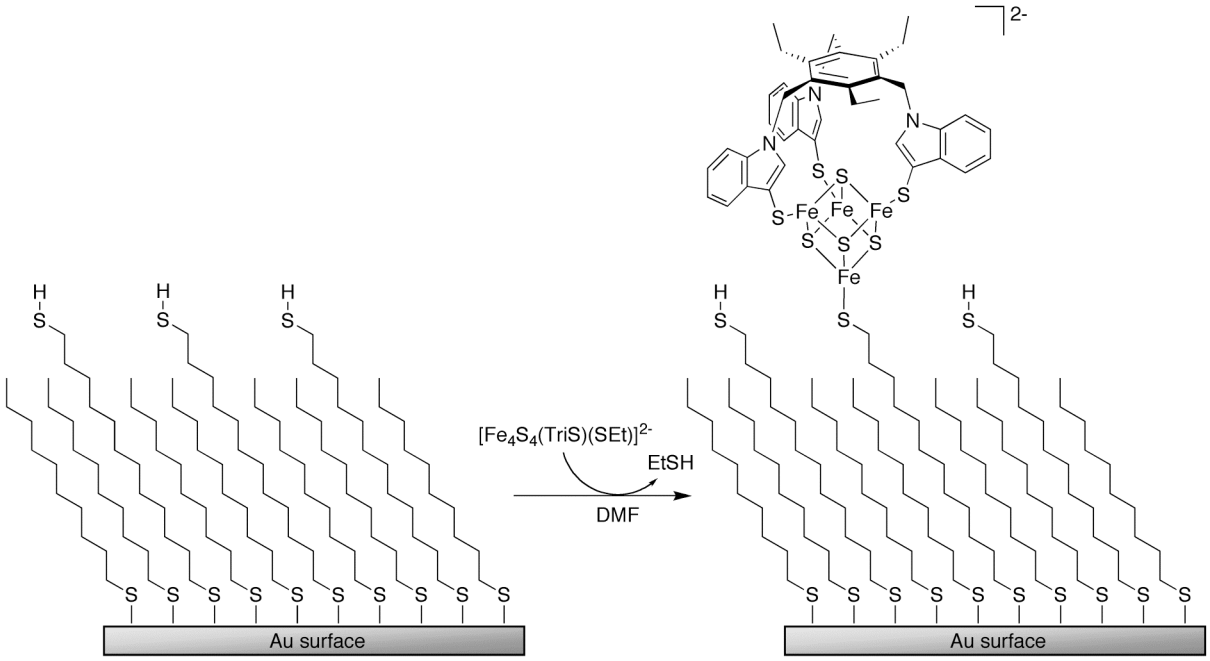

Scheme 3. The immobilization of $[Fe_4S_4(TriS)(SEt)]^{2-}$ on a SAM with surface thiol groups.

In conclusion, this thesis demonstrates the versatility and utility of $TriSH_3$ as a ligand in [4Fe-4S] cluster chemistry and presents several novel applications of 3:1 site-differentiated clusters. TriS-chelated [4Fe-4S] clusters not only represent the most conveniently accessible 3:1 site-differentiated [4Fe-4S] cluster family to date, but also prove to be reliable starting materials for further site-specific substitutions and incorporation into larger (biomimetic) structures. The clusters can be linked to ruthenium porphyrins, to self-assembled monolayers, to biologically relevant bimetallic subsites, or to each other *via* a metal-containing bridge. General properties of $TriS^{3-}$-chelated clusters include good solubility, reliable purity, and intermediate redox potentials. As biology yields new insights into the properties and function of 3:1 site-differentiated [4Fe-4S] clusters, $TriS^{3-}$-chelated analogues could prove to be an important tool in further biomimetic modelling studies. Possible applications may also be found in research fields more tangentially related to biology. For example, the [4Fe-4S]-Ru assembly in Chapter 4 combines a redox-active cluster unit with a metal ion widely applied for its (photo-)catalytic properties. The biologically inspired incorporation of [4Fe-4S] clusters into homogeneous catalysts and other functional materials may lead to synergistic effects similar to those seen in natural systems. Concomitantly, fundamental insights gained from studies such as those in this thesis could prove invaluable in realizing the full potential of 3:1 site-differentiated [4Fe-4S] clusters in novel biological and chemical applications.

References

[1] (a) Beinert, H.; Holm, R. H.; Münck, E. *Science* **1997**, *277*, 653–659. (b) Johnson, M. K. *Curr. Opin. Chem. Biol.* **1998**, *2*, 173–181.

[2] Beinert, H.; Kennedy, M. C.; Stout, C. D. *Chem. Rev.* **1996**, *96*, 2335–2373.

[3] (a) Nicolet, Y.; Piras, C.; Legrand, P.; Hatchikian, C. E.; Fontecilla-Camps, J. C. *Structure* **1999**, *7*, 13–23. (b) Peters, J. W.; Lanzilotta, W. N.; Lemon, B. J.; Seefeldt, L. C. *Science* **1998**, *282*, 1853–1858.

[4] Venkateswara Rao, P.; Holm, R. H. *Chem. Rev.* **2004**, *104*, 527–559.

[5] Walsdorff, C.; Saak, W.; Pohl, S. *J. Chem. Soc., Dalton Trans.* **1997**, 1857–1861.

[6] Tard, C.; Liu, X.; Ibrahim, S. K.; Bruschi, M.; De Gioia, L.; Davies, S. C.; Yang, X.; Wang, L.-S.; Sawers, G.; Pickett, C. J. *Nature* **2005**, *433*, 610–613.

[7] Silakov, A.; Reijerse, E. J.; Albracht, S. P. J.; Hatchikian, E. C.; Lubitz, W. *J. Am. Chem. Soc.* **2007**, *129*, 11447–11458.

Samenvatting en Toekomstbeeld

[4Fe-4S] clusters zijn een van de meest voorkomende cofactoren in de natuur, waar ze belangrijke rollen spelen in eiwit-struktuurstabilisatie, elektronentransport, katalyse en detectie van intracellulaire ijzerconcentraties.[1] Wanneer het actieve centrum van een enzym een [4Fe-4S] cluster bevat, is de coördinatie-omgeving van dit cluster *3:1 gedifferentieërd*, wat inhoudt dat het ligand gebonden aan één van de vier ijzeratomen significant verschilt van de liganden gebonden aan de andere drie ijzeratomen. Voorbeelden zijn aconitase, waarin een van de vier ijzeratomen het substraat bindt,[2] en ijzerhydrogenase, waarin het unieke ijzeratoom gebonden is aan een di-ijzergroep via een bruggend cysteinylthiolaat.[3]

Ter inleiding biedt **Hoofdstuk 1** van dit proefschrift een overzicht van natuurlijke en synthetische [4Fe-4S] clusters met 3:1 gedifferentieërde coördinatie-omgevingen. Er is een groot en groeiend aantal enzymen waarin de aanwezigheid van 3:1 gedifferentieërde [4Fe-4S] clusters kristallografisch is aangetoond, met de familie van radicale *S*-adenosylmethionine-enzymen als de meest tot de verbeelding sprekende recente ontdekking. In veel gevallen leiden nieuwe ontdekkingen tot nieuwe vragen en wetenschappelijke uitdagingen, waarmee het beperkte inzicht en begrip van biologische, 3:1 gedifferentieërde [4Fe-4S] clusters in het bijzonder, en katalytische ijzer-zwavelclusters in het algemeen, worden benadrukt. Een manier om de (bio)chemie van deze intrigerende metaalverbindingen te begrijpen is de benadering van het synthetisch analoog, waarin synthetische [4Fe-4S] clusters worden gemaakt, bestudeerd en vergeleken met hun biologische tegenhangers.[4] In de synthetische clusters wordt de 3:1 differentiatie meestal bewerkstelligd door het gebruik van tripodale trithiolaatliganden. Deze liganden cheleren drie van de vier ijzeratomen, waardoor één ijzeratoom beschikbaar blijft voor verdere modificaties. De identiteit van het tripodale ligand heeft een fundamenteel effect op de eigenschappen van het gebonden [4Fe-4S] cluster, en leidt tot specifieke voordelen maar ook nadelen in een beoogde toepassing.

Het meestbelovende 3:1 differentiërende [4Fe-4S] clusterligand is $TriSH_3$, gepubliceerd door Pohl *et al.* in 1997 (Figuur 1).[5] Helaas maakten de auteurs bij de synthese van $TriSH_3$ gebruik van toxische thiolbeschermings- en -ontschermingsreagentia. Ten behoeve van een verbeterde toegankelijkheid van synthetische, 3:1 gedifferentieërde [4Fe-4S] clusters, presenteert **Hoofdstuk 2** van dit proefschrift een nieuwe synthetische route naar $TriSH_3$. In deze route wordt indool-3-thiol beschermd door middel van chloromethyl*ethyl*ether in plaats van het carcinogene chloromethyl*methyl*ether. De beschermgroepen worden in een later stadium ontschermd met behulp van $AgNO_3$ en HCl in plaats van de conventionele ontschermingsreagentia $Hg(OAc)_2$ en H_2S. De nieuwe route vermijdt op deze wijze niet alleen het gebruik van minder gebruiksvriendelijke chemicaliën; tevens is de opbrengst van de $TriSH_3$ synthese tweemaal zo hoog in vergelijking met de oorspronkelijke procedure.

De reactie van $TriSH_3$ met $(n\text{-}Bu_4N)_2[Fe_4S_4(SEt)_4]$ in DMF levert het 3:1 gedifferentieërde cluster $(n\text{-}Bu_4N)_2[Fe_4S_4(TriS)(SEt)]$ op. Volledige omzetting kan worden bereikt in deze reactie door verwijdering van het vluchtige EtSH coprodukt. Het nieuwe cluster vertoont een goede oplosbaarheid en uitmuntende zuiverheid op basis van spectroscopische, microanalytische en elektrochemische karakterisering.

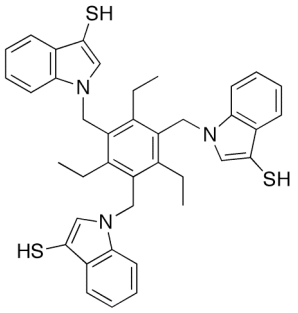

Figuur 1. Het tripodale $TriSH_3$ ligand.

Hoofdstuk 2 illustreert de synthetische veelzijdigheid van $(n\text{-}Bu_4N)_2[Fe_4S_4(TriS)(SEt)]$ aan de hand van de reactie met de thiol-gefunctionaliseerde Fe(II) verbinding $[Fe(tpySH)_2](PF_6)_2$ (tpySH = 2,2':6',2''-terpyridine-4'-thiol). Het produkt is het eerste [4Fe-4S] clusterdimeer dat verbonden is via een metaalbevattende brug (Figuur 2). In cyclische voltammetrie bij 100 mV/s ondergaat het dimer een enkele, cluster-gecentreerde overgang met een piekverschil van 82 mV, wat aantoont dat de [4Fe-4S] clusters in het dimeer zich gedragen als onafhankelijke redox-eenheden. In DMF oplossing vertoont het dimeer een elektronische absorptie bij 375 nm, veroorzaakt door een π–π^* overgang gelocaliseerd op de $tpyS^-$ C–S functionaliteit. De aanwezigheid van deze absorptie duidt op een thioquinonoïde elektronendistributie in de bruggende $\{Fe(tpyS)_2\}$ groep.

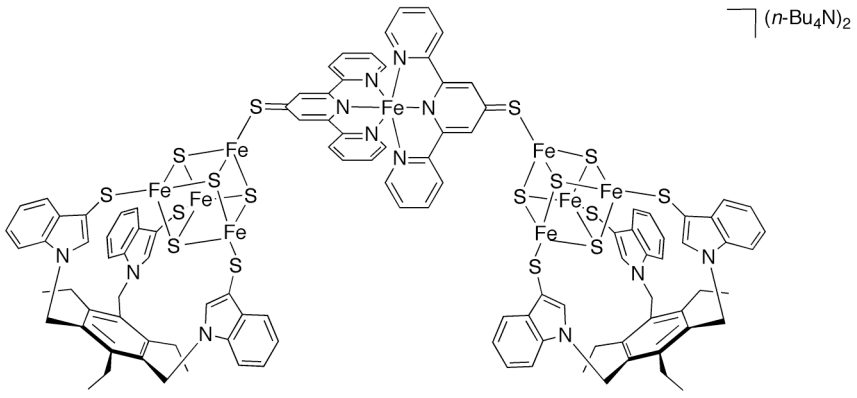

Figuur 2. Het [4Fe-4S] clusterdimeer $(n\text{-}Bu_4N)_2[\{Fe_4S_4(TriS)(\mu\text{-}Stpy)\}_2Fe]$.

De drie indolyl-3-thiol-armen in het $TriSH_3$ ligand vertonen een inherente strukturele ordening voor het binden van een [4Fe-4S] cluster in een centrale holte. Ondanks het grote aantal bekende, symmetrisch-gesubstitueerde clusters van het type $[Fe_4S_4(SR)_4]^{2-}$, zijn

synthetische clusters met monodentate liganden op basis van indool-3-thiol niet eerder beschreven. Om deze leemte in de [4Fe-4S] clusterchemie te vullen beschrijft **Hoofdstuk 3** van dit proefschrift de synthese van een serie symmetrisch-gesubstitueerde [4Fe-4S] clusters met *N*-gesubstitueerde indool-3-thiolaatliganden (Schema 1). De nieuwe clusterfamilie vertoont 2–/3– redoxovergangen bij potentialen tussen –1.17 en –1.22 V t.o.v. de standaard calomel elektrode (SCE) in CH_2Cl_2, afhankelijk van de identiteit van de *N*-substituent. Deze redoxpotentialen vallen in een bereik tussen de potentiaalbereiken waarin clusters met louter alifatische of aromatische thiolaten 2–/3– redoxovergangen vertonen. In DMF oplossing ondergaan de indool-3-thiolaatclusters laagste-energie-overgangen tussen de 500 (*N*-pentyl) en 511 (*N*-benzyl) nm. Deze elektronische overgangen behoren voor zover bekend tot de minst energetische overgangen ooit waargenomen voor [4Fe-4S] clusters.

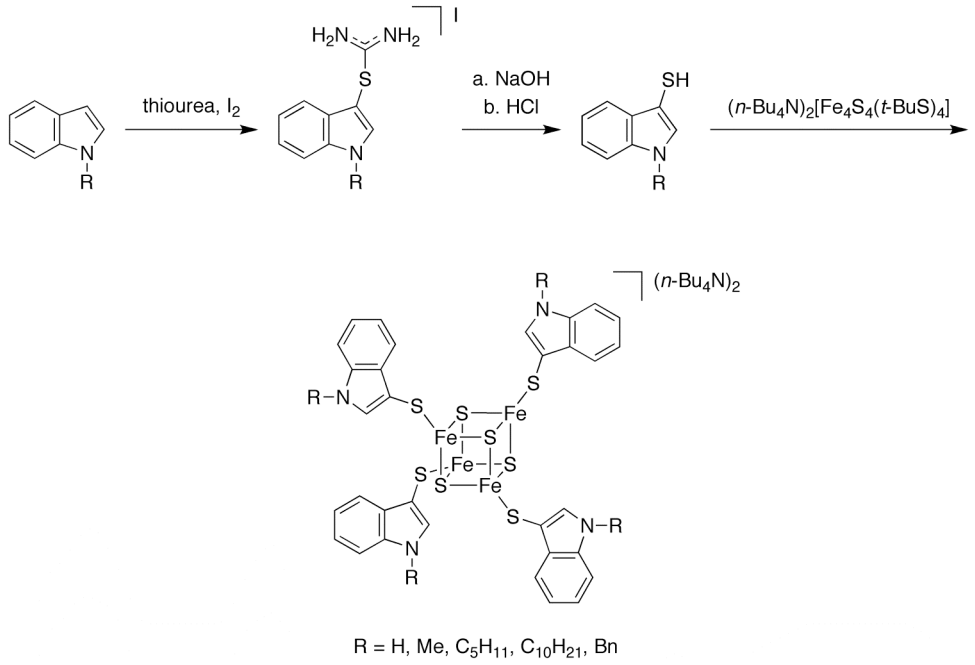

Schema 1. Synthese van een serie [4Fe-4S] clusters met *N*-gesubstitueerde indool-3-thiolaatliganden.

Hoofdstuk 4 verbreedt en verdiept de chemie van $TriS^{3-}$-gecheleerde [4Fe-4S] clusters door de bestudering van de reactie van $(n\text{-}Bu_4N)_2[Fe_4S_4(TriS)(SEt)]$ met drie verschillende thiolen. De reactie met ethylcysteïnaat (EtCysSH) levert analytisch zuiver $(n\text{-}Bu_4N)_2[Fe_4S_4(TriS)(SCysEt)]$ op en bewijst daarmee dat $(n\text{-}Bu_4N)_2[Fe_4S_4(TriS)(SEt)]$ plaatsspecifiek kan reageren met alifatische thiolen zonder voorafgaande activering van de unieke ijzerpositie. De reactie met 4-pyridinethiol resulteert in een 3:1 gedifferentieërd [4Fe-4S] cluster met een vrije pyridylgroep. Deze groep kan reageren met de rutheniumporfyrine [Ru(TTP)(CO)(MeOH)] (TTP = 5,10,15,20-tetra(*p*-tolyl)porfyrinato dianion), met als resultaat het eerste [4Fe-4S]-Ru complex (Schema 2). In CD_2Cl_2 worden de ^1H NMR signalen van de cluster- en porfyrine-delen van dit complex beiden beïnvloed door de brugvorming. De grootste verschuivingen doen zich echter voor bij de signalen van het $n\text{-}Bu_4N^+$ tegenion, wat duidt op ionpaarvorming. Elektrochemisch wordt het [4Fe-4S] cluster nauwelijks beïnvloed

door de binding met het rutheniumporfyrine: de 2–/3– cluster-redoxovergangen doen zich voor bij –1.13 en –1.11 V t.o.v. SCE in CH_2Cl_2 voor respectievelijk het uitgangscluster en het gebrugde produkt. Het rutheniumporfyrine is elektrochemisch gevoeliger voor axiale substituent-effecten. Vergeleken met de TTP reductie in het ongesubstitueerde pyridinecomplex [Ru(TTP)(CO)(C_5H_5N)] ($E_{1/2}$ = –1.61 V t.o.v. SCE) is de TTP reductie in het [4Fe-4S]-Ru complex sterk anodisch verschoven (E_{red} = –1.75 V vs. SCE). De carbonyl rekvibratie in het [4Fe-4S]-Ru complex is ietwat lager (1937 respectievelijk 1940 cm^{-1}) als gevolg van elektronendonatie door de clustergebonden thiolaatgroep.

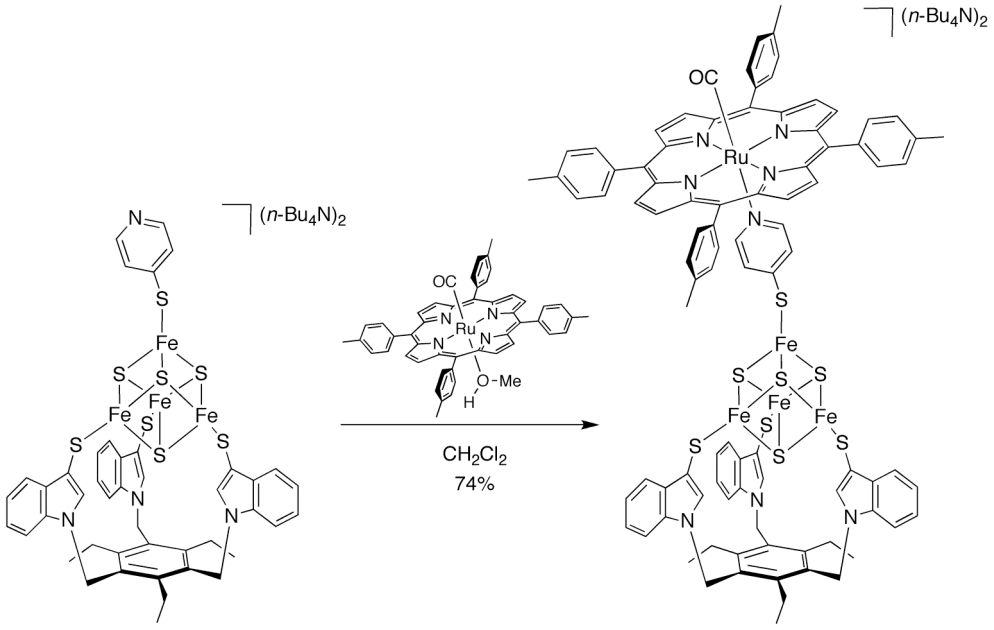

Schema 2. Synthese van een [4Fe-4S]-Ru complex.

De derde reactie beschreven in **Hoofdstuk 4** is de reactie van (n-$Bu_4N)_2[Fe_4S_4$(TriS)(SEt)] met p-fluorothiophenol tot (n-$Bu_4N)_2[Fe_4S_4$(TriS)(SC_6H_4-p-F)]. Hoewel alle andere spectroscopische studies en elementanalyse een volledig plaatsspecifieke substitutie suggereren, toont ^{19}F NMR de vorming van geringe hoeveelheden bijprodukten aan ten gevolge van decoördinatie van $TriS^{3-}$ donorarmen. De gevoeligheid van de ^{19}F resonantie voor de coördinatie-omgeving bewijst het nut van het gebruik van ^{19}F NMR in combinatie met een geschikt, fluorhoudend ligand om het substitutiegedrag van [4Fe-4S] clusters te bestuderen.

Hoofdstuk 5 beschrijft de biomimetisch meest relevante toepassing van een $TriS^{3-}$-gecheleerd cluster: een nieuw model voor het actieve centrum van ijzerhydrogenase (Figuur 3). Het model is het $TriS^{3-}$ analoog van een LS^{3-}-bevattend model eerder beschreven door Pickett *et al.*[6] en het verschil in tripodale ligand blijkt een verstrekkende invloed te hebben op de eigenschappen van het model als geheel. Terwijl reductie van Picketts model leidt tot het verbreken van de labiele brug tussen het [4Fe-4S] cluster en de di-ijzergroep, resulterend in de waarneming van twee, van elkaar afhankelijke redukties in cyclische voltammetrie, blijft

de brug in het $TriS^{3-}$-bevattende model intakt. De enige waargenomen reduktie vindt plaats bij –1.54 V t.o.v. het ferroceen/ferrocinium koppel in MeCN, dichtbij de analoge potentiaal in afwezigheid van de ijzercarbonyl-groep (–1,51 V). Tezamen met de grote kontaktverschuiving van het bruggende ligandsignaal in ^{1}H-NMR, duidt de afwezigheid van een kathodische verschuiving na introductie van de ijzercarbonyl-groep op een sterke koppeling tussen de [4Fe-4S] en di-ijzer-redoxeenheden. Eenzelfde sterke koppeling is aanwezig in het enzym zelf.[7] Helaas is het nieuwe model instabiel in de aanwezigheid van het 2,6-dimethylpyridinium kation, wat studies betreffende de aktiviteit van het model in elektrokatalytische protonreduktie sterk heeft bemoeilijkt.

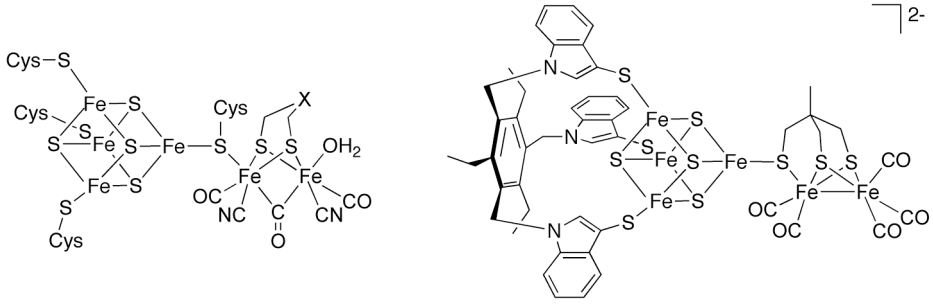

Figuur 3. Schematische weergave van het actieve centrum van ijzerhydrogenase (links, X = CH_2 of NH) en een $TriS^{3-}$-gecheleerd struktureel model (rechts).

Net als het overgrote deel van de [4Fe-4S] clusterstudies in de literatuur, beschrijven Hoofdstukken 2–5 de eigenschappen van clusters in oplossing. Daarentegen beschrijft **Hoofdstuk 6** van dit proefschrift de immobilisatie van [4Fe-4S] clusters op zelf-geassembleerde monolagen (SAMs), een eerste stap richting de bestudering van [4Fe-4S] clusters op gecontroleerde grensvlakken. Om de immobilisatie te bewerkstelligen, reageert (n-$Bu_4N)_2[Fe_4S_4(TriS)(SEt)]$ met een gemengde SAM bestaande uit 1-decaanthiol en 1,12-dodecaandithiol op Au(111). Liganduitwisseling tussen de aan het oppervlak gelegen thiolgroepen en het clustergebonden EtS^- ligand resulteert in een interactie die sterk genoeg is om grondige wasstappen te doorstaan (Schema 3). Röntgen-fotoelektronenspectroscopie (XPS) toont de aanwezigheid van ijzer aan op het SAM oppervlak. “Time of flight” secundaire ionenmassaspectrometrie detecteert fragmenten afkomstig van de [4Fe-4S] clusterkern en van het $TriS^{3-}$ ligand.

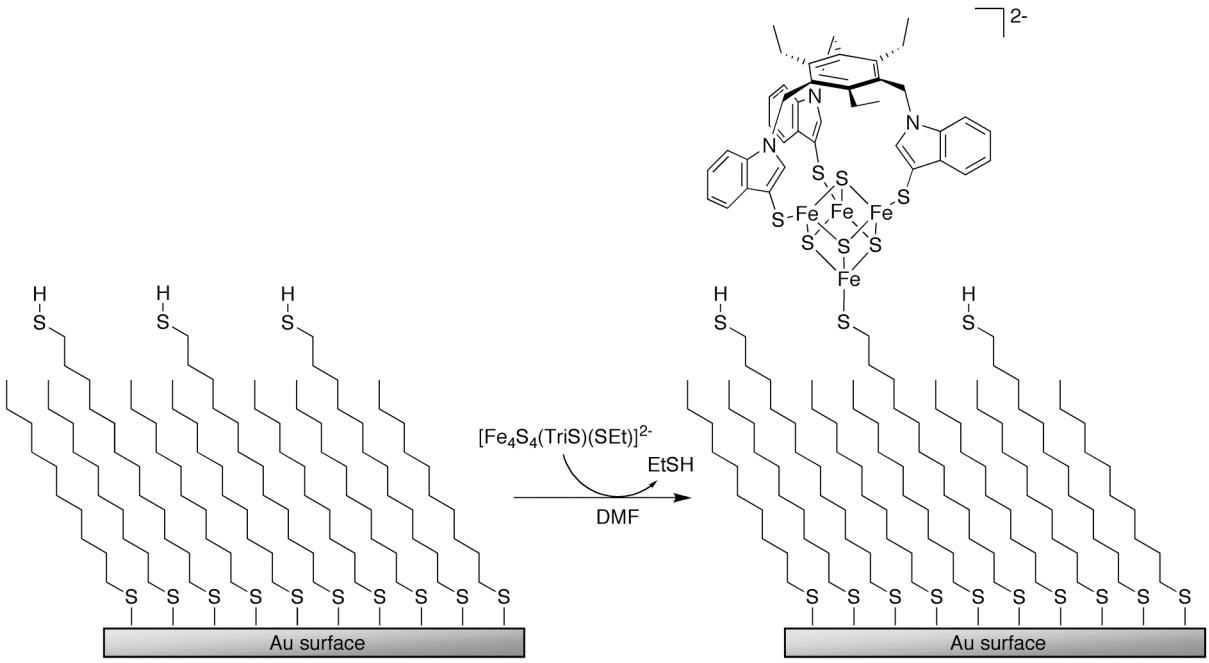

Schema 3. De immobilisatie van $[Fe_4S_4(TriS)(SEt)]^{2-}$ op een SAM met thiolgroepen aan het oppervlak.

Samenvattend bewijst dit proefschrift de veelzijdige toepasbaarheid van $TriSH_3$ als ligand in de [4Fe-4S] clusterchemie en presenteert het een reeks nieuwe toepassingen van 3:1 gedifferentieërde [4Fe-4S] clusters. $TriS^{3-}$-gecheleerde [4Fe-4S] cluster zijn niet alleen de meest toegankelijke 3:1 gedifferentieërde [4Fe-4S] clusterfamilie tot nu toe, maar hebben zich ook bewezen als betrouwbare uitgangsmaterialen voor verdere, plaatsspecifieke substituties en de synthese van grotere (biomimetische) strukturen. $TriS^{3-}$-gecheleerde clusters kunnen worden gebonden aan rutheniumporfyrines, zelf-geassembleerde monolagen, biologisch relevante bimetallische eenheden, of aan elkaar via metaalhoudende bruggen. Algemene kenmerken van de clusters zijn hun goede oplosbaarheid, betrouwbare zuiverheid en redoxpotentialen liggend tussen de redoxpotentialen van [4Fe-4S] clusters met enkel alifatische of enkel aromatische thiolaatliganden. Terwijl de biologie nieuwe inzichten blijft verschaffen in de eigenschappen en functies van 3:1 gedifferentieërde [4Fe-4S] clusters, kunnen $TriS^{3-}$-gecheleerde analogen een belangrijk hulpmiddel blijken in verdere, biomimetische modelstudies. Er liggen ook mogelijke toepassingen in onderzoeksvelden minder verwant aan de biologie. Zo combineert het [4Fe-4S]-Ru complex in Hoofdstuk 4 een redox-actief cluster met een metaalion dat veel wordt toegepast vanwege zijn (foto)katalytische eigenschappen. De biologisch geïnspireerde opname van [4Fe-4S] clusters in homogene katalysatoren en andere functionele materialen kunnen mogelijk leiden tot synergistische effekten zoals ook gezien in de natuur. Tegelijkertijd kunnen de fundamentele inzichten verkregen in studies zoals die beschreven in dit proefschrift, van groot belang zijn voor het volledig kunnen benutten van de veelzijdige eigenschappen van 3:1 gedifferentieërde [4Fe-4S] clusters in zowel biologische als chemische toepassingen.

Referenties

[1] (a) Beinert, H.; Holm, R. H.; Münck, E. *Science* **1997**, *277*, 653–659. (b) Johnson, M. K. *Curr. Opin. Chem. Biol.* **1998**, *2*, 173–181.
[2] Beinert, H.; Kennedy, M. C.; Stout, C. D. *Chem. Rev.* **1996**, *96*, 2335–2373.
[3] (a) Nicolet, Y.; Piras, C.; Legrand, P.; Hatchikian, C. E.; Fontecilla-Camps, J. C. *Structure* **1999**, *7*, 13–23. (b) Peters, J. W.; Lanzilotta, W. N.; Lemon, B. J.; Seefeldt, L. C. *Science* **1998**, *282*, 1853–1858.
[4] Venkateswara Rao, P.; Holm, R. H. *Chem. Rev.* **2004**, *104*, 527–559.
[5] Walsdorff, C.; Saak, W.; Pohl, S. *J. Chem. Soc., Dalton Trans.* **1997**, 1857–1861.
[6] Tard, C.; Liu, X.; Ibrahim, S. K.; Bruschi, M.; De Gioia, L.; Davies, S. C.; Yang, X.; Wang, L.-S.; Sawers, G.; Pickett, C. J. *Nature* **2005**, *433*, 610–613.
[7] Silakov, A.; Reijerse, E. J.; Albracht, S. P. J.; Hatchikian, E. C.; Lubitz, W. *J. Am. Chem. Soc.* **2007**, *129*, 11447–11458.

Graphical Abstract

Chapter 1

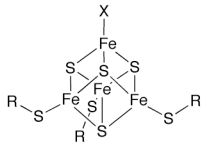

Chapter 2

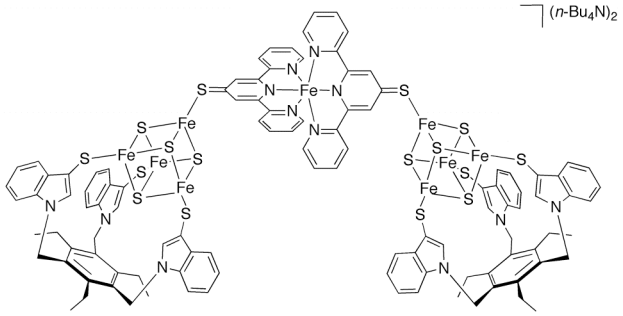

Chapter 3

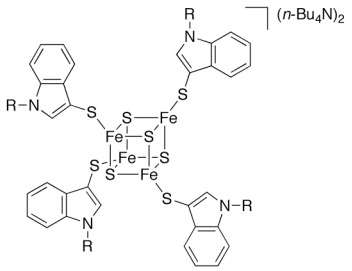

Chapter 4

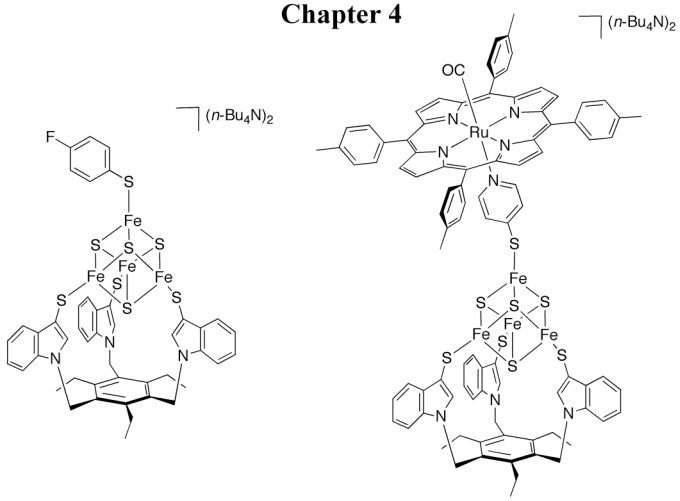

Chapter 5

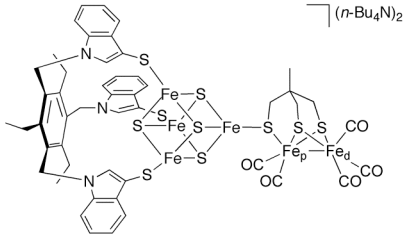

Chapter 6

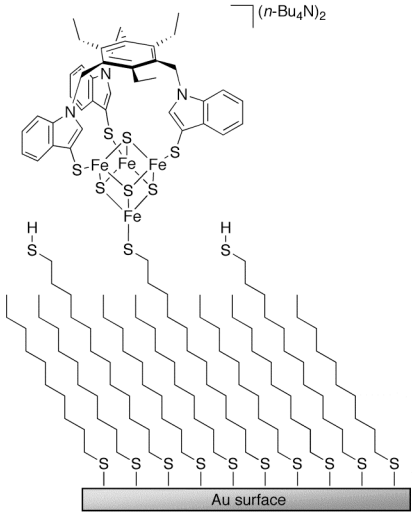

Curriculum Vitae

Erwin van der Geer was born on May 29th, 1981, in Katwijk, the Netherlands. After attending schools in the Netherlands, Italy, and Switzerland, he obtained an International Baccalaureate from the American Community Schools of Athens, Greece, in 1998. In the same year he started an MSc. program in chemistry at Leiden University. He conducted his MSc. thesis research in the group of Prof. Jan Reedijk, focusing on the synthesis and characterization of novel, anti-tumor polypyridyl ruthenium compounds. For this research, he was awarded the Unilever Research Prize in 2002. Erwin completed two other research projects for Prof. Peter Sadler (University of Edinburgh, the United Kingdom) and Prof. Mark Schofield (Williams College, the United States) before obtaining his MSc. degree *cum laude* in 2003. In that same year, he began his Ph.D. thesis in the Chemical Biology and Organic Chemistry group of Utrecht University, supervised by Prof. Bert Klein Gebbink, Prof. Gerard van Koten, and Prof. Bart Hessen. Parts of this thesis have been presented at the Netherlands Catalysis and Chemistry Conference (Noordwijkerhout, the Netherlands), the 3rd SFB Symposium on Metal-Mediated Reactions Modeled after Nature (Jena, Germany), and the 8th European Biological Inorganic Chemistry Conference (EuroBIC 8, Aveiro, Portugal). Since November 1st, 2007, Erwin has been working for Shell Global Solutions as a technologist in gas to liquids conversion.

Erwin van der Geer werd geboren op 29 mei, 1981 in Katwijk aan den Rijn. Zijn schooltijd bracht hij door in achtereenvolgens Nederland, Italië en Zwitserland, waarna hij in 1998 zijn International Baccalaureate behaalde aan de American Community Schools te Athene, Griekenland. In hetzelfde jaar begon hij met de studie scheikunde aan de Universiteit Leiden. Zijn doctoraalonderzoek, in 2002 beloond met een Unilever Researchprijs, werd uitgevoerd in de onderzoeksgroep van Prof. dr. Jan Reedijk en betrof de synthese en karakterisatie van nieuwe, antitumor-actieve, polypyridyl rutheniumcomplexen. Erwin werkte aan nog twee onderzoeksprojecten voor Prof. dr. Peter Sadler (University of Edinburgh, het Verenigd Koninkrijk) en Prof. dr. Mark Schofield (Williams College, de Verenigde Staten) alvorens in 2003 *cum laude* af te studeren. In datzelfde jaar begon hij met zijn promotieonderzoek in de vakgroep Chemische Biologie en Organische Chemie van de Universiteit Utrecht, onder begeleiding van Prof. dr. Bert Klein Gebbink, Prof. dr. Gerard van Koten en Prof. dr. Bart Hessen. Delen van dit proefschrift werden gepresenteerd op het Netherlands Catalysis and Chemistry Conference (Noordwijkerhout), het 3rd SFB Symposium on Metal-Mediated Reactions Modeled after Nature (Jena, Duitsland) en het 8th European Biological Inorganic Chemistry Conference (EuroBIC 8, Aveiro, Portugal). Sinds 1 november 2007 werkt Erwin voor Shell Global Solutions als technoloog in gas-naar-vloeistof (GTL) conversie.

List of Publications

Coordination of 9-Ethylguanine to the Mixed-Ligand Compound a-[Ru(azpy)(bpy)Cl_2] (azpy = 2-Phenylazopyridine and bpy = 2,2'-Bipyridine). An Unprecedented Ligand Positional Shift, Correlated to the Cytotoxicity of This Type of [RuL_2Cl_2] (with L = azpy or bpy) Complex
Hotze, A. C. G.; van der Geer, E. P. L.; Caspers, S. E.; Kooijman, H.; Spek, A. L.; Haasnoot, J. G.; Reedijk, J. *Inorg. Chem.* **2004**, *43*, 4935–4943.

Characterization by NMR Spectroscopy, X-ray Analysis and Cytotoxic Activity of the Ruthenium(II) Compounds [RuL_3](PF_6)$_2$ (L = 2-Phenylazopyridine or o-*Tolylazopyridine) and [RuL'_2L''](PF_6)$_2$ (L', L'' = 2-Phenylazopyridine, 2,2'-Bipyridine)*
Hotze, A. C. G.; van der Geer, E. P. L.; Kooijman, H.; Spek, A. L.; Haasnoot, J. G.; Reedijk, J. *Eur. J. Inorg. Chem.* **2005**, *13*, 2648–2657.

Controlling ligand substitution reactions of organometallic complexes: tuning cancer cell cytotoxicity
Wang, F.; Habtemariam, A.; van der Geer, E. P. L.; Fernández, R.; Melchart, M.; Deeth, R. J.; Aird, R.; Guichard, S.; Fabbiani, F. P. A.; Lozano-Casal, P.; Oswald, I. D. H.; Jodrell, D. I.; Parsons, S.; Sadler, P. J. *Proc. Nat. Acad. Sci. USA* **2005**, *102*, 18269–18274.

*Multipole refinement of indole-3-*N,N,N′,N′*-tetramethylthiouronium nitrate*
Lutz, M.; Spek, A. L.; van der Geer, E. P. L.; van Koten, G.; Klein Gebbink, R. J. M. *Acta Cryst.* **2008**, *C64*, o87–o90 (Appendix 2 of this thesis).

Indole-3-thiouronium nitrate
Lutz, M.; Spek, A. L.; van der Geer, E. P. L.; van Koten, G.; Klein Gebbink, R. J. M. *Acta Cryst.* **2008**, *E64*, o194 (Appendix 2 of this thesis).

Indole-3-thiouronium iodide
Lutz, M.; Spek, A. L.; van der Geer, E. P. L.; van Koten, G.; Klein Gebbink, R. J. M. *Acta Cryst.* **2008**, *E64*, o195 (Appendix 2 of this thesis).

N-*Substituted Indole-3-Thiolate [4Fe-4S] Clusters with a Unique and Tunable Combination of Spectral and Redox Properties*
van der Geer, E. P. L.; Li, Q.; van Koten, G.; Klein Gebbink, R. J. M.; Hessen, B. *Inorg. Chim. Acta*, in press (Chapter 3 of this thesis).

A [4Fe-4S] Cluster Dimer Bridged by Bis(2,2':6',2''-Terpyridine-4'-Thiolato)iron(II)
van der Geer, E. P. L.; van Koten, G.; Klein Gebbink, R. J. M.; Hessen, B. *Inorg. Chem.*, accepted (Chapter 2 of this thesis).

3:1 Site-Differentiated [4Fe-4S] Clusters: Visualizing Ligand Substitutions by ^{19}F NMR and Synthesis of a [4Fe-4S]-Ruthenium Assembly
van der Geer, E. P. L.; van Koten, G.; Klein Gebbink, R. J. M.; Hessen, B., to be submitted (Chapter 4 of this thesis).

Effects of the Chelating [4Fe-4S] Ligand on a Model for the Iron-Only Hydrogenase H Cluster
van der Geer, E. P. L.; Panday, D.; van Koten, G.; Klein Gebbink, R. J. M.; Hessen, B., to be submitted (Chapter 5 of this thesis).

Synthesis and Crystal Structures of tpySAc and $[FeCl_3(tpySAc)]\cdot MeCN$ (tpySAc = 4'-Acetylthio-2,2':6',2''-Terpyridine)
van der Geer, E. P. L.; Gagliardo, M.; Lutz, M.; Spek, A. L.; van Klink, G. P. M.; van Koten, G.; Klein Gebbink, R. J. M., to be submitted (Appendix 1 of this thesis).

*Comment on "Theoretical studies on the ground states in M(terpyridine)$_2^{2+}$ and M(*n*-butyl-phenylterpyridine)$_2^{2+}$ (M = Fe, Ru, Os) and excited states in Ru(terpyridine)$_2^{2+}$ using density functional theory"*
Wadman, S. H.; van der Geer, E. P. L.; Havenith, R. W. A.; van Klink, G. P. M.; van Koten, G.; Hessen, B.; Klein Gebbink, R. J. M., to be submitted.

3:1 Site Differentiation in Natural and Synthetic [4Fe-4S] Clusters
van der Geer, E. P. L.; van Koten, G.; Klein Gebbink, R. J. M.; Hessen, B., manuscript in preparation (Chapter 1 of this thesis).

A 3:1 Site-Differentiated [4Fe-4S] Cluster Immobilized on a Self-Assembled Monolayer
van der Geer, E. P. L.; van den Brom, C. R.; Arfaoui, I. E.; Houssiau, L.; Rudolf, P.; van Koten, G.; Klein Gebbink, R. J. M.; Hessen, B., manuscript in preparation (Chapter 6 of this thesis).

Dankwoord

Het geeft een fantastisch gevoel om nu, vier jaar en een paar maanden na het begin van mijn promotieonderzoek, rustig door mijn hoofdstukken te bladeren en me te realiseren dat de klus bijna geklaard is. Het proefschrift is natuurlijk bedoeld als een verslag van mijn wetenschappelijke resultaten, maar het boek zit voor mij persoonlijk ook barstensvol herinneringen aan leuke experimenten, nieuwe ideeën, teleurstellende tegenvallers en spannende doorbraken. Natuurlijk zit het ook vol met de herinneringen die minstens zo belangrijk zijn: de collega's met wie ik samen heb gewerkt en de mensen die mij de afgelopen jaren door dik en dun hebben gesteund. Ze verdienen het zonder meer om hier, aan het eind van het proefschrift, in het zonnetje gezet te worden.

Allereerst mijn promotoren, de professoren Bart Hessen, Bert Klein Gebbink en Gerard van Koten. Beste Bart, ik kan me nog goed herinneren dat ik bij mijn eerste bezoek aan het Kruytgebouw meteen gegrepen werd door je enthousiasme voor het onderzoeksvoorstel dat resulteerde in dit proefschrift, en waardoor ik voor een promotie in Utrecht koos. Sindsdien heb ik veel geleerd van je vermogen om een efficiënte doelgerichtheid te combineren met wetenschappelijke diepgang. Veel succes met je nieuwe levenspad; met het enthousiasme dat je ook ten toon spreidde in de scheikunde, zal dat zeker lukken! Beste Bert, het was ontzettend fijn om een promotor te hebben met veel ervaring in de clusterchemie. Hartelijk bedankt voor alle keren dat ik bij je aan kon kloppen om in alle rust samen de resultaten naast elkaar te leggen en een volgend experiment te bedenken. Beste Gerard, je voegde je wat later bij mijn lijst van promotoren, maar deed dat desondanks met zoveel interesse en energie dat ik optimaal kon profiteren van je kennis en ervaring. Aan onze samenwerkingen bij het voorbereiden van je nanotechnologie- en afscheidslezingen heb ik veel plezier beleefd.

Gelukkig kon ik tijdens mijn onderzoek ontzettend veel lachen, gezellige momenten beleven aan de koffie-/lunch-/borreltafel en mooie discussies voeren met mijn directe collega's. Mijn kantoorgenoten Elena, Nesibe, Guido, Alexsandro, Marianne en Anne zorgden altijd voor een gezellige kamer W803. Elena and Nesibe, I really loved the dinners; good luck with the remaining months of your promotions! Guido, de grappen op kantoor en op zaal waren onvergetelijk!

Sipke, de samenwerkingen, de cursussen (inclusief lange pauzes in A'dam) en de chemische discussies waren echt super; hartstikke leuk dat je mijn paranimf wilt zijn! Nilesh, I really enjoyed the train rides, the many nice evenings, jogs etc. with you and Meenal; it was also an honor to be your paranymph! The same goes for you, Marcella, and I'm glad Vicky and I keep in touch with you and Robert past our Utrecht days. Hopefully our tpySAc paper will be out soon!

Aidan (congrats, you beat me to it!), Bart (bedankt voor de mooie paarse porfyrines!), “co-Piet” Birgit, Jie, Pieter, Silvia, Kees, Niels, Marcel, Dennis, Morgane, Jeroen, Preston, Catelijne, Maaike, Rob K., Rob C., Jérôme, Alexey, Monika, Sylvestre, Thomas, Kamil, Harm, Patrick, Judith, Henk, Peter, Gerard van Klink, Johann, Jan, Layo, Jacco en Ed wil ik ook graag bedanken voor de fijne vier jaar.

Een speciale alinea is op zijn plaats voor de studenten die ik met veel plezier heb begeleid. Qian, I really enjoyed working with you and seeing your transition from the MSc. student just in from China to the Ph.D. student you are now. Well done on all the work in Chapter 3! Nicole, jij hebt de basis gelegd voor de verbeterde tpySAc synthese, bedankt daarvoor! Dinesh, jou heb ik de moeilijkste projecten gegeven en toch heb je daar fantastische resultaten uit weten te halen. Veel succes in jouw promotie-onderzoek! Robert-Jan, bedankt voor de uitputtende literatuurstudie, waardoor het schrijven van Hoofdstuk 1 een stuk makkelijker werd. Jij ook veel succes als AiO!

Binnen de Universiteit Utrecht zou ik ook graag Martin Lutz en Ton Spek willen bedanken voor het kristallografische werk in dit proefschrift. Martin, het was erg fijn dat je altijd bereid was weer zo’n weinig hoopgevend clusterkristal te meten; gelukkig zijn er toch nog leuke kristalstrukturen uit onze samenwerking gekomen!

Milka, Margo en Hester, hartelijk bedankt voor alle administratieve zaken die jullie altijd perfekt wisten, en weten, te regelen. De medewerkers van de audiovisuele dienst (in het bijzonder Jan den Boesterd) en de glasblazerij wil ik ook graag bedanken voor hun vakwerk.

Tijdens mijn promotie heb ik het geluk gehad dat ik niet alleen in Utrecht, maar ook in Groningen kon samenwerken met topwetenschappers. Coen van den Brom, het was erg leuk om het oppervlakte-werk van je te leren; dankzij jou heeft het begrip “schoon” nu voor mij een hele nieuwe dimensie gekregen! De diners bij jou thuis waren altijd erg gezellig; bedankt voor de voortreffelijke gastvrijheid. Imad Arfaoui, thanks for all the STM characterizations and, together with Bert de Boer, Monika Lubomska, and Lacra Popescu, for the preparations for my trips to Groningen. Sergio Bambirra, bedankt voor het moeilijke ESI-MS werk; de ESI-MS uitjes naar Groningen waren niet alleen nuttig, maar ook altijd leuk! Steven Boot, bedankt voor de hulp bij de CV metingen. Prof. dr. Petra Rudolf, hartelijk bedankt voor de fijne samenwerking en het feit dat ik altijd terecht kon voor vragen over het oppervlaktewerk. I would also like to thank Prof. Laurent Houssiau (Namur) for conducting the ToF-SIMS measurements in Chapter 6.

Als Leids alumnus was het altijd leuk om weer terug te zijn in de Gorlaeus Laboratoria. Stefania Grecea, Lies Bouwman en Prof. dr. Jan Reedijk, hartelijk dank voor de gastvrijheid toen ons CV apparaat kapot was!

Geluk op je werk en in je privéleven gaan vaak hand in hand, en ik kon tijdens mijn AiO-schap gelukkig altijd rekenen op mijn vrienden, kennissen en familie. Karin, we begonnen tegelijkertijd aan ons Utrechts avontuur. Voor jou zit het er nu ook bijna op; succes met de laatste loodjes! Ik ben blij dat je mijn paranimf wilt zijn. Jasper en Martijn, hopelijk volgen er met jullie nog veel avondjes films pakken, spellen spelen, biertjes drinken en uitjes naar De Lantaarn. Paul, hartstikke mooi dat we collega's gaan worden; hopelijk zullen we met jou en Debbie nog veel toeristische plekken in Nederland bezoeken. Wouter, het was altijd ontzettend leuk om—na een dag labwerk—me met jou uit te leven op de squashbaan. Aan alle leden van Harmoniekapel Werkmans Wilskracht: bedankt voor alle gezelligheid en ook voor het feit dat jullie het niet erg vonden dat ik de afgelopen vier jaar steevast te laat op de repetitie verscheen! Mijn nieuwe collega's bij Shell zou ik hier ook graag willen bedanken voor hun gastvrije ontvangst.

En dan mijn familie, met in de eerste plaats mijn ouders. Pap, Mam, zonder jullie zou ik niet zijn wie en waar ik nu ben. Het was en is van onschatbare waarde dat ik altijd op jullie kan rekenen, en het is daarom dat ik graag dit boekje aan jullie opdraag. Natasja, Gertjan, Jeroen en Linda, bedankt voor alle gezelligheid; ik vind het ontzettend fijn dat jullie zo dichtbij wonen! Mijn oma's, ooms, tantes, neven en nichten wil ik ook bedanken voor hun interesse in mijn studie en promotieonderzoek. I would also like to thank my future parents-in-law for their interest and support.

This last paragraph is reserved for the one person who made all the difference in the past few years. Vicky, you came all the way over here, adjusted and settled into a life together with me, and still always found the time and energy to be so loving and supportive throughout the hectic Ph.D. years. You make me truly and fundamentally happy. It's been quite the year, with our job switches, the finishing of the thesis, moving, and planning a wedding, but as we predicted, the reaping has begun! Nothing makes me happier, or more proud, than to know I get to spend the rest of my life with you.

Erwin